National Library of Canada
Acquisitions and Bibliographic Services Branch
395 Wellington Street
Ottawa, Ontario
K1A 0N4

Bibliothèque nationale du Canada
Direction des acquisitions et des services bibliographiques
395, rue Wellington
Ottawa (Ontario)
K1A 0N4

Your file Votre référence

Our file Notre référence

NOTICE

The quality of this microform is heavily dependent upon the quality of the original thesis submitted for microfilming. Every effort has been made to ensure the highest quality of reproduction possible.

If pages are missing, contact the university which granted the degree.

Some pages may have indistinct print especially if the original pages were typed with a poor typewriter ribbon or if the university sent us an inferior photocopy.

AVIS

La qualité de cette microforme dépend grandement de la qualité de la thèse soumise au microfilmage. Nous avons tout fait pour assurer une qualité supérieure de reproduction.

S'il manque des pages, veuillez communiquer avec l'université qui a conféré le grade.

La qualité d'impression de certaines pages peut laisser à désirer, surtout si les pages originales ont été dactylographiées à l'aide d'un ruban usé ou si l'université nous a fait parvenir une photocopie de qualité inférieure.

Canada

A COOLING SYSTEM USING TWO-PHASE CLOSED THERMOSYPHON FOR TELECOMMUNICATION MCM: EXPERIMENT AND SIMULATION

by

SEOK-HO RHI

A thesis submitted in partial fulfilment of

the requirements for the degree of

MASTER of APPLIED SCIENCE

in the

DEPARTMENT OF MECHANICAL ENGINEERING

UNIVERSITY OF OTTAWA

OTTAWA, ONTARIO, CANADA

DECEMBER 1995

ISBN 0-612-11593-3

UNIVERSITÉ D'OTTAWA
UNIVERSITY OF OTTAWA

ACKNOWLEDGMENT

First of all, the author is greatly indebted to Professor. Y. Lee. His advice, encouragement, and valuable suggestions during the program are particularly appreciated.

Many thanks to the technical staffs of the Mechanical Engineering workshops of their fast manufacture and repair.

The author wishes to express his deep appreciation to Dr. I. Pioro, a research associate of Professor Y.Lee, with whom the present experimental program was carried out together.

The author wishes to acknowledge to his parents for their moral and material support. Also the author wishes to express his sincere thanks to Messrs. M. W. Kim, B. S. Kim, and J. K. Ryou for their help and encouragement during the program.

The scholarships provided by the Nepean-Kanata Branch of the Rotary International and by the Chung-Buk National University through the kindness of Dean. C. G. Lee are gratefully acknowledged.

The research funding was provided by the the Electronics and Telecommunications Research Institute of Korea (E. T. R. I).

ABSTRACT

The present study is concerned with a cooling package system for multichip modules (MCM) in telecommunication systems. Due to the higher device operation speed and higher packaging density, the resulting heat flux is known to be 1 to 2 W/cm^2, which is one or two orders of magnitude higher than those of conventional systems, and beyond the capacity of high performance air cooling systems. A cooling system which can deal with a high heat flux of up to 4 W/cm^2 is the one that employs two-phase closed thermosyphons, (i.e., wickless heat pipes) and the present study presents the results of experimental and simulation study on a cooling system using two-phase closed thermosyphons for the cooling of MCM.

TABLE OF CONTENTS

Acknowledgment i

Abstract ii

Table of Contents iii

List of Tables vii

List of Figures ix

Nomenclature xiii

1. Introduction ..... 1 - 1

    1.1 Thermosyphon ..... 1 - 2

        1.1.1 Characteristics of TCT ..... 1 - 3

        1.1.2. Operating Principles of a TCT ..... 1 - 4

        1.1.3 Selection of Working Fluid ..... 1 - 5

    1.2 Multichip Modules (MCM) ..... 1 - 6

        1.2.1 Thermal Management of MCM ..... 1 - 6

        1.2.2 ATM Switching System of MCMs ..... 1 - 8

    1.3 Objectives of Present Study ..... 1 - 9

2. Literature Survey ..... 2 - 1

3. Experiments ..... 3 - 1

3.1 Design Considerations ..... 3 - 1

3.2 Experimental Apparatus ..... 3 - 2

3.2.1 Main TCT Assembly ..... 3 - 3

3.2.2 Cooling System in the Condenser Section ..... 3 - 5

3.2.3 Heat Generation Section ..... 3 - 6

3.2.4 Charging System ..... 3 - 8

3.3 Working Fluids ..... 3 - 8

3.4 Experimental Procedure ..... 3 - 9

3.5 Data Reduction ..... 3 - 12

4. Analysis: Computer Simulation ..... 4 - 1

4.1 Code Development ..... 4 - 1

4.1.1 Thermal Resistance Network ..... 4 - 2

4.1.2 Thermal Properties ..... 4 - 3

4.1.3 Operating Limit ..... 4 - 4

4.1.4 Fin Efficiency ..... 4 - 6

4.1.5 Programming Method ..... 4 - 7

4.2 Simulation Windows ..... 4 - 8

4.2.1 Main Window ..... 4 - 9

4.2.2 Data Input Window ..... 4 - 10

4.2.3 Processing Window ..... 4 - 11

4.2.4 Tool Box Window ..... 4 - 11

4.3 Simulation ..... 4 - 11

5. Results and Discussion ..... 5 - 1

5.1 Comparison between Experiment and Simulation ..... 5 - 4

5.1.1 Effect of Air Flow Velocity, u_{max} ..... 5 - 6

5.1.2 Effect of Saturation Temperature, T_s ..... 5 - 8

5.1.3 Heat Transfer Capacity versus Temperature Difference between Surface of Heat Generation Section and Air Temperature, ΔT_T .... 5 - 9

5.1.4 Effect of Evaporator - Condenser Length Ratio, L^* ..... 5 - 10

5.1.5 Effect of Contact Resistance ..... 5 - 11

5.1.6 Effect of Transportation Zone ..... 5 - 11

5.2 Experimental Results which can not be simulated ..... 5 - 12

5.2.1 Effect of Quantity of Working Fluid, V^* ..... 5 - 12

5.2.2 Effect of Non-condensible Gas ..... 5 - 14

5.2.3 Effect of No Forced Air Flow on the Condenser Section, $u_{max} = 0$ .. 5 - 15

5.2.4 Cooling Fan Noise Test ..... 5 - 16

6. Concluding Remarks ..... 6 - 1

6.1 Conclusion ..... 6 - 1

6.2 Recommendation ..... 6 - 3

APPENDIX A Thermal Resistances ..... 7 - 1

APPENDIX B Correlations for Boiling Heat Transfer Coefficient ..... 7 - 3

APPENDIX C Correlations for Condensing Heat Transfer Coefficient ..... 7 - 5

APPENDIX D Correlations for Forced and Natural Convection Heat Transfer Coefficient ..... 7 - 6

APPENDIX E Fin Efficiency ..... 7 - 8

APPENDIX F Shape Factors ..... 7 - 10

APPENDIX G Simulation Windows ..... 7 - 11

APPENDIX H Error Analysis ..... 7 - 14

REFERENCE ..... 8 - 1

TABLES ..... 9 - 1

FIGURES ..... 9 - 27

LIST OF TABLES

Table 2.1 Recent Studies on the Cooling System for MCM ..... 9 - 1

Table 3.1 Some Physical Properties of Working Fluids Used ..... 9 - 2

Table 3.2 Solubility of Non-Condensible Gas in Working Fluids ..... 9 - 2

Table 5.1 Maximum Heat Transfer Capability of Working Fluids ..... 9 - 3

Table 5.2 WF - FC-72, 1 TCT, $L^+ = 1.56$ ..... 9 - 4

Table 5.3 WF - FC-72, 1 TCT, $L^+ = 3.13$ ..... 9 - 5

Table 5.4 WF - FC-72, 1 TCT, $L^+ = 4.69$ ..... 9 - 6

Table 5.5 WF - FC-72, 1 TCT, $L^+ = 6.25$ ..... 9 - 7

Table 5.6 WF - FC-72, 2 TCT, $L^+ = 6.25$ ..... 9 - 8

Table 5.7 WF - FC-72, 3 TCT, $L^+ = 6.25$ ..... 9 - 9

Table 5.8 WF - ethanol, $L^+ = 6.25$ ..... 9 - 10

Table 5.9 WF - R-113, 1 and 2 TCTs, $L^+ = 6.25$ ..... 9 - 11

Table 5.10 WF - R-113, 3 TCT, $L^+ = 6.25$ ..... 9 - 12

Table 5.11 WF - R-11, $L^+ = 6.25$ ..... 9 - 13

Table 5.12 WF - FC-87, 1 and 2 TCTs, $L^+ = 6.25$ ..... 9 - 14

Table 5.13 WF - FC-87, 3 TCTs, $L^+ = 6.25$ ..... 9 - 15

Table 5.14 WF - acetone, $L^+ = 6.25$ ..... 9 - 16

Table 5.15 WF - water, $L^+ = 6.25$ ..... 9 - 17

Table 5.16 WF - FC-87, 1 TCT, $L^+ = 6.25$ (Effect of V^+) ..... 9 - 18

Table 5.17 WF - FC-87, 3 TCTs, $L^+ = 6.25$ (Effect of V^+) ..... 9 - 19

Table 5.18 WF - acetone, 3 TCTs, $L^+ = 6.25$ (Effect of V^+) ..... 9 - 20

Table 5.19 WF - R-113, 1 TCT, $L^+ = 6.25$ (Effect of V^+) ..... 9 - 21

Table 5.20 WF - FC-87, 3 TCTs, $V^+ = 9.38$ (Effect of L^+) ..... 9 - 22

Table 5.21 WF - acetone, 3 TCTs, $V^+ = 9.38$ (Effect of L^+) ..... 9 - 22

Table 5.22 WF - FC-72, $L^+ = 6.25$ (Effect of Non-Condensible Gas) ..... 9 - 23

Table 5.23 WF - FC-87, $L^+ = 6.25$ ($u_{max} = 0$) ..... 9 - 23

Table 5.24 WF - acetone, $L^+ = 6.25$ ($u_{max} = 0$) ..... 9 - 24

Table 5.25 WF - FC-87, $L^+ = 6.25$ (Temperature of Fan off) ..... 9 - 24

Table 5.26 WF - FC-87, $L^+ = 6.25$ (Temperature during Startup) ..... 9 - 25

LIST OF FIGURES

Figure 3.1(a) Experimental Apparatus ..... 9 - 27

Figure 3.1(b) Experimental Setup ..... 9 - 28

Figure 3.2 Evaporator Section ..... 9 - 29

Figure 3.3(a) Test Assembly ..... 9 - 30

Figure 3.3(b) Test Thermosyphon Assembly ..... 9 - 31

Figure 3.4 Heater Assembly ..... 9 - 32

Figure 3.5 Syringe used for Charging Working Fluids and Removing Non-Condensible Gas from TCT ..... 9 - 33

Figure 3.6 Temperature vs. Time from Startup (FC-87) ..... 9 - 34

Figure 4.1 Model for Simulation ..... 9 - 35

Figure 4.2 Thermal Resistance Network ..... 9 - 36

Figure 4.3 Flow Chart for Simulation ..... 9 - 37

Figure 4.4(a) h_c by different correlations with h_c of Rohsenow ..... 9 - 38

Figure 4.4(b) h_c by different correlations with h_c of Rohsenow ..... 9 - 39

Figure 4.4(c) U_T obtained by Simulation Code with various correlations for h_c ..... 9 - 40

Figure 4.4(d) U_T obtained by Simulation Code with various correlations for h_c ..... 9 - 41

Figure 4.5(a) Effect of ΔT_T on U_T with Various Working Fluids through Simulation (FC-72) ..... 9 - 42

Figure 4.5(b) Effect of L^* on U_T through Simulation (FC-72) ..... 9 - 43

Figure 4.5(c) Effect of u_{max} on U_T through Simulation (FC-72) ..... 9 - 44

Figure 4.5(d) Effect of T_s on U_T through Simulation (FC-72) ..... 9 - 45

Figure 4.5(e) Effect of T_{air} on U_T through Simulation (FC-72) ..... 9 - 46

Figure 4.5(f) Effect of Contact Resistance on U_T through Simulation (FC-72) ..... 9 - 47

Figure 4.5(g) Effect of Fin Type on U_T through Simulation (FC-72) ..... 9 - 48

Figure 5.1 Temperature Distribution of Heater (FC-72) ..... 9 - 49

Figure 5.2 Effect of T_s on U_T (All working fluids) ..... 9 - 50

Figure 5.3(a) Comparison between Experiment and Simulation on Temperature Distribution of TCT Assembly (FC-72) ..... 9 - 51

Figure 5.3(b) Comparison between Experiment and Simulation on Temperature Distribution of TCT Assembly (R-113) ..... 9 - 52

Figure 5.3(c) Comparison between Experiment and Simulation on Temperature Distribution of TCT Assembly (R-11) ..... 9 - 53

Figure 5.3(d) Comparison between Experiment and Simulation on Temperature Distribution of TCT Assembly (ethanol) ..... 9 - 54

Figure 5.3(e) Comparison between Experiment and Simulation on Temperature Distribution of TCT Assembly (FC-87) ..... 9 - 55

Figure 5.3(f) Comparison between Experiment and Simulation on Temperature Distribution of TCT Assembly (acetone) ..... 9 - 56

Figure 5.3(g) Comparison between Experiment and Simulation on Temperature Distribution of TCT Assembly (Water) ..... 9 - 57

Figure 5.4(a) Effect of u_{max} on U_T (FC-72) ..... 9 - 58

Figure 5.4(b) Effect of u_{max} on U_T (R-113) ..... 9 - 59

Figure 5.4(c) Effect of u_{max} on U_T (R-11) ..... 9 - 60

Figure 5.4(d) Effect of u_{max} on U_T (ethanol) ..... 9 - 61

Figure 5.4(e) Effect of u_{max} on U_T (FC-87) ..... 9 - 62

Figure 5.4(f) Effect of u_{max} on U_T (FC-72, 2 TCTs) ..... 9 - 63

Figure 5.4(g) Effect of u_{max} on U_T (FC-72, 3 TCTs) ..... 9 - 64

Figure 5.4(h) Effect of u_{max} on U_T (acetone) ..... 9 - 65

Figure 5.4(i) Effect of u_{max} on U_T (water) ..... 9 - 66

Figure 5.5(a) Effect of T_s on U_T (FC-72) ..... 9 - 67

Figure 5.5(b) Effect of T_s on U_T (R-113) ..... 9 - 68

Figure 5.5(c) Effect of T_s on U_T (R-11) ..... 9 - 69

Figure 5.5(d) Effect of T_s on U_T (ethanol) ..... 9 - 70

Figure 5.5(e) Effect of T_s on U_T (FC-87) ..... 9 - 71

Figure 5.5(f) Effect of T_s on U_T (acetone) ..... 9 - 72

Figure 5.5(g) Effect of T_s on U_T (water) ..... 9 - 73

Figure 5.5(h) Effect of T_s on U_T (R-11, FC-87, and acetone) ..... 9 - 74

Figure 5.6(a) Effect of ΔT_T on q (FC-72) ..... 9 - 75

Figure 5.6(b) Effect of ΔT_T on q (R-113) ..... 9 - 76

Figure 5.6(c) Effect of ΔT_T on q (R-11) ..... 9 - 77

Figure 5.6(d) Effect of ΔT_T on q (ethanol) ..... 9 - 78

Figure 5.6(e) Effect of ΔT_T on q (FC-87) ..... 9 - 79

Figure 5.6(f) Effect of ΔT_T on q (acetone) ..... 9 - 80

Figure 5.6(g) Effect of ΔT_T on q (water) ..... 9 - 81

Figure 5.6(h) Effect of ΔT_T on q (R-11, FC-87, and acetone) ..... 9 - 82

Figure 5.7(a) Effect of L^* on T_h and T_s (FC-72) ..... 9 - 83

Figure 5.7(b) Effect of L^* on T_h and T_s (FC-87) ..... 9 - 84

Figure 5.7(c) Effect of L^* on T_h and T_s (acetone) ..... 9 - 85

Figure 5.8 Effect of Transportation Zone on U_T (FC-72) ..... 9 - 86

Figure 5.9(a) Effect of V^* on ΔT_T (FC-87, 1 TCT) ..... 9 - 87

Figure 5.9(b) Effect of V^* on ΔT_T (FC-87, 3 TCTs) ..... 9 - 88

Figure 5.9(c) Effect of V^* on ΔT_T (acetone) ..... 9 - 89

Figure 5.9(d) Effect of V^* on ΔT_T (R-113) ..... 9 - 90

Figure 5.10 Effect of Non-Condensible Gas (FC-72) ..... 9 - 91

Figure 5.11(a) Effect of Absence of the Cooling Fan (FC-87) ..... 9 - 92

Figure 5.11(b) Effect of Absence of the Cooling Fan (acetone) ..... 9 - 93

Figure 5.11(c) Temperature from Fan off (acetone) ..... 9 - 94

Figure 5.12 Cooling Fan Noise Test ..... 9 - 95

NOMENCLATURE

A	surface area (m^2)
Ar	Archimedes number, $Ar = (g\, l_c^3(\rho_l-\rho_v))/(v_l^2\rho_l)$
Bo	Bond number, $\sigma/[g(\rho_l - \rho_g)\delta_w^2]$
k	thermal conductivity (W/m K)
C	constant for Eq. D.1 in Appendix D
c_p	specific heat (J/kg K)
C_{SF}	shape correction factor
d	inner diameter (m)
D	ıter diameter of tube (m)
Exp.	experimental
Fr	Froude number, $Fr = (w_{lw}^2\rho_l)/(gl_{ev}(\rho_l-\rho_v))$
f_{wave}	$f_{wave} = 1.15 / (1-0.63(P/P_{cr}))^{3.3}$ for Eq. C.3 in Appendix C.
g	acceleration due to gravity (m/s^2)
h	heat transfer coefficient (W/m^2 K)
h_{LG}	latent heat of vaporization (J/kg)
l	length (m)
L^+	length ratio between the evaporator and the condenser, l_c / l_e

M	molecular weight
N_{fin}	number of fins
Nu	Nusselt number
P	pressure (Pa), pitch in Appendix F (m)
P_r	pressure ratio between critical pressure and operation pressure, p/p_{cr}
Pr	Prandtle Number
Q	heat transfer rate (W)
q	heat flux (W/cm^2)
r	tube inner radius (m)
R	resistance (K/W)
Ra	Rayleigh number
Re	Reynolds Number
Re_φ	$Re_\varphi = Q/(\pi d h_{LG} \mu_l)$
R_p	roughness parameter
Sim.	simulation
T	temperature (°C)
TCT	two-phase closed thermostphon
u	velocity (m/s)
U	overall heat transfer coefficient (W/m^2 K)
V	volume (m^3)
V^+	dimensionless volume ratio of working fluid, V_l/V_{ev}
WF	working fluid

Subscripts

a	atmospheric
air	surrounding air
b	bare tube in the transportation zone
c	condenser section
conv	convection
cr	critical
e	evaporator section or heated zone, equivalent in Appendix E
f	fin, film in Appendix D
fil	filler
g	vapor
h	heater
i	inner
l	liquid
lam	laminar
nconv	natural convection
p	liquid pool
pl	holding plate of evaporator
s	saturation
T	total,
turb	turbulance
w	wall

Greek Letter Symbols

η	efficiency.
δ	thickness (m)
μ	dynamic viscosity (kg/s·m)
ρ	density (kg/m^3)
σ	surface tension (N/m)

Chapter 1

INTRODUCTION

Thermal management for electronic and electrical elements has become an important and serious issue with the rapid increase of microchip power and power densities. This is particularly true in the design of electronic packages. The desire for greater speed and power with electronic devices has given rise to a continuing increase in the circuit densities and power dissipation of the most advanced design chips found in integrated electronic packages. These modern electronic devices produce a large amount of heat during operation. In future, rapid development requires a new cooling system that can dissipate a large amount of heat in place of the conventional forced convection cooling provided by fans and ambient air. Modern electrical and electronic elements with their compact sizes and powerful capabilities release a large amount of heat. These heat fluxes can be one or two orders of magnitude higher than those handled by conventional cooling systems, and beyond the capacity of the high-performance air cooling systems. One such example is the **multichip modules (MCM) used in asynchronous transfer mode (ATM)** switching systems.

The high packaging density of MCM decreases signal propagation delay, thus simplifies synchronization between links, and reduces inductance as well as electromagnetic emission.

Immersion or direct liquid cooling is an alternative solution [1], but this in turn introduces new problems because of the direct contact of the electronic components with liquid. That is why we decided to combine the advantages of the traditional conventional air cooling systems with the advantages of fluid cooling systems, particularly with phase change. For this purpose two-phase closed thermosyphons were used as the high efficiency autonomous heat transferring devices which remove heat from the MCM, transfer the heat over some distance and dissipate it to the surrounding air. The major difference between the two-phase closed thermosyphons used in the present study and conventional thermosyphons is that the former has a very long transport zone between the evaporator and condenser sections, which dictates that the previous experimental results on the conventional thermosyphons can not be directly used.

A two-phase closed thermosyphon is a cooling system which can deal with high heat fluxes of electrical and electronic elements of the next generation. Because of the advantageous characteristics of the two-phase closed thermosyphons, they are widely used in many engineering fields including the cooling of electronic devices [1-9].

1.1 Thermosyphon

It has been known for a long time that very effective heat transfer can be obtained by means of evaporation and condensation of the working fluid. **Heat pipes and two-phase closed thermosyphons** are closed systems that utilize these processes. Both systems are very similar in terms of the functions that transport and distribute a large amount of heat by means of evaporation and condensation of the working fluid with a very small temperature difference along its working length, but have an important difference in the mechanism of the condensate return. The **two-phase**

closed thermosyphon (TCT) depends on gravity alone, whereas a heat pipe employs capillary force for the condensate return to the evaporator. Therefore, the TCT is ineffective in the absence of gravity force or in the case that the condensate has to be returned to the evaporation section against gravity.

The TCT is a simple tube which contains a small amount of working fluid inside. When the heat is applied to the lower section of the tube, some of the liquid vaporizes, rises toward the upper end and condenses when the temperature of the upper end is lower than the saturation temperature of the vapor. The condensed liquid comes down along the surface of the tube wall due to the gravitational force. On the other hand, the heat pipe has a wick structure inside the wall. This wick provides a capillary force for the condensed liquid as return even against the gravity. The TCTs are sometimes referred as wickless heat pipes or gravity assisted heat pipes. Except for terrestrial applications, the heat pipe orientation is not necessarily restricted to the horizontal and the evaporator can be above the condenser. However, in most applications, the device may be made to operate with the condenser elevated and in such cases the TCT is simpler and more cost effective than the heat pipe.

1.1.1. Characteristics of TCT

A large amount of heat can be transferred by a TCT. Specially, its simplicity of design is very attractive. The most attractive feature of a TCT is that it derives the power necessary for the circulation through the phase change of the working fluid from the heat transfer process. Consequently, no external power supply is needed.

In general, the important and common characteristics of a TCT that make it very useful in heat

transfer process are the following :

a. It has no mechanical parts and a simple structure with isothermal surfaces. Therefore, it will work for a long period of time without any maintenance or deterioration of the working fluid and tube material.

b. It is light and easily controlled.

c. It can act as a thermal diode and a heat flux transformer.

d. It can transport a large or a very small amount of heat

e. It reacts quickly.

f. It is almost noiseless in operation.

Due to these excellent characteristics, TCTs and heat pipes have been widely used in various engineering fields. In recent years, especially in the electronics field, they have been used as a cooling system for heat transfer augmentation [1-9].

The applications of TCTs and heat pipes are very numerous. For example, they are employed in electric and magnetic fields [9], in solar systems [10], in heat energy storage systems [11], in Stirling engines [12], in heat exchangers [13-15], in medical instruments [16] etc.

1.1.2. Operating Principles of a TCT

A TCT operates on a closed two-phase cycle of liquid-vapor phase. This closed two-phase process utilizes the latent heat of vaporization to transfer heat from the hot section with very small temperature gradients. Heat at the lower portion of a TCT vaporizes the working fluid. During this phase change process, the fluid picks up the heat associated with its latent heat of vaporization. The vapor in the evaporator region is at a higher temperature. Hence at a higher pressure than the vapor

in the condenser, the vapor rises with aid of buoyancy forces and flows to the cooler condenser where it gives up the latent heat of vaporization. The gravitational force then causes the condensate film to flow back down the inside wall of the TCT and the process repeats.

Although the inside surface of the TCT may occasionally be lined with grooves or a porous structure to promote the return of the condensate to the evaporator or to increase the associated heat transfer coefficient, a TCT basically depends on the local gravitational acceleration for the return of the liquid from the evaporator to the condenser. Therefore, for a proper operation, the evaporator of a TCT must be located below the condenser, or dryout of the evaporator may occur. The heat transfer performance and operation of a TCT strongly depends on the size, shapes, working fluids and tube materials. And the heat transfer characteristics of a TCT are limited by a host of thermophysical constraints, including the thermal properties of the working fluid, evaporator dry-out or critical heat flux (CHF), entrainment of return condensate (flooding limit) and the effectiveness of the condensation process.

1.1.3 Selection of Working Fluid

The selection of a suitable working fluid is the most important aspect of the design and manufacturing process, because the basis for the operation of a TCT is the vaporization and condensation of the working fluid. Factors that affect the selection of an appropriate working fluid include the operating temperature range, compatibility with the thermosyphon materials, dielectric properties for use in an electrical field, solubility in water, thermophysical properties etc. The selection of working fluid within the TCT also depends on several thermal properties of the fluid. The most important properties of the working fluid are the vapor pressure, latent heat of

vaporization and surface tension. In addition, the thermal conductivity, viscosity, and the liquid and vapor densities of them will also influence the working fluid selection of a TCT

Most of TCTs used in the industry have a short transporting section and its thermal capacity is mainly limited by the overall heat transfer coefficient, which depends on the thermophysical properties of the working fluid and working saturation pressure. Generally any liquid which can be boiled without decomposition may be used as the working fluid, but in practice there can be many restrictions. For application in electronic devices, such restrictions can be: a low range of working temperatures, a prohibition of flammable fluids, a electrically conductive fluids etc.

1.2. Multichip Modules (MCM)

1.2.1. Thermal Management of MCM

Hybrid microcircuit thin- and thick-film technologies, known and used for over 30 years, are the basis for MCMs. In fact, in spite of all the definitions proposed for MCMs to distinguish them from hybrid circuits and in spite of their wide publicity, MCMs are essentially an extension of hybrid circuits. Basically, MCMs may be considered as the new generation of hybrid circuits that provides at least order-of-magnitude reductions in weight and volume.

The thermal management of MCMs can be components of a large assembly or a stand-alone subsystem. Emphasis is placed on the thermal management as an integral part of the MCM design process which extends from a logic synthesis to the design for the final assembly and test. The trends both in the semiconductor technology and in the electronic system design are such that the heat dissipation per unit volume of electronics has been increasing with time and will become a major factor in the design of compact three-dimensional electronic systems of the future.

As an example of the MCM evolution, computers have progressed from the vacuum-tube-based ENIAC (Electronic Numerical Integrator and Computer), which occupied an 80-foot square room and performed approximately 5000 instructions per second (0.005 MIPS) in the late 1940s, to desktop computers in the 1980s that performed several orders of magnitude more quickly. The ENIAC dissipated approximately 140 KW of electric power. On the other hand , notebook computers of tne mid-1990s dissipate less than 50 W [17, 18]. The dramatic decreases in size, weight, and power dissipation of computers were made possible by progress in the semiconductor technology. However, the decrease in power dissipation does not mean that thermal management should be ignored in designing modern computers and advanced electronics. Indeed, in some advanced portable computers employing the latest generation of microprocessors, such as Intel's Pentium chip, special liquid cooling techniques are required to keep the microprocessor chips from overheating [18].

The quality of MCM thermal design is only as good as the accuracy to which the power dissipated in the individual chips and resistors is known. In most thermal design analyses, it is assumed that the power is evenly dissipated over the surface of the chip die. In general, two main fields of thermal management are applied to the design of electronic packages of MCMs: thermal control and thermal analysis.

Thermal control is the selection of heat transfer technology and equipment to meet specific thermal requirements in the design of the electronic package being considered. The goals are typically removing the heat dissipated by the MCMs, constraining the maximum MCM temperatures below specific values, and minimizing the thermal gradients. Additional factors that often must be considered in the thermal control design of MCMs are the noise levels that limit fan selection and

power consumption of the thermal control mechanisms themselves. Thermal control is necessary to ensure stable and predictable performance. High operating temperatures can result in degradation of performance in two ways: loss of noise margin and reduced operation speed.

Thermal analysis is becoming one of the most important steps of the MCM design process. The main aim of thermal analysis is to predict the temperatures and heat fluxes that will occur in an electronic assembly during field operation. Results of thermal analysis are also used to determine the suitability of competing thermal control designs. The fast development of MCMs with high performance and high power dissipation is requiring more considerably more thermal management.

1.2.2. ATM Switching System of MCMs

A high throughput ATM switching system requires high-speed interconnections and high density packaging to reduce the interconnection lengths. The main use of ATM switching systems will be high-speed data communications and multi-media communications including voice, video, and data [19]. The purpose of ATM switching systems is to satisfy the requirements to accommodate almost the same number of subscribers as the switching system of a conventional telephone network. In this system, the ATM switch will be constructed of many ATM switching elements consisting of switching chips and control chips with high speed interconnections. These are required to operate at high speed for high throughput performance, thus high density packaging is required. The use of MCMs in an ATM switching system makes it possible to construct ATM switching elements within a single package. High-speed signal transmission between the LSIs (Large Scale Integration) mounted on the MCM can thus be achieved due to the low dielectric constant of the polyimide insulator.

To make a high throughput ATM switch hardware using MCM technology, the following must be achieved [19] :

a. High-speed signal interconnection between MCMs

b. Pretesting of LSIs before device mounting;

c. Module cooling.

The paramount aspect in the MCM's operation is to manage its thermal performance of MCM, specifically to maintain the junction temperature to operate safely below 75-85 °C. Currently, the total power dissipation of a MCM is up to about 50 W [19]. In the future this will certainly be higher. Therefore, the thermal management of MCM's is an important issue to resolve for the high-speed telecommunication ATM.

1.3 Objectives of Present Study

The objectives of the present study are to apply TCT's for cooling of MCM's in the ATM switching system, to make an experimental investigation into the heat transfer performance of a cooling system using specially designed TCT's, and to develop a simulation code for the design of the proposed cooling system.

The present study presents the results of an experimental study on a cooling system using TCT's for the cooling of an MCM. The aim was to make the cooling capacity of the present experimental system up to a heat flux of 4 W/cm^2 which is about twice the value generally accepted as the limit by forced air cooling with heat pipes [20].

Results obtained in the present experimental study include:

- the heat transfer capability versus the temperature difference between the surface of the

heat generation section and the air temperature;

- the effect of various working fluids;
- the effect of the amount of working fluid charged in the system;
- the relationship between the cooling air velocity and the heat capacity;
- the characteristics of the cooling of the condenser section with its length; and
- the effect of the contact resistance between the heating surface and the evaporator and the heat transfer capacity of the system;

The objective of the simulation code development is to provide the following information using the different empirical correlations for evaporation, condensation and forced convection and the shape factors available from the literature:

- the heat transfer rate versus the temperature difference between the surface of the heat generation section and the air temperature;
- the saturation temperature of the heat pipe and the heat transfer capacity of the system;
- the effect of contact resistance or the heat transfer capacity of the system;
- the characteristics of the cooling of the condenser section with various heat transfer enhancement mechanisms (e.g. fins);
- the effect of the electrical insulation of the transport section on the heat transfer capability of the system;
- the choice of the working fluid; and
- the presentation of the above in graphs.

The prediction by simulation only and the comparison between experimental results and the simulation will be presented.

Chapter 2

LITERATURE SURVEY

Since the first interest in the single phase thermosyphon arose from the application for turbine blades by Schmidt [21], some basic studies have been carried out in an attempt to obtain greater understanding of the operation of the TCT as well as establishing its performance characteristics.

Cohen and Baylay [22] found in their study of a single phase open loop thermosyphon that the heat transfer coefficient was independent of the quantity of the working fluid above a certain amount level, and directly dependent on the tube diameter in a gas turbine blade. An additional observation was dry-out at the bottom of the tube when a small quantity of liquid was used.

The first comprehensive analysis of the two-phase closed thermosyphon (TCT) was made by Lee and Mital [23]. They carried out experiments to find the effects of several parameters such as the amount of working fluid, the evaporator-condenser length ratio (L^+), the mean operating pressure, the heat flux and the type of working fluid to obtain the performance of the TCT using a copper tube of 1.37 m in length and 25.4 mm in diameter. In their experimental study, they found that the heat transfer coefficient is independent of the quantity of the working fluid above a certain amount and increases with increasing L^+, system pressure, and applied heat flux. Lee and Bedrossian [13]

studied the effect of L^- in a heat exchanger using both heat pipes and TCTs. They found that the length of the condenser is much important than that of the evaporator for increasing heat transfer performance. Lee and Clements [24] showed that the heat transfer coefficient decreases with increasing diameter of the TCT.

Shiraishi et al. [25] introduced a mathematical model to predict the heat transfer characteristics of TCT's. They also showed that the overall thermal resistance is very sensitive to the operating pressure, the heat flux, and the quantity of the working fluid from their experimental results.

Nguyen-chi et al. [26] observed two different heat transfer limitations of TCT's; dry-out and burn-out, or the so- called flooding limit. They investigated the entrainment, or flooding limit in more detail, and observed the maximum performance at the flooding limit. The influence of the liquid fill charge, inclination angle, and operating temperature on maximum performance were also observed. They showed that the critical heat flux due to dry-out increases with increasing filling ratio and operating temperature, but decreases with increasing length ratio. The critical heat flux due to burn-out was found to increase with the operating temperature and the tube diameter. Also they showed that Wallis' correlation of the flooding limit [27] agrees well with their experimental data.

Ueda and Myashita [28] observed the performance limitation that occurs due to an unsuitable charge of working fluid. They corrected the correlation of flooding limit proposed by Wallis. Ma et al. [29] studied various flow patterns from visual observation. They found that the filling ratio and heating power were the factors affecting the change of flow patterns. And from the visual observation, they mentioned the importance of the volume ratio of the working fluid in the thermosyphon operation. They also proposed a correction of constant C_w from Wallis' correlation of the flooding limit [27] to values within the range 0.615 to 0.848.

Imura et al. [30] carried out some experimental studies on various effects such as the effect of tube diameter, heated length, working fluid, liquid charge and inside temperature on the critical heat flux in TCT's. The dimension of the test thermosyphon used was 19.4 mm inner diameter with heating and cooling lengths of 300-300 mm. They suggested an improved correlation for the flooding velocity based on their experimental results, and surveyed many correlations of the flooding velocity in TCT's. Their correlation was, however, based on Wallis' correlations with different conditions, and consequently are not really applicable to the present study, considering the inner diameter of our TCTs is only 5.6 mm. This is about 20 - 30 % of the diameter of the TCT used by Imura et al.

Flooding constraints can be a problem for the liquid filling charge in a TCT. Studies on the effect of the liquid filling charge and the optimum filling charge were carried out by several researchers [29-32].

Imura et al. [30] presented the effect of the liquid filling charge in terms of the ratio of the volume of the liquid pool at that of the evaporator (V^+). They suggested that the optimum range of V^+ is between 0.25 and 0.3 and also suggested a useful formula for V^+. However, they also concluded that the value and formula suggested are not applicable for the case where the length of the heater and the inner diameter of TCTs are very small. For such cases, they suggested a correction factor to be used for the case where the length of the evaporator is much less than other sections, or the inner diameter is much smaller than in conventional thermosyphons. The results of this study were used to calculate the appropriate amount of working fluid to be charged in the test thermosyphon for the present study. (This will be discussed again in Chapter 5)

In addition, the optimum quantity for the working fluid in a TCT was determined empirically

by several experimenters as 10 - 25 % of the pipe volume [29, 31, 32, 33]. This optimum filling charge for the operation of a TCT, which would maximize the transferable heat flow for given operating conditions, is not yet theoretically available. Bartsch and Unk [32] observed visually the evaporation and condensation process within a TCT made of glass with ammonia as the working fluid. Their experimental and analytical approach to find the optimum quantity of working fluid resulted in a few equations for the optimum volume of the working fluid.

The presence of non-condensible gases plays an important role in the heat transfer performance of TCTs. Kobayashi et al. [34] and Tien et al. [35] investigated the behaviour of non-condensible gases in the flow field of vapor condensing within TCTs through analytical and experimental methods. Kobayashi et al. [34] observed that a comparatively thick gas-vapor interfacial layer appears, separating clearly the region of non-condensible gas from that of pure vapor. It was also noted that the gas region contains a certain amount of saturated vapor corresponding to the temperature of that region.

The above studies on the TCT involve large inside diameter, between 15 and 33 mm ($D_i \geq 1$ cm), and long heating and condensing sections. There are relatively few studies on small diameter TCTs with short evaporator sections and long transport sections.

Thermosyphons were used widely in space applications till the mid-1980's. With the fast development of electrical and electronic components and the rapid growth of the technology of the electronic chip, many reseachers have tried to apply TCT's as cooling systems for the electrical and electronic fields as described in Chapter 1.

The interest in the cooling of MCM's has continued because much of system parameters can be traced to reductions in the IC size from the initial several hundred microns down to approximately

10 μm in 1975, 2 μm in 1983 and essentially 1 μm or less today. With the continuing refinement of MCM technology [1, 19, 20, 36, 37, 38], efforts to develop a new cooling system continue. An overview of these efforts is presented in Table 2.1

Bar-Cohen [36] surveyed the thermal management of the 1980's. In his study, the maximum power dissipation of that decade's MCM's was from 4 W to 10 W for an 1 × 1 cm MCM, and simple air and liquid cooling methods were enough for the cooling of MCM's. He anticipated that the development of high density chips would be limited by conventional cooling systems, considering the power dessipation for an 1×1 cm chip would reach approximately 125 W in 1990's. His anticipation has been realized and the requirement for a next generation cooling system has become severe for many electronic companies. His anticipation of 125 W or higher per chip is now possible. Avram also examined the air and liquid cooling systems of several companies that had been used in industry and he emphasized that new cooling devices must be developed.

Sasaki et al. [37] introduced a new MCM of structure with fins and impressed air flow to reduce thermal resistance. The total power dissipation of their new structure was 26 W in a 70 × 70 mm MCM (i.e., 0.53 W/cm^2) consisting of 36 chips. This new module design was applied on MCM's of the early 1990's and can be easily found in the current 486s and advanced PCs. But there are also some limitation precluding this new MCM structure for the next generation of MCM's.

Doi et al. [19] determined that the total power dissipation of an MCM is about 50 W and for safe operation it is necessary to keep the junction temperature below 85 °C with a 40° C inlet temperature. They developed a new ATM switching system to satisfy the MCM operating conditions, having a low thermal resistance and a high-speed interconnection between the MCM and printed circuit board. Cooling fins were also applied to the module substrate to cool the MCM.

Lee et al. [38] studied a liquid cooling system for a high power multichip package in small moveable equipment. In the experiments, FC-72 and R-113 were used as liquids. They showed that their cooling system could remove 274 W of power with a 52 °C temperature difference between the inlet liquid and air. The thermal resistance encountered was 0.19 °C/W while pumping perfluorocarbon FC-72 at a flow rate of 1.1 L/min. Their total system size was 20.8 cm by 18.4 cm by 14.5 cm and consisted primarily of a liquid-to-air heat exchanger assembly, a pump, and an accumulator.

Nelson et al. [1] tried to integrate immersion cooling to transfer the heat from the chips to a final heat transfer medium outside the package in a MCM package. The package is a miniature immersion cooled system using an FC-72 working fluid with a pin-fin condenser that could be operated either in a submerged or vapor-space condensing mode. Their experimental system consisted of sixteen chips bonded on a 57 × 57 mm alumina substrate. It was determined that their cooling system was capable of handling over 160 W of power with thermal resistances, based on the chip area, as low as 2 K-cm^2/W. But their results made no mention of the effect of the direct contact between the MCM and the working fluid. A maximum cooling ability was measured to be between 5 and 30 W per chip of 8.97 × 8.97 mm area.

The possibility of heat pipes and TCT's as the cooling system for MCMs has been studied theoretically and experimentally [3, 20, 39, 40].

Pei and Heng [40] investigated a TCT cooling system with a remote condenser section for transferring heat from high power MCMs and single chip packages. Their phase change cooling systems, which used R-22 as the working fluid, essentially consisted of a compact evaporative cold plate connected by tubes to a separate fan-cooled condenser section which could be placed at a

convenient remote location. They studied a twin-tube TCT cooling system with an evaporative plate of 102 × 102 mm and a single tube TCT cooling system with the evaporative plate of 51 × 51 mm. It was found that their cooling system could transfer 160) W with the twin-tube TCT and 350 W with the single-tube TCT. But they made no mention of either the MCM's operating temperature or the details of the MCM to be simulated. It is necessary that the details of the MCM and the operating conditions be known.

Kishimoto et al. [20] carried out experiments for an cooling system for MCMs of the ATM switching system. They applied two-phase loop thermosyphons (wickless heat pipes) using a low velocity of the air as the cooling system of an ATM switching system. They presented two cooling systems: a TCT heat exchanger and an innovative thermosyphon cooling technology. A heat pipe cooling approach was detailed for high density, high-powered telecom systems that use large planar packaging with a heat flux of 0.2 W/cm^2. In addition, they developed a cooling technology for 40-Gb/s throughput high-speed ATM switching MCMs. Their heat flux limit was 1.6 W/cm^2. They used FC-87, Freon 142b and water as the working fluids. They suggested various configurations for future cooling technology by using heat pipes whose main purpose would be to maintain the junction temperature below 85 °C. A design limit on heat flux was determined at between 0.2 and 2 W/cm^2. This limitation is lower than possible future heat fluxes. This particular study showed the possibility of the two-phase loop thermosyphon with its applicability to the cooling systems of the next generation MCMs having higher power dissipation.

As seen above, there has been little investigation involving the cooling of telecom MCMs at heat fluxes of over 2 W/cm^2 using TCTs, and it is the objective of the present experimental and simulation studies to develop design information for a TCT system for the cooling of telecom MCMs

at heat flux of up to 4 W/cm^2, and to illustrate the limitation of computer simulation code in such cases.

Chapter 3

EXPERIMENTS

An experimental apparatus was designed to investigate the heat transfer characteristics of the proposed cooling system using TCTs and to simulate the MCM under controlled laboratory conditions. From the design of the system to the experimentation, all steps were carried out considering the MCM and its operating conditions.

3.1 Design Considerations

The test assembly for the present experimental study was manufactured with the following considerations:

a. Test TCT assembly

- Best TCT Material in terms of life time and reliability.
- Leak proof capsuling
- Compact size

b. Cooling capacity

- Heat flux : 4 W/cm^2

- Maximum surface temperature of the evaporator section: 75 °C

- Overall temperature difference (junction-to-air): 50 °C

c. Cooling method for the condenser section.

- Forced convection using a fan

- Allowable noise level of fan : less than 55 dB

d. Heat generation section

- Tight contact joint between the heater and the evaporator section

- Heat generated: up to 50 W

e. Working fluid

- Dielectric, non-flammable, and environmentally friendly working fluid

3.2. Experimental Apparatus

The present cooling system using TCT's has potential applications for real industry. Therefore, it is important to select the right component combination for the optimum performance and reliability as well as minimal noise and vibration. The above design considerations for the optimum design were considered and the chosen components were selected according to applicable standards such as MILITARY STANDARD, ASME etc.

The experimental apparatus, illustrated in Figs. 3.1 (a, b), mainly consists of the main TCT assembly, the cooling system in the condenser section, the heat generation section and the charging system.

3.2.1 Main TCT Assembly

The physical characteristics of the main TCT assembly used in the study are divided into three parts: the evaporation section with the thermosyphon's evaporators, the long smooth transporting sections, and the finned condensers.

A completely new design of the evaporator section was developed based on a novel yet simple concept. The evaporator section was made from a copper plate with dimensions of 35 × 35 × 9.5 mm. Three non-through holes were drilled on the centre line of one narrow side (35 × 9.5 mm) at the distances of 11.7 mm with the middle hole located centrally on the plate. Fig. 3.2 shows the dimensions of the evaporation section. From the beginning to the depth of 4 mm, the hole diameters were 6.4 mm and after that were 5.6 mm. The transportation and the condenser sections, i.e. the block of three thermosyphons, were made from three brass tubes with a 6.4 mm O.D., and a wall thickness of 0.4 mm. These three tubes were soldered into the three holes drilled in the evaporator section as shown in Fig. 3.3 (a). In this way three evaporators were created with inside diameters of 5.6 mm and the lengths of 32 mm each. The total length of the test thermosyphon was 1478 mm.

At a length of 200 mm, the tubes were bent in one direction and plane with the large side of the evaporator section at the angle of 140°. At the length of 800 mm, the tubes were bent again at the same 140° angle and in the same plane but in the opposite direction (i.e.. the each part of the tubes were parallel one to another and laid in one plane). This configuration is shown in Fig. 3.3 (a, b). This is to show that the TCTs should not be always straight.

As shown in Figs. 3.3 (a, b), from the top ends of the tubes, 66 fins were made from copper sheet with dimension of 35 × 20 × 0.5 mm and installed at a pitch of 3 mm. Three holes of the diameters of 6.4 mm were drilled in each fin. The fins were then soldered to the tubes. The overall

length of the forced convection condenser was 200 mm and the finned part of the tubes started at 23 mm from the top ends. With fins, the condenser area was 898 cm^2, which is 22.3 times of tube area. A temporary seal of the test thermosyphons was made with NUPRO vacuum valves (Swagelock Co. Product, B4HK-TW) so that the test thermosyphons could be used repeatedly.

To measure the temperature distribution over the length of the thermosyphons, 16 T-type thermocouples were used as shown in Fig. 3.1 (a). The 1 mm O.D. subminiature thermocouple assembly (OMEGA TMTSS-040G-6) with a transition joint was installed in the non-through hole drilled equidistantly between the two tube holes on the opposite side of the evaporation section and laid in the central plane parallel to the large sides. This hole was drilled to the depth of 17.5 mm. At a distance of 500 mm over each tube from the top edge of the evaporation section, three thermocouples (OMEGA GG-T-24, duplex insulated thermocouple wire) were soldered onto the tubes. Next, three thermocouples of the same type were soldered at a distance of 15 mm from the first fin. A single thermocouple was soldered to the corner of the first fin, and finally three thermocouples were soldered at the distance of 25 mm from the last fin. Nine thermocouples were located on the tubes and were covered with a thick insulation made from styrofoam. The evaporator section with its tubes and thermocouple assembly was installed into a nylon box (70 × 70 × 19 mm) having a machine cut opening (35 × 35 × 9.53 mm) and four slots (one for the thermosyphon assembly and three for the tubes). To detect non-condensible gases inside thermosyphons, the three thermocouples were located between the last fin and the vacuum valves.

All thermocouples were calibrated in situ and connected. A digital thermometer (OMEGA DP-460, resolution 0.1 °C and accuracy ± 5 °C) with a rotary selector switch was used.

3.2.2 Cooling System in the Condenser Section

In the condenser section, a fan was used for cooling. The finned parts of the TCT's were installed into the channel (290 mm long and in cross section rectangular with the dimensions: 201.5 × 35 mm) made from transparent acrylic (sheets with 6 mm thickness). The finned tubes were installed at the distance of 255 mm from the channel entrance. This front channel was installed perpendicularly to the desk board with a thickness of 18 mm into the opening cut. From the back of the desk board, another channel made from the same material was bonded to the first. The back channel was also rectangular in cross section but was tapered from the size of the front channel (201.5 × 35 mm), to the size of the fan (80 × 80 mm). The long sides (bottom and top) of the back channel were 278 mm long and formed an angle of 24° in the vertical plane between each other. The rectangular shape flange was mounted on the end of the back channel.

A cooling fan (120 V AC, 60 Hz, 12 W, 3100 rpm, $1.51*10^{-2}$ m^3/s, sound level - 38 dB) was screwed to another (same size) flange. The two flanges were connected one to another with a hinge.

A gasket from a soft rubber was installed between two flanges to prevent the air leakage. Twelve grooves were made on the internal surface of the channels for installing inserts (one from the front and one from the back). Thus, the heat transfer area of the finned tubes was decreased by means of changing the length (height) of the channels. Each insert from the bottom created a channel with dimensions and flow velocity as follows:

# of insert	Dimension of condenser	Maximum velocity without confinement	Maximum velocity between fins
Full channel	200 mm × 35 mm	0 ~ 1.65 m/s	0 ~ 4.4 m/s
1st insert	150 mm × 35 mm	0 ~ 1.8 m/s	0 ~ 4.8 m/s

2nd insert	100 mm × 35 mm	0 ~ 2.4 m/s	0 ~ 6.4 m/s
3rd insert	50 mm × 35 mm	0 ~ 2.54 m/s	0 ~ 6.8 m/s

A hot-wire probe (Wallac Inc. - type Ni-125 ANE) was installed from the bottom side of the front channel before the finned tubes at a distance of 180 mm from the air entrance as shown in Fig. 3.1 (b). The measuring head of the probe was in the center of the channel cross section (the same position as in the cross section area decreased by inserts). The hot-wire probe was connected to a thermo-anemometer (Wallac Inc. - type GGA22F), which had the ability to measure not only air velocity but also air temperature. The probe was calibrated for velocity and temperature, using the hot-wire calibrator set, and an NBS [National Bureau of Standards (USA), standard mercury in glass thermometer] standard thermometer. The cooling fan was connected to a variable autotransformer with an output of 0 - 140 V and up to 10 A.

3.2.3 Heat Generation Section

As shown in Fig. 3.4, the special flat plate heater provided by the Electronics and Telecommunications Research Institute of Korea was designed and manufactured for the simulation of MCM operation in real conditions. The heater consisted of a heating element made from BeO on a ceramic sheet plate with metal as an electrical conductor from one side and covered with thin layer of electrical insulating material and a copper box. The heating element of 35 × 35 mm was installed in the copper box (50 × 50 × 10.2 mm) with the cut opening (35 × 35 × 8 mm) and the heating layer facing into the box. The opening was covered with a plate. The thickness of the copper wall facing the heating layer was 2.2 mm. Heating of the element was accomplished by an

alternating current passing through the thin layer of BeO. The current was supplied by a variable autotransformer (type 116B, input - 120 V, output - 0 - 140 V and up to 10 A). Five T-type thermocouples made from thermocouple wire (OMEGA TT-T-30) were installed into the grooves manufactured on the inside surface of the heat transferring copper wall as illustrated in Fig. 3.4. The grooves were 1.4 mm wide and 1.2 mm deep. Thus, five thermocouples measuring the joints were situated across the heat transferring copper wall (four to the corners of the heating element and one to the center). The heater with the heat transferring copper wall face-up was installed in the opening cut in the nylon box (70 × 70 × 10.2 mm) with 7 holes in the back: five for thermocouples and two for power wires.

The face-up heat transferring copper wall was covered with a one component CHO-Therm T500 insulator-elastomer [Chomerics Inc., minimum breakdown voltage - 4,000 V, volume resistivity - 10×10^{14} Ohm-cm, thermal conductivity - 2.7 W/(m K), thickness - 0.25 mm and operating temperature range - -60°C ~ +200°C] - a filler for the tight contact between the heater and the evaporator of the TCT. The filler was made on a base of silicone with boron nitride. Such a composition allows to combine the properties of electrical insulation with a heat conducting material. The filler was then bonded to the copper surface. Two nylon boxes, one with the evaporation section and the other with the heater, were screwed together in a such way that the heater with the filler was put on the evaporation section. Six screws situated over perimeter of the nylon boxes allowed good contact between the heater and the evaporation section through the filler.

The test section with the heater was installed on the vertical desk board. The tubes were supported at two points by nylon bridges mounted on the desk board. The nylon boxes were screwed to the desk board and covered with additional thick insulation (Styrofoam box with external

dimensions: 163 × 130 × 135 mm (height - 163 mm), inside opening: 110 × 76 × 75 mm (depth - 75 mm)) to prevent heat loss to environment. The parts of the tubes soldered to the evaporation section and the fins were situated perpendicularly to the horizontal plane with the finned parts of the tube at the top.

3.2.4 Charging System

The charging system consisted of a vacuum pump, a McLeod gauge, vacuum valves and a special syringe to charge the desired amount of the working fluid into the test TCT as shown in Fig. 3.5.

3.3 Working Fluids

To find the best working fluid, refrigerants such as R-11, R-113, ethanol, water, FC-72, FC-87, and acetone were tried under various conditions. Some physical properties of working fluids used in the experiment are presented in Table 3.1. Theoretically, any kind of fluids could be used as the working fluid, and water is to be the best choice from considering thermophysical properties, as water has a high latent heat. Water permits transmitting of more heat than all other working fluids. In addition, water is cheap, easily available, and safe from fire. On the other hand there are some disadvantages of water, such as a high freezing temperature, a high vapor pressure at moderate temperatures, and a tendency to react with some substances (alkali metals, etc.) which are accompanied by the release of hydrogen which under certain conditions can cause an explosion.

For low temperature range applications, refrigerants with chlorine are commonly used. But

the use of these refrigerants by the Montreal Protocol in 1987 has already been restricted and is now completely prohibited due to the industrial pollutants [50]. The industrial pollutants are based on the atmospheric ozone layer, which filters damaging ultraviolet radiation. In the present experimental study, R-113 and R-11 were used just as references, because the use of CFC's is already prohibited, as they are ozone-depleting substances [50]. That is why we decided to apply new environmentally friendly fluids, such as the fluorinert liquids FC-72 and FC-87 which are suitable for a low temperature range and are in full accordance with the restrictions mentioned above. Unfortunately, the behaviour of these new coolants as boiling working fluids was seldom investigated (only for the conditions close to the pool boiling of FC-72 [1, 38, 51]), and no study was reported in the literature on the heat transfer rates in the a TCT except the study by Kishimoto et al. [20] for FC-87.

In the present study, FC-72 was used for the basic study and FC-87, R-113, R-11, acetone, water and ethanol were used as working fluids. With FC-72, experiments to investigate all possible effects were carried out in first series of experiments to find the heat transfer characteristics of the proposed system.

3.4 Experimental Procedure

Before starting the actual experiments, the thermosyphon tube was throughly cleaned by washing with ethanol and then with distilled water. It was then vacuum dried, tested for vacuum and leaks were checked for. The thermosyphon tube was connected to a Leybold mechanical vacuum pump (type ADEA 71 N4) to remove the inside air and other non-condensible gases. The pump usually reached 8×10^{-3} torr for a dry system.

After the thermosyphon was evacuated, a known amount of the working fluid was charged into the tube. The amount to be charged was kept in a charging syringe which made the working fluid flow into the tube due to the pressure difference. In the present study, usually the amount of the working fluid charged was about 6 ml for each thermosyphon which is 7.5 times larger than the volume of the thermosyphon evaporator. The experiment was carried out at different pressures (below, at, and above atmospheric). The initial pressure without the working fluid was not higher than $5 - 10 \times 10^{-3}$ torr.

Great care was taken to remove all air and other non-condensible gases from the charging system and test thermosyphons before a new working fluid was charged. In addition, special precautions were made to remove non-condensible gases from the working fluids. Usually non-condensible gases will be pushed out by moving vapor into the upper end of the tube during the operation. In this case they will create a gas "plug" in the condenser section which would prevent the vapor from condense. Due to this, the temperature at the upper end is lower than temperatures along the tube below this plug. In such case, the thermosyphon with the presence of non-condensible gases was connected to the vacuum pump and the vacuum valve was opened for the purpose of degassing.

The power to the evaporator heating section was increased very carefully in steps to the desired heat flux. To reach the steady state, it took usually approximately 1 hour. Voltage was seen to fluctuate within a range of $\pm$ 0.2 V. While supplying the power, great care was necessary because a maximum heat flux, depending on the quantity of working fluid in the tube, would be reached above which the wall temperature would begin to rise suddenly and rapidly. An immediate power reduction was then necessary to prevent the burn-out of the heater.

By using the thermo-anemometer, the air flow velocity and air temperature were measured. The air flow velocity had to be very carefully controlled by a slip switch because of the sensitivity of the switch itself. After changing the velocity setting, 10 minutes were required to achieve steady state readings. Once a steady velocity was obtained , the values were recorded.

The actual velocity of the flow was different according to the length of condenser because a change of the length of the wind duct in the condenser section led to a change of the air flow velocity as mentioned in Section 3.2.2. After a steady velocity and heating power were obtained, the temperature was checked for a steady value. To determine these temperatures, the thermocouple installed in the heater center was observed until it registered no temperature fluctuation (approximately 40-60 minutes) [Fig. 3.6]. When this was observed, all temperatures of thermocouples installed in the system were recorded.

In some experiments, the system did not work. This could be attributed to a large amount of non-condensible gases existed within the TCT's. In each experiment, after getting the steady power and temperature, the temperatures of thermocouples specially installed on the upper ends of the tubes were investigated to determine the presence of non-condensible gases. Top and condenser temperatures with the presence of non-condensible gases showed much lower values than those for other sections of TCTs. This implies that the vapor from the evaporator could not go up to the condenser section because the vapor is prevented by the non-condensible gases. In these cases, the non-condensible gases were removed as discussed above. When it was too difficult to remove the non-condensible gases, the experiment was restarted again from the beginning after removing all working fluid inside the TCT's. In the case of FC-87, this procedure was repeated many times because FC-87 can have a large amount of dissolved gas before it is charged, as seen in Table 3.2.

For the procedure of removing non-condensible gases when working fluid charged, the quantity of working fluid charged was about 10% more than required because it can be guessed that a small amount of working fluid was removed with the non-condensible gases.

Once the system was stable, all data was recorded step by step. After each test series for a given working fluid, the thermosyphon was throughly cleaned by repeated washing and then vacuum dried, as well as leak checked. After the system was evacuated, a known amount of new test working fluid was charged into the test tube and the subsequent series of tests was repeated using the same procedures.

3.5 Data Reduction

The tube overall heat transfer coefficient, U_T, of the test TCT for the cooling system is defined as:

$$U_T = \frac{q}{T_h - T_{air}} \tag{3.1}$$

The heat flux per unit area was calculated from the power measurement, which was done from the voltmeter and ammeter coupled into the power supply circuit of the main heater. The heat losses through the insulation of the heating and evaporation section were negligible because of the low heat flux generated in the heater and the good insulation of the heating and the evaporator sections.

The temperatures in the heated section and condensing section were measured by calibrated thermocouples. The saturation temperature of the working fluid was unobtainable because saturation temperature is a function of the heat transfer rates of the systems. However, from the study of Ref.

[23], we can assume the temperatures measured by the thermocouples installed in middle on the transportation zone as the saturation temperature. The errors involved in the calculation of the tube heat transfer coefficient were generally due to the inaccuracy of the temperature and the power measurements. Even if the readings of the power and the temperatures were recorded after the steady state had been reached, a little fluctuation was observed (± 0.2 V for voltage, ± 0.01 A for current and ± 0.2 °C for temperature).

Chapter 4

ANALYSIS : COMPUTER SIMULATION

Since a purely analytical solution for the system is not possible due to the complexity included in the system, a resistance network method was used in the computer simulation code.

4.1 Code Development

A simulation computer code was developed from the following environments:

a. Program language: Microsoft Visual Basic 3.0

b. Programming environment: Microsoft Windows 3.1 and 95.

c. Working environment: Microsoft Windows 3.1 or higher version

d. Programming method: Gauss-Seidel iteration method based on the thermal resistance network

A simulation computer code for the cooling system of the present study was developed for general use. A simulation model which was derived from the ideal model shown in Fig. 4.2 is based on a thermal resistance network as shown in Fig. 4.2.

4.1.1 Thermal Resistance Network

Under the steady-state conditions of the test, a thermal resistance model as shown in Fig. 4.1 was used to estimate the heat transfer rate of the present experimental cooling system. Each thermal resistance between the hot section and the cold section can be written as:

$$R_T = R_{12} + R_{23} + R_{34} + R_{T45} \tag{4.1}$$

$$R_{T45} = \frac{1}{R_f} + \frac{1}{R_n}$$

$$R_f = R_{45} + R_{56} + R_{67}$$

$$R_n = R_{45}' + R_{56}' + R_{67}'$$

where R_T is total resistances between the hot section and the cold section.

R_{12} : thermal resistance of the filler

R_{23} : thermal resistance of the evaporator wall

R_{34} : thermal resistance of boiling

R_{45} : thermal resistance of condensation

R_{56} : thermal resistance of the condenser wall

R_{67} : thermal resistance of forced convection from the condenser section

R'_{45}, R'_{56} , R'_{67}: thermal resistances of the transportation zone

Each of these thermal resistance is presented in Appendix A. In this thermal resistance model, the overall thermal resistance is defined by the basic definition as:

$$R_T = R_{12} + R_{23} + R_{34} + R_{T45} = \frac{1}{U_T} \tag{4.2}$$

As shown in Appendix A, the thermal resistance method requires a number of empirical correlations for the various thermal resistances. Several empirical correlations for boiling (Appendix B), condensation (Appendix C), enhanced forced convection (Appendix D), and free convection (Appendix D) were collected and evaluated for the applicability.

The conduction shape factors needed for the evaporator section were estimated by analytical solutions from the literature. Analytical solutions of the shape factor for two cases are given in Appendix F.

4.1.2 Thermal Properties

The thermal properties of the working fluids, such as the density and viscosity versus saturation temperature, were calculated using the generally accepted method and approximations given in Ref. [85]. These calculations were necessary because of the lack of published data, especially for FC-72 and FC-87. Results of calculations involving FC-72 and FC-87 when compared with a few known thermal properties showed about ± 10 % difference. The thermal properties of other working fluids are formulated into empirical equations using a data regression for the temperature range of -50 °C to 150 °C. The analysis of these equations for the thermal properties of each working fluid showed the difference of about ± 5 %.

4.1.3 Operating Limit

In a TCT, the heat is transported axially by the vapor generated in the heating section. The vapor flows up the tube and condenses in the cooling section. The condensate is then returned to the heating section by gravity.

A TCT is a high-performance heat transfer device; however, when the heat- transport rate is increased greatly, a limiting point may be reached where a sharp rise in wall temperature or sharp deterioration in heat transfer coefficients take place in the heating section. This performance limit has been studied by many investigators and it is known that the limit can be classified into three types

One type of performance limit occurs at very low liquid fill charges. There is a required minimum quantity of working fluid for the TCT to have a continuous circulation of vapor and condensate in accordance with the heat transport rate. If the quantity of working fluid is less than the required minimum, the falling liquid film cannot reach the bottom of the heating section, resulting in dry-out of the heating section, or that the wall temperature slowly rises. Thus, this type is usually called the dry-out limit.

Vapor bubbles are generated in the liquid pool of the evaporator section, and this nucleate boiling becomes more intense with increasing heat flux. At a certain critical radial heat flux, individual vapor bubbles are combined to form rather quickly a vapor film at the wall. This vapor film insulates the evaporator surface from the evaporating liquid. Owing to the poor thermal conductivity of the vapor, only part of the heat input to the wall is a sudden increase of the evaporator wall temperature. This boiling limit is burn-out limit. This limit prevails for relatively large liquid fill charges.

A flooding limit also occurs for large fill charges, high axial heat flows, but small radial evaporator heat fluxes. The high axial heat flow causes a relatively high velocity between the counter-current vapor and liquid flows, and consequently an increase of the shear stresses at the vapor/liquid interface. Large surface waves are thereny induced at the vapor/liquid interface. Thus an instability of the liquid flow is created leading to an entrainment of liquid. The entrained liquid is transported to the condenser by the vapor flow and collected there. The high shear stresses can also cause the returning condensate flow to be completely stopped. Then the condensate flow breaks up at the flooding point. In any case, the intense entrainment or flooding causes an insufficient liquid supply to the evaporator. This leads to a local dry-out and subsequently a complete dry-out of the evaporator.

An exact solution to the flooding limit is not available from existing literature. Moreover, the present study involves a small diameter and long thermosyphon. Therefore, in this case the hydraulic characteristics of the vapor flow are more important than the heat transfer characteristics.

In the present simulation computer code, the flooding limit of the proposed system is also included in the code to identify whether a particular operating condition is possible or not. Wallis' correlation for flooding velocity in vertical tubes [27] was used as a correlation of the flooding limit as shown in following Eq. 4.3.

$$j_g^{*\,1/2} + m j_f^{*\,1/2} = C \tag{4.3}$$

where j_g^* and j_f^* are the dimensionless superficial velocities of the gas and liquid and are defined as:

$$j_g^* = j_g \rho_g^{\,1/2} [gD(\rho_f - \rho_g)]^{-1/2}$$

$$j_f^* = j_f \rho_f^{1/2} [gD(\rho_f - \rho_g]^{-1/2}$$

In general, m is unity and the value recommended of C lies between 0.88 and 1. In the simulation code, the value of C calculated from j_g^* and j_f^* was compared with the value 1.

4.1.4 Fin Efficiency

Heat transfer from a prime surface can be increased by attaching fins or extended surfaces. Use of a finned cooling surface is particularly effective in the case where the heat transfer coefficient between the wall and one fluid is substantially greater than the heat transfer coefficient to the other fluid. Thus, for example, fins on pipes are very effective when liquid flows inside the pipe and gas flows on the outside. Fins are also used on the liquid side and even with condensing vapors having low heat transfer coefficients.

The method of designing cooling fins of various shapes is based on the same principles as those used for calculating the cooling capacity of rods of constant cross-section. The greater the distance from the base of the fins, the smaller the heat flow, so that for a constant cross section, the temperature gradient decreases along the fin length. Theoretically, if the heat transfer coefficient is constant, a fin bounded by a pair of parabolas is the most efficient [52]. In practice, a fin of such shape is too difficult to manufacture, thus it is usual to design fins having trapezoidal sections. The present design consisted of sixty-six thin rectangular fins attached to the cylindrical base of the tubes because of the difficulties of manufacturing fins of the best shape for heat transfer.

The fin efficiency of circular or rectangular fins attached to the TCTs involves mathematically

Bessel functions, which can usually be represented in tabular and graphical forms. For analysis and simulation, approximate, but reasonabl accurate empirical expressions presented by McQuiston and Tree [52] were used. They commented that the difference between experimental results and results calculated by their empirical equation is ± 3 - 4 %. The main equation for the fin efficiency is Eq. 4.4 and other equations are given in Appendix E.

$$\eta_f = \frac{\tanh(m\psi)}{m\psi} \tag{4.4}$$

4.1.5 Programming Method

Programming of the simulation code started with the definition of the thermal resistance network. For the thermal resistance network, we need some assumptions to be defined as following:

a. The problem is steady state.

b. Each resistance field has a lumped surface with a uniform temperature distribution.

c. The conductivities of each component are constant.

d. Radiation exchanges with the surroundings are negligible.

Based on these assumptions, the simulation code was programmed with the following parameters: the initial temperature of the heater, the inlet air temperature of the forced convection side with the specification of thermal resistance fields in each nodal point, and possible operation limits which can restrict the simulation result. The thermal resistance of each nodal point and other definitions needed were described in previous sections. These nodal resistances can be solved by the typical Gauss-Seidel iteration method in terms of temperature and resistance [59].

$$T_i = \frac{\sum_j T_j/R_{ij}}{\sum_j 1/R_{ij}} \tag{4.5}$$

An initial value for T_i was approximated by the following:

$$T_i = \frac{T_h + T_{air}}{2} \tag{4.6}$$

Each iteration's value of the nodal temperature T_i is calculated according to Eq. 4.5, using the most recent T_j. This nodal calculation is repeated till the convergence criterion is met according to:

$$|T_i^{n+1} - T_i^n| \leq \epsilon \tag{4.7}$$

where n is the number of iterations. In the simulation code, ϵ is defined as the accuracy, ranging from 0.1 to 0.00001. Obviously, increasing the precision of ϵ will lengthen the computational time to derive the nodal temperature. A flow chart of the simulation code is presented in Fig. 4.3.

4.2 Simulation Windows

The simulation code consists of following windows (interfaces generated).

a. Main window (Fig. G-1 in Appendix G)

   - creation of data file

   - selection of single or multiple range

b. Data Input window (Fig. G-2 in Appendix G)

- dimensions of the TCT.

- selection of empirical correlations for evaporation and condensation.

- selection of fin types (rectangular or circular)

- selection of correlation for forced convection for the condensing region.

- selection of shape factor

- selection of precision (ϵ=1/10 - 1/100000)

c. Processing window (Fig. G-3 in Appendix G)

- selection of working fluid.

- view of results (single and multiple)

- graphical presentation

- input of correction factor

Overall, the simulation code consisted of 21different windows including above 3 windows. In addition, 19 other windows operate to assist the operation of the above 3 windows.

4.2.1 Main Window

The main window is used to control all sub-windows. Data files are created from a start menu and a specific graphical package can be called to present the results. It is also possible to select a simulation range; that is, a single range (fixed condenser and evaporator length) or multiple range (various lengths of condenser and evaporator sections). Having selected the desired range, one advances to the data input window.

4.2.2 Data Input Window

The data input window allows the specification of the dimensions and the various parameters of the simulated TCT. All necessary dimensions of a TCT such as the diameter, lengths, and material thermal conductivities can be specified: Correlations for heat transfer coefficients can be specified; evaporation (8 empirical correlations), condensation (3 correlations), and forced convection (3 correlations). The detailed equation of each correlation is presented in Appendix B, C, and D, respectively.

Three different conduction shape factors are also used as shown in Appendix F. In a two dimensional system where only two temperature limits are involved, it is possible to define conduction shape factor *S*. This shape factor has been worked out for several geometries as shown in Appendix F. The effect of *S* can be negligible, but in the simulation code all possible parameters were considered. Shape factors for a row of pipes in a semi-infinite solid block, a row of pipes bounded by two parallel planes, or an arbitary numeric value are installed in the simulation code.

The present test assembly has rectangular fins with an annular base. In the simulation code, two kinds of fin were provided: rectangular fins and circular fins with an annular base. Discussion on the fin efficiency was presented in Section 4.1.4. As stated previously, a mathematical solution of fin efficiency involves Bessel functions, but in the present simulation code, the complex exact solution would reduce the speed of computation. Therefore, in the simulation code, the empirical equation as discussed in Section 4.1.4 was adopted. This empirical correlation has a ± 3 - 4 % error. Based on all these described parameters, the calculation would be proceed.

4.2.3 Processing Window

The processing window provides the processing of the simulation code with the selection of a working fluid. Also, this processing window presents the simulation's results, such as the cooling rate, saturation temperature and pressure.

From the 'Flooding Limit' of Wallis' correlation [27] , the possibility of the simulation with the particular dimensions is also determined and presented. The processing window allows many trials with different working fluids to contrast their heat transfer capabilities. No attempt was made to include the operational limits because "dry-out" and "burn-out" as these in TCTs are not yet well documented.

4.2.4 Tool Box Window

The Tool box window is able to provide the repetitive trials with a change of specific parameters (e.g. the shape factor, data file name, fin specification, some correlation sources, and correction factor). This tool box window includes useful menus that can be used in the process (e.g. result view, graphical view of the simulated temperature profile).

4.3 Simulation

Simulation was carried out with the developed computer code. Figs 4.4 (a, d) show the heat transfer coefficients for boiling and condensation respectively, by various correlations of h_e with h_c of Rohsenow [41] [Figs. 4.4 (a)] and various correlations of h_c with h_e of Bier et al [52] [Figs. 4.4 (b)]. Figs. 4.4 (c, d) illustrate the U_T obtained by the simulation code with different h_e by h_c of Rohsenow [41] [Figs. 4.4 (c)] and different h_c by h_e of Bier et al. [52] [Figs. 4.4 (d)] respectively.

As seen in the figures, each correlation generates distinct relationships. The results with h_c's of Gross [58] and Shiraishi [43, 58] showed much higher values than all those represented in Fig. 4.4 (a). Fig 4.4 (b) also shows a large difference in h_c's depending on the correlation used. Therefore, Fig. 4.4 (a, b) impiies that it is necessary to find a satisfactory correlation for a given condition or, at least, some modification of an existing correlation. This will be discussed in Chapter 5 through the comparison between the experiments and the computer simulation.

Fig. 4.5 (a) shows the effect of different working fluids on the overall heat transfer coefficient, U_T, and it can be seen that water is the best theoretically as discussed in Chapter 3. The simulation can show only the approximate range of the heat transfer capability with different working fluids. Figs. 4.5 (b-d) show the effects of L^*, u_{max}, and T_{air}. It is seen that U_T increases with increasing L^*, u_{max}, and T_s. Fig. 4.5 (e) presents the effect of T_{air} with a fixed T_h showing that an increase in ambient air temperature decreases the heat transfer rate.

Fig. 4.5 (f) shows the effect of the contact resistance of the filler between the heater and evaporator. As expected, an increase of the contact resistance leads to the decrease of the heat transfer capacity.

In the condenser section, sixty-six rectangular fins was installed to enhance the convective heat transfer coefficient. In the simulation computer code, two types of fin (rectangular and circular with the annular base) made available to compare the heat transfer capability with different enhancing fins. In the present study, rectangular fins with an annular base were attached to the condenser section. Fig. 4.5 (g) shows the effect of fin type on U_T. The system having circular fins of the same area has a higher heat transfer capability than a system with rectangular fins. In the present study, rectangular fins were used because of greater ease of fabrication and assembly.

As shown in Figs. 4.4 (a-d), it is clearly seen that a computer code alone can not give any meaningful quantitative results unless it is accompanied by some experimental results, implying that no computer code should be developed without a benchmark experimental verification.

Chapter 5

RESULTS AND DISCUSSION

The results of the present experimental study are shown in Tables 5.1 to 5.26. The thermal performance of the present MCM cooling system will be first evaluated in terms of the overall heat transfer coefficient (U_T). The present experimental results allow the evaluation of the various characteristics of the system's overall heat transfer coefficient.

The overall heat transfer coefficient depends on the dimensionless volume of the working fluid (V^*), the evaporator-condenser length ratio (L^*), the air flow velocity in the condenser section (u_{max}), the saturation temperature (T_s), the heat flux (q), and the choice of the working fluid. The effect of each of these parameters will be discussed here, except the effect of the tube inner diameter. It must be noted, however, that the TCT's inner diameter, though not considered in this study, is another parameter which would influence the value of U_T.

The obvious aim of the present experiment is to achieve the maximum heat transfer rate which also satisfies the expressed design limits. These design limits were mentioned in Section 3.1. To explain each term clearly, it is necessary to define the maximum heat transfer rate and the corresponding maximum U_T used in the present discussion. Considering the objective of the present

experimental study is to develop a safe and effective cooling system for the MCM's of the ATM switching system, it is meaningful to assess the results within the operating conditions of MCM's. As mentioned in Chapter 4, the computer simulation alone can not give any meaningful quantitative results unless it is accompanied by some experimental results. In this section, to verify our simulation study, the results of the simulation are compared with those from the experimental trials. However, there are some parameters which the simulation study can predict at the moment for which comparison with experimental results is not possible. These are the effect of the amount of the working fluid (V^+), the presence of non-condensible gas in the TCT, and the noise level. For these cases, the corresponding experimental results alone will be discussed.

The commissioning test of the whole apparatus revealed that the reading of the five heater thermocouples did not show a uniform temperature across the heater surface as shown Fig. 5.1. The reason for this non-uniformity of surface temperature could be the fact that the size of the heater is a little larger than the evaporator cross-section, which has a surface area of 35 mm × 35 mm, and that the resistance layer may not be uniformly formed. The relevant areas of the heater have the following dimensions:

	Dimension (mm)	Area (mm^2)
Outer surface area	50 × 50	2,500
Area of the heat generation section	38 × 38	1,444
Area of the evaporator section	35 × 35	1,225

Therefore, it can be seen that the area of the heater outer surface is 104 % larger than the area of the evaporator section, and the heat generation section is 18 % larger than the evaporator area. For this reason, the arithmetic average temperatures of the heater were taken for evaluation and discussion.

In the preliminary tests, R-11, R-113, FC-72, FC-87, acetone, ethanol and water were used as the working fluids and their representative results are shown in Fig. 5.2. As stated in Section 3.3, to follow the Montreal Protocol, the focus of the study was with FC-72, FC-87, and acetone as the working fluids.

Individual working fluids vary in their heat transfer capacity because of their different thermophysical properties, which lead to unique saturation temperatures and pressures. The main thermophysical property affecting the high heat transfer rate under boiling is the latent heat of vaporization. The vapor density and viscosity, as well as the liquid surface tension and viscosity, also influence the vapor flow activity.

Although water has a high latent heat, the results showed a low heat transfer capacity relative to the U_T of other working fluids, as shown in Fig. 5.2. This is thought to be due to a low operating temperature (the saturation temperature of 30-60 °C) and a low operating pressure (less than 0.2 bar). The effects of each working fluid on various parameters will be discussed in later sections.

The maximum of U_T for each working fluid shown in Fig. 5.2 is very close to the maximum heat transfer rate of each working fluid. Also, from inspection of Fig. 5.2, it can be concluded that desirable working fluids for our restricted range of the parameters are R-11, acetone, FC-87 and R-113. For this range in Fig. 5.2, acetone and R-113 were working under sub-atmospheric pressures and R-11 and FC-87 at up to 2.5 - 3 bar.

5.1 Comparison between Experiment and Simulation

Comparisons between the experimental and simulation results for two and three TCTs are not made because the basic assumption of the simulation code is that the temperature distribution of the heater is uniform. Therefore, the non-uniformity of the heater temperature forced uo to restrict the comparison between the experiment and the code to the single TCT case only.

It will be shown that the success of the computer code based on the analytical thermal resistance network methods depends on the choice of empirical correlations for various thermal resistances. By considering 8 empirical correlations for the boiling heat transfer coefficients (h_e), 3 for the condensation (h_c), 3 for forced convection (h_{conv}) and 3 for shape factor (S), there could be as many as 216 possible solutions for a given condition from the simulation code and every one of them could be the right one.

However, since the solution was based on the thermal resistance network method, the key to check the correctness of the code is to compare the temperature distribution within the TCT assembly obtained by the simulation with that of experiments as shown in Figs. 5.3 (a-g).

The simulated interior temperature distributions could be quite different from the experimental results, depending on the choice of the empirical correlations used for boiling and condensation. The use of Bier et al.'s correlation for boiling [52] and Gross'correlation for condensation [60, 61] gave the best fit among all the correlations for the temperature distribution as seen in Fig. 5.3 (a) for the conditions described in the figures with FC-72 as the working fluid. However, even this combination of boiling and condensation correlation did not give a good agreement with different working fluids. Therefore, to achieve the best fit between the experimental and simulation results, it was considered that some modification is needed for the boiling and

condensation heat transfer correlations (h_e and h_c) for a particular working fluid.

To modify a given combination of the boiling and condensation heat transfer correlations, the following expression by Park [55] was used for the heat transfer coefficient in the evaporator section and the condenser sections.

The modified heat transfer coefficients for boiling and condensation (h_e and h_c) are expressed, respectively, as.

$$h_e = C_e x_e^{m_e} \tag{5.1}$$

where x_e is the original Bier et al's correlation [52] given as Eq. B.4 of Appendix B

$$h_c = C_c x_c^{m_c} \tag{5.2}$$

where x_c is the original Gross' correlation [60, 61] given as Eq. B.7 of Appendix B

The constants C_e and C_c, and exponents m_e, and m_c were also determined from the experimental data so as to correlate the data best.

The values obtained are tabulated as follows:

Working Fluid	C_e	C_c	m_e	m_c
FC-72	0.6	0.8	1	1
R-113	0.37	0.7	1	1
R-11	0.4	1.2	1	1
Ethanol	0.6	0.08	1	1
FC-87	0.47	1	1	1

Working Fluid	C_e	C_c	m_e	m_c
Acetone	1.6	0.7	1	1
Water	0.02	0.08	1	1

The simulation used the shape factor of Eq. F.1 (0.103 m) of Appendix F and Churchill et al's correlation [59] for the forced convection given as Eq. D.3 of Appendix D.

Figs. 5.3 (a-g) show the comparison of the experimental results with those of the simulation using the original and modified h_e and h_c.

With the modified correlations of the boiling and the condensation heat transfer coefficients, it is now possible to compare the simulation results with the experimental results and consider the effects of the various parameters.

5.1.1 Effect of Air Flow Velocity, u_{max}

The velocity of air is a factor which affects the heat transfer capability of the system. The effect of the air velocity in the finned condenser section on the heat transfer capacity of the proposed system is shown in Figs. 5.4 (a-e), where the experimental results are compared against the simulation. It is seen that the total thermal resistance was reduced due to the forced convection. However, it can also see as shown in Fig. 5.4 (a) that an increase in the air velocity larger than 2 - 3 m/s would not significantly increase the over-all heat transfer capacity of the assembly. The observed effect of the heat transfer capacity increasing with air velocity was observed in all working fluids as illustrated in Fig. 5.4 (a-e). It was already discussed that due to the non-uniformity of the

heater surface, the simulation was confined to the case with one TCT. In Figs 5.4 (f-i), the experimental results with 2 and 3 TCTs are shown for the three working fluids of FC-72, acetone and water.

Air flow velocity is an important factor in the improvement of the heat transfer capacity of the system because the external flow velocity of the condenser section affects the activity of two-phase flow in TCT. In the case where the vapor is cooled by a low flow velocity, the relatively large quantity of the rising vapor from evaporator will impede the return flow of the condensed liquid. Conversely, a high air flow velocity can reduce the vapor flow against the increased counterflow of condensed liquid. Overall, a high flow velocity does not imply a high heat transfer ability. Therefore, the flow of the vapor or liquid inside the TCT must be balanced by an optimum convection air flow velocity. The overall relationship is a complex function of various parameters, such as the type of working fluid, TCT dimensions, etc.

Even when the heat transfer capacity of the working fluids was different, a similar tendency was observed as seen in Figs. 5.4 (a-i). With ethanol as the working fluid, increasing the velocity seem to have little effect on the improvement of U_T as shown in Fig. 5.4 (d). Furthermore, the comparison of the experimental results with the simulation for the cases of Q = 10 and 25 W did not show good agreement. In general, the comparison of the experimental results and the simulation is excellent for the cases with the working fluids FC-72, R-113, and R-11 and fails for the cases with working fluids ethanol and FC-87. But it is seen that the simulation correctly predicts the effect of the air velocity on U_T.

5.1.2 Effect of Saturation Temperature, T_s

In defining the heat transfer coefficients h_c and h_e, it is meaningful to use T_s. It is seen that the higher T_s, the higher U_T for a given working fluid from the literature [23, 55]. In the experiment, saturation temperature was to be the temperature of the transportation zone in Chapter 3. In the analysis, i.e., simulation, T_s was obtained by interaction.

Figs. 5.5 (a-g) show that the overall heat transfer coefficient of the test thermosyphon, U_T, increases considerably with an increase in the saturation temperature (T_s) in all working fluids. This may be due to the fact that the boiling heat transfer coefficient (or overall heat transfer coefficient) always increases with increasing system pressure. The thermal properties for working fluids in TCT's are a function of saturation temperature and pressure. Increasing the heat input leads to an increase in the saturation temperature and pressure. This means that the vapor density within the thermosyphon increases with high pressure. An increase in the saturation temperature from the increased pressure diminishes the effect of surface tension and increases the return flow of the condensate because of the decrease of liquid viscosity. Due to these factors, the condensed liquid moves quickly from the condensing section, which in turn increases the heat transfer coefficient. These thermo-physical phenomena are shown in Figs. 5.5 (a-g). Comparison between the experiment and simulation results shows a good agreement except in the case of ethanol as shown in Fig. 5.5 (d). In Fig. 5.5 (h), the effects of T_s on U_T for the cases of 2 and 3 TCTs were illustrated, which also indicates that in all cases an increase in T_s increases U_T.

5.1.3 Heat Transfer Capacity versus Temperature Difference between Surface of Heat Generation Section and Air Temperature, ΔT_T

Figs. 5.6 (a-g) show the effect of the over-all temperature difference on the heat flux obtained from the experiment and simulation. A design restriction on the over-all temperature difference (T_h to T_{air}) is 50 °C, as indicated in Section 3.1. The agreement between the experiment and simulation is very good. The effect of the number of TCT's is shown in Fig. 5.6 (h). In all cases, an increase in ΔT_T increases q.

The conditions of the present experimental study are defined by practical restrictions, i.e., the over-all temperature difference should be less than 50°C, the heater temperature should be less than 75 °C, and the maximum heat dissipation rate should be up to 4 W/cm^2.

From the experiment, three working fluids of R-11, FC-87, and acetone satisfy all these three design conditions as seen in Fig. 5.6 (h). FC-87 was somewhat high in the heater temperature. But as mentioned in the previous section, if the non-uniform temperature distribution due to the unbalanced area ratio of the evaporator section is taken into account, FC-87 may be acceptable.

Working fluids which are able to transfer a large amount of heat with a smaller temperature difference are always desirable for the cooling system. Acetone was seen to have a considerably lower temperature difference than other working fluids except for R-11. From Fig. 5.6 (h), acetone is shown to be satisfactory for the designated maximum heat flux of 4 W/cm^2. Acetone is also seen to transfer the heat up to a rate of 5 W/cm^2. Acetone as the working fluid has a high heat transfer capability over a small temperature difference. The maximum temperature difference was observed at 52.4 °C with the maximum heat flux of about 5 W/cm^2.

Table 5.1 shows the maximum heat transfer capacity of each working fluid. The maximum

heat transfer capacity is defined as the ability to satisfy the design conditions.

5.1.4 Effect of Evaporator - Condenser Length Ratio, L^*

The effect of condenser length is also an important parameter to determine the heat transfer capability of the system. In Figs. 5.7 (a, b), for FC-72 and FC-87 as the working fluid the system was definitely seen to be affected by the condenser length. For the case of FC-72 as the working fluid with increasing air velocity, the temperatures decreased gradually with increasing values of L^*. However, when L^* is at 6.25 (the condenser length is 200 mm) temperatures seem to increase again. The explanation is that with the increase of L^*, T_s will decrease because the vapor flow rate will rise due to an increase in the pressure difference between the evaporator and condenser section. An increase in L^* means that the area of the condensing region increases with a constant length of the evaporator; the length of the evaporator was 32 mm [Fig. 3.2]. The opposite is true where its upper limit of the pressure difference was seen to impede the return of the condensed liquid and to increase the heater temperature, as shown in Fig. 5.7 (a). This implies that the TCTs need an optimum condenser length based on the selection of the working fluid and its thermal properties. Also, Fig. 5.7 (a) indicates that the simulation results agree well with the experimental results. This figure illustrates that the combination of the boiling and condensing heat transfer coefficient correlations is very important. For the case with FC-87 as the working fluid, the phenomenon seen in Fig. 5.7 (a) was not observed [Fig. 5.7 (b)]. The effect of L^* was observed to be very similar to the effect of u_{max}. Fig. 5.7 (c) shows the relationship of T_h and T_s vs. L^* for the case of acetone as the working fluid with 3 TCTs, and again the phenomena seen in Fig. 5.7 (a) for the case of FC-72 as the working

fluid was not observed. It can be also seen that the higher the heat transfer rate of the system, the less the effect of L^* as shown in Figs. 5.7 (b, c), which is consistent from the physical point of view.

5.1.5 Effect of Contact Resistance

It can be seen in Figs. 5.3 (a-g), when the filler material between the heater and the evaporator surface are properly selected and packed as we have done in the present study, the effect of the contact resistance of the filler can be correctly simulated from the property data of the filler provided by the manufacturer of the filler materials. It is extremely important that this resistance be as small as possible to obtain the high heat transfer of the cooling system using proposed TCT.

5.1.6 Effect of Transportation Zone

The transportation zone (TZ) between the evaporator and condenser section of the usual TCTs is relatively short. However, in the present study, the TZ section is an order or two larger than the dimension of the evaporator. However, the TZ section is either adiabatic or subject to only natural convection. Since the present simulation code with a proper selection of various empirical correlations for a given working fluid agrees with the experimental results, only the simulation was used to see the effect of the length of the TZ and the results, are shown in Fig. 5.8. As expected, it seems that the effect is almost negligible.

It must be pointed out at this point that one of the benefit of a computer simulation is seen in the present case: i.e., when benchmark experimental results agree well with those of the simulation, some of the experimental study can be eliminated.

5.2 Experimental Results which can not be simulated

As stated in page 5-2, there are some variables whose effects can not yet be simulated because of the lack of the understanding or influence with respect to the physics involved, such as the amount of working fluid in a TCT, the presence of non-condensible gas and the noise level of the fan used. Therefore, these cases where the simulation is not possible are discussed in the following.

5.2.1 Effect of Quantity of Working Fluid, V^+

In this study, the quantity of working fluid inside the thermosyphon was defined as the ratio of the volume of the working fluid in the thermosyphon to the inside volume of the evaporator section:

$$V^+ = \frac{(\pi r^2 l_p)}{(\pi r^2 l_e)} = \frac{V_p}{V_e} \tag{5.3}$$

To determine the optimum amount of a working fluid in TCT, it is assumed that the heat transfer in a TCT takes place in two modes. That is, the heat transfer in the evaporator is that of pool boiling, whereas the evaporative heat transfer is taking place from the falling condensate liquid film above the pool of working fluid. The amount of the working fluid is a crucial information for the designers of cooling systems using TCTs because it is known to affect the heat transfer performance of the systems.

The important constraint in the operation of a thermosyphon is the effect of V^+. The quantity of the working fluid was found to vary directly with an increase or decrease of the heat transfer performance of the system as mentioned in section 4.1.3.

There are a few analytical studies on the amount of working fluid in heat pipes or TCT's, based on very simplified assumptions which grossly underestimate the real situations [29 - 32].

Imura et al. [30] suggested a useful formula for V^+ in terms of the average temperature of the top-inside, bottom-inside, and adiabatic wall and the critical heat flux given as:

$$q_{cr}\frac{4l_e}{d}/h_{LG}[\sigma g\rho_g^2(\rho_l-\rho_g)]^{1/4} = 0.64(\frac{\rho_l}{\rho_g})^{0.13} \tag{5.4}$$

$$V^+ = (1/5\sim 1/3) + \frac{0.8l_c+l_a}{l_a}\frac{4}{d}\left(\frac{3\mu_l l_e q_{cr}}{\rho_l^2 g h_{LG}}\right)^{1/3} + \frac{\rho_g}{\rho_l}\left[\frac{l_c+l_a}{l_e} - \frac{0.8l_c+l_a}{l_a}\frac{4}{d}\left(\frac{3\mu_l l_e q_{cr}}{\rho_l^2 g h_{LG}}\right)^{1/3}\right] \tag{5.5}$$

They mentioned that 1/5 ~ 1/3 of the first term is not sufficient in the case where l_e is much less than (l_c+l_a) and concluded that a further study on the matter is needed. However, Eq. 5.5 is useful to estimate the minimum amount of a working fluid.

The calculation by Eq. 5.5 for the present system and the range of temperatures showed that $V^+ = 2.65$ for the case where FC-72 was the working fluid. This implies for the present case that we can initially charge the TCT with approximately 2 ml of FC-72.

With such information, one can determine the optimum amount of a given working fluid and a series of experiments was carried out to determine the optimum V^+. The TCT used in the present study was designed with a very long transport zone (1,200 mm) and a relative long condenser section (up to 200 mm), compared to 32 mm of the evaporator length. The values of L^+ used in experimental studies reported in the literature are in the range between 1 and 1.5 [29-32] whereas the values for the TCT used in the present study were between 1.56 and 6.25. Therefore, it is expected that the

value of V^+ on the overall temperature difference at different heat transfer rates for the working fluids of FC-87 and acetone is shown in Figs. 5.9 (a) & (b) and 5.9 (c), respectively. In fig. 5.9 (d), the effect of V^+ on the overall temperature difference at different air velocities on the condenser section for the working fluid of R-113 is illustrated. The amount of a working fluid should be sufficient enough to transfer the heat in the evaporator section as well as the amount of vapor and the returning condensate film in the transport zone and the condenser section. Therefore, as illustrated in figures, V^+ is strongly affected not only by the heat transfer rate (heat flux) and the air velocity on the condenser section but also by working fluids. This implies that any extrapolation of the effect of V^+ for other working fluids requires caution.

5.2.2 Effect of Non-Condensible Gas

It has been well known that the performance of a thermosyphon will deteriorate in the presence of non-condensible gases which evolve from dissolved gases in the working fluid and the absorbed gas in the thermosyphon structure. When present in the system, the non-condensible gases are swept along with the vapor flow and accumulate at the condenser end. This will form a gas plug that represents a barrier to the flowing vapor and a small amount of gas may shut down the operation of a TCT. To eliminate the sources of the non-condensible gases the working fluid must be systematically purged of the dissolved gases. However, the presence of non-condensible gas can be utilized in a positive manner to control the system temperature [35].

Usually the presence of the non-condensible gas results from contact between air and fluid during manufacturing, storage, or charging processes. For example, up to 6 ml of air can be naturally dissolved under atmospheric pressure and room temperature in 100 ml of water as shown in Table.

3.2. Therefore, the dissolved air in TCTs must be eliminated under vacuum before it is charged with a working fluid.

This contamination problem is especially serious for the new fluorinert liquids FC-72 and FC-87, due to their extremely high solubility of air (as much as 10 times greater than for water). Fig. 5.10 shows the temperature profile of the TCT assembly before and after degassing at a constant heat flux. It is obvious that the presence of the non-condensible gases decreases system performance. The presence of non-condensible gases leads to an increased heater temperature and decreased condenser temperature. The presence of the non-condensible gases in the TCT reduces the condensing area and raises the system temperature just as in the case where the length of the condenser section is reduced. In the experiment, a special technique and procedure proposed by Lee et al [68] were used for the removal of the non-condensible gases [Fig. 3.5]. In the present experiments, the test TCT assembly had 3 additional thermocouples on the top of the tube passing through the condenser section. These thermocouples identify the presence of non-condensible gas which are then removed from the thermosyphon.

5.2.3 Effect of No Forced Air Flow on the Condenser Section, $u_{max} = 0$

In the absence of TCT deterioration, the most probable failure mechanism of the system would be the case when the fan used for the removable of heat from the condenser section fails. Therefore, in the event of fan failure, the heat transfer capacity of the system must be known. Figs. 5.11 (a) and (b) show the heat transfer capability of the proposed system without a fan (free convection) with working fluid of FC-87 and acetone, respectively. It is seen in the figures that the present cooling system can achieve a cooling capacity of up to 30 W (2.45 W/cm^2) for FC-87 as the working fluid

and 35 W (2.85 W/cm^2) for acetone, which are higher than the 2 W/cm^2 known as the maximum heat flux of the current MCM of ATM switching system. Therefore, this implies that the present cooling system can satisfy the heat transfer requirements without a fan when FC-87 and acetone are used as the working fluid.

Since the configuration of the present experimental setup of the cooling channel of the condenser section is different from that with no cooling channel, the comparison with simulation is not attempted.

Fig. 5.11 (c) shows the temperature transient for the case where there was no forced air flow on the condenser section.

5.2.4 Cooling Fan Noise Test

During the experiment, a noise test was carried out. The result is shown in Fig. 5.12. The test results were 45-50 dB within 0.5 m from the fan and 55-60 dB within 0.1 m from the fan. This meant that the noise level of the cooling fan installed satisfied the noise level suggested. Acoustic noise levels needed to conform to FCC classes A and B and Military Standard 461 for the office environment [36]. That noise level is less than 52 dB.

Chapter 6

CONCLUDING REMARKS

6.1 Conclusion

An experimental and analytical study on the heat transfer characteristics of a cooling system using TCT for ATM's MCM are presented in the present thesis. R-11, R-113, FC-72, FC-87, water, ethanol, and acetone were used as the working fluids. The present experimental and simulation study provides some practical information on an application of TCT's for the cooling of MCM's. In the present study, it is shown that the two-phase closed thermosyphon cooling system of the present design has satisfied the aim of handling a high heat flux of up to 4 W/cm^2 with an over-all temperature difference of 50 °C when acetone or FC-87 as the working fluid is used. From the experimental and simulation study, the following conclusions are made:

1. The effect of the quantity of working fluid was identified for 7 working fluids. The optimum range of V^+ varies between about 6 and 9.4.
2. The effect of non-condensible gases affect the heat transfer capability of the system. In the presence of non-condensible gases, it is difficult to estimate.
3. The effect of heater temperature versus air velocity was identified for a given working fluid.

For all working fluids, increasing the air velocity to the condenser section led to a reduced heater temperature and to an increased heat transfer capacity. The cooling air velocity to the condenser section affects the heat transfer capacity of the system.

4. The overall heat transfer coefficient of the system was found to increase gradually with an increasing saturation temperature.
5. The contact resistance was seen to affect the heat transfer capacity of the system.
6. The effect of L^+ showed a similar trend in all working fluids except with FC-72. Increasing L^+ would decrease the saturation temperature of the system.
7. The heat transfer capability of the present system without a fan dramatically fell for the cases of the working fluids FC-87 and acetone. In each case, the resultant temperature distribution exceeded the design limits. The present cooling system, however, was capable of handling the heat flux of up to 2 W/cm^2.
8. The simulation code was developed to predict the heat transfer capability of the present cooling system. It showed that the simulation through the accepted empirical correlations must be accompanied with experiment. The simulation code allows the combination of all possible parameters. The simulation by the modified correlations of Bier et al. [52] for boiling and Gross [60, 61] for condensation resulted in a close agreement with the experimental results.

6.2 Recommendation

To avoid the deterioration of the system due to the accumulation of non-condensible gas, it is suggested that about 50 % length of V^+ in the equivalent length based on the diameter of TCT, be added to the top of the condenser section to accommodate the non-condensible gas which may appear eventually.

APPENDIX A
THERMAL RESISTANCES

The heat transfer flow rate of the system is defined as:

$$Q = \frac{\Delta T}{\Sigma R} \tag{A.1}$$

1. Thermal resistance through the filler

$$R_{12} = \frac{\delta_{pl}}{k_{filt} A_h} \tag{A.2}$$

2. Thermal resistance through the plate

$$R_{23} = \frac{1}{k_{pl} S} \tag{A.3}$$

3. Thermal resistance due to the evaporation

$$R_{34} = \frac{1}{h_e \pi d l_h} \tag{A.4}$$

4. Thermal resistance due to the condensation

$$R_{45} = \frac{1}{h_c \pi d l_c} \tag{A.5}$$

(for R'_{45}, $l_c = l_b$)

5. Thermal resistance through the tube

$$R_{56} = \frac{\ln(D/d)}{2\pi k_t l_c} \tag{A.6}$$

(for R'_{56}, $l_c = l_b$)

6. Thermal resistance due to the forced convection through a finned area.

$$R_{67} = \frac{1}{h_{conv}\eta_{total}A_{total}} \tag{A.7}$$

where η_{total} is defined as Eq. E.1 in Appendix E.

7. Thermal resistance due to the free convection through the transportation zone.

$$R'_{67} = \frac{1}{h_{nconv}A} \tag{A.8}$$

APPENDIX B

CORRELATIONS FOR BOILING HEAT TRANSFER COEFFICIENT

1. Rohsenow (1952) [52, 53, 56, 59]

$$\frac{c_{pl}\Delta T_s}{h_{LG}} = C_{SF}\left[\frac{q}{\mu_l h_{LG}}\sqrt{\frac{\sigma}{g(\rho_l-\rho_g)}}\right]^{0.33}\left[\frac{c_{pl}\mu_l}{k_l}\right]^{s} \qquad \text{(B.1)}$$

2. Foster and Zuber (1955) [52]

$$h_e = 0.00122\frac{\Delta T_s^{0.24}\Delta P_s^{0.75}c_{pl}^{0.45}k_l^{0.75}}{\sigma^{0.5}h_{LG}^{0.24}\mu_l^{0.29}\rho_g^{0.24}} \qquad \text{(B.2)}$$

3. Mostinskii (1963) [52]

$$h_e = A^{*}q^{0.7}F(p) \qquad \text{(B.3)}$$

$$A^{*} = 3.596\times10^{-5}\,P_{cr}^{0.69}$$

$$F(p) = 1.8\,P_r^{0.17} + 4P_r^{1.2} + 10P_r^{10}$$

4.Bier et al. (1983) [52]

$$h_e = A^{*} q^{0.7} F(p) \tag{B.4}$$

$$F(p) = 0.7 + 2P_r\left(4 + \frac{1}{1-P_r}\right)$$

5. Cooper (1984) [52]

$$h_e = 55 q^{0.67} P_r^{(0.12-0.2 log Rp)} (-\log_{10} P_r)^{-0.55} M^{-1/2} \tag{B.5}$$

6. Shiraishi (1987) [43, 58]

$$h_e = 0.32 * \frac{\rho_l^{0.65} k_l^{0.3} C_{pl}^{0.7} g^{0.2}}{h_{LG}^{0.4} \rho_v^{0.25} \mu_l^{0.1}} q^{0.4} \left[\frac{P}{P_a}\right]^{0.23} \tag{B.6}$$

7. Gross (1990) [58]

$$Nu = 4(ArFr^{1/2})^{1/3} Pr_l^{1/2} (Bo/10)^n \tag{B.7}$$

n = 1/2 for Bo < 10, 1/6 for Bo >10

8. Zhang et al. (1991) [58]

$$Nu = 81.19 \left(\frac{\rho_l}{\rho_v}\right)^{0.0756} \left(\frac{\rho_l c_{pl}}{k}\right)^{-0.0274} \left(\frac{Dq}{h_{LG}\mu_l}\right)^{0.3621} \tag{B.8}$$

APPENDIX C

CORRELATIONS FOR CODENSING HEAT TRANSFER COEFFICIENT

1. Nusselt (1916) [59]

$$h_c = 0.943\left[\frac{k_l^3 \rho_l(\rho_l-\rho_g)gh_{LG}}{\mu_l \Delta T_s\, l_c}\right]^{1/4} \tag{C.1}$$

2. Rohsenow (1956) [41]

$$h_c = 0.943\frac{k_l}{l_c}\left[\frac{l_c^3 \rho_l(\rho_l-\rho_g)g}{\mu_l\, \Delta T_s\, k_l}\left[h_{LG}+0.68c_{pl}\Delta T_s\right]\right]^{1/4} \tag{C.2}$$

3. Gross (1987) [60, 61]

$$Nu = \sqrt{(Nu_{lam} f_{wave})^2+(Nu_{turb})^2} \tag{C.3}$$

$$Nu_{lam} = 0.925(Re_\varphi)^{-1/3}$$

$$Nu_{turb} = 0.021(Re_\varphi)^{*1/3}$$

APPENDIX D

CORRELATIONS FOR FORCED AND NATURAL CONVECTION HEAT TRANSFER COEFFICIENT

1. Empirical correlations for forced convection from a finned area

a. Knudsen and Katz. (1958) [59]

$$\frac{hd}{k_f} = C\left(\frac{u_\infty d}{\nu_f}\right)^n Pr^{1/3} \qquad \text{(D.1)}$$

C=0.683, n=0.466 for 40 < Re < 4000

b. Fand (1965) [59]

$$Nu_f = (0.35 + 0.65Re_f^{0.52})Pr_f^{0.3} \qquad \text{(D.2)}$$

c. Churchill and Bernstein. (1977) [59]

$$Nu = 0.3 + \frac{0.62Re^{1/2}Pr^{1/3}}{\left[1+(0.4/Pr)^{2/3}\right]}\left[1+\left(\frac{Re}{282{,}000}\right)^{5/8}\right]^{4/5} \qquad \text{(D.3)}$$

2. Empirical equations for natural convection from the transportation zone (1956) [62]

$$\overline{Nu} = \frac{4}{3}\left[\frac{7RaPr}{5(20+21Pr)}\right]^{1/4} + \frac{4(272+315Pr)l_b}{35(64+63Pr)D} \qquad \text{(D.4)}$$

APPENDIX E

FIN EFFICIENCY

The fin effiency is difined as [52]:

$$\eta_{total} = 1 - \frac{A_{fin}}{A_{total}}(1 - \eta_f) \tag{E.1}$$

$$A_{fin} = N_{fin}\pi\left[2\frac{D_{fin}^{\ 2} - D^2}{4} + D_{fin}\delta_{fin}\right]$$

$$A_{tube} = \pi D(l_c - N_{fin}\delta_{fin})$$

$$A_{total} = A_{fin} + A_{tube}$$

$$\eta_{fin} = \frac{\tanh(m\psi)}{m\psi}$$

$$m = \sqrt{\frac{2h_{conv}}{k_{fin}\delta_{fin}}}$$

$$h_{conv} = \frac{Nuk}{D}$$

$$\psi = \frac{D_i}{2}[(\frac{r_c}{r_i})-1][1+0.35\ln(\frac{r_c}{r_i})]$$

a. for annular fins

$$\frac{r_c}{r_i} = \frac{r_o}{r_i}$$

b. for rectangular fins

$$\frac{r_c}{r_i} = 1.28\psi\sqrt{\beta-0.2}$$

APPENDIX F
SHAPE FACTOR

1. Row of pipes of equal diameter and at equal temperature in a semi-infinite mass - Fig. F-1 [63].

$$S = \frac{2\pi l_h}{\ln\left[\frac{P_t}{\pi r}\times\sinh\left(2\pi\frac{\delta_{pl}}{P_t}\right)\right]} \qquad \text{(F.1)}$$

2. Row of pipes of equal diameter and at equal temperature in a mass bounded by two parallel planes - Fig. F-2 [63].

$$S = \frac{2\pi l_h}{\ln\left[\frac{P_t}{\pi r}\times\sinh\left(\pi\frac{\delta_{pl}}{P_t}\right)\right]} \qquad \text{(F.2)}$$

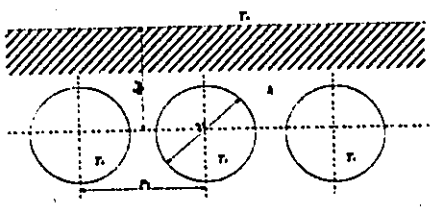

Figure F-1

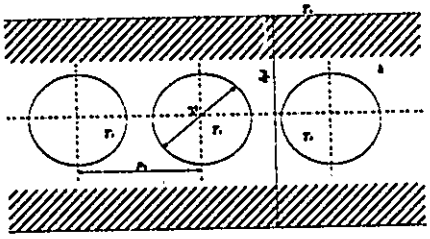

Figure F-2

APPENDIX G
SIMULATION WINDOWS

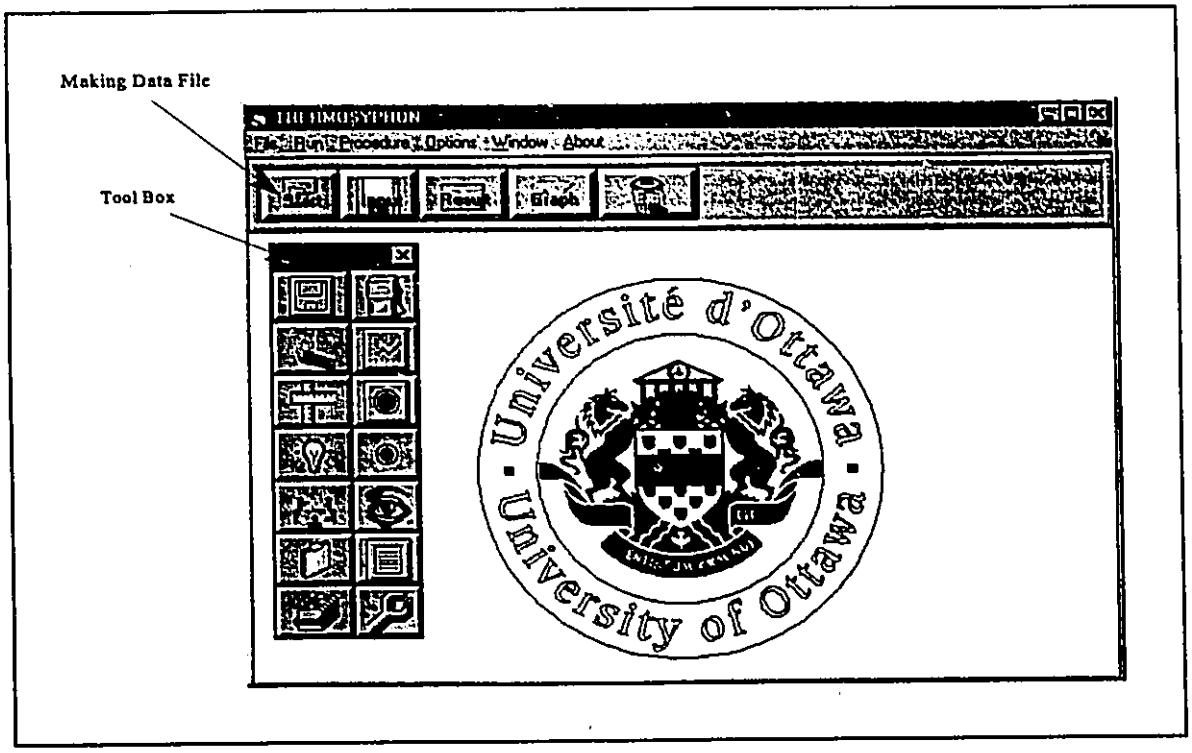

Figure G-1 Main Window

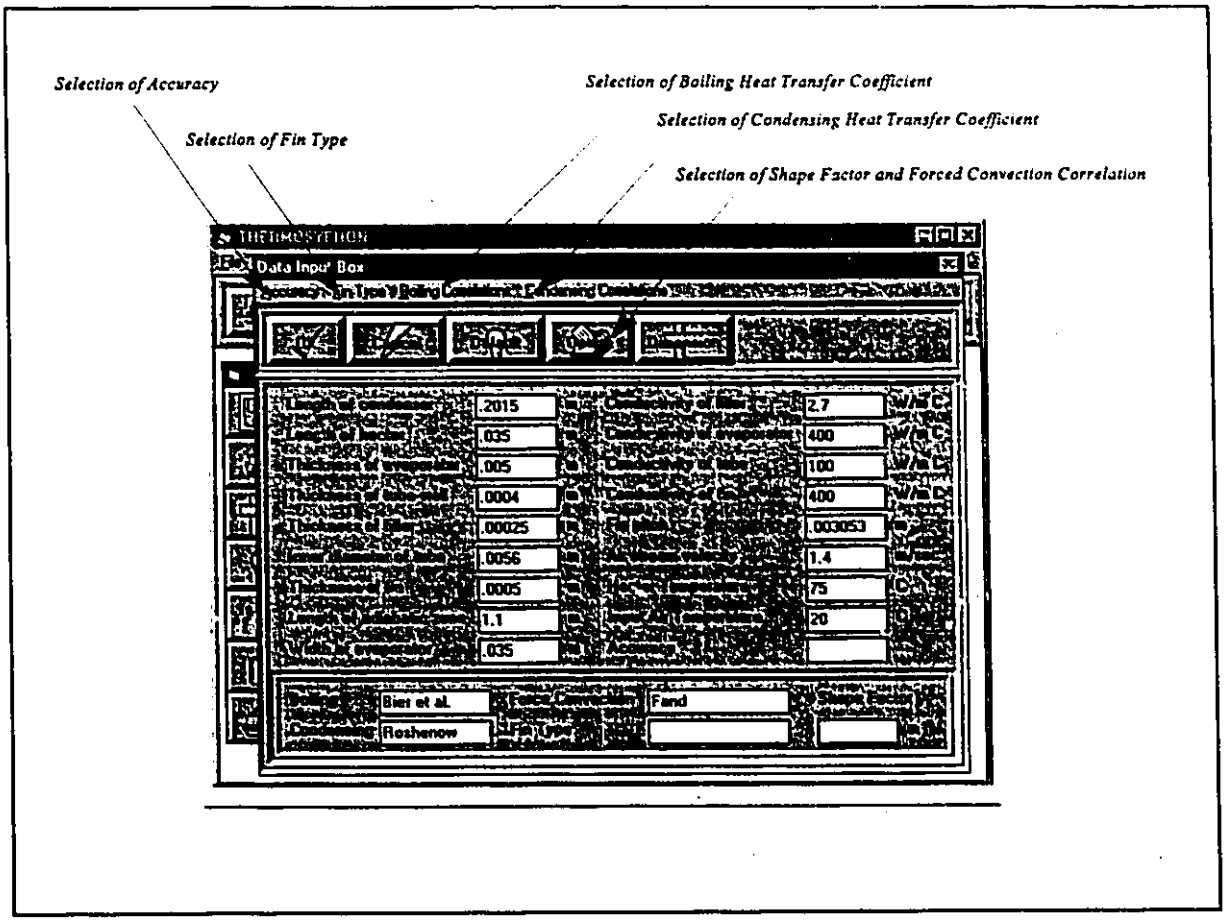

Figure G-2 Data Input Window

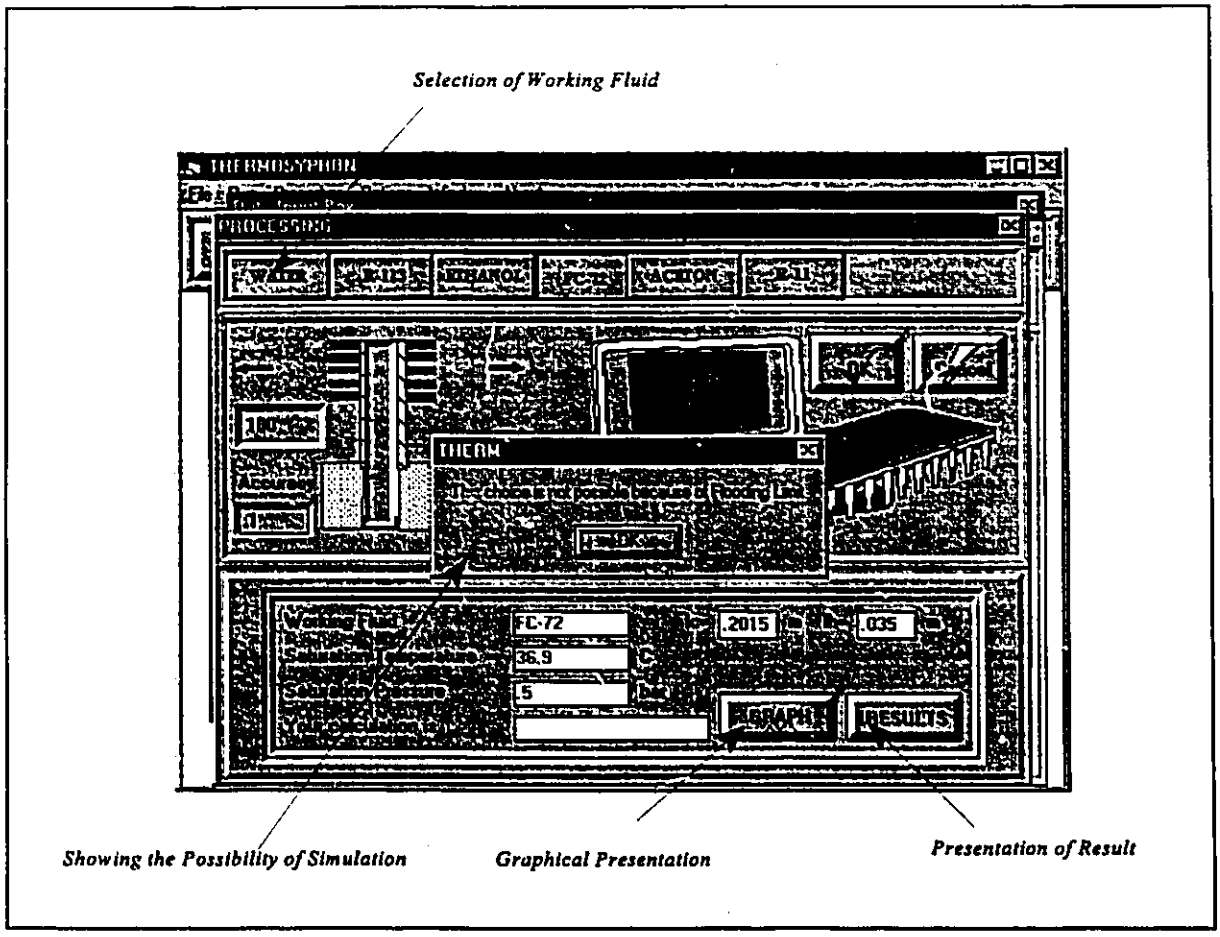

Figure G-3 Processing Window

APPENDIX H
ERROR ANALYSIS

The experimental errors were calculated using the method recommended by Kline and McClintok [93]. The evaluated uncertainties in the variables are:

L (length): ± 0.25 %

T (temperautr): ± 0.2 °C

E (voltage): ± 0.5 %

I (current): ± 3.5 %

Using these variables, the following was calculated.

1. Power

$$Q = VI = 20$$

$$\frac{\partial Q}{\partial I} = V = 50$$

$$\frac{\partial Q}{\partial V} = I = 0.4$$

$$w_Q = \left[\left(\frac{\partial Q}{\partial V} w_V\right)^2 + \left(\frac{\partial Q}{\partial I} w_I\right)^2 \right]^{\frac{1}{2}}$$

$$w_Q = \left[(0.4 \times 0.2)^2 + (50 \times 0.01)^2 \right]^{\frac{1}{2}}$$

$$= 0.506$$

$$Q = 20 \pm 0.506 \ (2.5\%)$$

2. Area

$$A = L_e \times L_e = 0.001225 \ m^2$$

$$\frac{\partial A}{\partial L_e} = 2L_e = 0.07$$

$$w_A = \left[\left(\frac{\partial A}{\partial L_e} w_{L_e}\right)^2 \right]^{\frac{1}{2}}$$

$$w_A = \left[(0.07 \times 0.00000875)^2 \right]^{\frac{1}{2}}$$

$$= 0.000000612$$

$$A = 0.001225 \pm 0.000000612 \ (0.05 \ \%)$$

3. Heat Flux

$$q = \frac{Q}{A} = \frac{20}{0.001225} = 16326$$

$$\frac{\partial q}{\partial Q} = \frac{1}{A} = \frac{1}{0.001225} = 816.3$$

$$\frac{\partial q}{\partial A} = -\frac{Q}{A^2} = -\frac{20}{0.0000015} = -13333333$$

$$w_q = \left[\left(\frac{\partial q}{\partial A} w_A\right)^2 + \left(\frac{\partial q}{\partial Q} w_Q\right)^2 \right]^{\frac{1}{2}}$$

$$w_q = \left[(-13333333 \times 0.000000612)^2 + (816.3 \times 0.506)^2 \right]^{\frac{1}{2}}$$

$$= 408.2$$

$$q = 16326 \pm 408.2 \ (2.5\%)$$

4. Overall heat transfer coefficient

$$U_T = \frac{q}{\Delta T_T} = \frac{16326}{39.18} = 416.7$$

$$\frac{\partial U_T}{\partial (q)} = \frac{1}{\Delta T_T} = 0.00065$$

$$\frac{\partial U_T}{(\partial \Delta T_T)} = -\frac{1}{(\Delta T_T)^2} = -10.4$$

$$w_{U_T} = \left[\left(\frac{\partial U_T}{\partial \Delta T_T} w_{\Delta T}\right)^2 + \left(\frac{\partial U_T}{\partial q} w_q\right)^2 \right]^{\frac{1}{2}}$$

$$w_{U_T} = \left[(-10.4 \times 0.2)^2 + (0.00065 \times 408.2)^2 \right]^{\frac{1}{2}}$$

$$= 2.1$$

$$U_T = 416.7 \pm 2.1(0.5\%)$$

REFERENCES

1. R. D. Nelson, S. Sommerfeldt and A. Bar-Cohen, "Thermal Performance of An Integral Immersion Cooled Multichip Module Package," IEEE Tr. cn Components, Packaging, and Manufacturing Technology, Part A, Vol. 17, No. 3, pp. 405-412, 1994.
2. J. Sotani, K. Nanba and N. Kageyama, "A Micro Heat - Pipe for Cooling Notebook PCs," 9th IHPC, Albuquerque, 1995.
3. F. Polášek and P. Štulc, " Cooling of Electronic Elements by Miniature Heat Pipes," 4IHPS, Preprints, Tsukuba, pp. 114-122, 1994.
4. V. Zbořil and P. Štulc, "Heat Pipes in Computer Modules," 5th IHPC, Preprint, Tsukuba, pp. 134-135, 1984.
5. T. P. Cotter, "Principles and Prospects for Micro Heat Pipes," 5th IHPC, Preprint IV, Tsukuba, pp. 126-127, 1984.
6. B. S. Larkin, "Temperature Control of Electronic Ssystems Using Inexpensive Heat Pipes," 5th IHPC, Preprints IV, Tsukuba, pp. 136-141, 1984.
7. X. Xia, J. Liu and H. Jang, "The Application of Heat Pipes To Semiconductor Thermoelectronic Refrigeration Device," 8th IHPC, Beijing, pp. 669-672, 1992.

8. A. Gerák, L. Horváth, F. Jelínex, P. Štulc and V. Zbořil, "Examples of Heat Pipe Application in Chemical, Electrical and Other Industry," 6th IHPC, Grenoble, pp. 676-684, 1987.

9. J. Zhuang and T. M. Xu, "Research And Industrial Application of Closed Two Phase Thermosyphons and Heat Pipes," 6th IHPC, Grenoble, pp. 761-771, 1987.

10. Y. V. Avakyan, L. P. Grakovich and D. K. Khrustalev, "Heap Pipes for Solar Systems," 6th IHPC, Grenoble, pp. 721-728, 1987.

11. Y. Lee and C. Z. Wu, "Solidification of Heat Transfer Characteristics in Presence of Two-Phase Closed Thermosyphons in Latent Heat Energy Storage Systems," 6th IHPC, Grenoble, pp. 729-733, 1987.

12. T. Alleau and A. Brichard, "Stirling Engine Coupled with A Sodium Boiler,"6th IHPC, Grenoble, pp. 748-754, 1987.

13. Y. Lee and A. Bedrossian, "The Characteristics of Heat Exchangers using Heat Pipes or Thermosyphon," Int. J. Heat and Mass Transfer., Vol. 21, pp. 221-229,1978.

14. D. Fetcu, V. B. Ungureanu and G. Bacanu, "Gravity-Assisted Wickless Heat Pipe Heat Exchanger," 8th IHPC, Beijing, Preprints E-12, 1992.

15. T. Wadowaski, A. Akabarzadeh and P. Johnson, "Characteristics of Gravity-Assisted Wickless Heat Pipe Heat Exchanger," 7th IHPC, Minsk, 1990.

16. A. Itoh and S. Itoh, "Control of the Metastasis of Cancer (Part 1)," 9th IHPC, Albuquerque, 1995.

17. J. J. Licari, "Multichip Module Design, Fabrication, and Testing," McGraw-Hill Inc., New York, 1995.

18. M. Pecht, "Handbook of Electronic Package Design," Marcel Dekker Inc., New York, 1991.

19. Y. Doi, H. Yamada and S. Sasaki, "An ATM Switch Hardware Technologies UsingMultichip Packaging," IEEE Tr. on Components, Hybrids, and Manufacturing Technology, Vol. 16, No. 1, pp. 60-65, 1993.

20. T. Kishimoto, A. Harada, S. Sasaki and T. Iwata, "Heat-Pipe Cooling Technologies for Telecom MCMs," 4th IHPS, Preprints, Tsukuba, pp. 106-113, 1994.

21. E. Schmidt, "General Discussion on Heat Transfer," Institution of Mechanical Engineers, London, Section IV, p. 361, 1951.

22. H. Cohen and F. J. Baylay, Heat Transfer Problems of Liquid Cooled Gas Turbine Blades, Proc. Inst. Mech. Eng, Vol. 169, pp. 1063-1080, 1955.

23. Y. Lee and U. Mital, "A Two-Phase Closed Thermosyphon," Int. J. Heat and Mass Transfer., Vol. 15, pp. 1695 - 1707, 1972.

24. B. Clements and Y. Lee, "Additional Parameters in Two-Phase Closed Thermosyphon: Effect of Tube Diameter and Wall Thickness," Int. J. Heat Mass Transfer., Vol. 24, No. 9, pp. 1554-1555, 1981.

25. M. Shiraish, K. Kikuchi and T. Yamanishi, "Investigation of Heat Transfer Characteristics of A Two Phase Cloosed Thermosyphon", 4th IHPC, London, pp. 95-104, 1981.

26. H. Nguyen-Chi and M. Groll, "Entrainment or Flooding Limit in A Closed Two-Phase Thermosyphon," 4th IHPC, London, pp. 147-162, 1981.

27. G. B. Wallis, "One-dimensional Two Phase Flow," McGraw-Hill Book Company, New York, 1969.

28. T. Ueda and T. Myashita, "On the Performance Limit Closed Two-Phase Thermosyphon,"

Heat Transfer-Japanese Research, Vol. 20, No. 6, pp. 602-617, 1991.

29. T. Ma, X. Liu and J. Wu, "Flow Pattern and Operation Limits in Two-Phase Closed Thermosyphon," 6th IHPC, Grenoble, pp. 576-581, 1987.

30. H. Imura, K. Sasaguchi and H. Kozai, "Critical Heat Flux in a Closed Two-Phase Thermosyphon," Int. J. Heat Transfer., Vol. 26, No. 8, pp. 1181-1188, 1983.

31. K. T. Feldman and R. Srinivasn, "Investigation of Heat Transfer Limits in Two-Phase Closed Thermosyphon," 5th IHPC, Tsukuba, pp. 30-35, 1984.

32. G. Bartsch and J. Unk, " A Contribution to Calculating the Optimum Quantity for Filling A Closed Two-Phase Thermosyphon," 6th IHPC, Grenoble, pp. 641-646, 1987.

33. K. Neigishi and T. Sawada, "Heat Transfer Performance of an Inclined Two-Phase Closed Thermosyphon," Int. J. Heat Mass Transfer., Vol. 26, No. 8. pp. 1207-1213, 1983.

34. Y. Kobayashi and T. Matsumoto, "Vapor Condensation in the Presence of the Non-Condensible Gas in the Gravity Assisted Termosyphon," 6th IHPC, Grenoble, pp. 565-570, 1987.

35. C. L. Tien and S. J. Chen, "Non-Condensible Gas in Heat Pipes," 5th IHPC, Preprints II, Tsukuba, pp. 2-6, 1984.

36. A. Bar-Cohen, "Thermal Management of Air- and Liquid-Cooled Multichip Modules," IEEE Tr. on Components, Hybrids, and Manufacturing Technology, Vol. CHMT-10, 2, pp. 159-171,1987.

37. S. Sasaki, T. Konchi and T. Ohsaki, "A New Module Using A Copper Polyimide Multilayer Substrate," IEEE Tr. on Components, Hybrids, and Manufacturing Technology, Vol. 12, No. 4, pp. 658-662, 1989.

38. T. Y. T. Lee, J. A. Andrews, P. Chow and D. Saums, "Compact Liquid Cooling System for Small, Moveable Electronic Equipment," IEEE Tr. on Components, Hybrids, and Manufacturing Technology, Vol. 15, No. 5, pp. 786-793, 1992.

39. G. P. Peterson, "Heat Pipes in the Thermal Control of Electronic Components," 3rd IHPS, Tsukuba, pp. 1 - 12, 1988.

40. J. Pei and S. Heng, "Thermosyphons for Cooling High Power Multichip Packages," 8th IHPC, Beijing, pp. 653-656, 1992.

41. Y. Wen and S. Guo, "Experimental Heat Transfer Performance of Two Phase Thermosyphon," 5th IHPC, Tsukuba, pp. 43-49, 1984.

42. M. K. Bezrodnyi and S. S. Volkov, "Study of Hydrodynamic Characteristics of Two-Phase Flow in Closed Thermosyphon," 4th IHPC, London, pp. 115-123, 1981.

43. M. Shiraishi, K.Kikuchi and T. Yamanishi, "Investigation of Heat Transfer Characteristics of A Two-Phase Closed Thermosyphon," 4th IHPC, London, pp. 95-104, 1981.

44. T. Spendel and M. Groll, "Thermal Behavior High-Performance Closed Two-Phase Thermosyphons," 5th IHPC, Tsukuba, Preprints IV, A9, pp. 36-42, 1984.

45. M. Xin, G. Chen and Y. Chen, "Flow and Heat Transfer in Two-Phase Thermosyphon," 6th IHPC, Grenoble, pp. 571-575, 1987.

46. Y. Zhang, Z. Sun and L. Huang, "Flow Patterns and Heat Transfer Crises in A Two-Phase Closed Thermosyphon," 6th IHPC, Grenoble, pp. 628-633, 1987.

47. A. B. Duncan and G. P. Peterson, "Review of Micro Scale Heat Transfer," Applied Mechanics Review, Vol. 47, No. 9, pp. 397-428, 1994.

48. G. P. Peterson, "Overview of Micro Heat Pipe Research And Development," Applied Mechanics Review, Vol. 45, No. 5, pp. 175-189, 1992.

49. D. E. Pope, "Thermal Characterization of a Tape Carrier Package," IEEE Tr. on Components, Packaging, and Manufacturing Technology, Part A, Vol. 18, No. 1, 1995.

50. Satutory Authority, "Ozone-depleting Substances Regulations," 3080, Canada Gazette Part I, Sept. 2, 1995.

51. M. D. Kelleher, R. Egger and Y. Joshi, "Modification of the Nucleate Boiling Hysteresis in the Pool Boiling of Fluorocarbons," 14th Inter. Heat Transfer Conf., Brighton, UK, Paper No.10-PB-14, Vol. 5, pp. 87-92, 1995.

52. G. F. Hewitt, G. L. Shiress and T. R. Bott, "Process Heat Transfer," CRC Press, London, 1994.

53. W. M. Rohsenow, "A Method of Correlating Heat Transfer for Surface of Liquids," Trans. ASME, Vol. 74, pp. 969-976., 1952.

54. D. Q. Kern, "Process Heat Transfer," McGraw-Hill Book Company, New York, 1950.

55. R. J. Park, "Two-Phase Closed Thermosyphon with Two-Fluid Mixtures," M.A.Sc. Thesis, University of Ottawa, 1992.

56. R. I. Vachon, G. H. Nix, G. E.Tanger, "Evaluation of Constants for the Rohsenow Pool-Boiling Correlation," J.of Heat Transfer, Vol. 90, pp. 239-247, 1968.

57. D. P. Dewitt, "Fundmentals of Heat and Mass Transfer," 3rd ed., John Wiley &Sons, New York, 1990.

58. X. Q. Chen, Z. Zhang and T. Ma, "Heat Transfer Correlation of the Evaporator Section in A Two-Phase Closed Thermosyphon," 8th IHPC, Beijing, pp. 354-359, 1992.

59. J. P. Holman, " Heat Transfer," 7th ed., McGraw-Hill Book Company, New York, 1989.

60. U. Gross, "Reflux Condensation Heat Transfer Inside A Closed Thermosyphon," Int. J. Heat Mass Transfer., Vol. 35, No. 2, pp. 279-294, 1992.

61. U. Groβ and E. Hahne, "Condensation Heat Transfer Inside A Closed Thermosyphon," 6th IHPC, Grenoble, pp. 618-623, 1987.

62. A. Bejan, "Heat Transfer," Jhon Wiley & Sons Inc., New York, 1993.

63. S. S. Kutateladze, "Fundamentals of Heat Transfer," Edward Arnold Ltd., New York, 1963.

64. F. Kaminaga, Y. Okamoto and T. Suzuki, "Study on Boiling Heat Transfer Correlation in A Closed Two-Phase Thermosyphon," 8th IHPC, Beijing, pp. 317-322, 1992.

65. W. H. McAdams, "Heat Transmission," 3rd ed., McGraw-Hill Book Company, New York, 1954.

56. S. H. Zahir, "A Two-phase Closed Thermosyphon at Low Temperature," M.A.Sc. Thesis, University of Ottawa, 1972.

67. J. He, T. Ma and Z. Zhang, "Heat Transfer Characteristics in the Evaporator Section of Two-Phase Closed Thermosyphon," 8th IHPC, Beijing, China, pp. 335-340, 1992.

68. Y. Lee, I. L. Pioro, and H. J. Park, "An Experimental Study on a Plate Type Two-Phase Closed Thermosyphon," 4th IHPS, Tsukuba, Japan, pp. 49-58, 1994.

69. C. Rajagopal, S. Subramaniyam and P. D. Grover, "Theoretical Analysis of Condensation in Vertical Heat Pipes," 6th IHPC, Grenoble, pp. 65-72, 1987.

70. K. Kobayashi, T. Yamamoto, T. Kuroki, K. Nagata, "Heat Transfer Performance of A Two-Phase Closed Thermosyphon," 5th IHPC, Tsukuba, pp. 36-42, 1984.

71. M. R. Vogel, "Liquid Cooling Performance for a 3-D Multichip Module and Miniature Heat Sink," IEEE Tr. on Components, Packaging, and Manufacturing Technology, Part A, Vol. 18, No. 1, 1995.

72. M. N. Ivanoski, V. P. Sorokin, and I. V. Yagodkin, "The Physical Principles of Heat Pipes," Claredon Press, New York, 1982.

73. E. U. Schlunder, "Heat Exchanger Design Handbook," Hemisphere Publishing Corp,1983.

74. W. K. Ho and C. L. Tien, "Reflux Condensation Characteristics of A Two-Phase Closed Thermosyphon," 4th IHPC, London, pp. 541-458, 1981.

75. T. Spendel, "Laminar Film Condensation Heat Transfer in Closed Two-Phase Thermosyphon," 4th IHPC, London, pp. 163-173, 1981.

76. S. J. Chen, J. G. Reed and C. L. Tien, "Reflux Condensation in a Two-Phase Closed Thermosyphon," Int. J. Heat Mass Transfer., Vol. 27, No. 9, pp. 1587-1594, 1984.

77. P. J. Berenson, "Experiments on Pool-Boiling Heat Transfer," Int. J. Heat Mass Transfer., Vol. 5, pp 985-999, 1962.

78. C. Z. Wu and Y. Lee, "Effect of L/D on Heat Transfer Characteristics fo Two-Phase Closed Thermosyhon," 8th IHPC, Beijing, China, pp. 345-348, 1992.

79. Z. J. Zuo and F. S. Gunnerson, "Numerical Modeling of the Steady State Two-Phase Closed Thermosyphon," Int. J. Heat Mass Transfer., Vol. 37, No. 17, pp. 2715-2722, 1994.

80. H. Uehara, "Filmwise Condensation for Wavy Flow on a Vertical Flow," Trans. of JSME, Vol. 48, No. 433, pp. 1751-1760, 1982.

81. F. Kaminaga and Y. Shigematsu, "Maximum Heat Flux and Condensation Heat Transfer," 9th IHPC,Albuquerque, 1995.

82. J. P. Holman, " Experimental Methods for Engineers," 6th ed., McGraw-Hill Book Company, New York, 1994.

83. J. E. Diehl and C. R. Koppany, "Flooding Velocity Correlation For Gas-Liquid Counterflow in Vertical Tubes," Heat Transfer Philadelphia-Chemical Engineering Progress Symposium Series, AICE, New York, Vol. 65, No. 92, pp. 77-83, 1969.

84. G. P. Peterson, "An Introduction to Heat Pipes," John Willy & Sons. Inc, New York,1994.

85. R. C. Reid, J. M. Prausnitz and K. S. Thomas, "The Properties of Gases and Liquids," 3rd edition, McGraw-Hill Book Company, New York, 1977.

86. K. Kaminaga, Y. Okamoto and T. Suzuki, "Study of Boiling Heat Transfer Correlation in A Closed Two-Phase Thermosyphon," 8th IHPC, Beijing, pp. 317-322, 1992.

87. N. Zuber, "On the Stability of Boiling Heat Transfer," Trans. ASME, Vol. 46, pp. 711-720, 1958.

88. W. A. Ranken and M. G. Houts, "Heat Pipe Cooled Reactors for Multi-Kilowatt Space Power Supplies," 9th IHPC, Albuquerque, 1995.

89. G. S. H. Lock, "The Tubular Thermosyphon," Oxford University Press, New York, 1992.

90. S. W. Chi, "Heat Pipe Theory and Practice," Hemisphere Publishing Corporation, New York, 1976.

91. S.J. Kline and F.A. McClintok, "Describing Uncertainties in Single-Sample Experiments," Mechanical Engineering, 3-8, January, 1953.

Table 2.1 Recent Studies on the Cooling System for MCM

Researcher	Cooling objective	Cooling Method	Max. Power Dessipation (W)	External Resistance (K/W)	Working Fluid or Coolant
Zbořil et al. (1984) [4]	computer chip module	Heat pipe of retangular cross section.	-	-	Water and ethanol
Cotter (1984) [5]	MCM	Micro heat pipes	-	-	Methanol
Larkin (1984) [6]	electronic circuitry	Heat pipes	-	-	R-22, R-114
Gerák et al. (1988) [8]	integrated circuits	Heat pipes	-	-	not mentioned
Sasaki et al (1989) [37]	MCM	Cooling fins in substrate	26	25	Air
Pei and Heng (1992) [40]	MCM	TCT	350 (single) 1600 (twin)	0.07 0.01	R-22
Doi et al. (1993) [19]	ATM switch with MCM	Cooling fins	50	13	Air
Polášek et al (1994) [3]	MCM	Heat Pipes	-	-	R-113
Kishimoto et al. (1994) [20]	ATM switch with MCM	TCT	160 ($1.6W/cm^2$)	5.6	FC-87, Freon 142b, Water
Nelson (1994) [1]	MCM	Immersion Cooling	16 /Chip	4.06	FC-72
Pope (1995) [49]	Tape carrier Package	Cooling Fins	5	2	Air
Vogel (1995) [71]	MCM	Liquid cooling	50	1.5	Polyalphaol-efin (PAO)

Table 3.1 Some Physical Properties of Working Fluids Used

No	Working Fluid	Saturation Temperature at 1 atm., °C	Freezing Temperature at 1 atm., °C	Flammability, % in air	Toxicity (max conc. in air), mg/m^3	Compability with Al
1	Water	100	0	-	-	Limited
2	Ethanol	78	-114	3.3-19	1000	Limited
3	Aceton	56	-93	2.6-13	200	Compat.
4	R113	48	-36	-	3000	Limited
5	R11	24	-111	-	3000	Limited
6	FC72	56	-90	-	-	-
7	FC87	30	-101	-	-	-

Table 3.2 Solubility of Non-Condensible Gas in Working Fluids

Working Fluid	Boiling Point	Solubility, at 1 atm. *ml*/100 *ml* liquid
FC-72	56 °C	48 (at 25 °C)
FC-87	30 °C	54 (at 25 °C)
Water	100 °C	2.6 O_2 (at 30 °C)
Water	100 °C	1.7 H_2 (at 30 °C)

Table 5.1 Maximum Heat Transfer Capacity of Working Fluids

W.F	# of TCT	Q_{max} (W)	q_{max} (W/cm^2)	L*	u_{max} (m/s)	V*	$T_{h\text{-}c}$ (°C)	$T_{h\text{-}a}$ (°C)	$\Delta T_{h\text{-}air}$ (°C)
R-11	1	25.0	2.04	6.25	4.07	7.5	71.2	75.7	48.9
	2	40.6	3.31	6.25	4.4	7.5	72.2	79.7	52.9
	3	59.6	4.87	6.25	4.4	7.5	62.7	74.2	47.4
Acetone	1	30	2.44	6.25	4.4	7.5	76.2	81.4	58.4
	2	50.0	4.08	6.25	4.4	7.5	64.6	74.0	53.2
	3	61.7	5.02	6.25	4.4	9.4	66.3	72.4	52.4
FC-87	1	20.0	1.63	6.25	4.4	7.5	62.3	65.9	46.6
	2	29.4	2.40	6.25	4.4	7.5	73.9	78.6	54.1
	3	45.3	3.69	6.25	3.4	7.5	69.8	78.3	54.0
R-113	1	20.7	1.69	6.25	4.3	7.5	69.7	73.6	46.8
	2	30.2	2.47	6.25	4.3	7.5	69.6	75.6	49.7
	3	40.0	3.27	6.25	4.1	7.5	68.7	76.4	50.6
FC-72	1	19.8	1.62	4.79	5.4	7.5	71.7	75.4	53.6
	2	30.2	2.47	6.25	3.8	7.5	73.9	79.7	58.2
	3	30.2	2.47	6.25	4.4	7.5	61.7	67.3	44.9
Water	1	19.4	1.58	6.25	4.04	7.5	63.9	67.3	43.5
	2	-	-	-	-	-	-	-	-
	3	30.0	2.45	6.25	3.7	7.5	67.2	64.5	40.5
Ethanol	1	30.3	2.47	6.25	4.4	7.5	66.3	72.7	48.0
	2	-	-	-	-	-	-	-	-
	3	30.0	2.45	6.25	4.4	7.5	67.6	72.8	48.1

Table 5.2 WF - FC-72, 1 TCT, $L^+ = 1.56$

WF - FC-72, 1 TCT, V^+ =7.5, L^+ =1.56											
# of TCT	L^+	V^+	Q	q	T_h	T_c	T_s	T_{air}	ΔT_T	u_{max}	U_T
1	1.56	7.5	10.2	0.84	60.4	56.7	39.1	21.5	38.9	0.0	214.5
1	1.56	7.5	10.2	0.84	53.9	50.2	32.3	21.5	32.4	6.8	256.6
1	1.56	7.5	10.2	0.84	53.7	50.2	32.6	21.5	32.2	4.4	258.4
1	1.56	7.5	10.2	0.84	53.9	50.0	32.7	21.5	32.4	3.8	259.6
1	1.56	7.5	10.2	0.84	54.7	50.2	32.2	21.5	33.2	3.3	258.0
1	1.56	7.5	10.2	0.84	71.4	51.1	33.7	21.5	49.9	2.4	251.8
1	1.56	7.5	15.0	1.22	65.3	66.1	43.8	22.0	43.3	0.0	247.9
1	1.56	7.5	15.0	1.22	65.1	59.7	36.1	22.1	43.0	6.8	283.3
1	1.56	7.5	15.0	1.22	65.2	59.6	36.0	22.1	43.1	4.4	284.9
1	1.56	7.5	15.0	1.22	65.7	59.9	36.5	22.1	43.6	3.8	283.7
1	1.56	7.5	15.0	1.22	65.9	60.1	37.2	22.1	43.8	3.3	281.0
1	1.56	7.5	15.0	1.22	84.0	60.4	37.5	22.1	61.9	2.4	279.5
1	1.56	7.5	19.6	1.7	74.7	77.0	48.9	22.1	52.6	0.0	258.2
1	1.56	7.5	19.6	1.7	76.0	67.4	38.3	22.1	53.9	6.8	304.0
1	1.56	7.5	19.6	1.7	76.3	68.7	39.3	22.1	54.2	4.4	296.5
1	1.56	7.5	19.6	1.7	76.3	69.1	39.7	22.1	54.2	3.8	294.9
1	1.56	7.5	19.6	1.7	77.2	69.1	39.3	22.1	55.1	3.3	294.7
1	1.56	7.5	19.6	1.7	77.2	70.1	41.2	22.1	55.1	2.4	289.8

Table 5.3 WF - FC-72, 1 TCT, $L^+ = 3.13$

WF - FC-72, 1 TCT, V^+ =7.5, L^+ =3.13											
# of TCT	L^+	V^+	Q	q	T_h	T_c	T_s	T_{air}	ΔT_T	U_T	u_{max}
1	3.13	7.5	10.3	0.84	59.5	55.9	37.0	21.1	38.4	218.1	0.0
1	3.13	7.5	10.3	0.84	52.2	48.5	29.2	21.1	31.1	268.8	6.1
1	3.13	7.5	10.3	0.84	52.3	48.6	29.4	21.1	31.2	268.0	4.4
1	3.13	7.5	10.3	0.84	53.0	49.1	29.6	21.1	31.9	262.6	3.8
1	3.13	7.5	10.3	0.84	53.2	49.5	30.3	22.0	31.2	268.(	3.2
1	3.13	7.5	10.3	0.84	52.6	49.3	30.7	22.2	30.4	274.8	2.4
1	3.13	7.5	10.3	0.84	54.3	50.6	31.4	22.0	32.3	258.8	1.9
1	3.13	7.5	15.0	1.22	73.5	68.2	44.9	22.2	51.3	238.5	0.0
1	3.13	7.5	15.0	1.22	63.7	57.9	32.7	22.1	41.6	294.0	6.1
1	3.13	7.5	15.0	1.22	62.5	56.7	32.6	22.1	40.4	303.3	4.4
1	3.13	7.5	15.0	1.22	63.0	57.3	33.0	22.1	40.9	299.3	3.8
1	3.13	7.5	15.0	1.22	63.3	57.4	33.3	22.1	41.2	297.2	3.2
1	3.13	7.5	15.0	1.22	62.3	56.1	33.6	22.1	40.2	304.2	2.4
1	3.13	7.5	15.0	1.22	62.5	57.2	33.8	22.1	40.4	302.8	2.2
1	3.13	7.5	19.6	1.6	85.6	78.4	49.2	21.5	64.1	249.2	0.0
1	3.13	7.5	19.6	1.6	77.9	62.0	38.3	21.5	56.4	283.6	6.1
1	3.13	7.5	19.6	1.6	77.5	70.5	40.0	22.8	54.7	292.0	4.4
1	3.13	7.5	19.6	1.6	73.8	35.4	35.9	21.5	52.3	305.6	3.8
1	3.13	7.5	19.6	1.6	74.1	66.8	36.3	21.5	52.6	303.8	3.2
1	3.13	7.5	19.6	1.6	74.1	66.9	36.8	21.5	52.6	303.7	2.4
1	3.13	7.5	19.6	1.6	74.1	67.2	37.3	21.5	52.6	303.8	1.9

Table 5.4 WF - FC-72, 1 TCT, $L^+ = 4.69$

WF - FC-72, 1 TCT, $V^+ = 7.5$, $L^+ = 4.69$											
# of TCT	L^+	V^+	Q	q	T_h	T_e	T_s	T_{air}	ΔT_T	u_{max}	U_T
1	4.69	7.5	10.2	0.84	60.7	56.7	36.8	21.5	39.2	0.0	213.4
1	4.69	7.5	10.2	0.84	50.9	47.1	25.9	21.5	29.4	4.4	284.4
1	4.69	7.5	10.2	0.84	50.7	46.9	26.1	21.5	29.2	3.8	286.1
1	4.69	7.5	10.2	0.84	55.0	51.5	31.5	21.5	33.5	3.2	249.9
1	4.69	7.5	10.2	0.84	56.0	52.2	31.7	21.5	34.5	2.4	242.5
1	4.69	7.5	10.2	0.84	56.0	52.3	31.8	21.5	34.5	1.9	242.3
1	4.69	7.5	10.2	0.84	56.2	52.5	31.9	21.5	34.7	1.7	240.8
1	4.69	7.5	15	1.22	75.3	70.1	43.2	21.5	53.8	0.0	227.5
1	4.69	7.5	15	1.22	62.3	56.8	29.1	21.5	40.8	4.4	299.9
1	4.69	7.5	15	1.22	62.4	57.0	29.4	21.5	40.9	3.8	299.6
1	4.69	7.5	15	1.22	62.0	56.6	28.8	21.5	40.5	3.2	302.2
1	4.69	7.5	15	1.22	63.3	57.8	29.9	22.2	41.1	2.4	297.7
1	4.69	7.5	15	1.22	63.1	57.7	30.3	22.2	40.9	1.9	299.6
1	4.69	7.5	15	1.22	63.9	58.4	30.7	22.2	41.7	1.7	293.5
1	4.69	7.5	19.6	1.6	87.0	79.9	47.7	22.0	65.0	0.0	245.8
1	4.69	7.5	19.6	1.6	75.4	67.8	30.4	21.8	53.6	5.4	298.1
1	4.69	7.5	19.6	1.6	74.6	67.2	30.8	21.7	52.9	4.4	302.4
1	4.69	7.5	19.6	1.6	74.1	66.7	31.3	21.8	52.3	3.8	305.8
1	4.69	7.5	19.6	1.6	72.8	65.3	31.2	21.8	51.0	3.2	313.4
1	4.69	7.5	19.6	1.6	76.4	69.2	37.1	23.2	53.2	2.4	300.2
1	4.69	7.5	19.6	1.6	76.3	69.1	37.0	23.6	52.7	1.9	303.0

Table 5.5 WF - FC-72, 1 TCT, $L^+ = 6.25$

WF - FC-72											
# of TCT	L^+	V^+	Q	q	T_h	T_e	T_s	T_{air}	ΔT_T	u_{max}	U_T
1	6.25	7.5	10.1	0.83	70.2	66.8	36.1	24.2	46.0	0	179.2
1	6.25	7.5	10.1	0.83	63.9	60.6	28.3	23.7	40.2	1.7	205.2
1	6.25	7.5	10.1	0.83	63.2	59.8	28.1	23.6	39.6	2.4	208.7
1	6.25	7.5	10.1	0.83	62.9	59.4	27	23.5	39.4	3.1	209.9
1	6.25	7.5	10.1	0.83	62.7	59.3	26.9	23.5	39.2	3.7	211.0
1	6.25	7.5	15.5	1.28	84.6	79.2	50.8	24.4	60.2	0	212.6
1	6.25	7.5	15.6	1.27	71.4	65.7	36.6	24.5	46.9	1.7	271.9
1	6.25	7.5	15.7	1.28	69.5	63.5	35.8	24.7	44.8	2.4	285.7
1	6.25	7.5	15.8	1.29	69.1	63.4	35.3	24.7	44.4	3.3	289.6
1	6.25	7.5	15.7	1.28	69	63.3	35	24.7	44.3	3.7	289.6
1	6.25	7.5	15.7	1.28	68.6	63.1	35.1	24.7	43.9	4.4	292.1
1	6.25	7.5	19.9	1.60	90.6	83.9	50.1	23.6	67.1	0	238.3
1	6.25	7.5	19.8	1.60	83.2	75.6	40.2	23.4	59.8	1.8	268.1
1	6.25	7.5	20.2	1.65	81.5	73.8	39.6	23.5	58.1	2.4	284.0
1	6.25	7.5	20.2	1.65	81.1	73.7	39	23.5	57.6	3.3	286.2
1	6.25	7.5	20.3	1.66	75.6	68.3	32.9	23.4	52.2	3.8	317.0
1	6.25	7.5	20.0	1.60	74.2	66.9	33.1	23.3	50.9	4.4	313.2

Table 5.6 WF - FC-72, 2 TCTs, $L^+ = 6.25$

WF - FC-72, 2 TCTs, $V^+ = 7.5$, $L^+ = 6.25$											
# of TCT	L^+	V^+	Q	q	T_h	T_e	T_s	T_{air}	ΔT_T	u_{max}	U_T
2	6.25	6	10.2	1.8	58.0	54.4	33.0	22.2	35.88	0.0	246.1
2	6.25	6	10.2	0.8	48.9	44.9	26.1	22.3	26.6	4.4	341.5
2	6.25	6	10.2	0.8	48.6	44.8	26.0	22.3	26.36	3.8	344.3
2	6.25	6	10.2	0.8	48.8	45.0	26.3	22.3	26.5	3.3	341.5
2	6.25	6	10.2	0.8	49.0	45.1	26.3	22.3	26.7	2.4	338.7
2	6.25	6	10.2	0.8	49.7	45.8	26.9	22.3	27.4	1.9	329.4
2	6.25	6	10.2	0.8	49.9	45.9	27.1	22.3	27.6	1.7	328.1
2	6.25	6	19.6	1.6	73.5	66.3	47.7	22.3	51.2	0.0	336.5
2	6.25	6	19.6	1.6	65.2	58.0	38.7	22.3	42.9	4.4	407.7
2	6.25	6	19.6	1.6	65.1	57.8	38.9	21.7	43.4	3.8	402.6
2	6.25	6	19.6	1.6	65.1	57.9	39.2	21.7	43.4	3.3	401.6
2	6.25	6	19.6	1.6	65.4	58.2	39.2	21.7	43.7	2.4	399.6
2	6.25	6	19.6	1.6	65.7	58.4	39.6	21.7	44.0	1.9	396.6
2	6.25	6	19.6	1.6	65.9	58.9	40.2	21,7	44.2	1.7	393.7
2	6.25	6	30.2	2.5	96.2	85.1	59.4	21.7	74.5	0.0	358.2
2	6.25	6	30.2	2.5	81.8	70.9	35.6	21.5	60.3	4.4	452.8
2	6.25	6	30.2	2.5	82.9	72.3	36.4	21.5	61.4	3.8	443.1
2	6.25	6	30.2	2.5	79.7	68.9	36.5	21.5	58.2	3.3	471.0
2	6.25	6	30.2	2.5	80.4	69.6	37.8	21.5	58.9	2.4	463.9
2	6.25	6	30.2	2.5	81.1	70.5	38.2	21.5	59.6	1.9	457.9

Table 5.7 WF - FC-72, 3 TCTs, $L^+ = 6.25$

WF - FC-72, 3 TCTs, $V^+ = 7.5$, $L^+ = 6.25$											
# of TCT	L^+	V^+	Q	q	T_h	T_e	T_s	T_{air}	ΔT_T	u_{max}	U_T
3	6.25	6	10.2	0.8	54.1	50.1	33.9	22.0	32.14	2.0	297.7
3	6.25	6	10.2	0.8	50.1	45.4	27.2	22.0	28.12	2.4	297.5
3	6.25	6	10.2	0.8	47.7	44.0	27.0	21.8	25.94	3.3	322.5
3	6.25	6	10.2	0.8	47.9	43.9	26.8	21.6	26.28	3.8	318.3
3	6.25	6	10.2	0.8	47.1	43.4	26.3	21.5	25.64	4.4	326.3
3	6.25	6	10.2	0.8	47.2	43.6	26.0	21.5	25.66	0.0	326.0
3	6.25	6	19.6	1.6	67.0	60.4	40.7	22.0	44.96	1.7	355.5
3	6.25	6	19.6	1.6	61.2	53.8	33.7	22.0	39.2	1.9	407.7
3	6.25	6	19.6	1.6	60.4	53.3	33.2	21.6	38.76	2.4	412.3
3	6.25	6	19.6	1.6	60.8	53.6	33.0	21.6	39.16	3.3	408.1
3	6.25	6	19.6	1.6	60.7	53.6	33.4	21.5	39.18	3.8	407.9
3	6.25	6	19.6	1.6	59.9	53.1	33.0	21.7	38.18	4.4	418.6
3	6.25	6	19.6	1.6	60.4	53.4	35.0	22.1	38.28	0.0	417.5
3	6.25	6	30.2	2.5	85.6	74.8	51.4	22.4	63.2	2.2	390.5
3	6.25	6	30.2	2.5	70.2	59.1	36.4	22.4	47.76	3.3	516.8
3	6.25	6	30.2	2.5	69.3	57.9	35.3	22.4	46.88	3.8	526.5
3	6.25	6	30.2	2.5	67.6	56.6	34.3	22.4	45.22	4.4	545.8
3	6.25	6	30.2	2.5	67.3	56.4	34.0	22.4	44.92	0.0	549.4
3	6.25	6	39.8	3.2	97.1	82.9	54.6	22.5	74.56	0.0	435.3

Table 5.8 WF - Ethanol, $L^+ = 6.25$

WF - Ethanol											
# of TCT	L^+	V^+	Q	q	T_h	T_c	T_s	T_{air}	ΔT_T	u_{max}	U_T
1	6.25	7.5	10.1	0.83	61.7	58.2	47.2	24.1	37.6	4.4	220.7
1	6.25	7.5	9.6	0.79	61.9	58.5	47.3	24.1	37.8	3.0	208.8
1	6.25	7.5	10.1	0.83	62.2	58.8	47.7	24.2	38.0	1.7	218.3
1	6.25	7.5	15.6	1.28	68.7	63.1	48.1	24.2	44.5	4.4	287.5
1	6.25	7.5	15.7	1.28	69.3	63.5	48.3	24.2	45.1	3.4	283.9
1	6.25	7.5	15.7	1.28	69.3	63.7	48.7	24.3	45.0	1.6	284.4
1	6.25	7.5	20.2	1.65	73.6	66.3	49.1	24.4	49.2	4.4	335.5
1	6.25	7.5	19.4	1.59	74.9	65.2	48.3	24.5	50.4	1.7	315.7
1	6.25	7.5	25.5	2.08	76.3	66.9	48.1	24.6	51.7	4.4	402.5
1	6.25	7.5	25.6	2.09	77.6	67.9	49.1	24.7	52.9	1.7	395.4
1	6.25	7.5	30.3	2.47	72.7	60.4	47.8	24.7	48.0	4.4	514.6
3	6.25	7.5	29.3	2.39	72.8	61.8	48.1	24.7	48.1	4.4	496.5
3	6.25	7.5	29.3	2.39	72.7	62.0	48.2	24.7	48.0	4.1	497.5
3	6.25	7.5	29.3	2.39	73.0	62.1	48.5	24.7	48.3	3.4	494.6
3	6.25	7.5	29.3	2.39	73.2	62.1	48.7	24.7	48.5	2.4	493.0
3	6.25	7.5	29.9	2.44	73.8	62.8	49.7	24.7	49.1	1.8	496.7
3	6.25	7.5	29.4	2.40	78.9	68.4	57.0	24.7	54.2	0.0	443.0

Table 5.9 WF - R-113, 1 and 2 TCTs, $L^+ = 6.25$

WF - R-113											
# of TCT	L^+	V^+	Q	q	T_h	T_e	T_s	T_{air}	ΔT_T	u_{max}	U_T
1	6.25	2.5	20.1	1.64	78.7	70.7	33.8	23.0	55.7	3.7	294.5
1	6.25	2.5	20.1	1.64	78.1	71.1	35.7	23.0	55.1	1.2	297.3
1	6.25	5	20.5	1.67	78.7	71.2	37.5	23.0	55.7	1.2	300.3
1	6.25	7.5	10.3	0.84	47.6	43.4	30.7	26.8	20.8	4.2	404.7
1	6.25	7.5	20.7	1.69	73.6	66.6	33.3	26.8	46.8	4.3	360.6
1	6.25	7.5	20.5	1.68	78.5	71.1	37.7	23.0	55.5	1.2	302.0
1	6.25	7.5	20.5	1.68	78.4	71.0	36.3	23.0	55.4	3.7	302.5
1	6.25	7.5	29.5	2.41	90.4	80.7	35.7	25.3	65.1	4.3	370.3
1	6.25	8.75	20.3	1.66	79.5	71.9	36.0	23.0	56.5	1.6	293.7
1	6.25	8.75	20.3	1.66	79.3	71.2	35.0	23.0	56.3	1.6	294.7
1	6.25	8.75	24.6	2.00	82.6	74.0	35.1	23.0	59.6	3.4	336.3
1	6.25	10	20.3	1.66	79.5	72.4	39.8	23.0	56.5	1.1	292.9
1	6.25	10	20.3	1.66	79.7	72.6	39.1	23.0	56.7	3.7	292.2
2	6.25	7.5	30.2	2.46	75.6	64.3	49.8	25.9	49.7	4.3	496.0
2	6.25	7.5	39.8	3.25	87.5	73.7	51.8	25.9	61.6	4.3	526.6

Table 5.10 WF - R-113, 3 TCTs, $L^+ = 6.25$

WF - R-113											
# of TCT	L^+	V^+	Q	q	T_h	T_e	T_s	T_{air}	ΔT_T	u_{max}	U_T
3	6.25	7.5	39.9	3.25	77.5	61.2	36.4	25.9	51.6	4.3	630.8
3	6.25	7.5	39.9	3.25	76.4	61.0	36.8	25.8	50.6	3.3	642.7
3	6.25	7.5	40.7	3.32	78.0	62.8	39.3	25.8	52.2	1.7	636.7
3	6.25	7.5	45.5	3.71	81.8	65.7	36.7	25.8	56.0	4.3	663.5
3	6.25	7.5	45.4	3.71	82.5	65.8	37.5	25.8	56.7	3.3	653.5
3	6.25	7.5	45.4	3.70	84.6	67.5	40.1	25.8	58.8	1.7	629.7
3	6.25	10	31.5	2.57	75.4	64.4	42.1	23.9	51.5	3.4	498.7
3	6.25	12.5	31.5	2.57	69.5	57.6	47.7	23.9	45.6	3.4	563.5
3	6.25	12.5	31.4	2.56	69.5	57.6	48.1	23.8	45.7	3.0	560.9
3	6.25	12.5	31.5	2.57	69.5	57.7	48.6	23.9	45.6	1.6	563.9
3	6.25	17.5	31.6	2.58	77.4	66.1	57.9	23.9	53.5	3.4	481.2
3	6.25	22.5	31.5	2.57	82.8	72.1	63.3	23.9	58.9	2.9	436.7

Table 5.11 WF - R-11, $L^+ = 6.25$

WF - R-11											
# of TCT	L^+	V^+	Q	q	T_h	T_e	T_s	T_{air}	ΔT_T	u_{max}	U_T
1	6.25	7.5	17.4	1.42	63.6	60.5	34.6	26.8	36.8	4.4	386.7
1	6.25	7.5	17.3	1.41	67.6	62.0	36.6	26.8	40.8	1.4	345.8
1	6.25	7.5	25.0	2.04	75.7	67.6	36.7	26.8	48.9	4.1	416.5
1	6.25	7.5	24.9	2.03	77.9	69.7	39.8	26.8	51.1	1.4	397.7
2	6.25	7.5	30.1	2.46	69.6	58.7	37.2	26.8	42.8	4.4	575.0
2	6.25	7.5	35.2	2.87	73.2	60.6	38.1	26.8	46.4	4.4	619.1
2	6.25	7.5	40.6	3.32	79.7	65.7	38.9	26.8	52.9	4.4	627.6
2	6.25	7.5	45.4	3.71	87.1	70.9	40.7	26.8	60.3	4.4	614.5
3	6.25	7.5	40.8	3.33	61.1	45.7	38.0	26.8	34.3	4.4	970.5
3	6.25	7.5	45.4	3.71	64.3	46.8	39.3	26.8	37.5	4.4	988.7
3	6.25	7.5	45.4	3.71	68.6	51.4	43.9	26.8	41.8	1.4	887.9
3	6.25	7.5	49.9	4.07	67.9	48.3	40.7	26.8	41.1	4.4	990.1
3	6.25	7.5	59.6	4.87	74.2	51.6	42.5	26.8	47.4	4.4	1027.6
3	6.25	7.5	60.0	4.89	75.9	52.8	44.1	26.8	49.1	3.0	996.9
3	6.25	7.5	60.1	4.91	80.1	57.1	48.5	26.8	53.3	1.5	921.2
3	6.25	7.5	50.0	4.08	68.7	48.8	41.1	26.8	41.9	4.3	974.6
3	6.25	7.5	50.2	4.10	69.8	49.9	42.4	26.8	43.0	3.0	952.8
3	6.25	7.5	50.1	4.09	72.8	53.6	45.9	26.8	46.0	1.6	888.8
3	6.25	7.5	64.6	5.27	82.8	58.4	49.3	26.8	56.0	1.6	941.8
3	6.25	7.5	63.6	5.19	79.4	54.4	44.7	26.8	52.6	3.0	986.5

Table 5.12 WF - FC-87, 1 and 2 TCTs, $L^+ = 6.25$

WF - FC87											
# of TCT	L^+	V^+	Q	q	T_h	T_c	T_s	T_{air}	ΔT_T	u_{max}	U_T
1	6.25	7.50	10.2	0.84	57.8	54.1	30.5	22.2	35.6	0.0	235.3
1	6.25	7.50	10.2	0.84	48.6	44.8	28.1	21.6	27.0	1.9	310.1
1	6.25	7.50	10.2	0.84	48.1	44.3	27.7	21.6	26.5	2.4	315.4
1	6.25	7.50	10.2	0.84	47.4	43.7	27.1	21.2	26.2	3.2	319.5
1	6.25	7.50	10.2	0.84	47.3	43.4	26.9	21.1	26.2	3.8	319.3
1	6.25	7.50	10.2	0.84	47.0	43.2	26.7	21.1	25.9	4.4	322.8
1	6.25	7.50	19.6	1.60	81.7	74.7	48.1	21.0	60.7	0.0	263.5
1	6.25	7.50	19.6	1.60	68.6	61.2	32.3	21.5	47.1	1.9	339.6
1	6.25	7.50	19.6	1.60	68.4	60.9	31.8	21.4	47.0	2.4	340.2
1	6.25	7.50	19.6	1.60	68.2	60.9	31.5	21.4	46.8	3.2	341.5
1	6.25	7.50	19.6	1.60	66 8	59.6	30.9	21.3	45.5	3.8	350.9
1	6.25	7.50	19.6	1.60	65.9	58.8	30.6	21.3	44.6	4.4	358.0
2	6.25	3.13	10.3	0.84	54.7	50.6	29.6	24.5	30.2	4.4	276.8
2	6.25	3.13	19.6	1.60	64.8	57.9	31.2	24.5	40.3	4.4	396.4
2	6.25	3.13	29.4	2.40	78.6	68.2	33.6	24.5	54.1	4.4	443.8
2	6.25	3.13	35.5	2.90	89.7	75.9	35.5	24.5	65.2	4.4	444.9

Table 5.13 WF - FC-87, 3 TCTs, $L^+ = 6.25$

WF - FC-87											
# of TCT	L^+	V^+	Q	q	T_h	T_e	T_s	T_{air}	ΔT_T	u_{max}	U_T
3	6.25	7.50	39.8	3.25	78.0	63.1	35.2	21.3	56.7	1.9	572.8
3	6.25	7.50	39.8	3.25	76.2	61.3	33.9	21.5	54.7	2.4	593.8
3	6.25	7.50	39.8	3.25	74.0	59.1	34.4	22.8	51.2	3.2	634.6
3	6.25	7.50	39.8	3.25	74.0	58.8	34.8	22.8	51.2	3.8	635.3
3	6.25	7.50	39.8	3.25	73.3	58.3	34.1	22.8	50.5	4.4	644.1
3	6.25	7.50	45.3	3.70	99.3	82.4	56.5	22.7	76.6	0.0	482.5
3	6.25	7.50	45.3	3.70	82.0	64.4	38.3	22.7	59.3	2.2	623.6
3	6.25	7.50	45.3	3.70	81.1	63.5	37.5	22	59.1	2.4	625.5
3	6.25	7.50	45.3	3.70	78.5	61.7	37.4	24.3	54.2	3.2	682.5
3	6.25	7.50	45.3	3.70	78.6	61.9	37.1	24.3	54.3	3.8	680.5
3	6.25	7.50	45.3	3.70	78.3	61.3	36.6	24.3	54.0	4.4	685.3
3	6.25	7.50	53.3	4.35	88.9	68.6	40.4	23.8	65.1	1.9	667.9
3	6.25	7.50	53.3	4.35	88.4	68.5	40.1	23.8	64.6	2.4	673.1
3	6.25	7.50	53.3	4.35	85.5	64.9	36.6	22.1	63.4	3.2	686.3
3	6.25	7.50	53.3	4.35	84.4	64.1	36.0	22.1	62.3	3.8	698.8
3	6.25	7.50	53.3	4.35	84.3	63.9	35.8	22.8	61.5	4.4	707.9

Table 5.14 WF - acetone, $L^+ = 6.25$

WF - Acetone											
# of TCT	L^+	V^+	Q	q	T_h	T_e	T_s	T_{air}	ΔT_T	u_{max}	U_T
1	6.25	6.0	10.1	0.83	40.1	36.2	24.7	22.7	17.4	4.4	476.5
1	6.25	6.0	20.3	1.66	50.6	43.1	27.4	22.6	28.0	4.4	592.0
1	6.25	6.0	30.1	2.46	81.4	71.4	28.9	23.0	58.4	4.4	421.4
2	6.25	7.5	50.0	4.08	74.0	55.1	30.6	20.8	53.2	4.4	766.3
2	6.25	7.5	39.8	3.25	63.7	48.7	28.8	20.6	43.1	4.4	754.8
2	6.25	7.5	31.3	2.56	55.0	43.2	27.0	20.2	34.8	4.4	735.2
2	6.25	7.5	20.2	1.65	45.7	37.9	25.2	20.2	25.5	4.4	647.6
3	6.25	7.5	10.3	0.84	41.3	37.8	29.3	22.4	18.9	4.4	443.5
3	6.25	7.5	19.6	1.6	48.5	41.2	31.0	22.4	26.1	4.4	613.0
3	6.25	7.5	30.2	2.46	56.4	45.3	32.6	24.1	32.3	4.4	762.1
3	6.25	7.5	40.6	3.32	63.7	48.4	34.9	24.6	39.1	4.4	850.0
3	6.25	7.5	51.0	4.16	70.6	51.4	36.5	24.8	45.8	4.4	907.9
3	6.25	7.5	60.0	4.9	77.4	54.4	38.2	25.0	52.4	4.4	935.8
3	6.25	7.5	60.4	4.93	91.0	69.7	39.0	25.0	66.0	3.4	747.2
3	6.25	9.4	59.6	4.86	93.6	71.3	40.0	23.8	69.8	1.9	696.3
3	6.25	9.4	59.6	4.86	92.0	69.6	38.2	23.8	68.2	2.4	713.0
3	6.25	9.4	59.6	4.86	90.6	68.3	36.2	23.8	66.8	3.3	727.8
3	6.25	9.4	59.6	4.86	90.2	67.8	35.3	23.8	66.4	3.8	731.9
3	6.25	9.4	39.4	3.21	63.3	47.9	36.6	24.4	38.9	1.9	824.8
3	6.25	9.4	39.4	3.21	61.8	46.3	34.2	24.4	37.4	3.4	858.3
3	6.25	9.4	39.4	3.21	61.4	45.7	33.5	24.4	37.0	3.8	868.0
3	6.25	9.4	39.4	3.21	61.5	45.7	33.2	24.4	37.1	4.4	866.2

Table 5.15 WF - water, $L^+ = 6.25$

WF - Water											
# of TCT	L^+	V^+	Q	q	T_h	T_e	T_s	T_{air}	ΔT_T	u_{max}	U_T
1	6.25	7.5	10.0	0.82	49.8	46.6	31.4	23.6	26.2	3.7	311.0
1	6.25	7.5	15.8	1.29	59.1	53.4	33.9	23.7	35.4	3.7	364.4
1	6.25	7.5	19.4	1.59	67.3	60.8	35.0	23.8	43.5	4.0	364.1
1	6.25	7.5	23.5	1.92	81.9	74.4	35.8	23.8	58.1	4.0	330.0
3	6.25	7.5	9.6	0.78	45.7	42.4	26.9	23.8	21.9	3.7	356.9
3	6.25	7.5	19.5	1.59	52.6	45.5	30.6	23.9	28.7	3.7	554.3
3	6.25	7.5	30.1	2.46	64.5	54.0	32.6	23.9	40.6	3.7	605.6
3	6.25	7.5	38.4	3.13	79.3	65.2	34.5	23.9	55.4	3.7	565.9
3	6.25	7.5	30.3	2.47	68.3	57.1	33.8	23.9	44.4	3.7	556.5
3	6.25	7.5	30.3	2.47	68.4	57.3	34.3	24.0	44.4	2.7	556.8
3	6.25	7.5	30.3	2.47	69.0	58.1	35.0	24.0	45.0	2.1	549.8
3	6.25	7.5	30.3	2.47	69.2	58.3	35.4	24.0	45.2	1.7	546.7
3	6.25	7.5	30.3	2.47	69.4	58.5	35.7	24.0	45.4	1.4	544.0
3	6.25	7.5	30.3	2.47	85.5	74.5	51.7	24.0	61.5	0.0	402.0

Table 5.16 WF - FC-87, 1 TCT, $L^+ = 6.25$ (Effect of V^+)

WF - FC87											
# of TCT	L^+	V^+	Q	q	T_h	T_e	T_s	T_{air}	ΔT_T	u_{max}	U_T
1	6.25	1.88	10.4	0.85	57.7	53.8	29.8	24.5	33.2	4.4	255.0
1	6.25	1.88	15.0	1.22	64.9	59.6	31.8	24.5	40.4	4.4	302.7
1	6.25	1.88	19.7	1.61	86.1	79.7	32.3	24.5	61.6	4.4	261.0
1	6.25	3.13	11.0	0.90	45.5	41.6	25.4	20.7	24.8	4.4	360.8
1	6.25	3.13	14.7	1.20	51.8	46.4	26.8	20.7	31.1	4.4	386.4
1	6.25	3.13	20.2	1.65	60.2	53.2	28.4	20.7	39.5	4.4	416.8
1	6.25	3.13	24.6	2.00	68.2	59.2	29.4	20.7	47.5	4.4	421.8
1	6.25	3.13	29.4	2.40	85.1	74.1	30.6	20.7	64.4	4.4	372.9
1	6.25	6.25	10.1	0.82	54.9	50.8	25.7	20.7	34.2	4.4	239.9
1	6.25	6.25	14.9	1.22	62.2	56.7	26.6	20.7	41.5	4.4	292.7
1	6.25	6.25	20.2	1.65	70.5	63.2	28.3	20.7	49.8	4.4	330.5
1	6.25	6.25	24.5	2.00	77.4	68.5	29.1	20.7	56.7	4.4	352.2
1	6.25	6.25	29.4	2.40	98.6	87.9	30.3	20.7	77.9	4.4	308.0
1	6.25	9.38	10.1	0.82	72.5	69.6	28.7	24.3	48.2	4.4	170.6
1	6.25	9.38	14.8	1.21	84.2	79.6	29.1	24.2	60.0	4.4	201.7
1	6.25	9.38	19.6	1.60	92.2	85.6	30.6	24.2	68.0	4.4	235.4

Table 5.17 WF - FC-87, 3 TCTs, $L^+ = 6.25$ (Effect of V^+)

WF - FC87											
# of TCT	L^+	V^+	Q	q	T_h	T_c	T_s	T_{air}	ΔT_T	u_{max}	U_T
3	6.25	3.13	34.5	2.82	77.3	63.3	34.7	24.9	52.4	4.4	537.9
3	6.25	3.13	41.3	3.37	85.2	68.7	36.0	24.9	60.3	4.4	558.9
3	6.25	3.13	30.2	2.47	72.3	60.1	34.0	24.9	47.4	4.4	520.7
3	6.25	4.69	30.3	2.47	71.3	59.3	33.8	24.9	46.4	4.4	532.8
3	6.25	4.69	34.6	2.82	75.2	61.6	34.7	24.9	50.3	4.4	561.2
3	6.25	4.69	41.2	3.36	82.2	65.9	36.0	24.9	57.3	4.4	586.3
3	6.25	6.25	30.4	2.48	70.8	58.8	33.8	24.9	45.9	4.4	540.5
3	6.25	6.25	35.3	2.88	75.6	61.8	34.7	24.8	50.8	4.4	566.8
3	6.25	6.25	39.5	3.22	80.5	64.9	35.6	25	55.5	4.4	580.5
3	6.25	6.25	45.7	3.73	83.4	64.9	36.8	25.1	58.3	4.4	640.0
3	6.25	6.25	51.3	4.18	89.2	69.1	38.2	25.1	64.1	4.4	652.9
3	6.25	9.38	31.6	2.58	66.2	54.1	34.0	24.8	41.4	4.4	623.7
3	6.25	9.38	34.5	2.81	69.4	56.2	34.5	24.8	44.6	4.4	631.3
3	6.25	9.38	39.2	3.20	73.5	58.7	35.3	24.8	48.7	4.4	657.6
3	6.25	9.38	45.5	3.71	79.3	62	36.2	24.8	54.5	4.4	681.5
3	6.25	9.38	51.2	4.18	87.9	68.1	38.5	24.7	63.2	4.4	660.9

Table 5.18 WF - acetone, 3 TCTs, $L^+ = 6.25$ (Effect of V^+)

WF - Acetone											
# of TCT	L^+	V^+	Q	q	T_h	T_e	T_s	T_{air}	ΔT_T	u_{max}	U_T
3	6.25	3.13	20.4	1.67	50.3	42.6	29.3	24.6	25.7	4.4	650.3
3	6.25	3.13	30.1	2.46	58.5	47.2	31.0	24.5	34.0	4.4	722.7
3	6.25	3.13	42.0	3.43	65.9	49.6	33.3	24.5	41.4	4.4	828.5
3	6.25	3.13	49.8	4.07	71.3	51.5	34.7	24.5	46.8	4.4	870.0
3	6.25	3.13	61.5	5.02	83.0	59.3	36.6	24.5	58.5	4.4	858.7
3	6.25	6.25	20.6	1.68	46.3	37.8	26.1	22.9	23.4	4.4	717.3
3	6.25	6.25	29.4	2.40	50.2	38.7	25.6	21.2	29.0	4.4	827.0
3	6.25	6.25	41.1	3.35	58.1	42.1	28.0	20.7	37.4	4.4	894.8
3	6.25	6.25	50.0	4.08	64.5	44.8	29.6	20.5	44.0	4.4	926.4
3	6.25	6.25	55.2	4.50	81.4	60.4	30.8	20.3	61.1	4.4	736.5
3	6.25	9.38	20.2	1.65	44.8	36.5	25.0	20.2	24.6	4.4	669.6
3	6.25	9.38	29.4	2.40	51.0	39.5	26.4	20.0	31.0	4.4	774.2
3	6.25	9.38	41.0	3.35	57.7	42.0	28.3	20.0	37.7	4.4	888.1
3	6.25	9.38	49.5	4.04	63.5	44.6	29.1	20.0	43.5	4.4	927.9
3	6.25	9.38	56.0	4.57	67.8	46.0	30.4	20.0	47.8	4.4	956.5
3	6.25	9.38	61.7	5.04	72.4	47.8	31.8	20.0	52.4	4.4	962.2

Table 5.19 WF - R-113, 3 TCTs, $L^+ = 6.25$ (Effect of V^+)

WF - R-113, Q = 30 W, L+ = 6.25, T_{air} =25 °C			
# of TCT	V^+	ΔT_T	u_{max}
3	2.5	61.0	1.7
3	5	51.3	1.7
3	7.5	52.2	1.7
3	10	49.0	1.7
3	12.5	44.9	1.7
3	2.5	57.3	2.5
3	5	50.8	2.5
3	7.5	47.0	2.5
3	10	51.4	2.5
3	12.5	45.1	2.5
3	2.5	56	3.7
3	12.5	45.2	3.7
3	17.5	53.2	3.7
3	22.5	58.8	3.7

Table 5.20 WF - FC-87, 3 TCTs, $V^+ = 9.38$ (Effect of L^+)

WF - FC-87								
# of TCT	L^+	V^+	Q	q	T_h	T_s	T_{air}	u_{max}
3	1.56	9.38	50.1	4.09	97.6	49.7	24.8	4.4
3	3.13	9.38	50.2	4.10	93.9	44.6	24.8	4.4
3	4.69	9.38	51.2	4.18	89.9	40.9	24.8	4.4
3	6.25	9.38	51.2	4.18	87.9	38.5	24.7	4.4

Table 5.21 WF - acetone, 3 TCTs, $V^+ = 9.38$ (Effect of L^+)

WF - Acetone								
# of TCT	L^+	V^+	Q	q	T_h	T_s	T_{air}	u_{max}
3	1.56	9.38	40.8	3.33	90.08	45.87	24.4	4.4
3	3.13	9.38	40.8	3.33	90.20	45.50	24.4	4.4
3	4.69	9.38	40.8	3.33	90.58	41.40	24.4	4.4
3	6.25	9.38	40.8	3.33	91.96	39.83	24.4	4.4
3	1.56	9.38	51.2	4.18	73.3	47.6	24.4	4.4
3	3.13	9.38	51.2	4.18	67.96	41.83	24.4	4.4
3	4.69	9.38	51.2	4.18	64.56	38.13	24.4	4.4
3	6.25	9.38	51.2	4.18	61.46	36.13	24.4	4.4
3	1.56	9.38	59.6	4.87	66.54	47.4	24.4	4.4
3	3.13	9.38	59.6	4.87	62.42	41.6	24.4	4.4
3	4.69	9.38	59.6	4.87	59.68	37.86	24.4	4.4
3	6.25	9.38	59.6	4.87	57.90	35.03	24.4	4.4

Table 5.22 WF - FC-72, $L^+ = 6.25$ (Effect of Non-condensible gas)

WF - FC-72, $V^+ = 7.5$, $L^+ = 6.25$, $u_{max} = 3.7$ m/s, $T_{air} = 24.8$ °C		
Thermocouple	with Non-condensible gas (°C)	degassing (°C)
Heater	70.2	59.0
Evaporator	67.8	55.4
Transportation Zone	42.7	31.7
Condenser	25.0	27.0
Air	24.8	24.8

Table 5.23 WF - FC-87, $L^+ = 6.25$, $u_{max} = 0$ (Effect of Absence of Cooling Fan)

WF - FC-87, $L^+ = 6.25$											
# of TCT	L^+	V^+	Q	q	T_h	T_c	T_s	T_{air}	ΔT_T	u_{max}	U_T
3	6.25	9.38	20.4	1.66	62.4	54.8	41.7	24.5	37.9	0.0	438.5
3	6.25	9.38	24.6	2.00	67.6	58.8	44.0	24.5	43.1	0.0	464.6
3	6.25	9.38	28.4	2.32	76.1	65.3	48.6	24.5	51.6	0.0	448.9
3	6.25	9.38	34.2	2.79	86.2	73.1	53.4	24.5	61.7	0.0	452.4
3	6.25	12.50	20.3	1.66	59.4	51.8	38.4	21.8	37.6	0.0	440.7
3	6.25	12.50	24.6	2.00	65.2	55.8	40.6	20.7	44.5	0.0	450.8
3	6.25	12.50	28.1	2.29	71.5	60.8	44.5	20.8	50.7	0.0	452.7
3	6.25	12.50	33.2	2.71	78.4	65.6	47.1	20.5	57.9	0.0	467.9
3	6.25	12.50	43.9	3.58	92.3	75.4	52.5	20.4	71.9	0.0	498.5

Table 5.24 WF - acetone, $L^+ = 6.25$, $u_{max} = 0$ (Effect of Absence of Cooling Fan)

WF - acetone											
# of TCT	L^+	V^+	Q	q	T_h	T_e	T_s	T_{air}	ΔT_T	u_{max}	U_T
3	6.25	9.38	50.0	4.08	89.6	69.1	61.7	24.1	65.5	0.0	622.7
3	6.25	9.38	42.6	3.48	82.9	65.5	58.1	24.2	58.7	0.0	593.0
3	6.25	9.38	36.8	3.00	77.9	62.8	55.5	24.2	53.7	0.0	559.1
3	6.25	9.38	30.3	2.47	69.6	57.7	50.4	24.2	45.4	0.0	544.1
3	6.25	9.38	20.4	1.67	60.6	52.3	45.1	24.2	36.4	0.0	459.0
3	6.25	9.38	10.3	0.84	47.2	43.0	36.7	24.0	23.2	0.0	362.1

Table 5.25 WF - FC-87, $L^+ = 6.25$ (Temperature of Fan off)

WF - acetone, 3 TCTs, V+ =6.25, umax =4.4 m/s, Tair = 21.5, Q = 53.3 W	
Time (min)	Temperature of the Heater center (°C)
0	58.2
1	59.6
2	62.5
3	64.8
4	66.2
5	67.7
6	69.0
10	72.3

WF - acetone, 3 TCTs, V+ =6.25, umax =4.4 m/s, Tair = 21.5, Q = 53.3 W	
Time (min)	Temperature of the Heater center (°C)
0	58.2
15	75.5
20	77.5
27	79.1
35	79.2
40	79.7
45	80.1
51	80.2
55	80.3

Table 5.26 WF - FC-87, $L^+ = 6.25$ (Temperature from Startup)

WF - FC-87, 3 TCTs, L^+ =6.25, $V^+ = 12.5$, $T_{air} = 24.5$ °C, u_{max} =4.4 m/s									
Time (hour)	Q	q	T_h	T_e	T_s	T_{air}	ΔT_T	u_{max}	U_T
1	51.1	4.18	86.2	63.0	38.2	21.5	64.7	4.4	644.7
2	50.2	4.10	87.3	63.2	39.0	22.4	64.9	4.4	631.4
4	51.6	4.22	88.1	67.4	40.2	22.9	65.2	4.4	647.0
5	51.2	4.18	87.4	67	39.9	22.9	64.5	4.4	648.4
6	51.3	4.18	87.6	67.1	39.9	23.1	64.5	4.4	648.8

WF - FC-87, 3 TCTs, L^+ =6.25, V^+ = 12.5, T_{air} = 24.5 °C, u_{max} =4.4 m/s									
Time (hour)	Q	q	T_h	T_e	T_s	T_{air}	ΔT_T	u_{max}	U_T
7	51.2	4.18	87.6	67.2	39.9	23.3	64.3	4.4	650.2
8	51.2	4.18	86.7	66.7	39.4	23.3	63.4	4.4	659.0
9	51.3	4.19	87.3	66.9	39.6	23.5	63.8	4.4	656.7
14	50.1	4.09	86.6	66.4	39.1	24.3	62.3	4.4	656.7
17	50.1	0.00	85.1	65.1	37.8	24	61.1	4.4	656.7
19	50.1	0.00	85.3	65.2	38.4	24.2	61.1	4.4	656.7

1. Heating Element
2. Cooper Plate
3. Filler
4. Heating Plate
5. Nylon Box
6. Brass Tube
7. Back Channel
8. Fan
9. Fins
10. Probe
11. Front Channel
12. Grooves
13. Thermocouples Assembly
14. Thermocouple
15. Valves
16. Measuring vessel with piston
17. Additional Thermosyphon

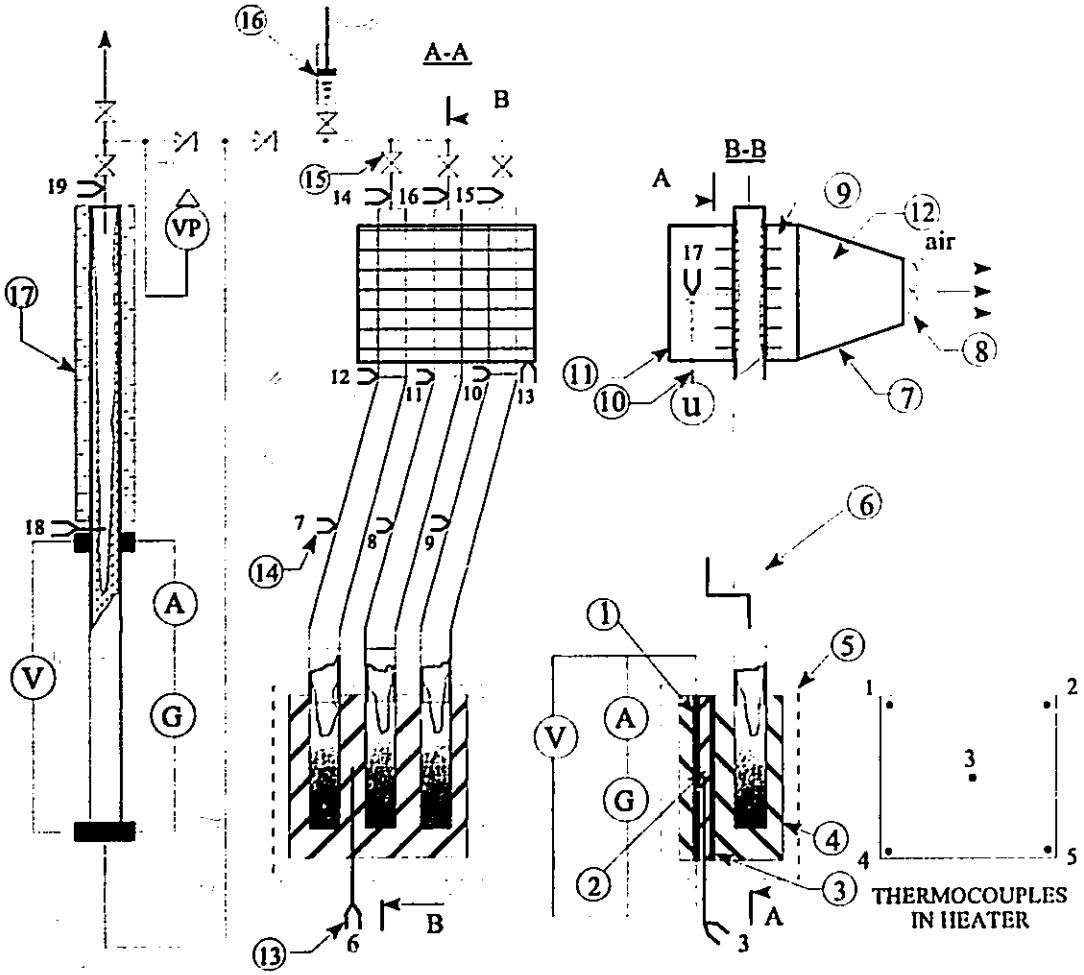

Figure 3.1(a) Experimental Apparatus

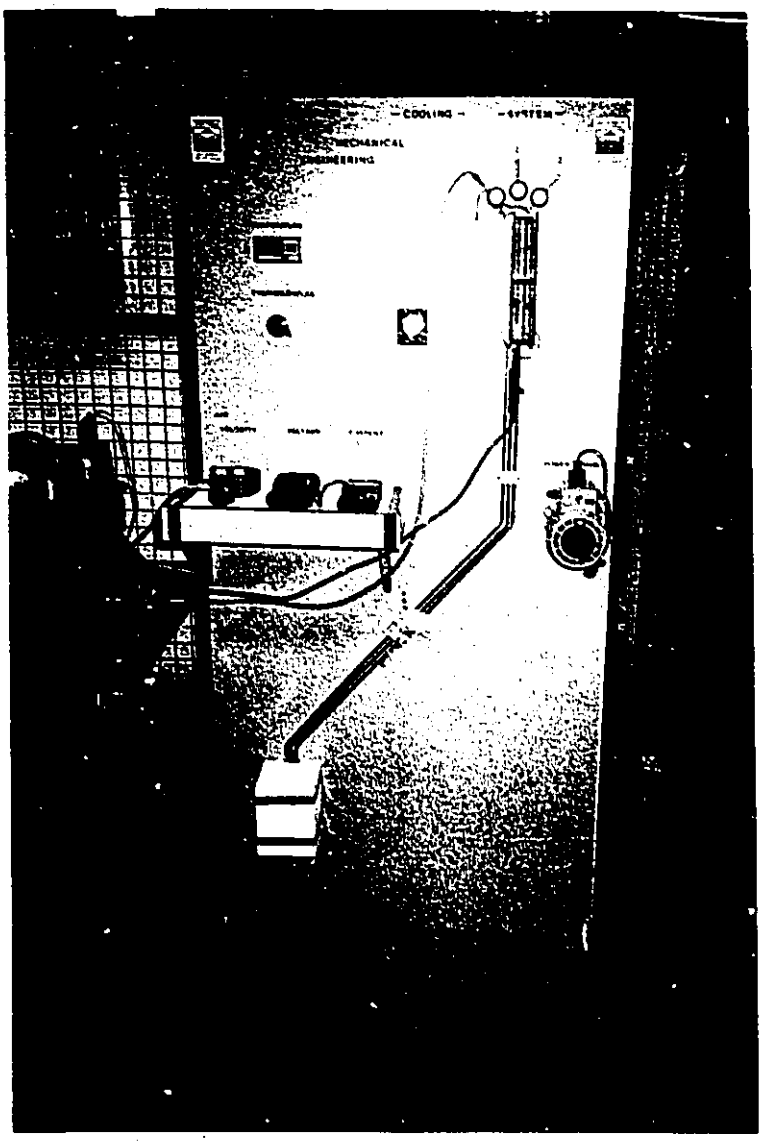

Figure 3.1(b) Experimental Setup

Item	Thermosyphon Evaporator
Unit	mm
Date	May 1995

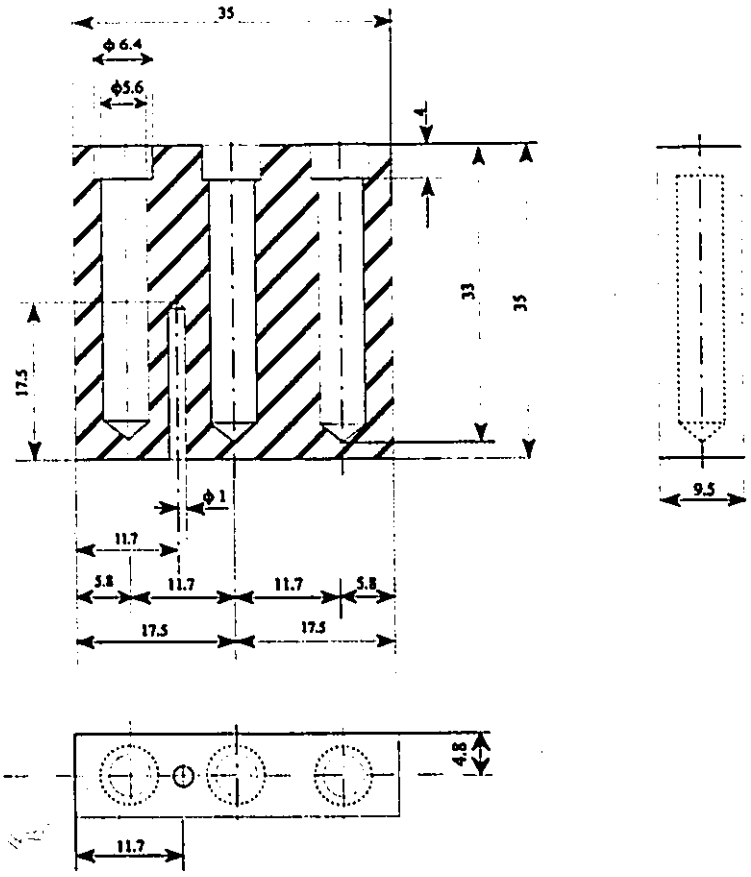

Figure 3.2 Evaporator Section

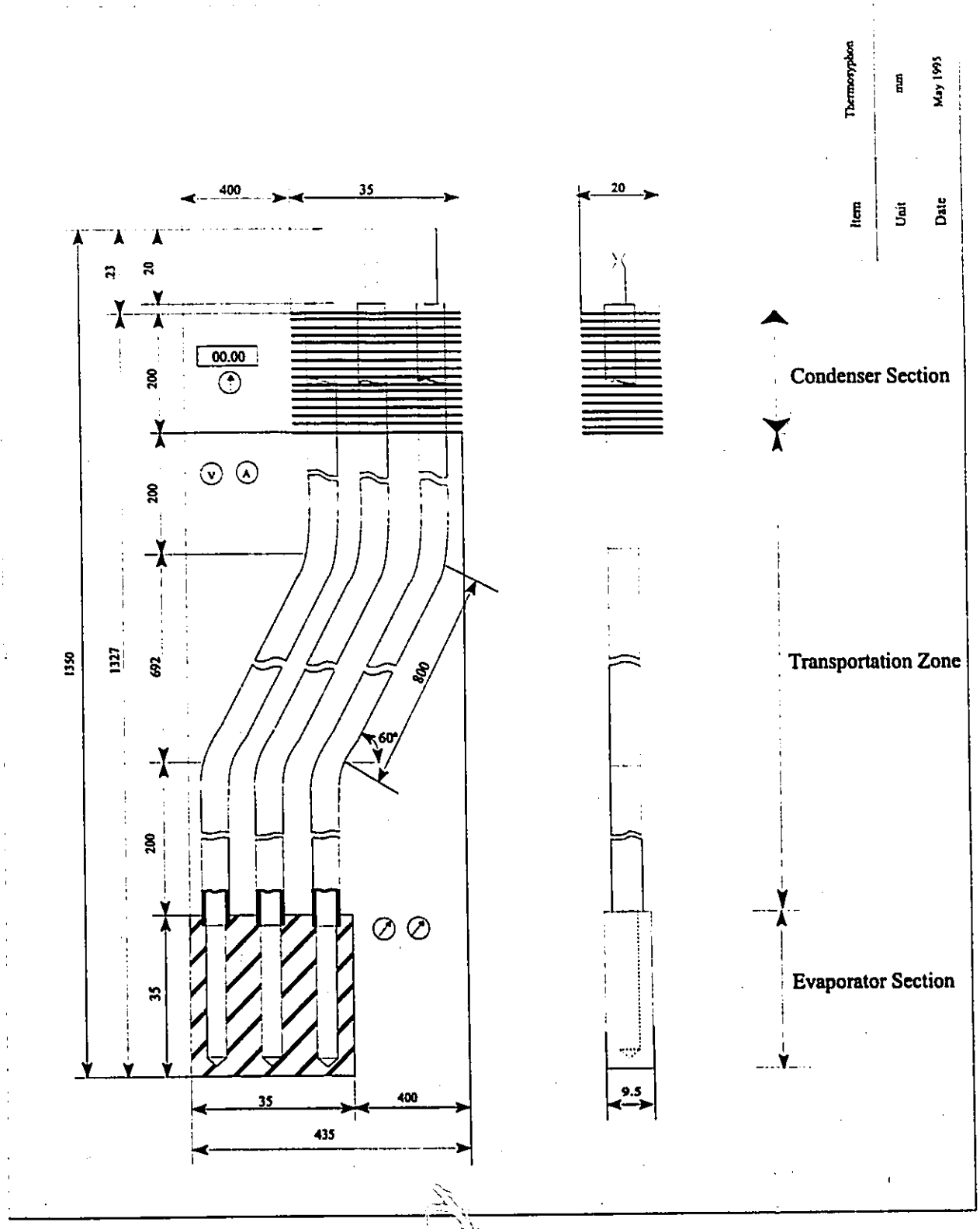

Figure 3.3(a) Test Assembly

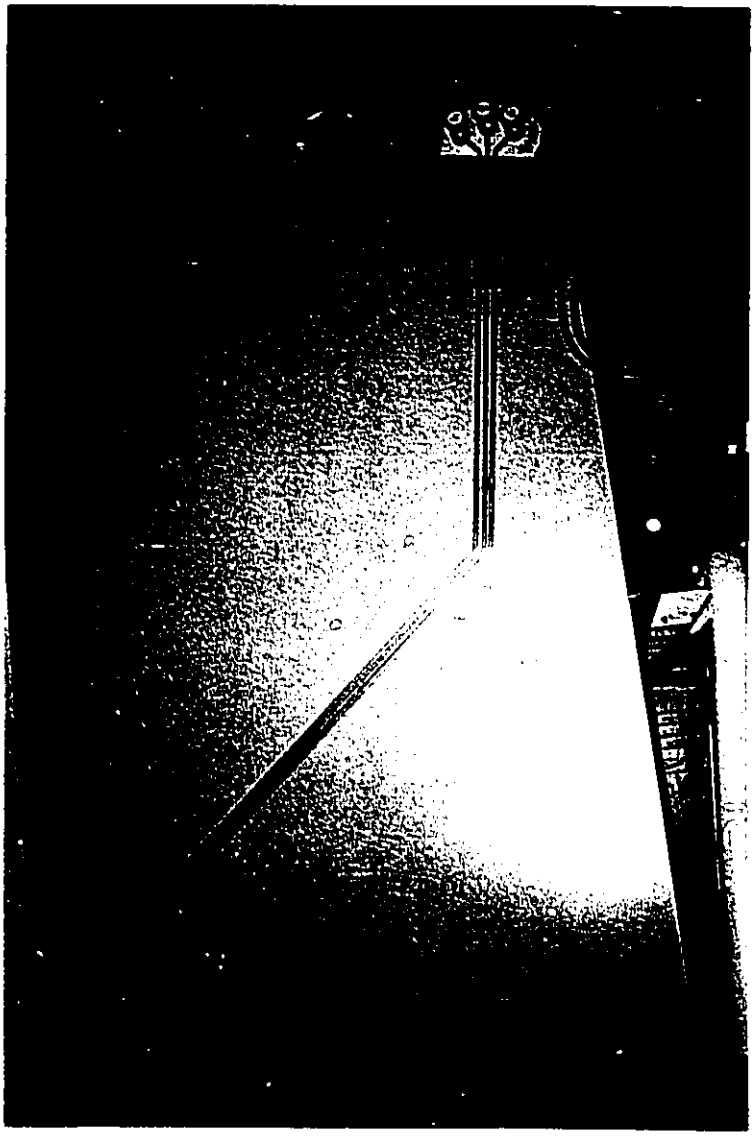

Figure 3.3(b) Test Thermosyphon Assembly

Item	Material
Heater	Copper

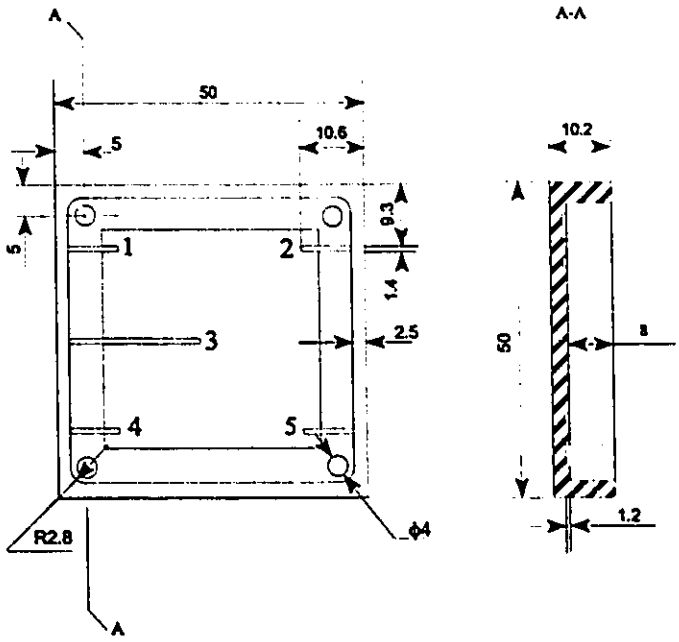

Figure 3.4 Heater Assembly

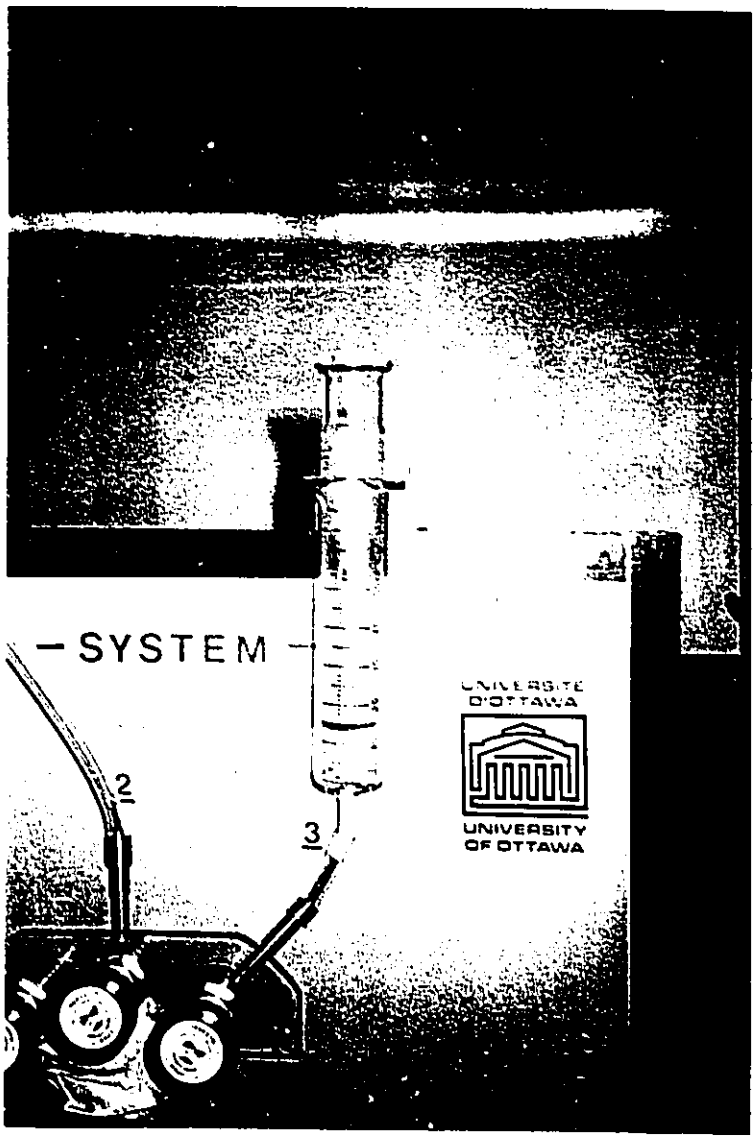

Figure 3.5 Syringe used for Charging Working Fluids and Removing Non-Condensible Gas from TCT

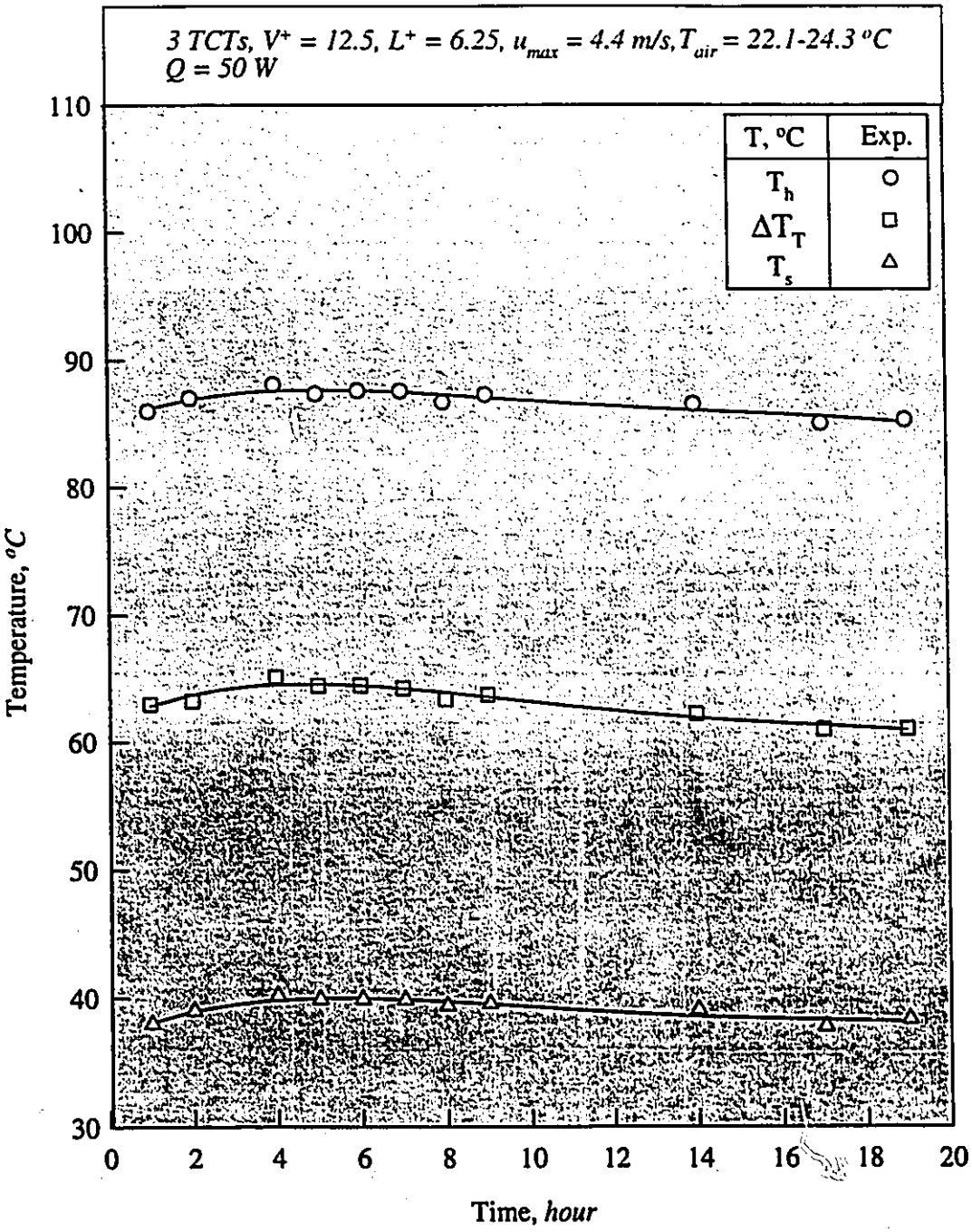

Figure 3.6 Temperature vs. Time from Startup; WF = FC-87

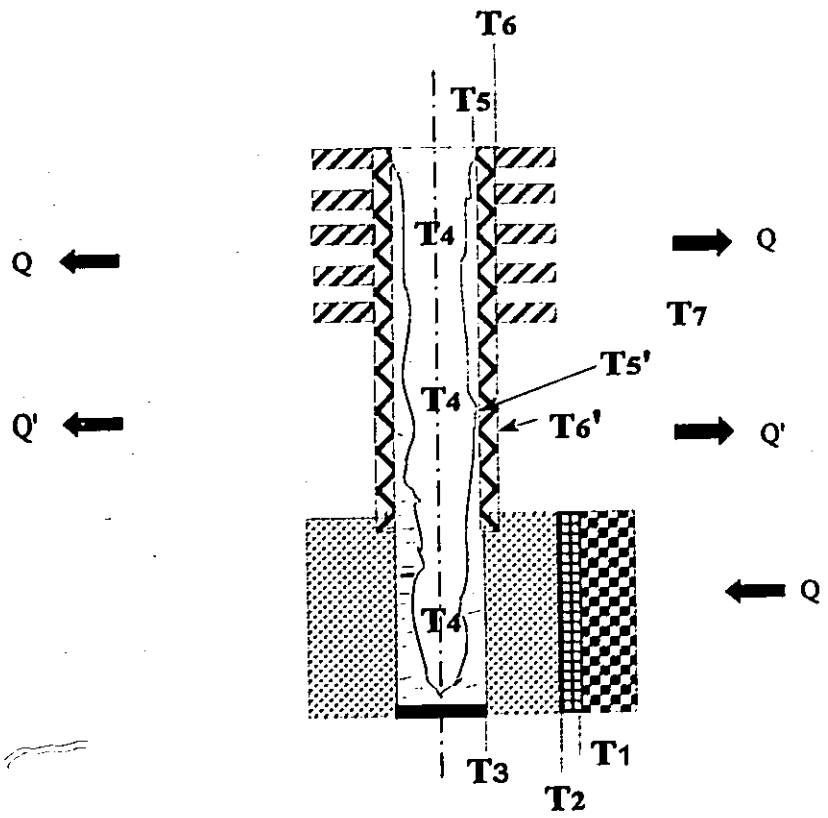

Figure 4.1 Model for Simulation

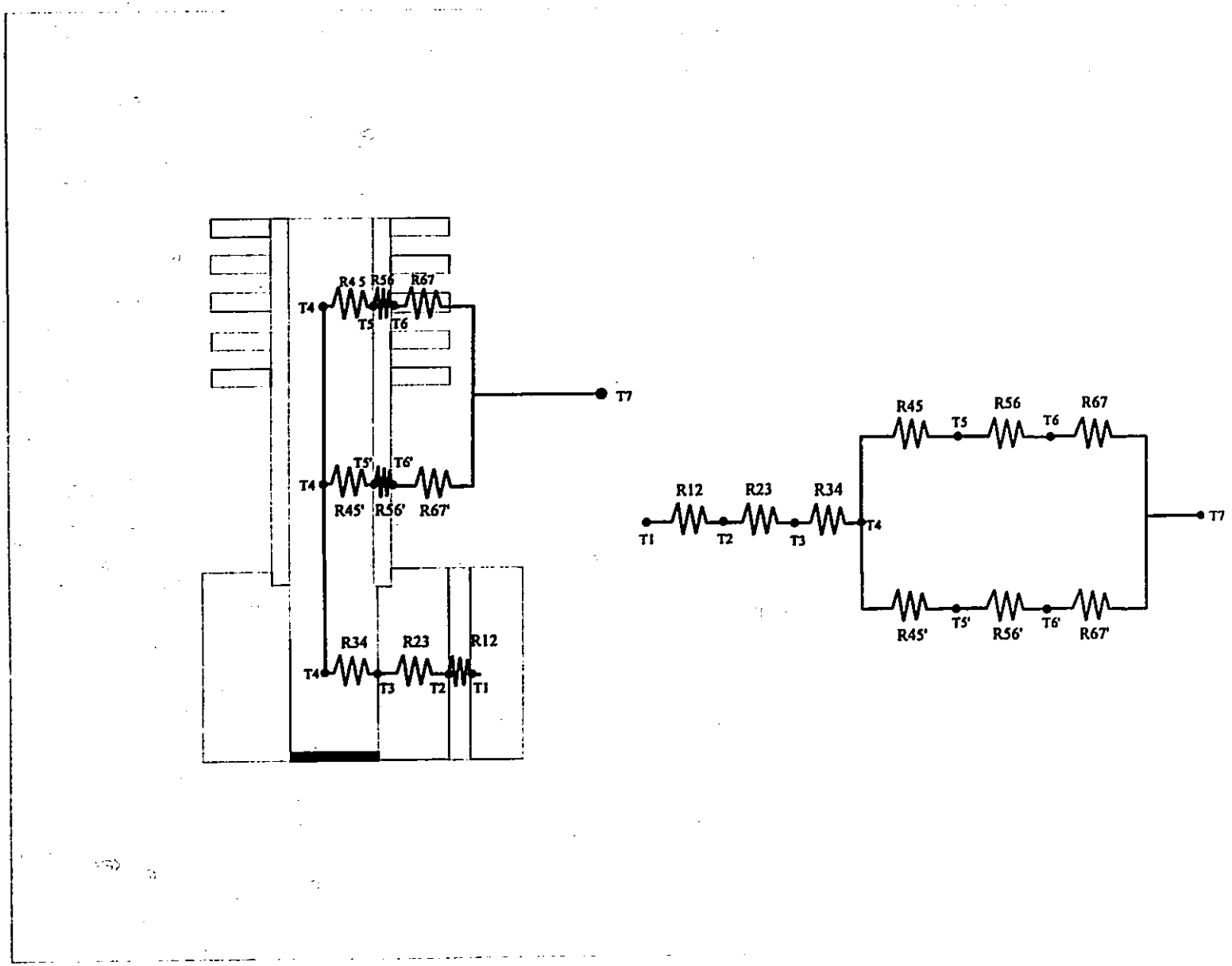

Figure 4.2 Thermal Resistance Network

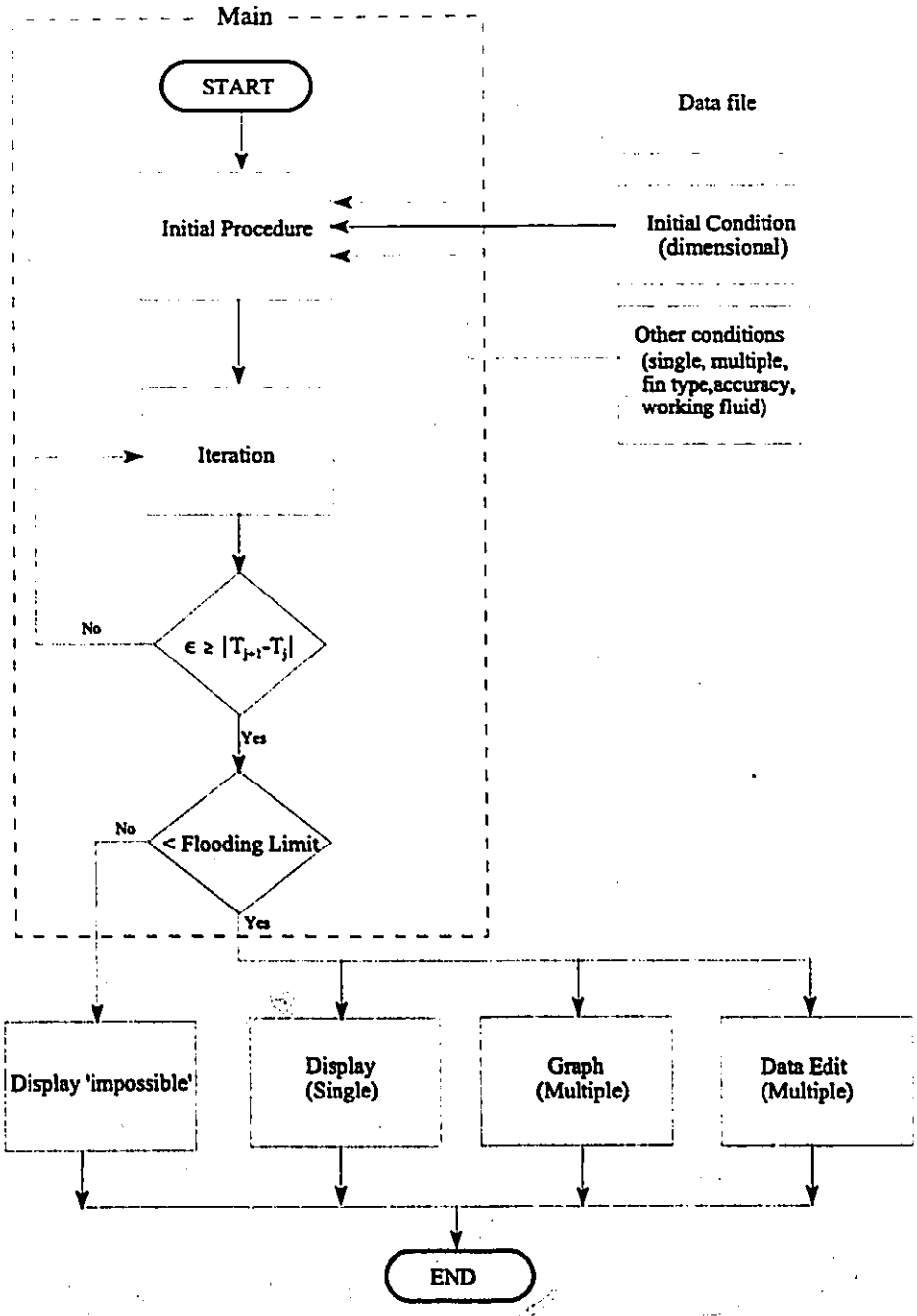

Figure 4.3 Flow Chart for Simulation.

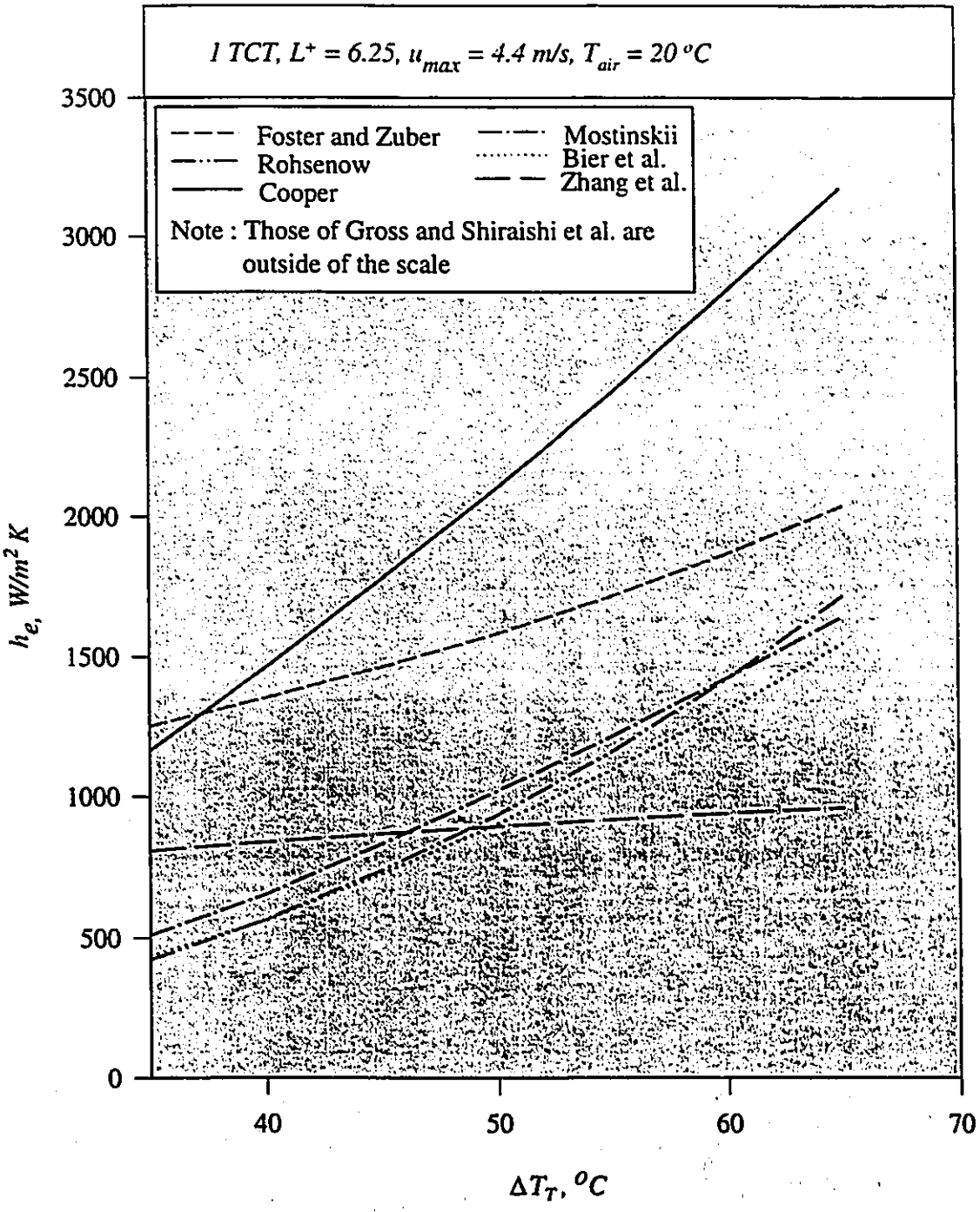

Figure 4.4(a) h_c by different correlations with h_c of Rohsenow [41]; WF = FC-72

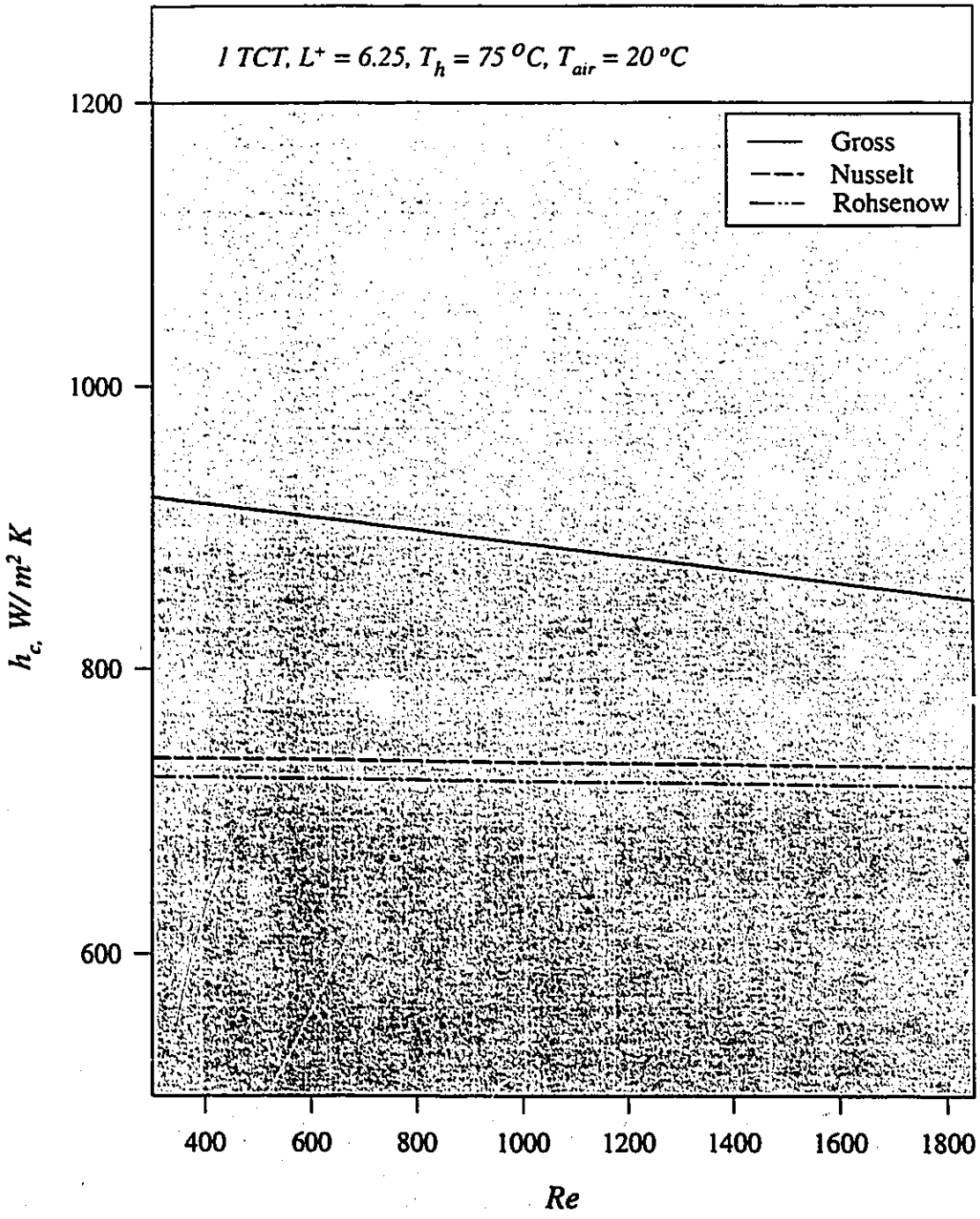

Figure 4.4(b) h_c by different correlations with h_e of Bier et al [52]; WF = FC-72

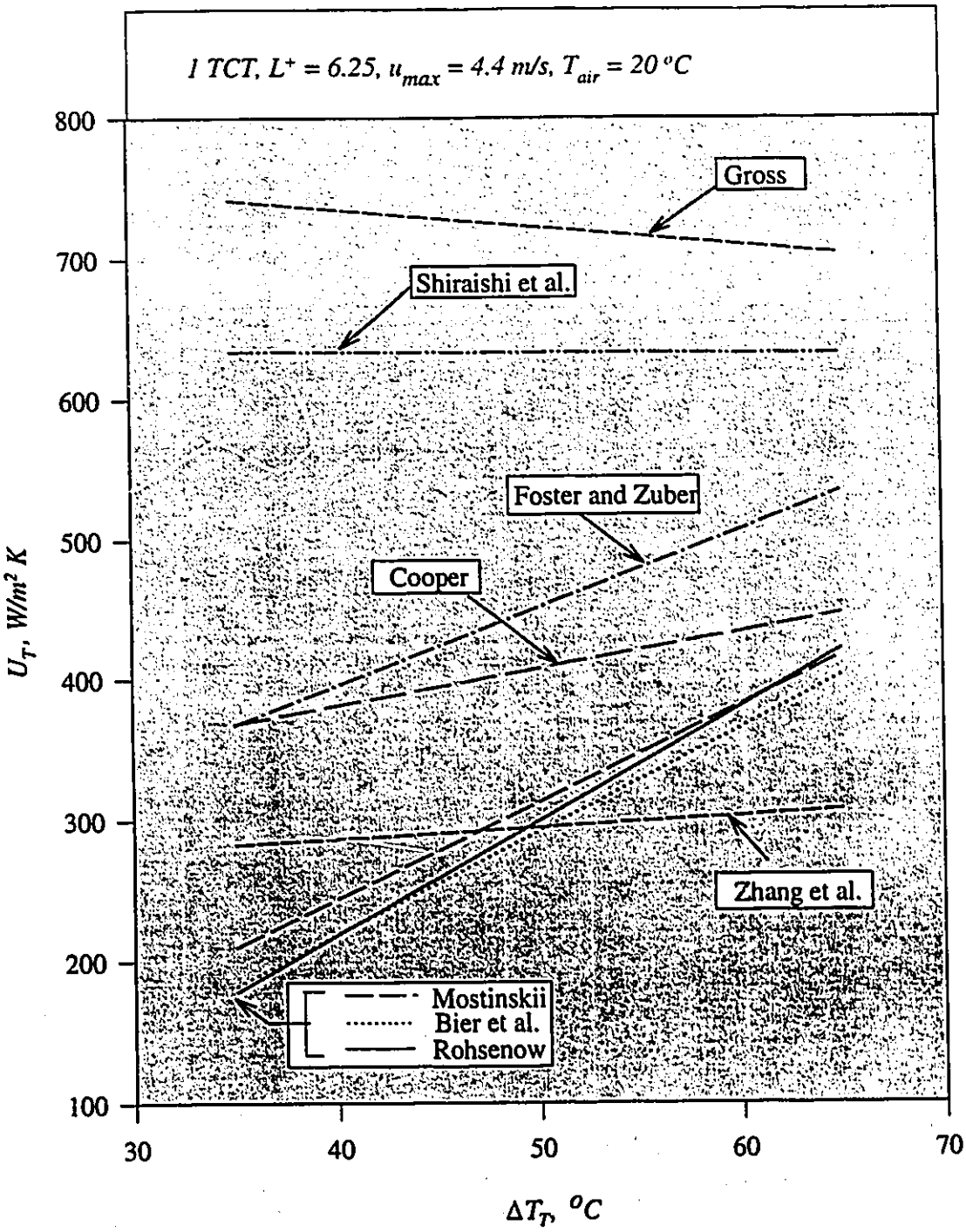

Figure 4.4(c) U_T obtained by Simulation Code with various correlations for h_c; with h_c of Rohsenow [41], WF = FC-72

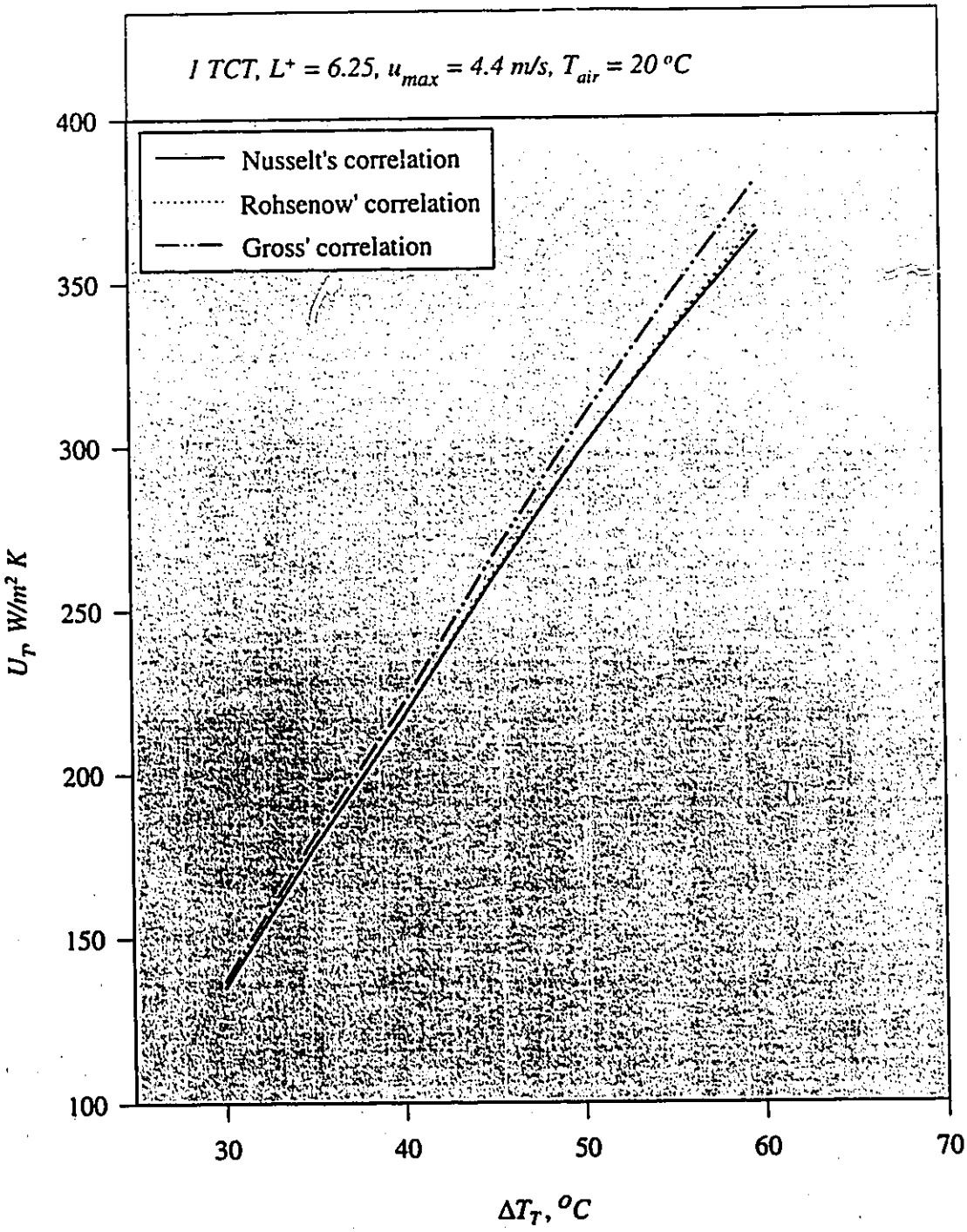

Figure 4.4(d) U_T obtained by Simulation Code with various correlations for h_c; with h_c of Bier et al. [52], WF = FC-72

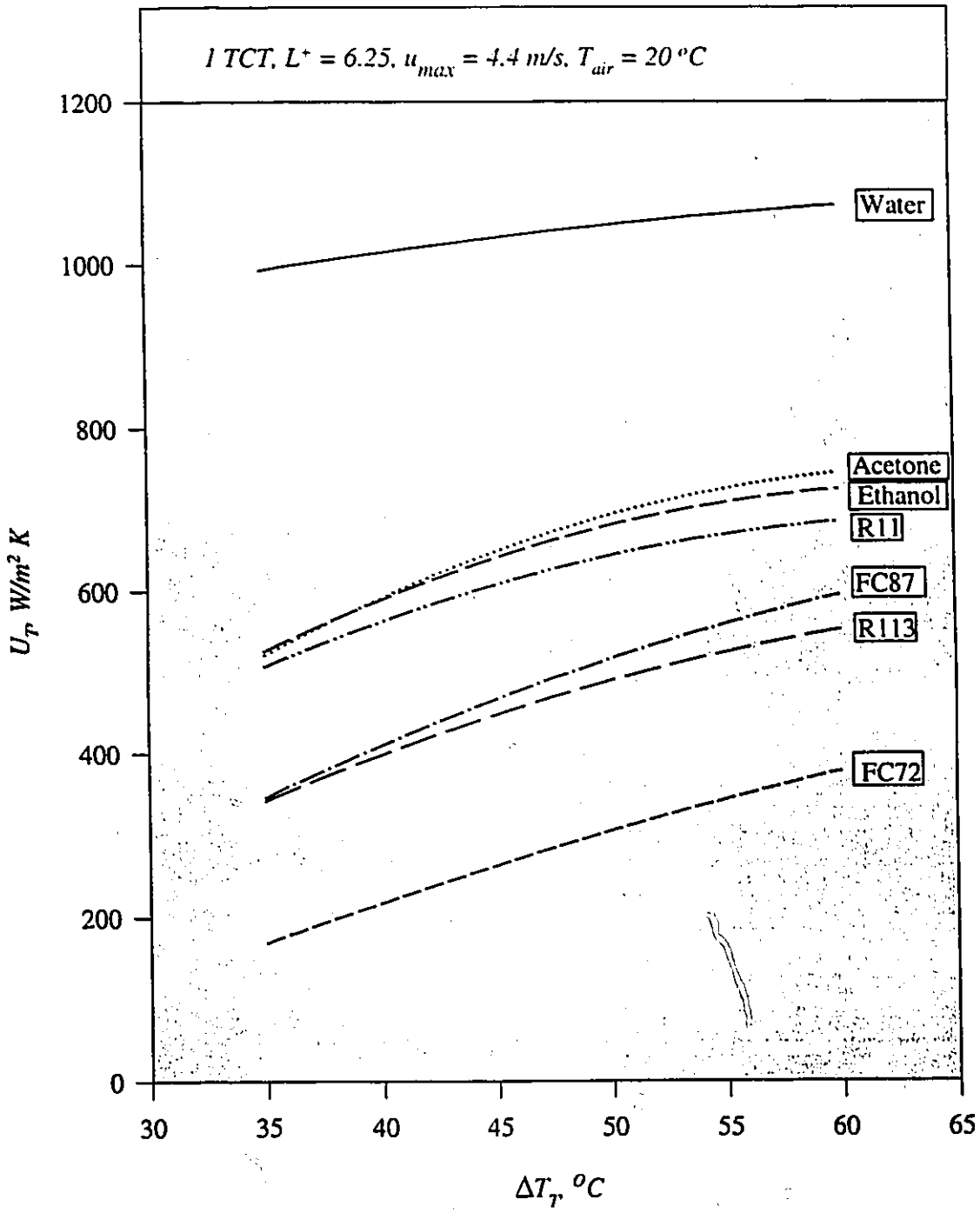

Figure 4.5(a) Effect of ΔT_T on U_T with Various Working Fluids through Simulation

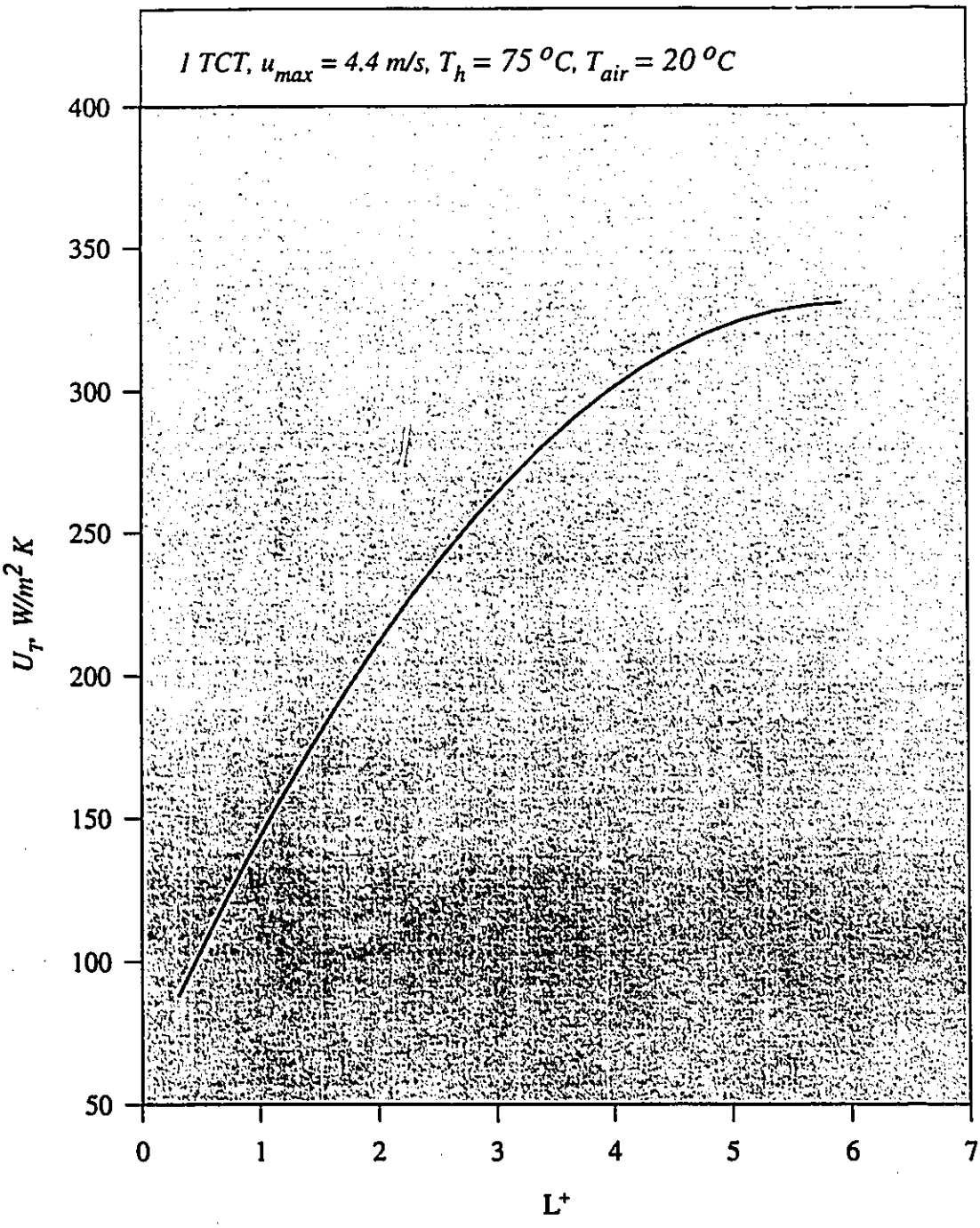

Figure 4.5(b) Effect of L^+ on U_T through Simulation; WF = FC-72

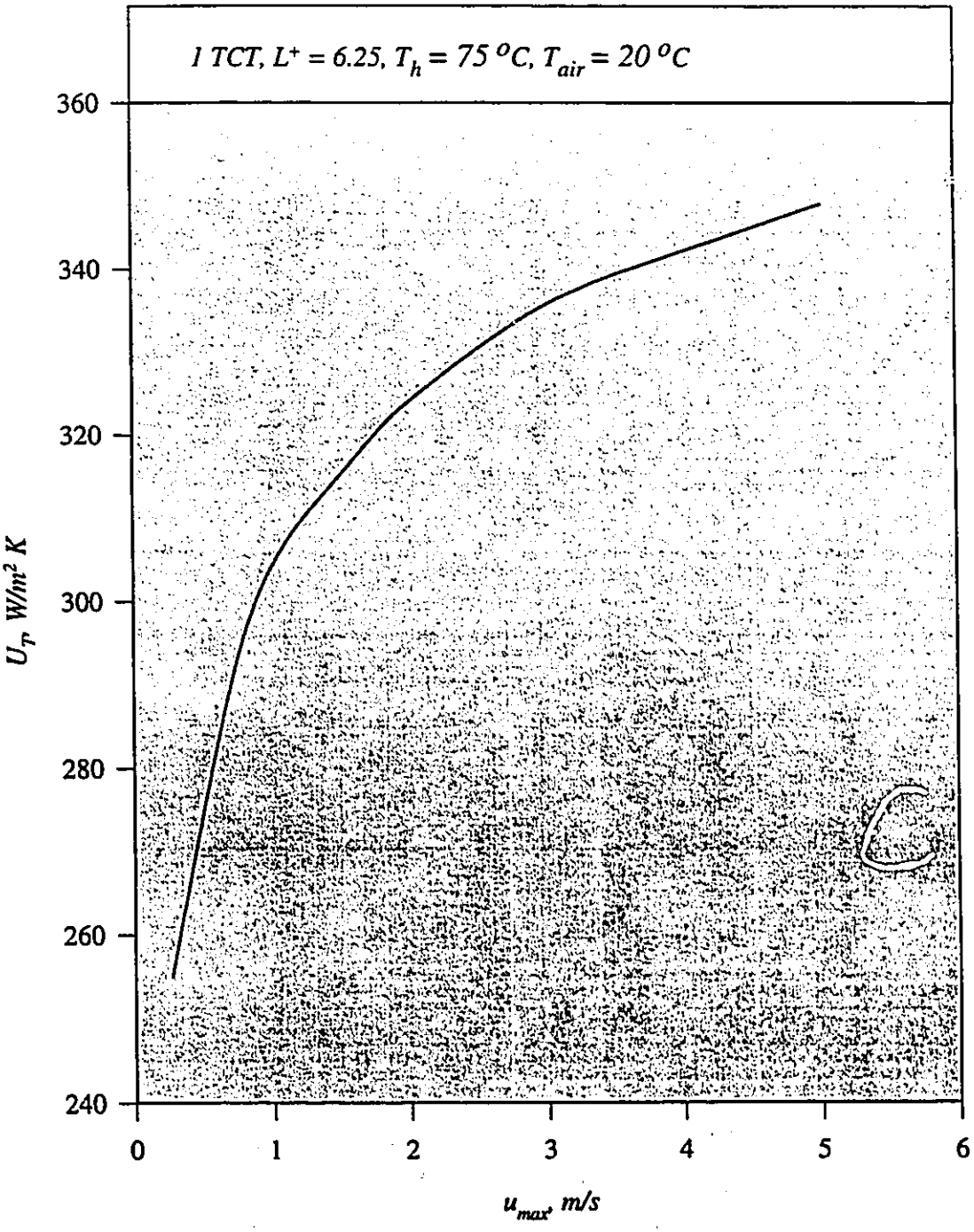

Figure 4.5(c) Effect of u_{max} on U_T through Simulation; WF = FC-72

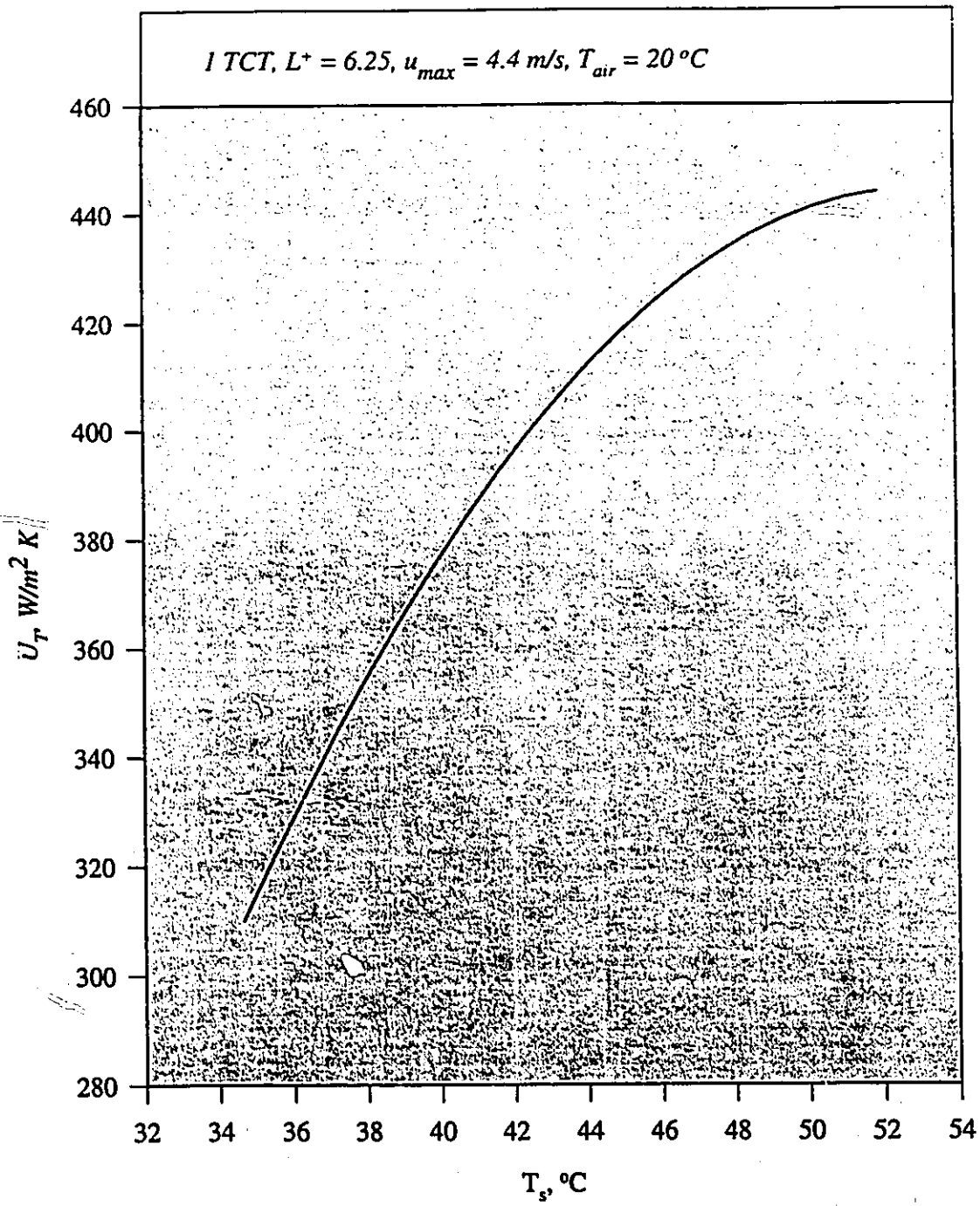

Figure 4.5(d) Effect of T_s on U_T through Simulation; WF = FC-72

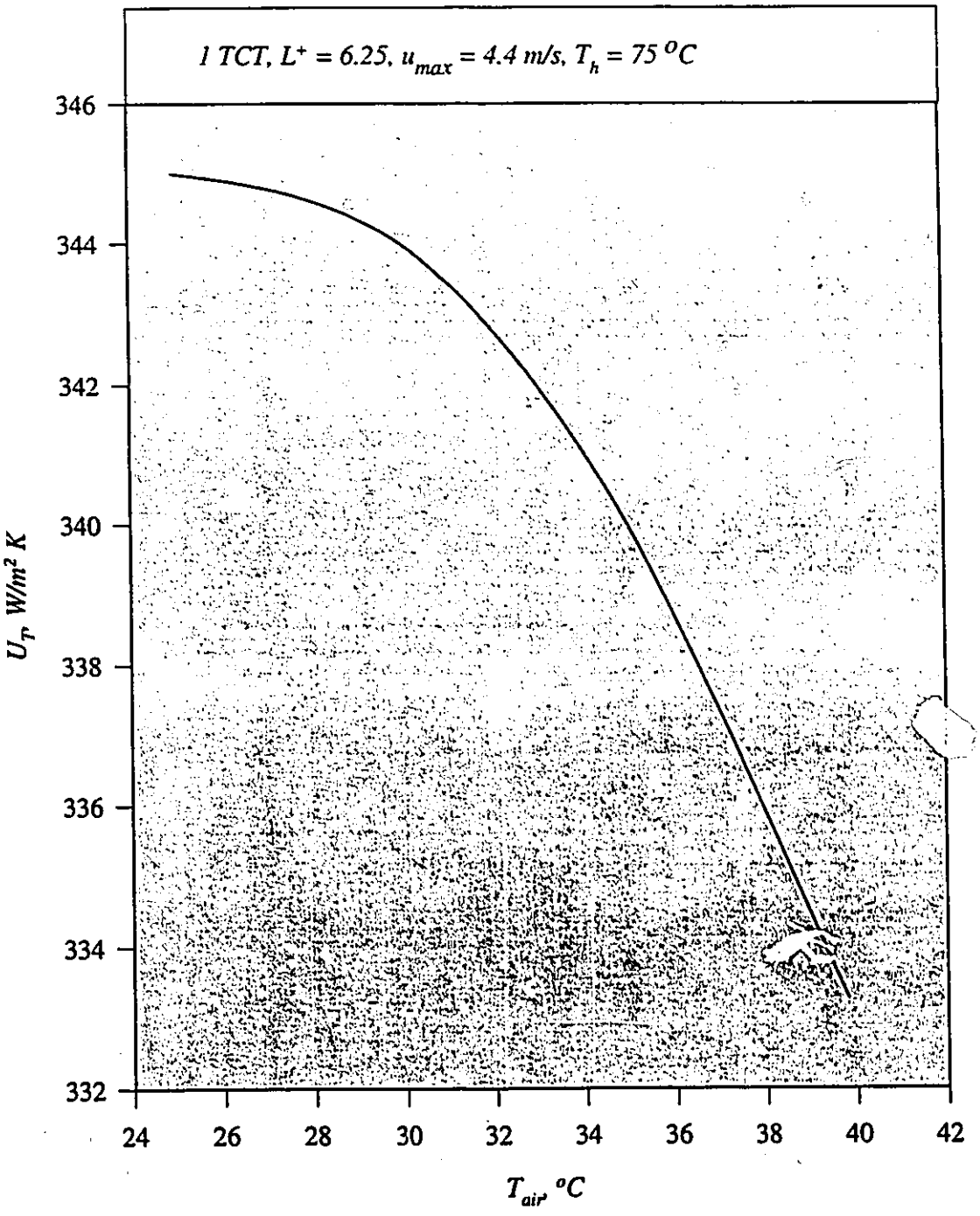

Figure 4.5(e) Effect of T_{air} on U_T through Simulation; WF = FC-72

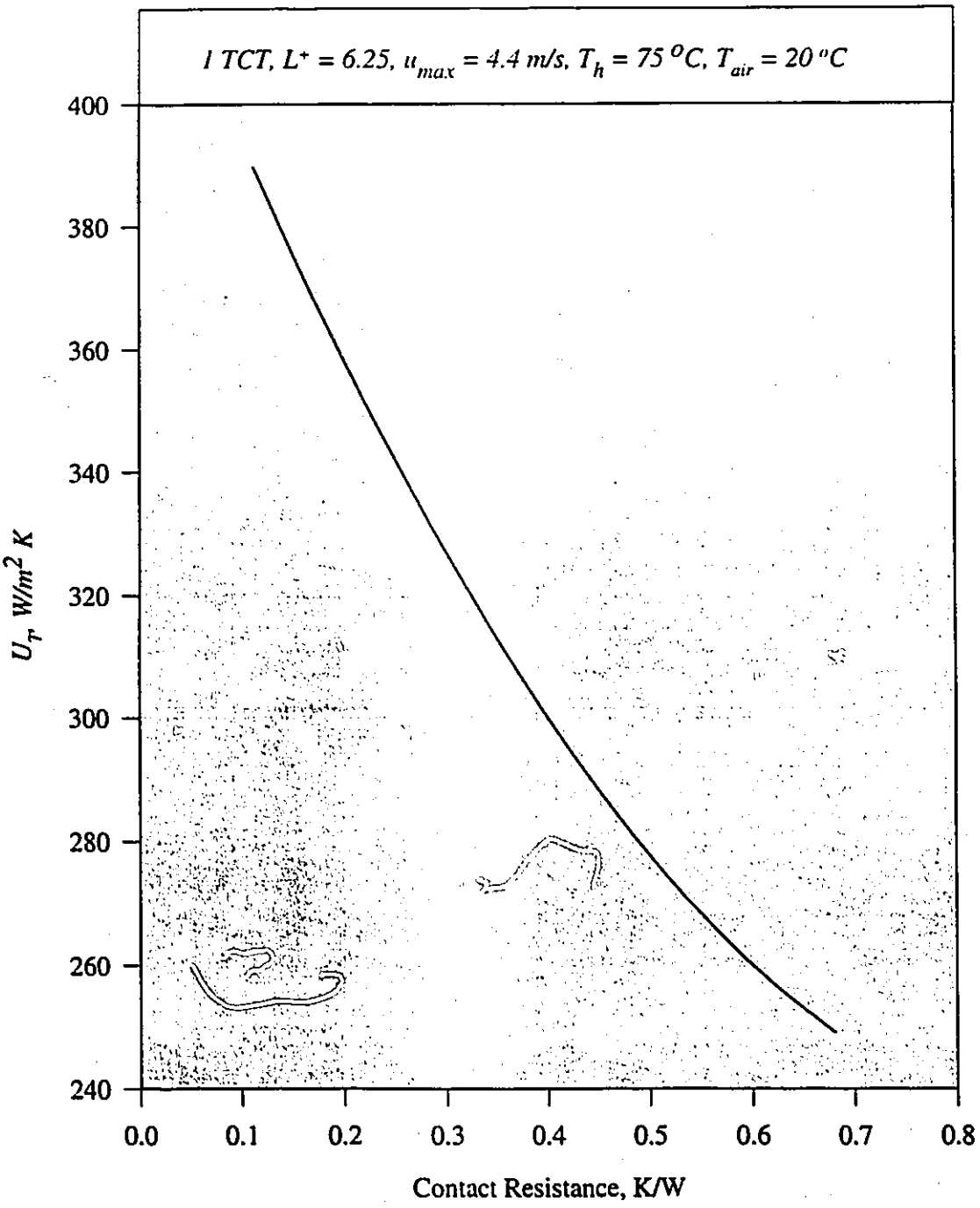

Figure 4.5(f) Effect of Contact Resistance on U_T through Simulation; WF = FC-72

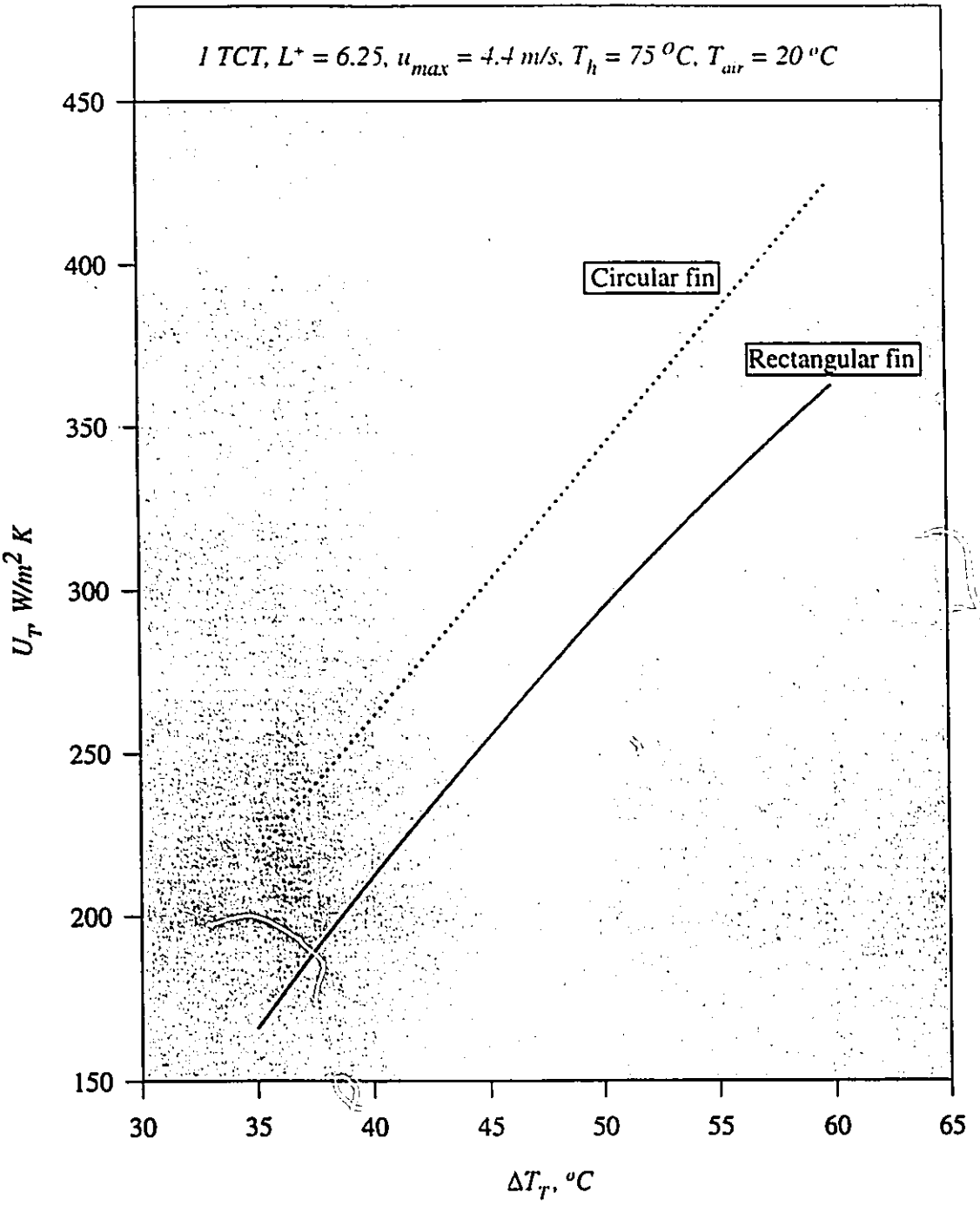

Figure 4.5(g) Effect of Fin Type on U_T through Simulation; WF = FC-72

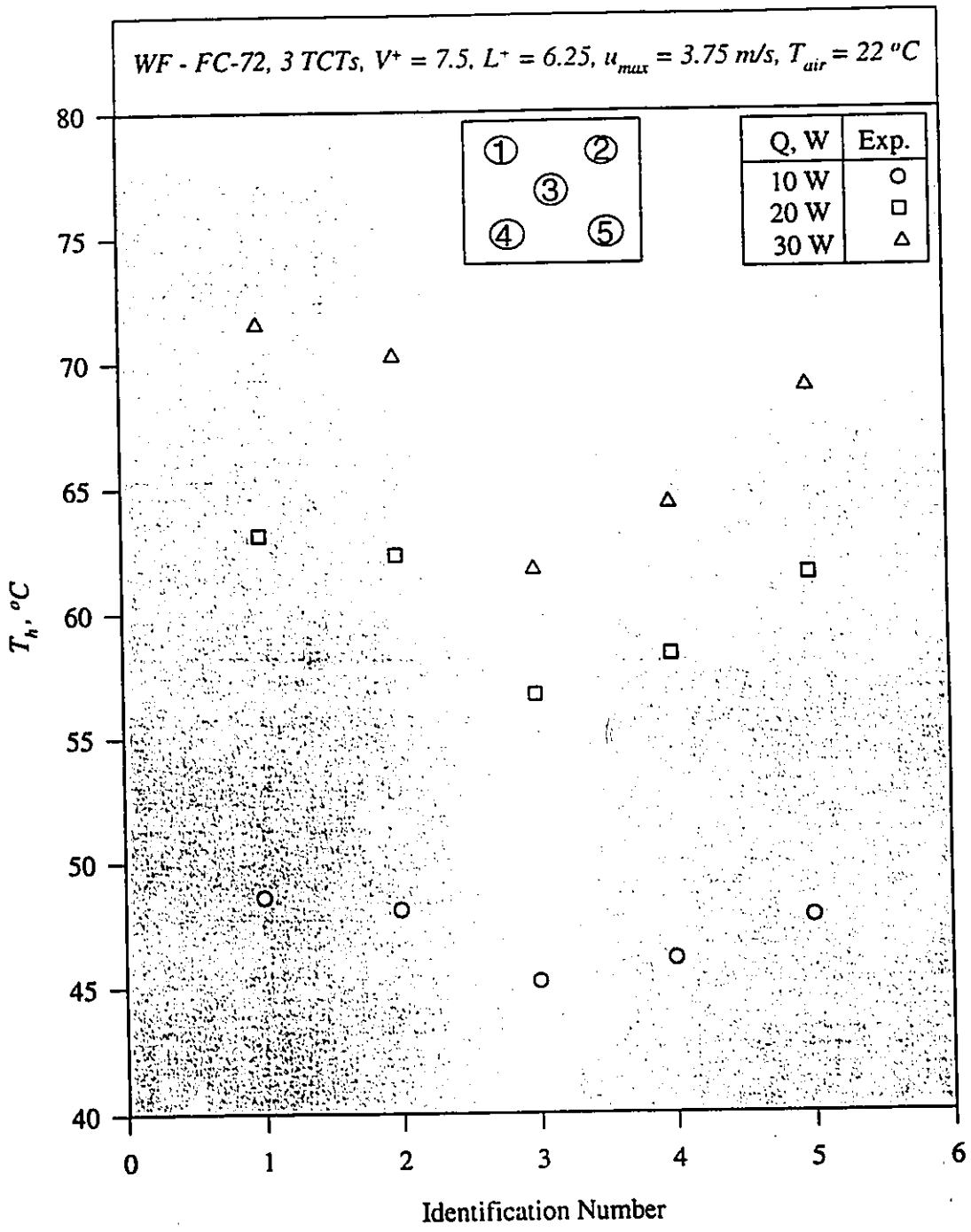

Figure 5.1 Temperature Distribution of Heater

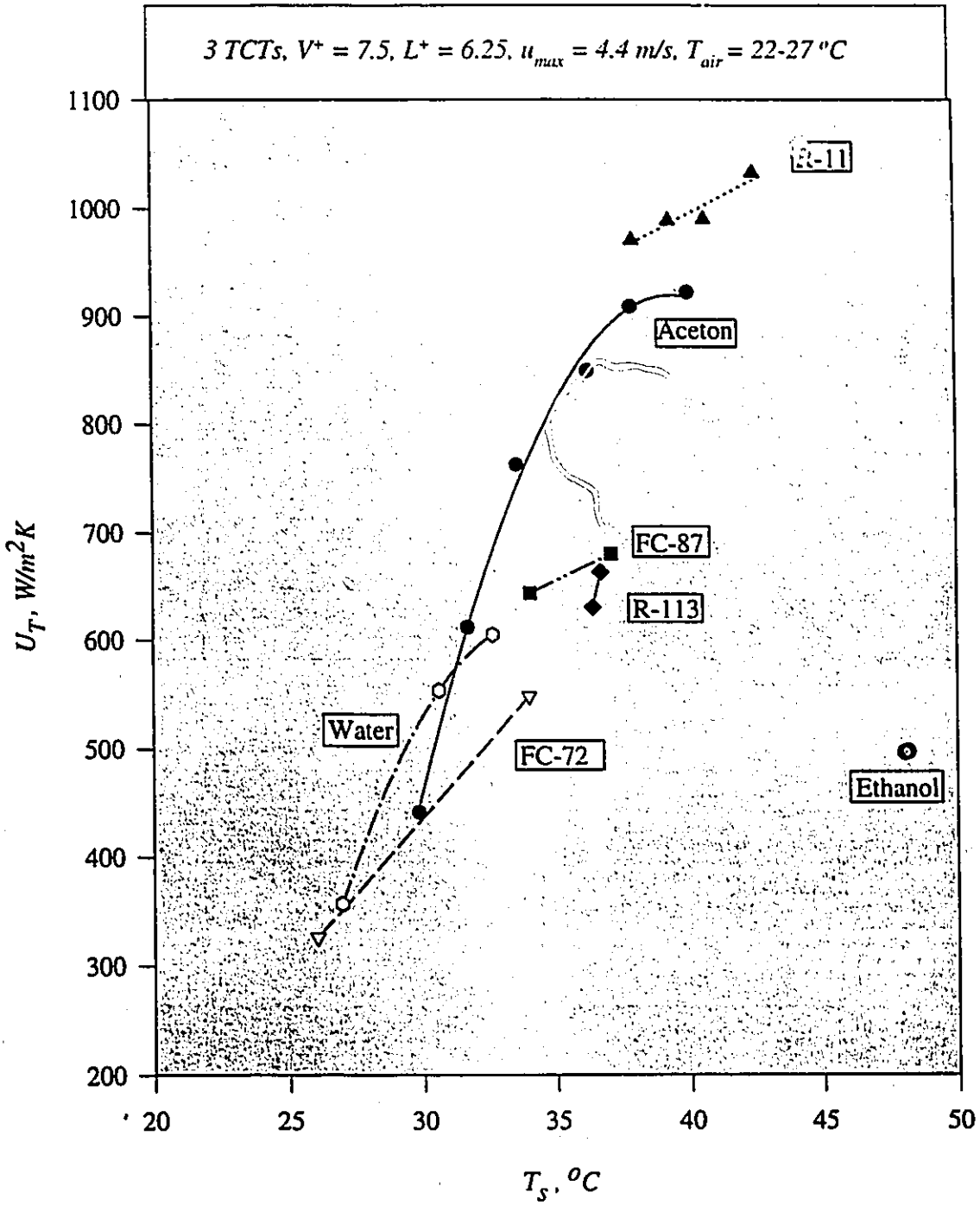

Figure 5.2 Effect of T_s on U_T

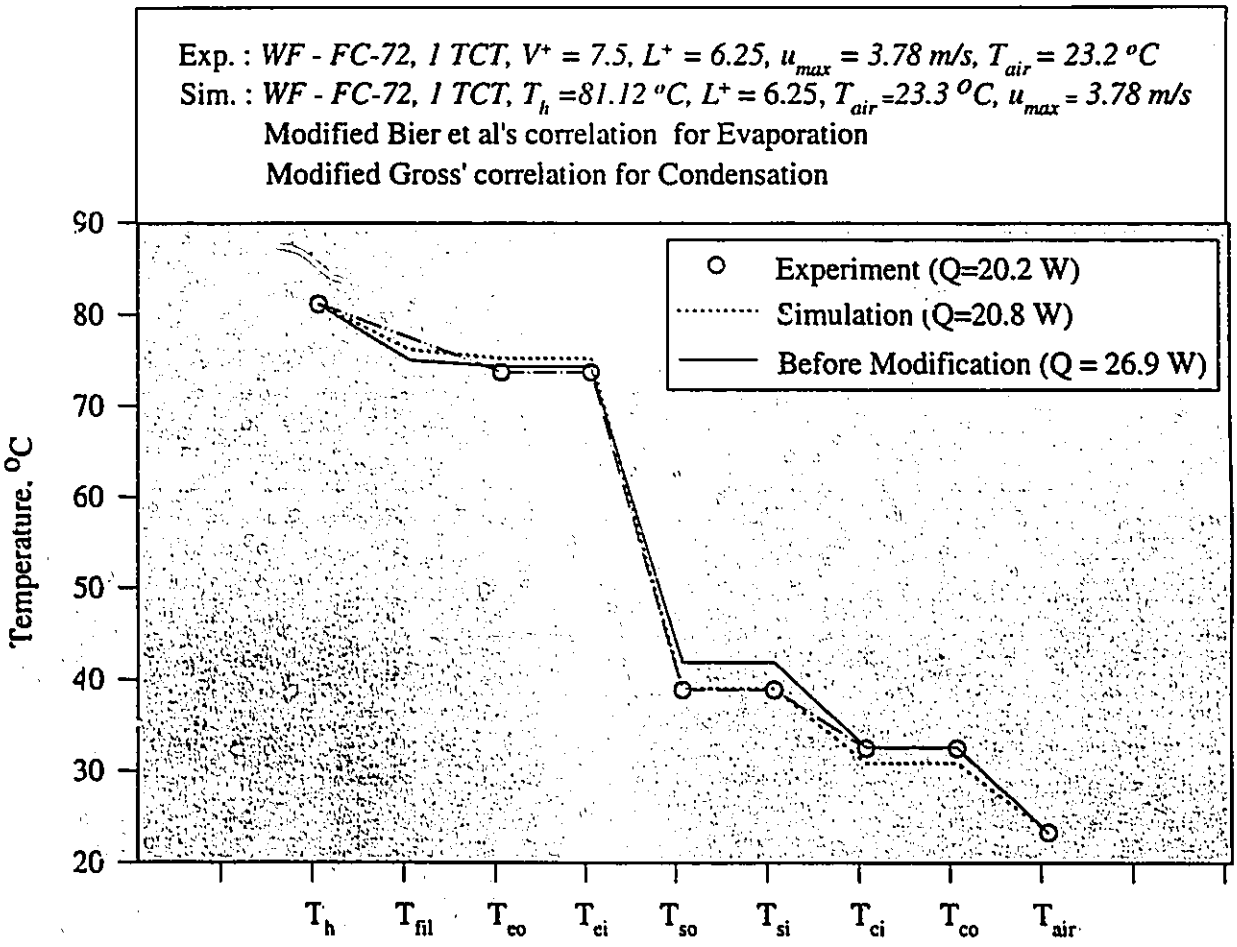

Figure 5.3(a) Comparison between Experiment and Simulation on Temperature Distribution of TCT Assembly

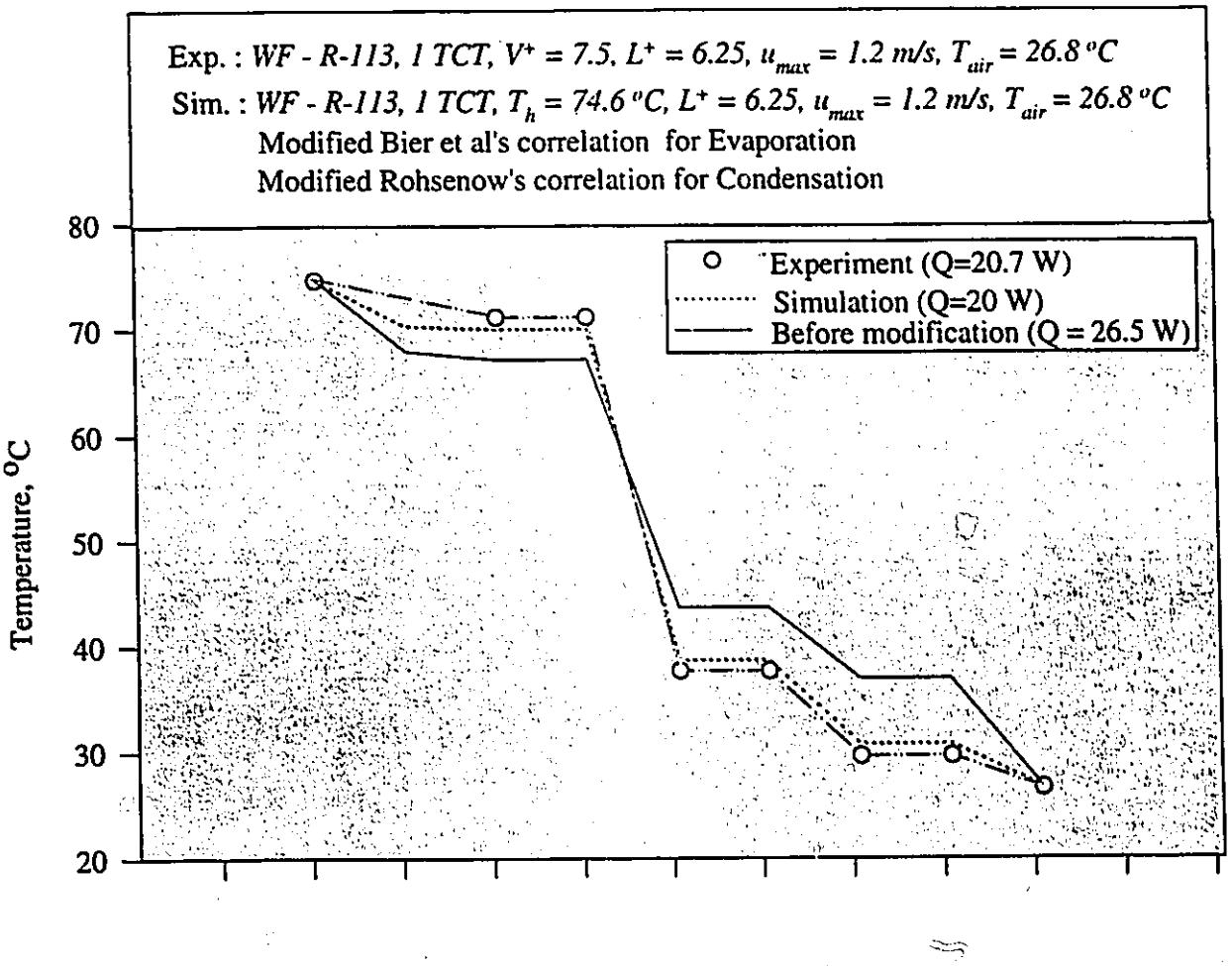

Figure 5.3(b) Comparison between Experiment and Simulation on Temperature Distribution of TCT Assembly

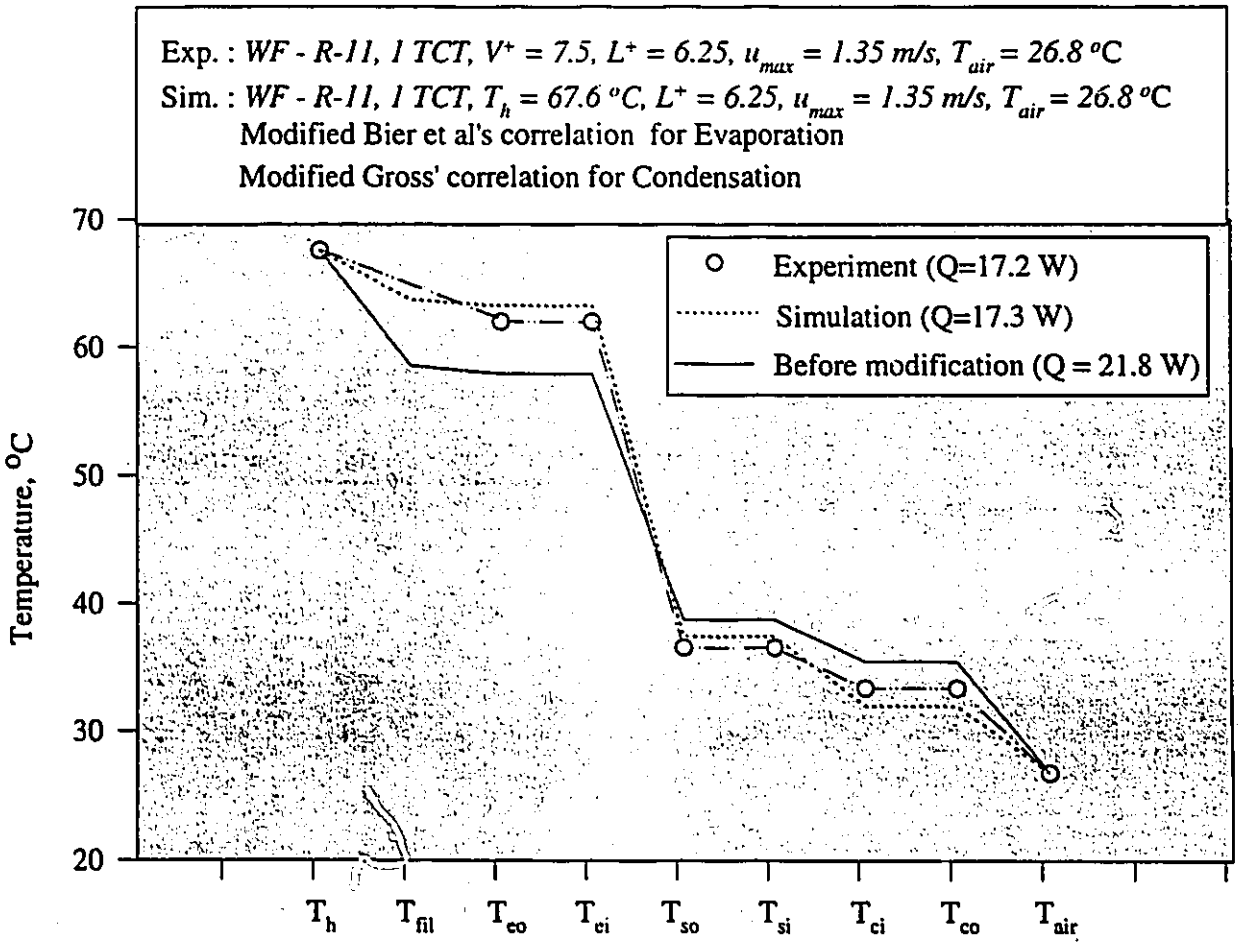

Figure 5.3(c) Comparison between Experiment and Simulation on Temperature Distribution of TCT Assembly

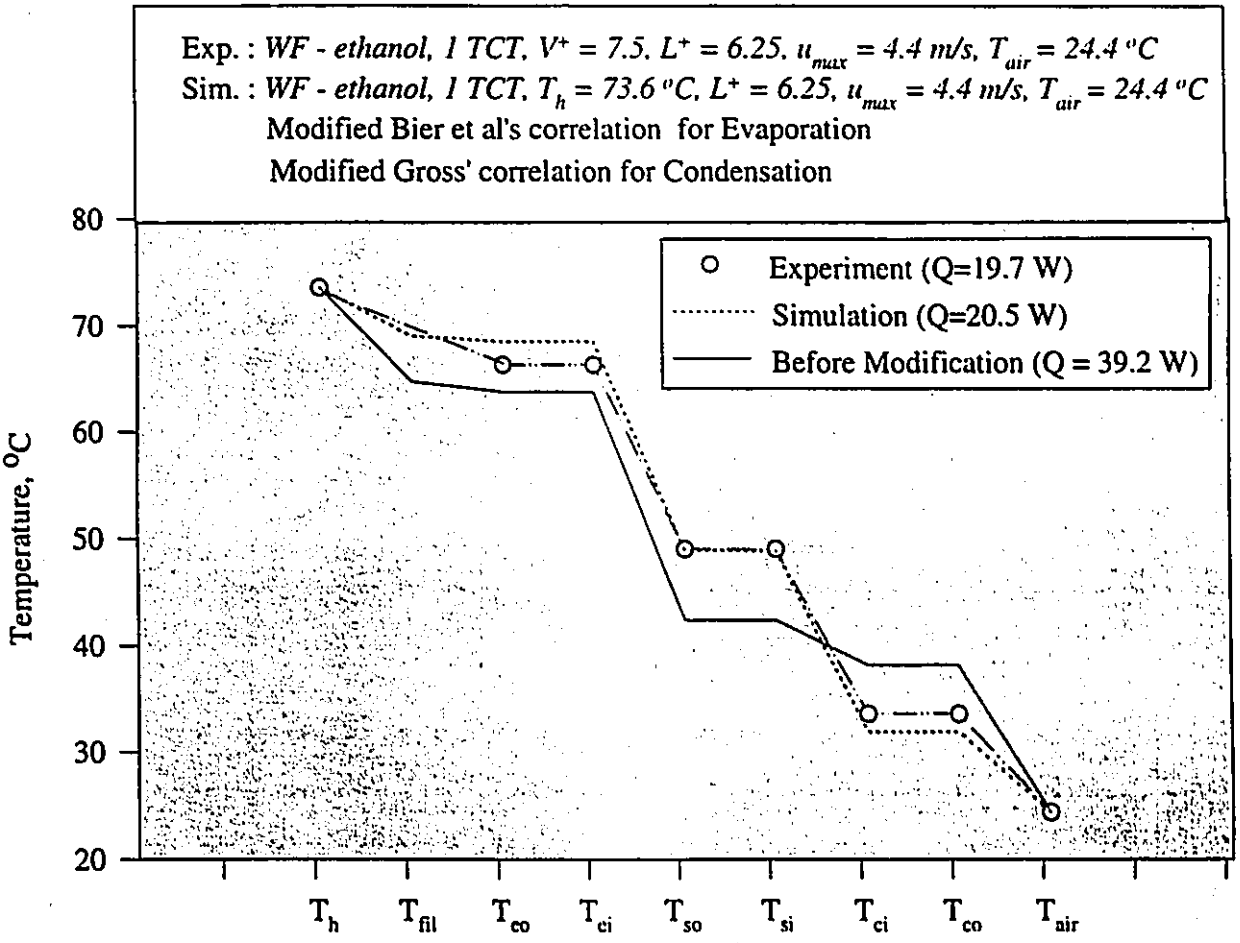

Figure 5.3(d) Comparison between Experiment and Simulation on Temperature Distribution of TCT Assembly

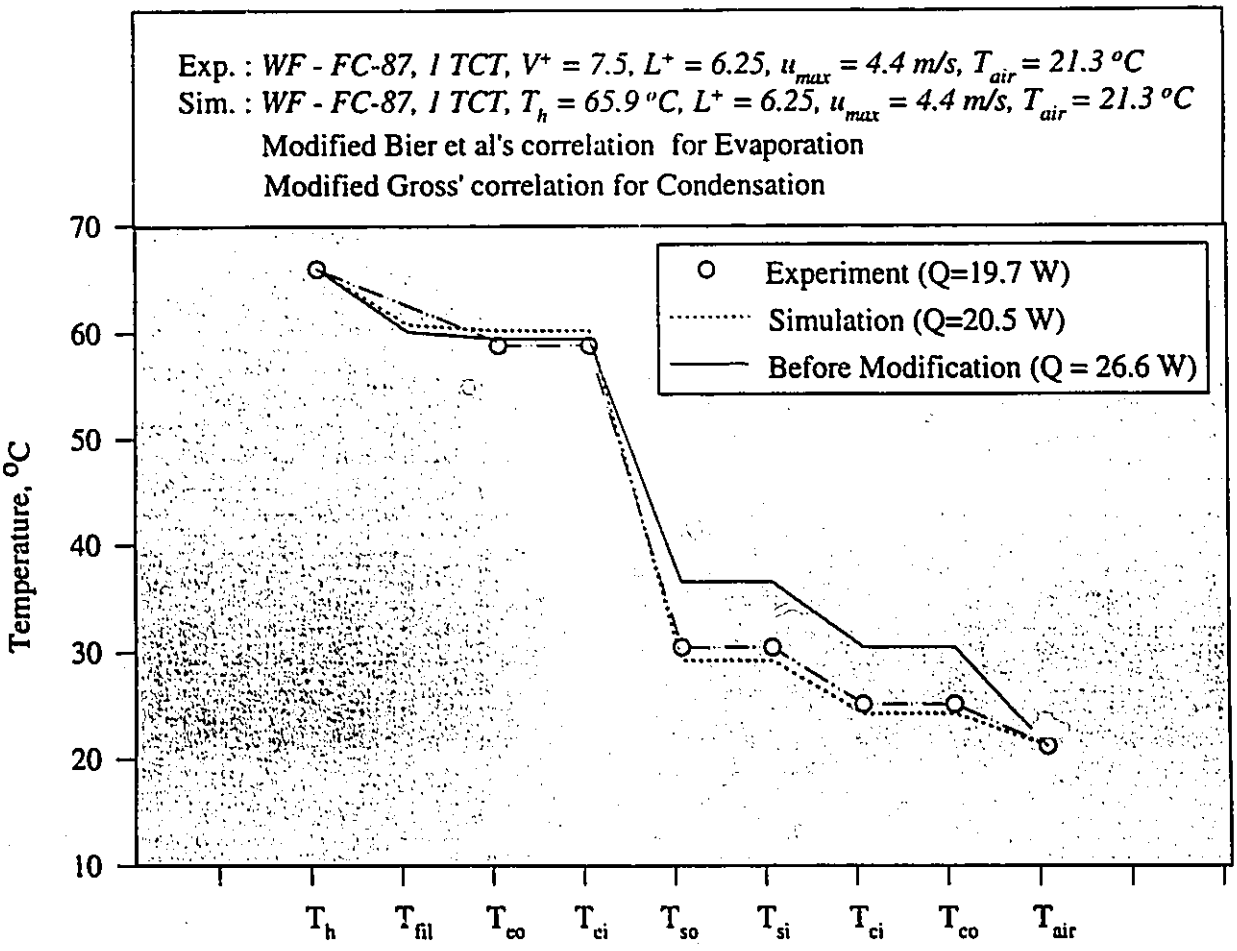

Figure 5.3(e) Comparison between Experiment and Simulation on Temperature Distribution of TCT Assembly

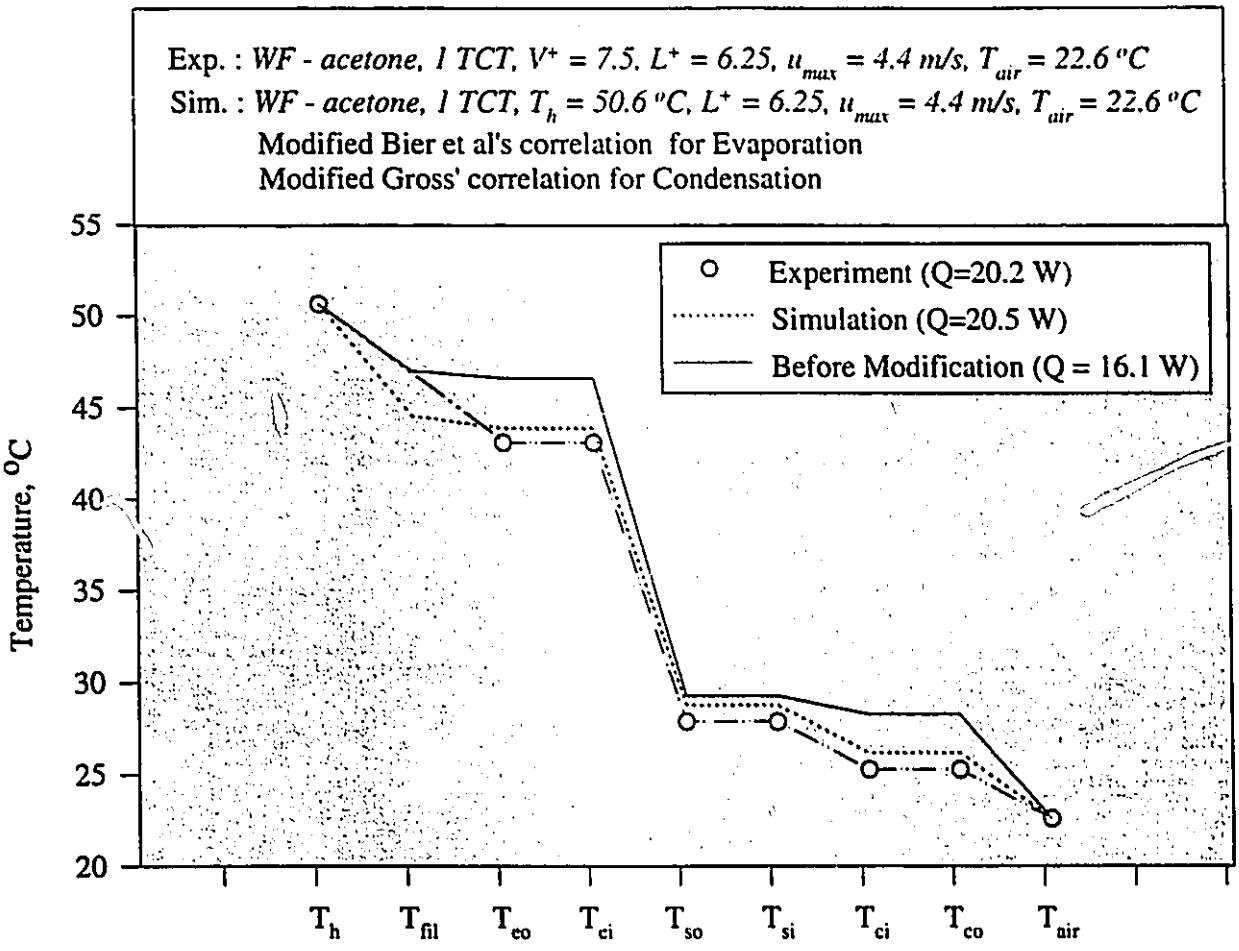

Figure 5.3(f) Comparison between Experiment and Simulation on Temperature Distribution of TCT Assembly

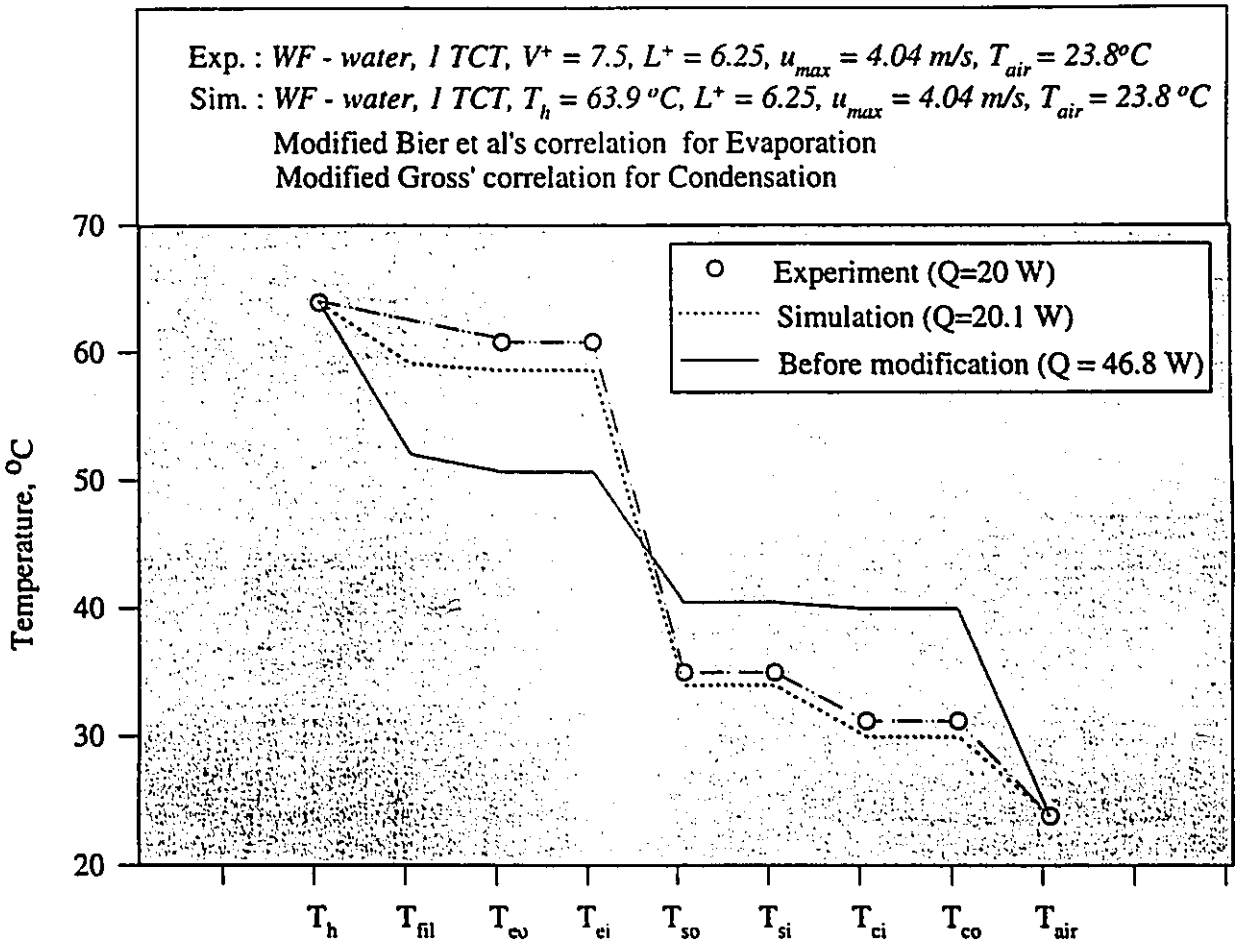

Figure 5.3(g) Comparison between Experiment and Simulation on Temperature Distribution of TCT Assembly

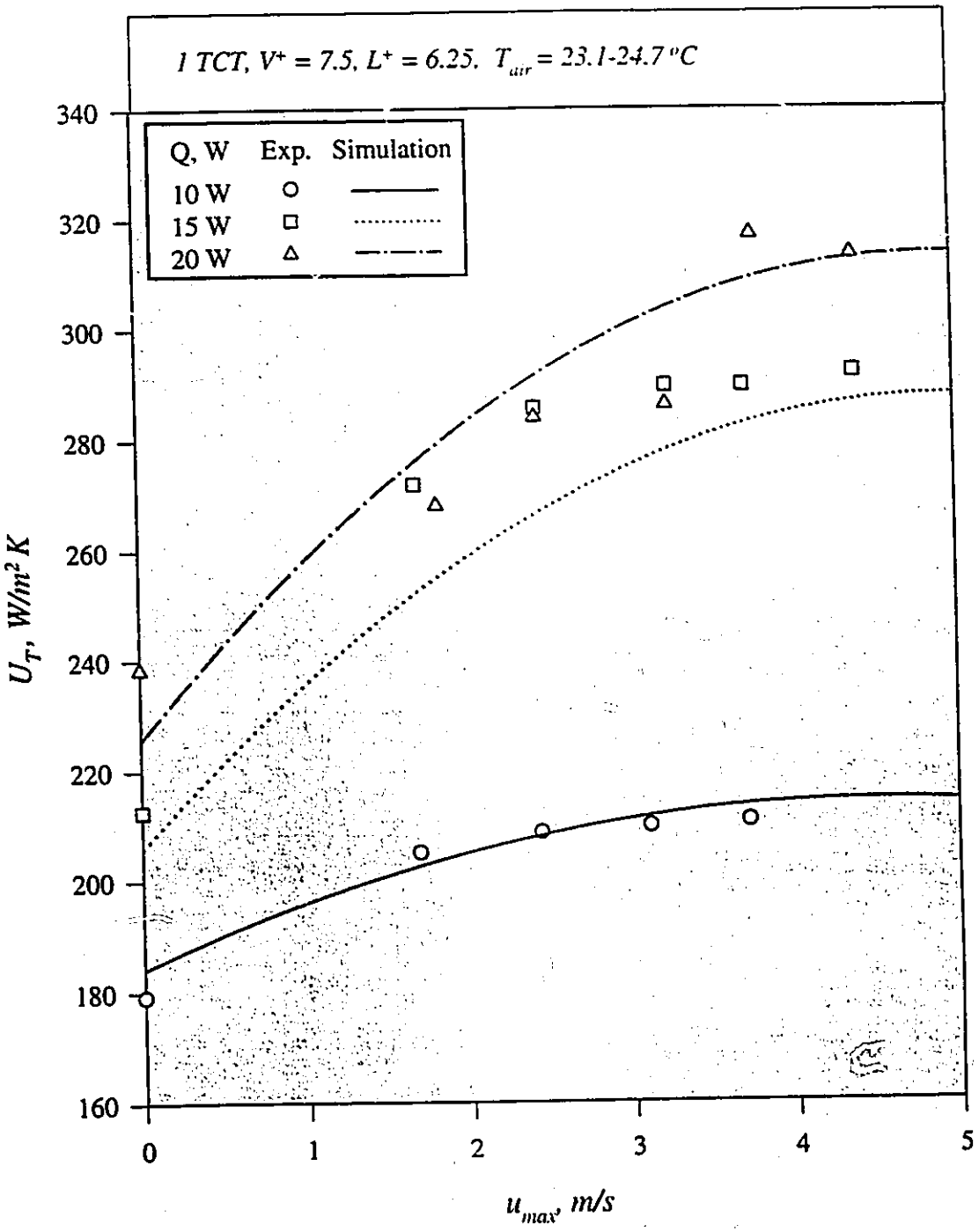

Figure 5.4(a) Effect of u_{max} on U_T; WF = FC-72

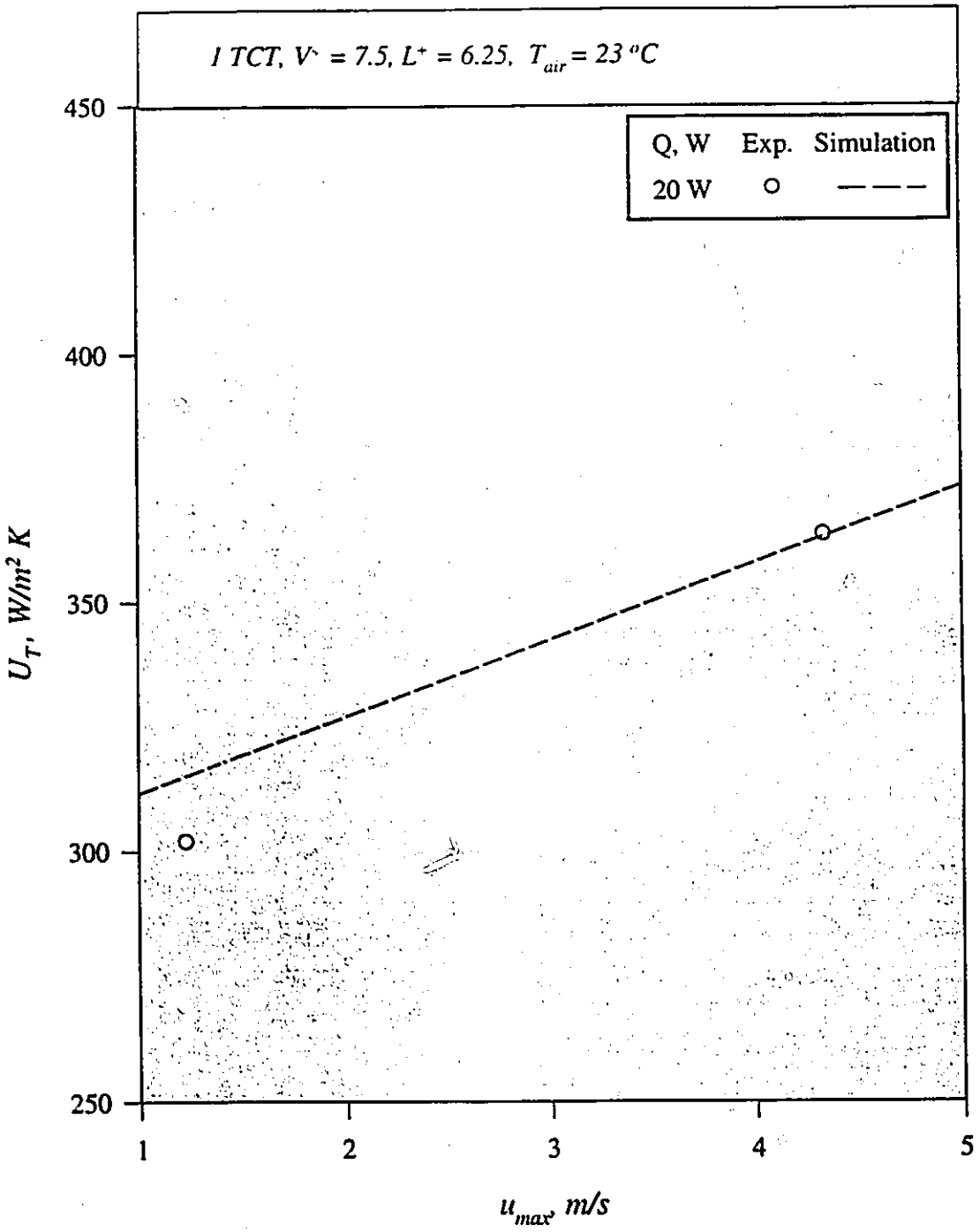

Figure 5.4(b) Effect of u_{max} on U_T; WF = R-113

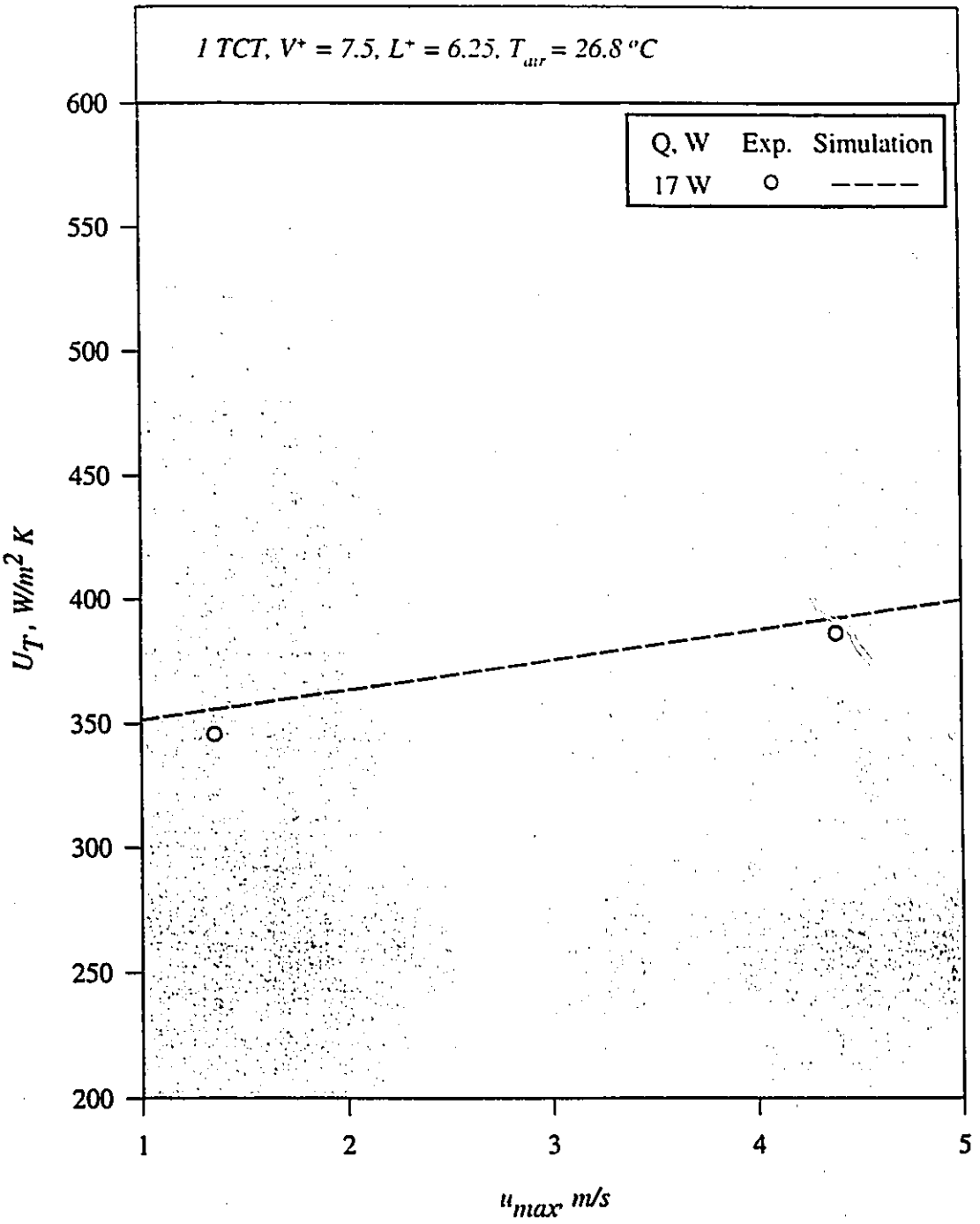

Figure 5.4(c) Effect of u_{max} on U_T; WF = R-11

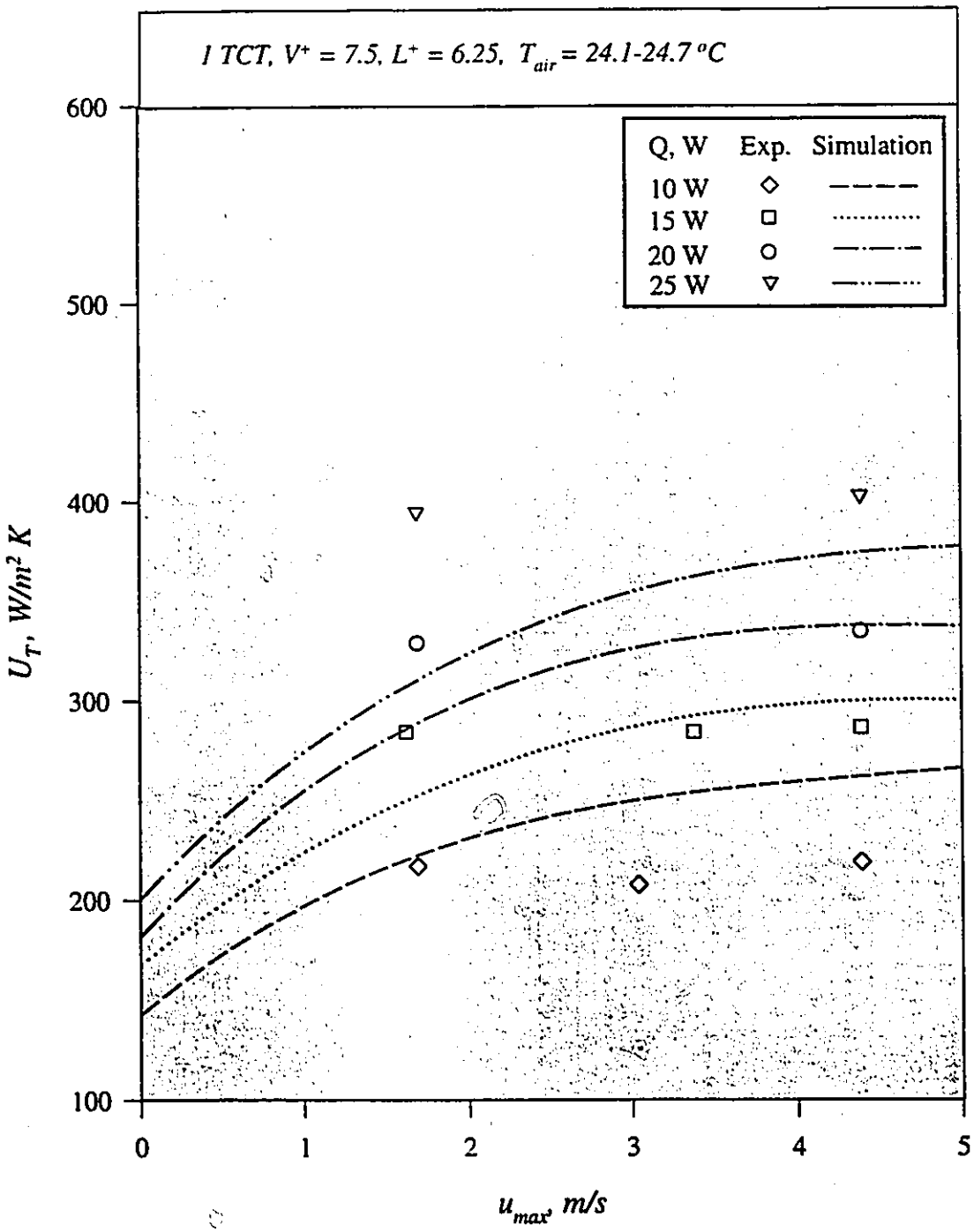

Figure 5.4(d) Effect of u_{max} on U_T; WF = ethanol

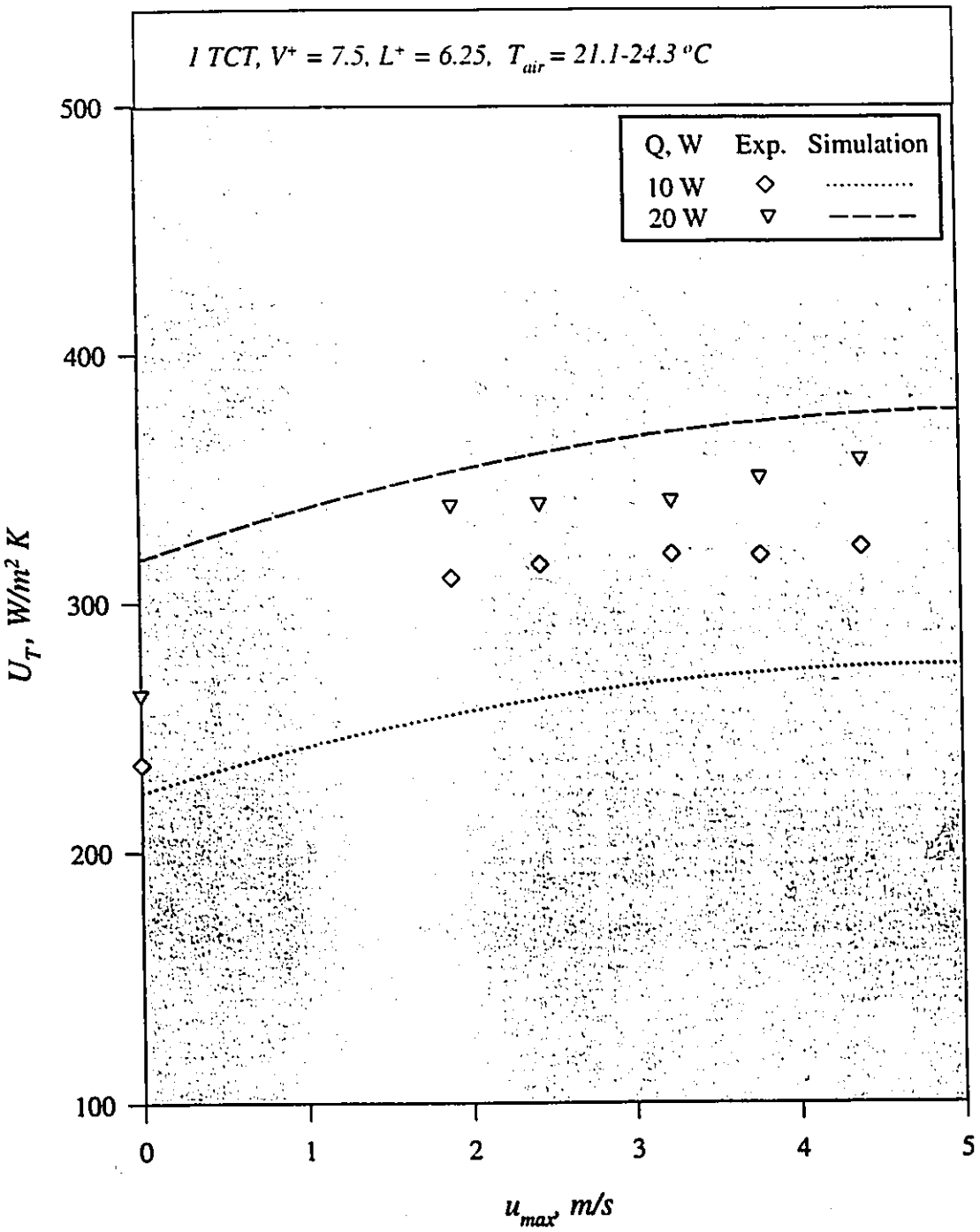

Figure 5.4(e) Effect of u_{max} on U_T; WF = FC-87

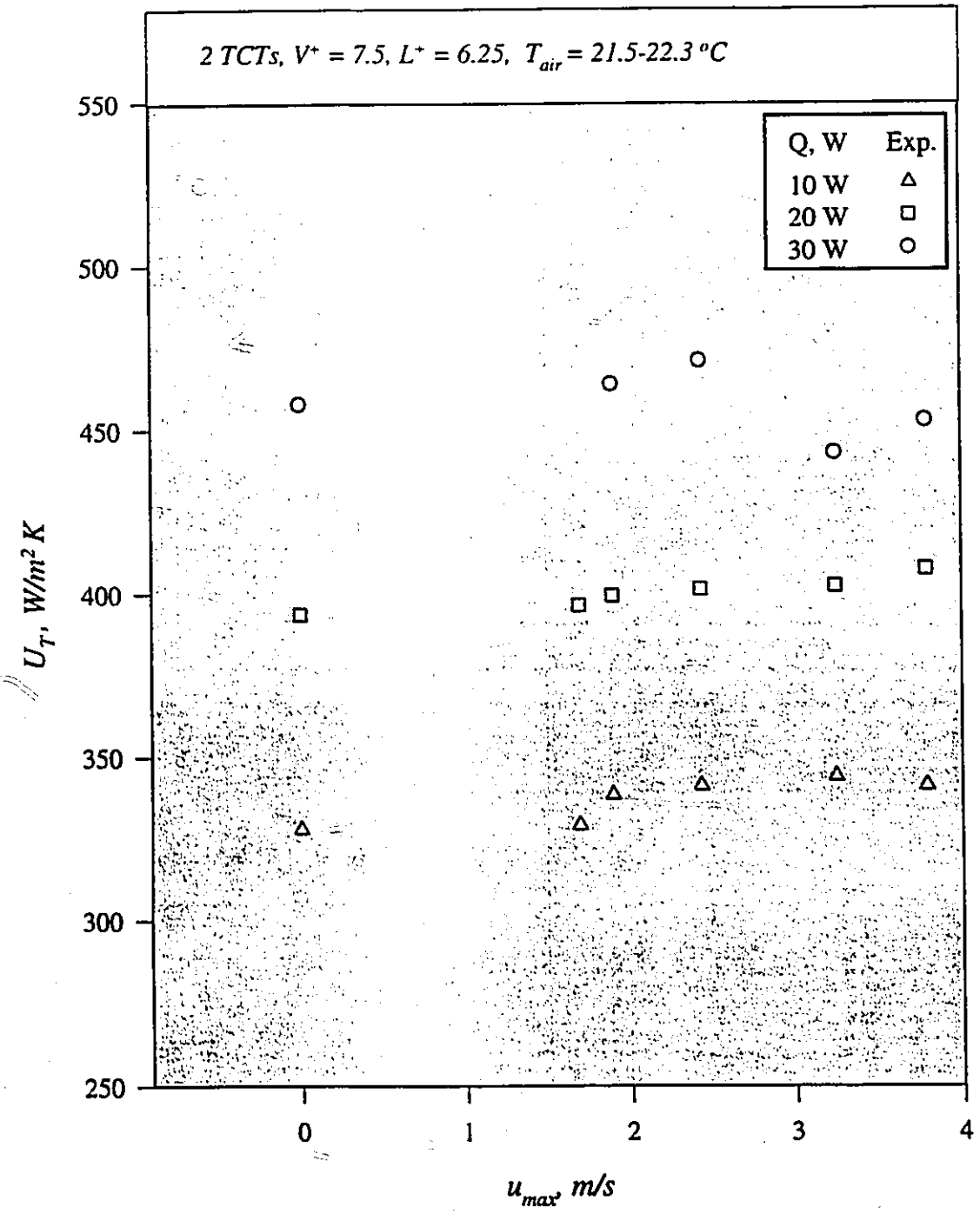

Figure 5.4(f) Effect of u_{max} on U_T; WF = FC-72

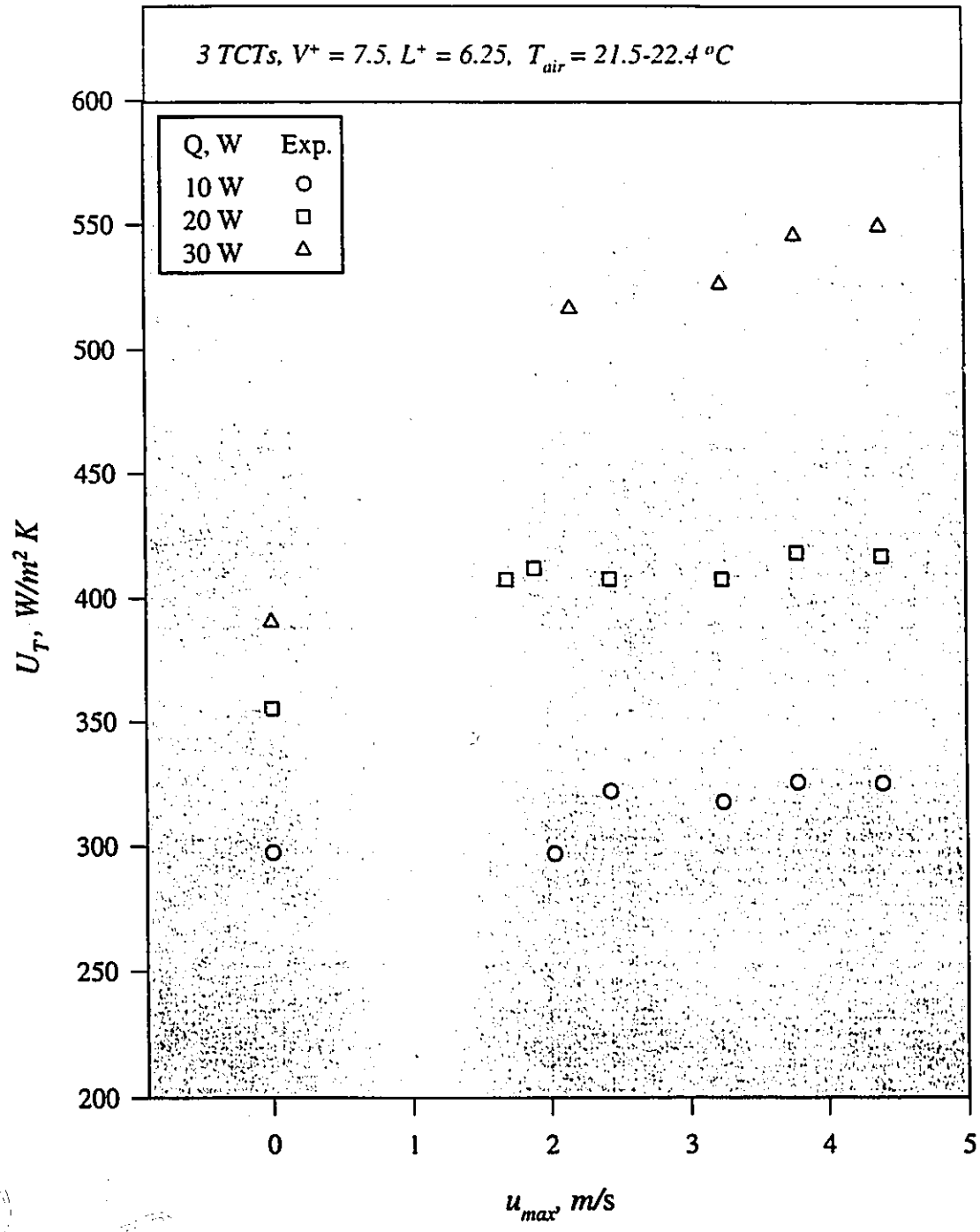

Figure 5.4(g) Effect of u_{max} on U_T; WF = FC-72

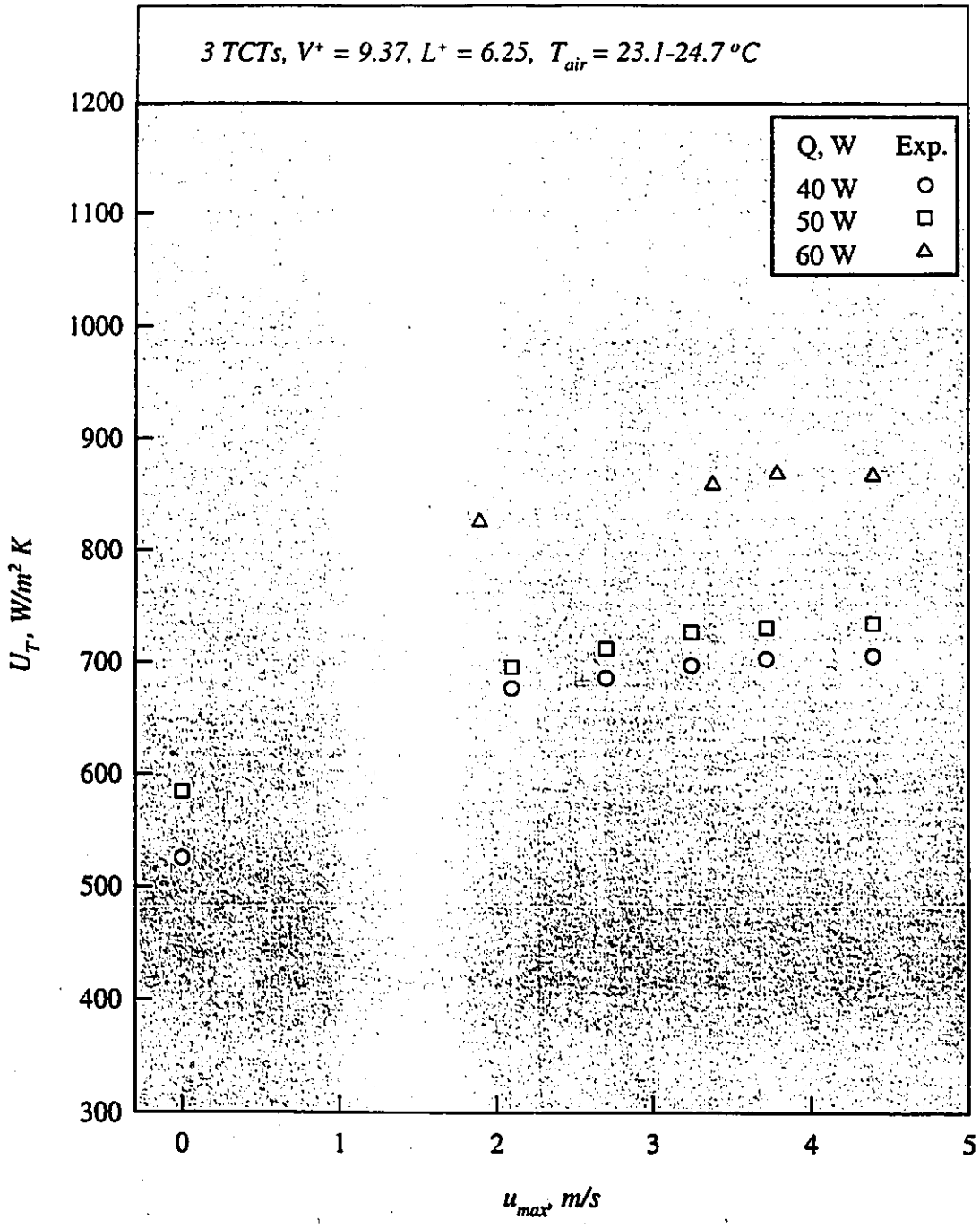

Figure 5.4(h) Effect of u_{max} on U_T; WF = acetone

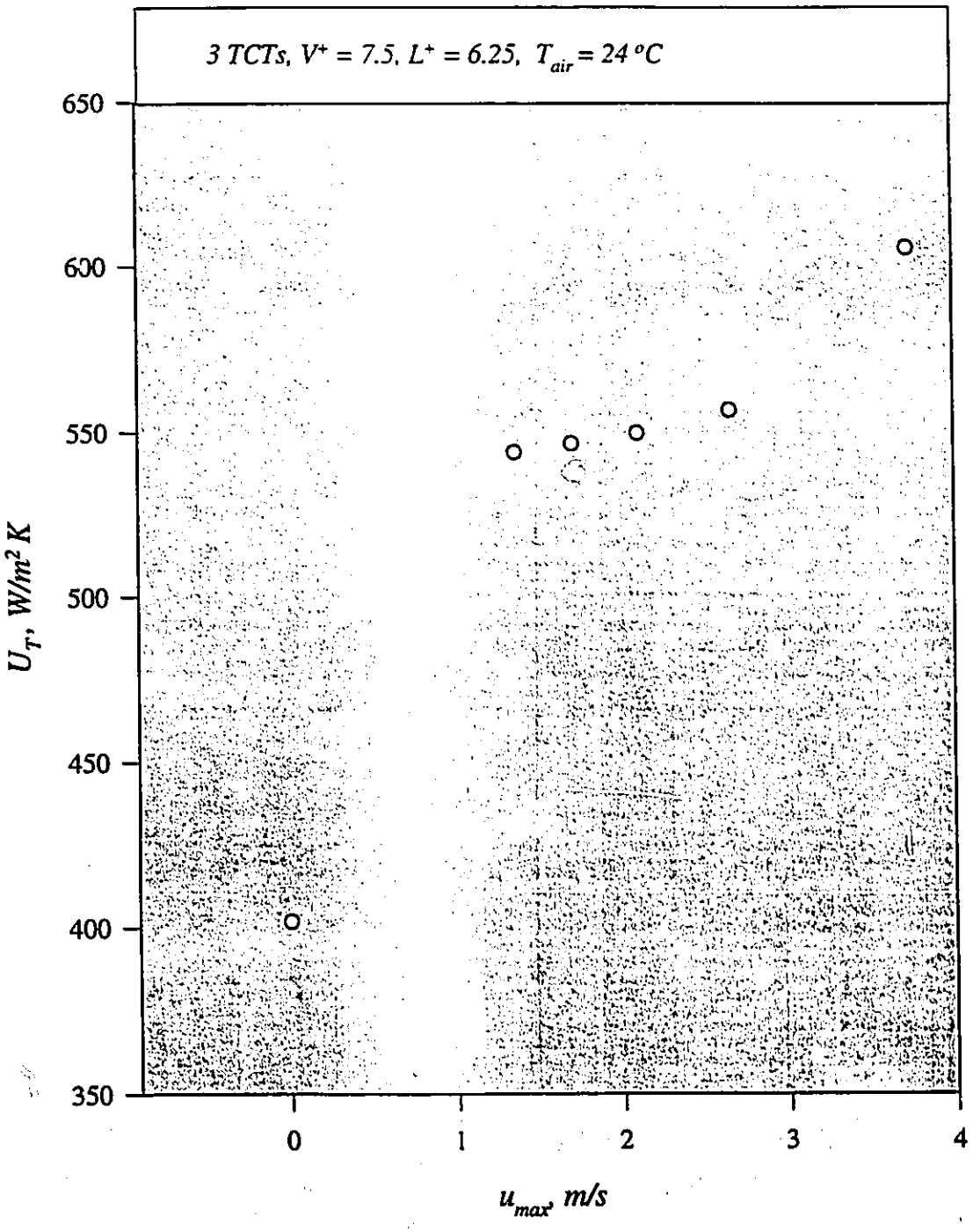

Figure 5.4(i) Effect of u_{max} on U_T; WF = water

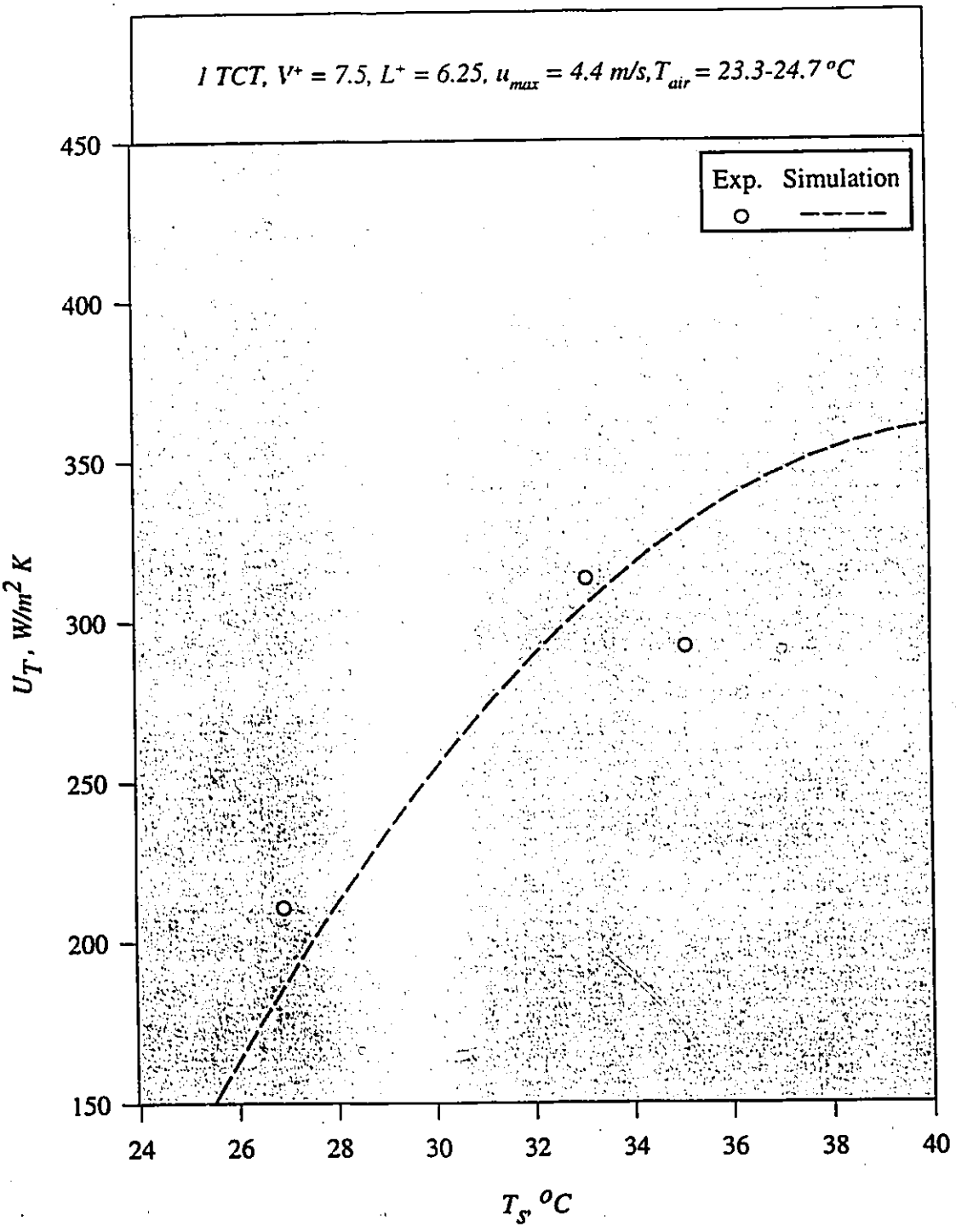

Figure 5.5(a) Effect of T_s on U_T; WF = FC-72

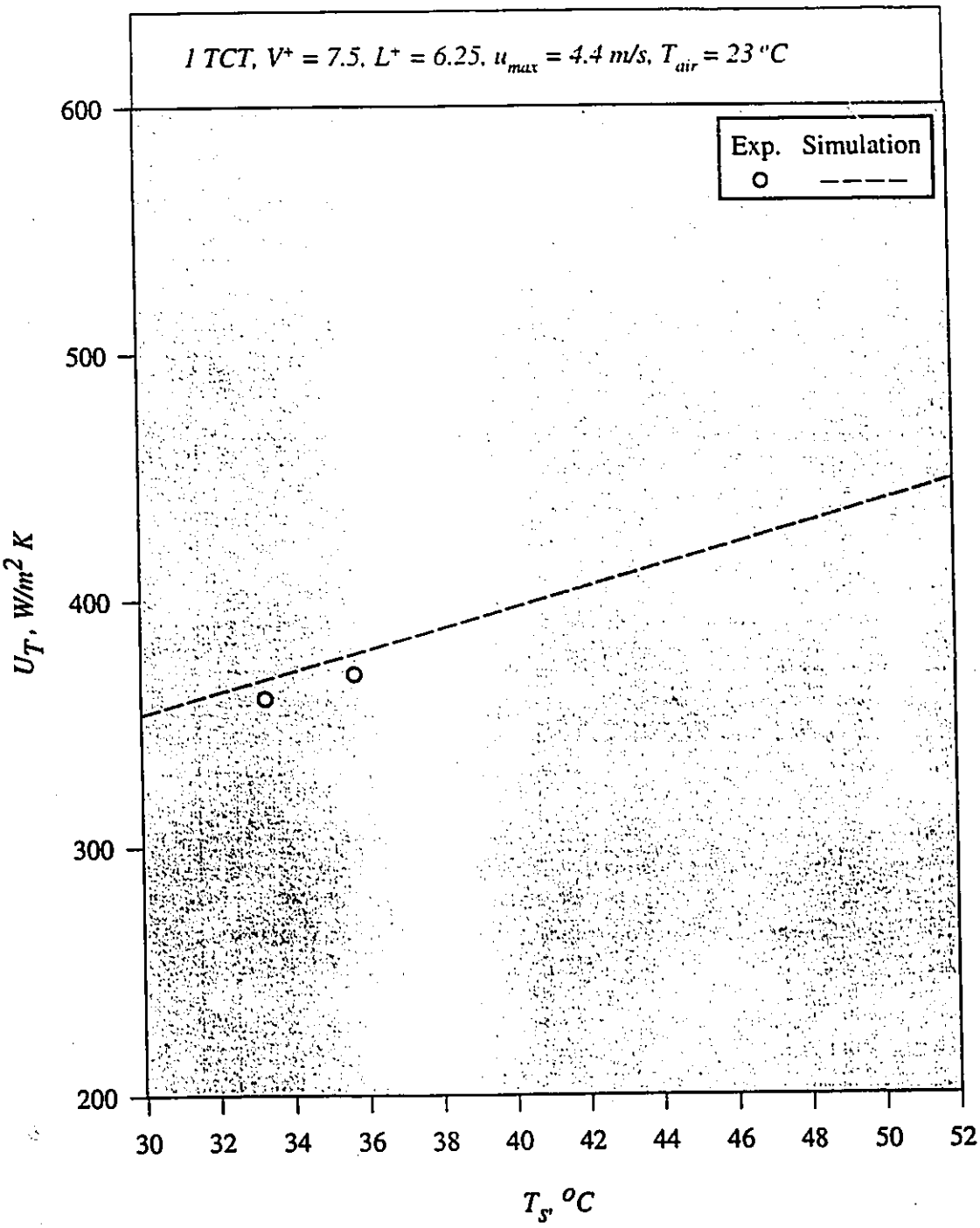

Figure 5.5(b) Effect of T_s on U_T; WF = R-113

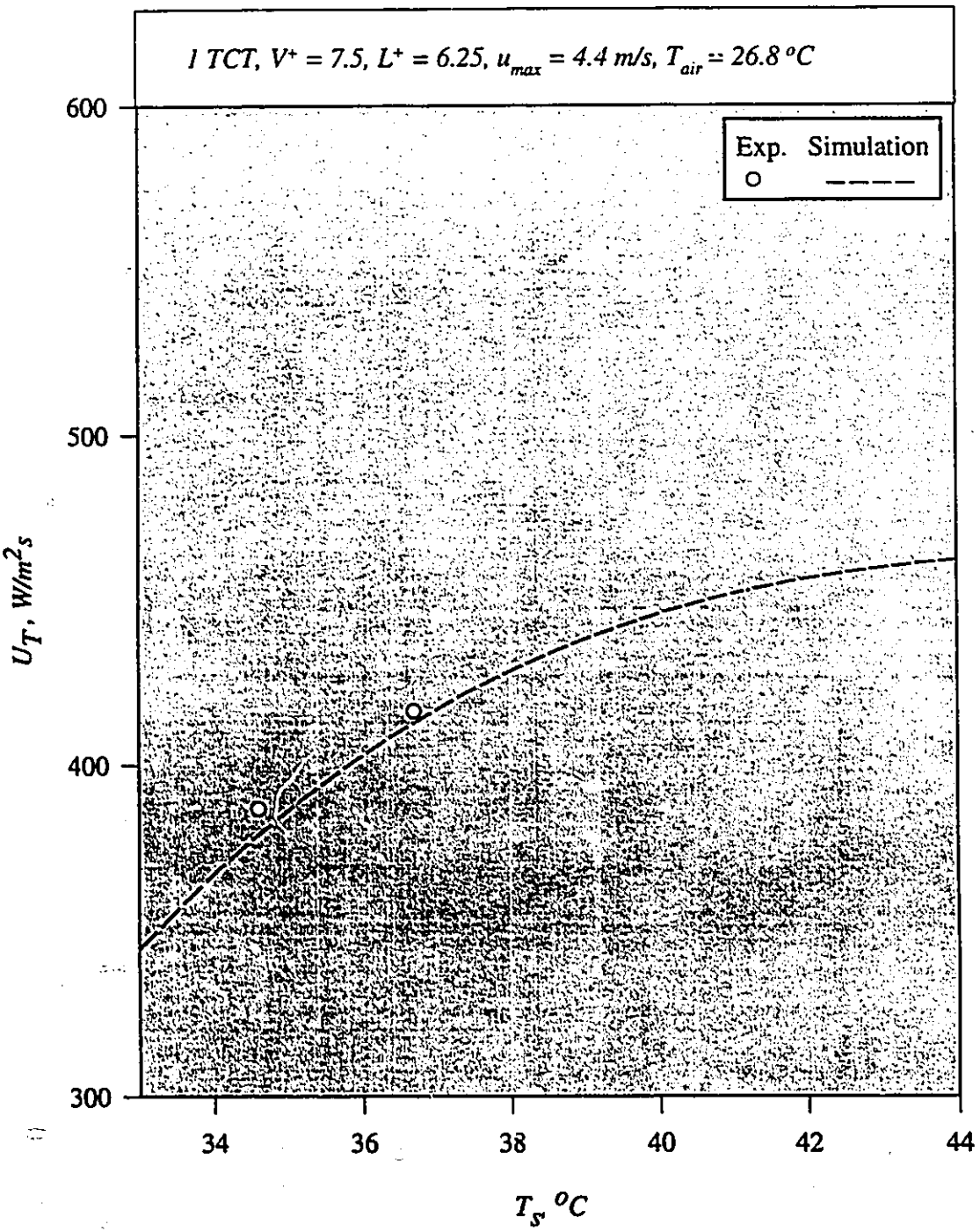

Figure 5.5(c) Effect of T_s on U_T; WF = R-11

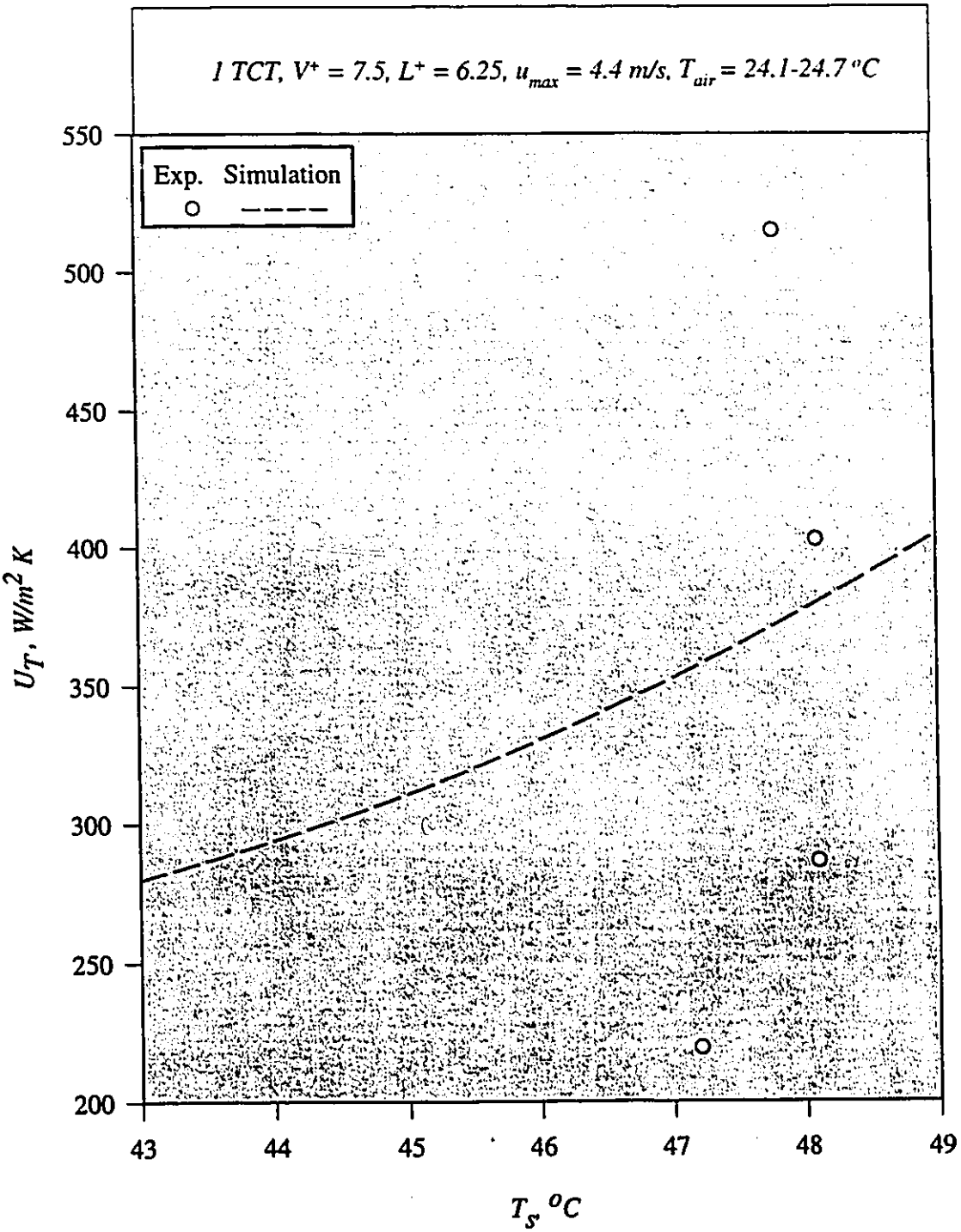

Figure 5.5(d) Effect of T_s on U_T; WF = ethanol

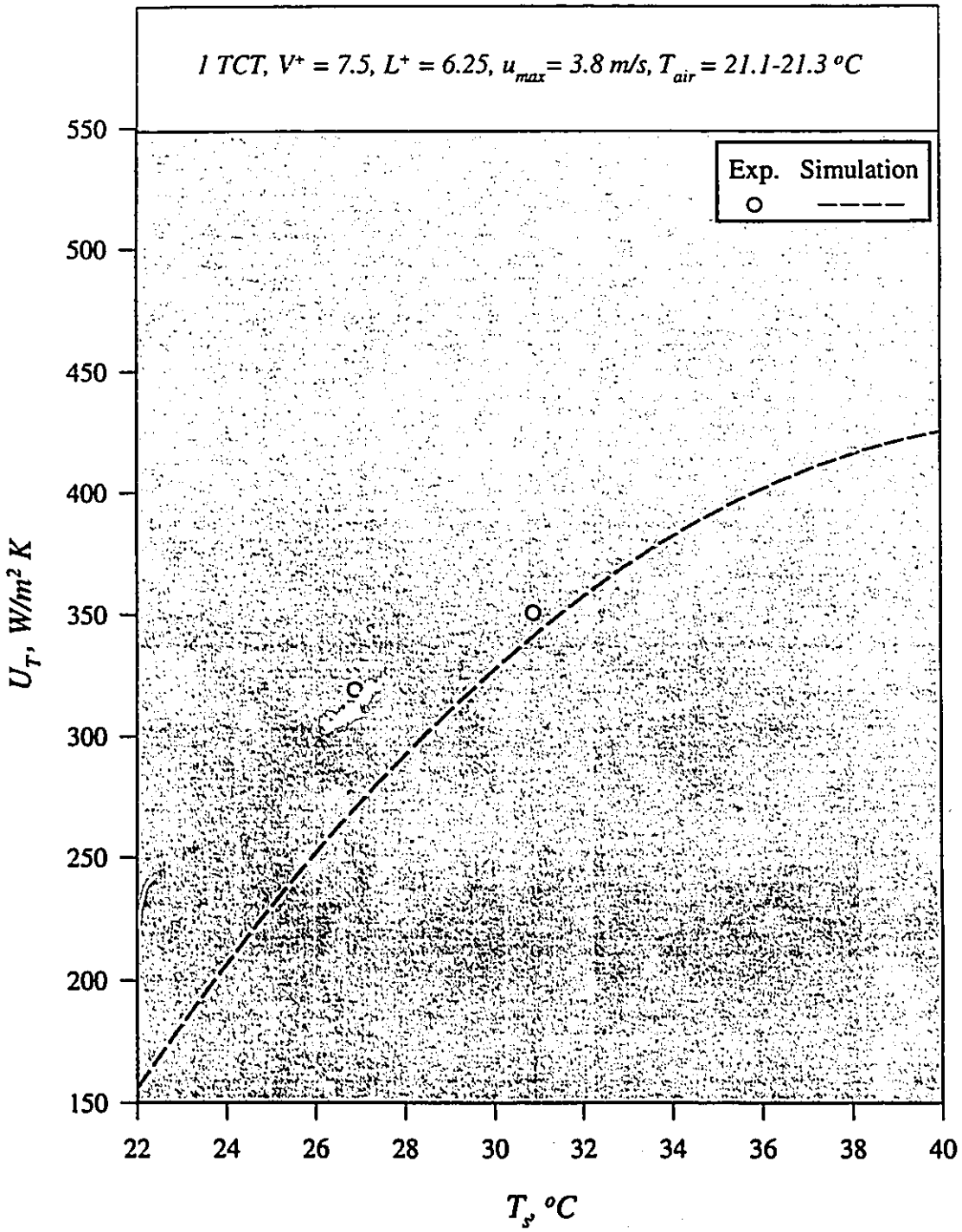

Figure 5.5(e) Effect of T_s on U_T; WF = FC-87

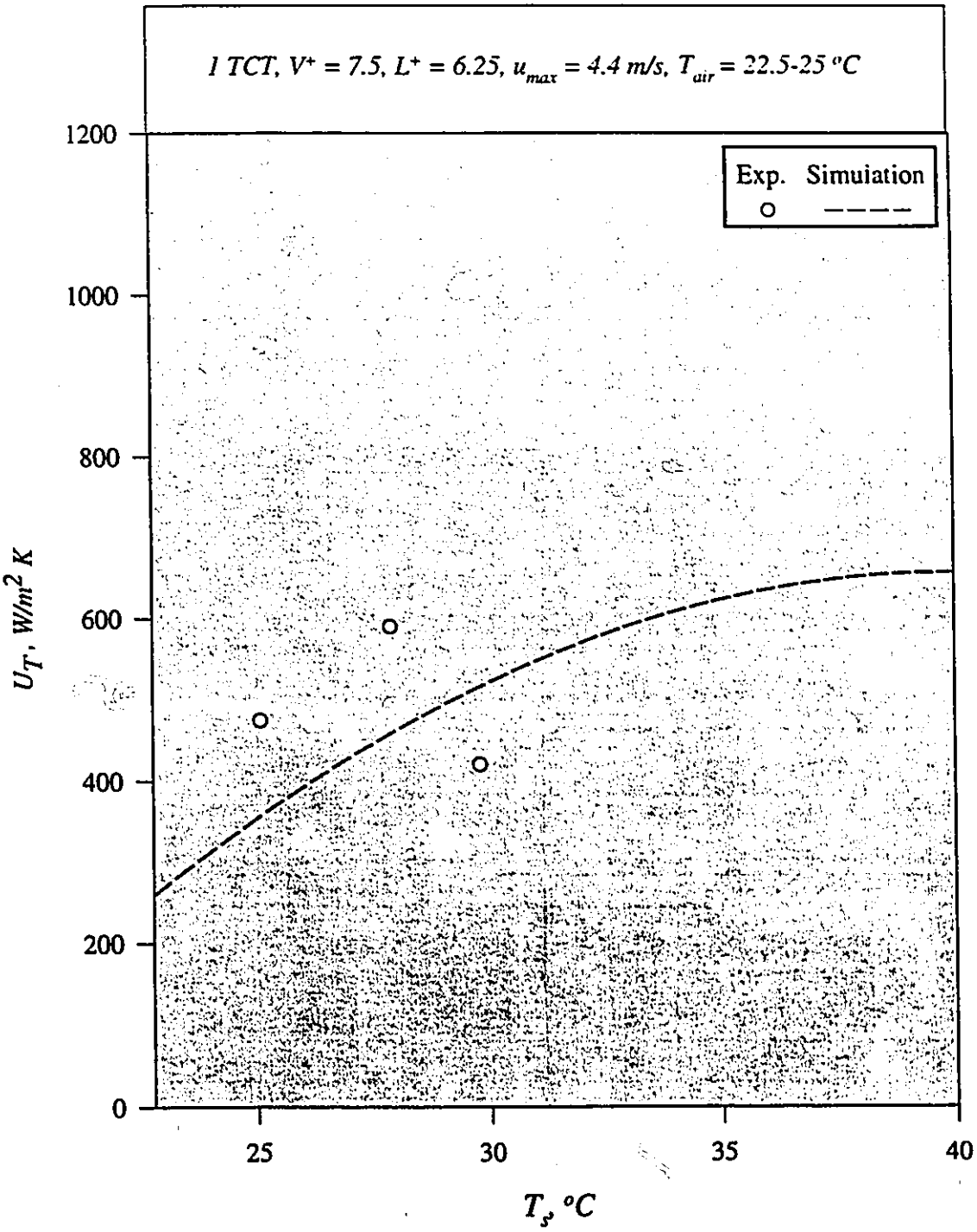

Figure 5.5(f) Effect of T_s on U_T; WF = acetone

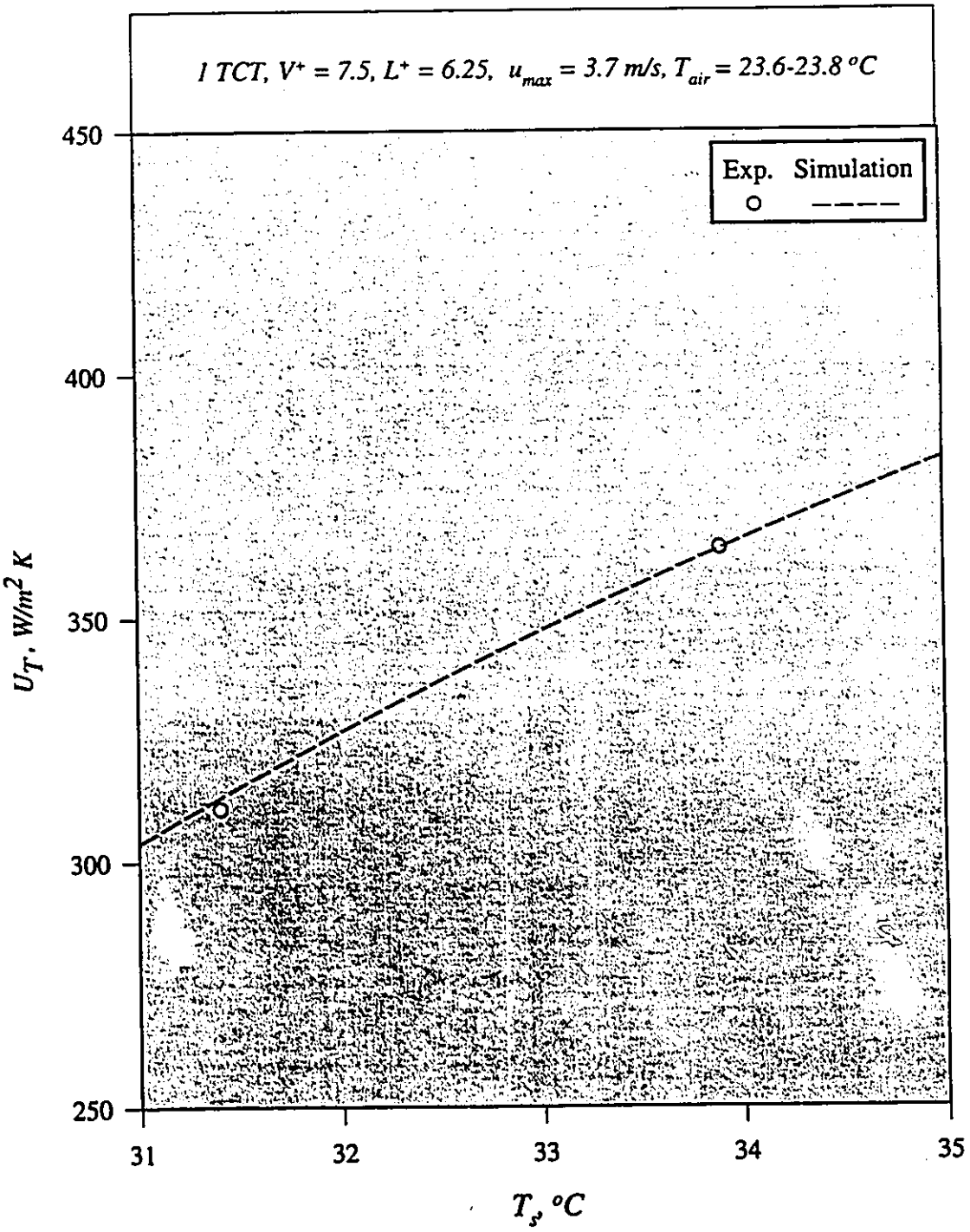

Figure 5.5(g) Effect of T_s on U_T; WF = water

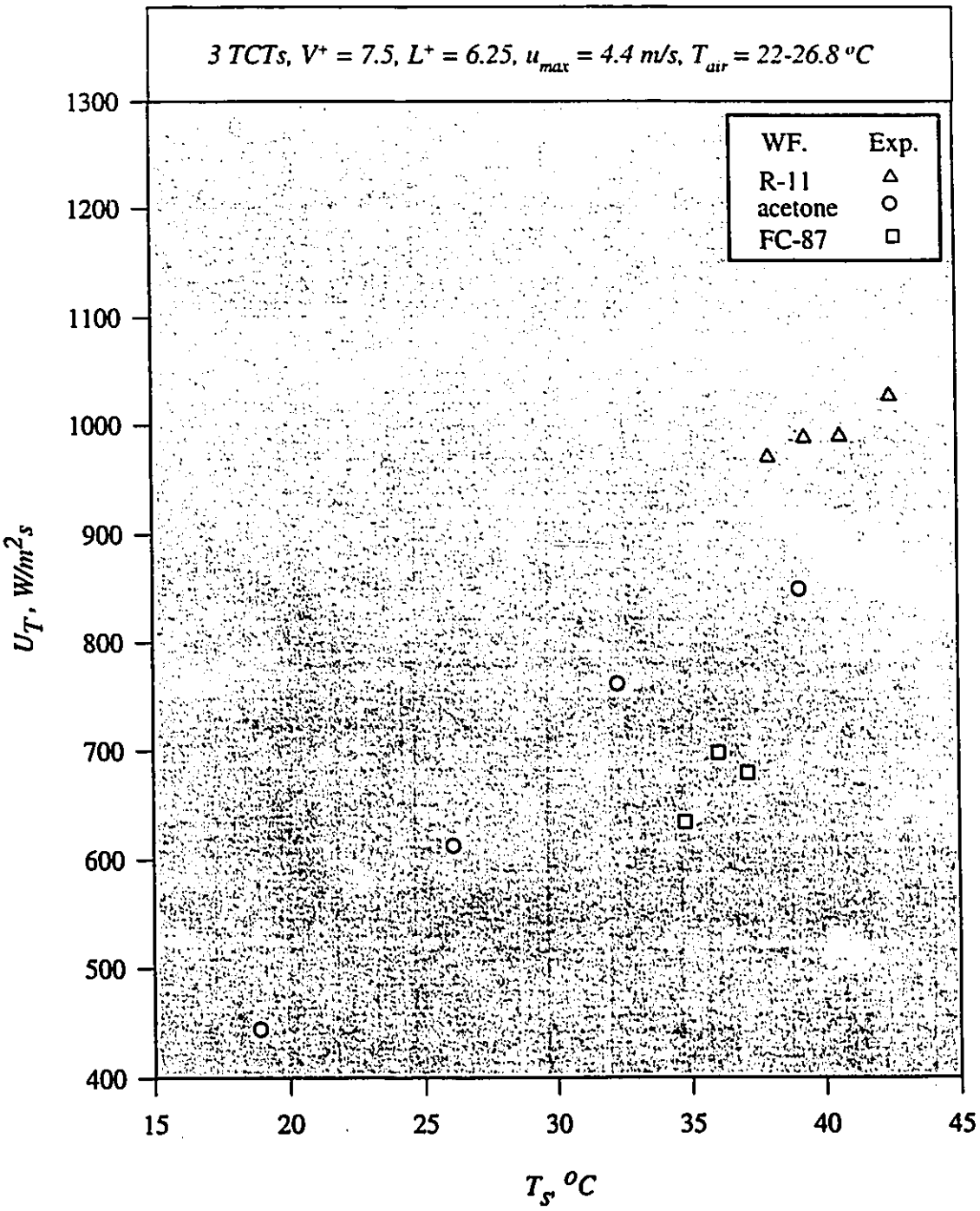

Figure 5.5(h) Effect of T_s on U_T; WF = R-11, FC-87, and acetone

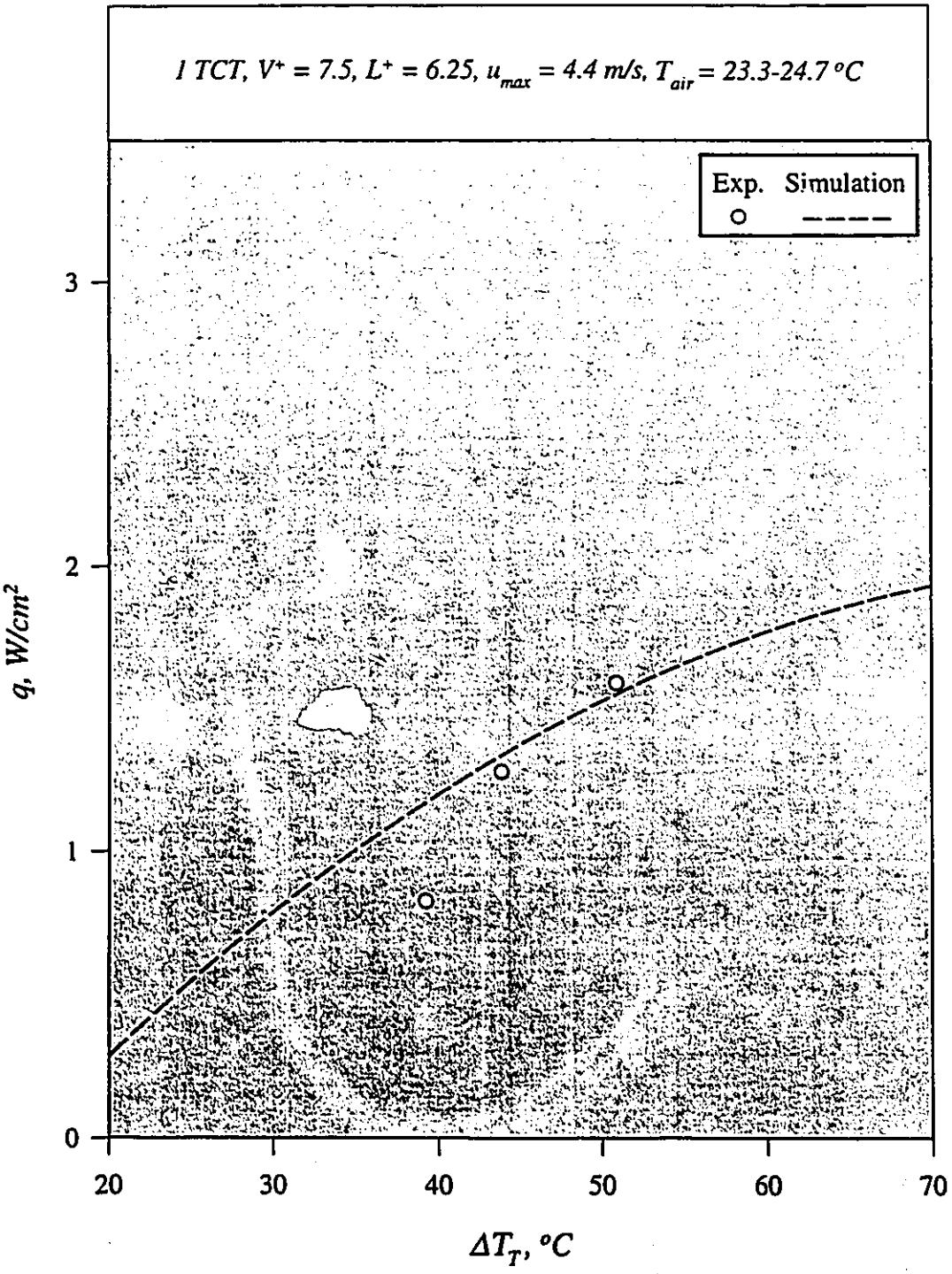

Figure 5.6(a) Effect of ΔT_T on q; WF = FC-72

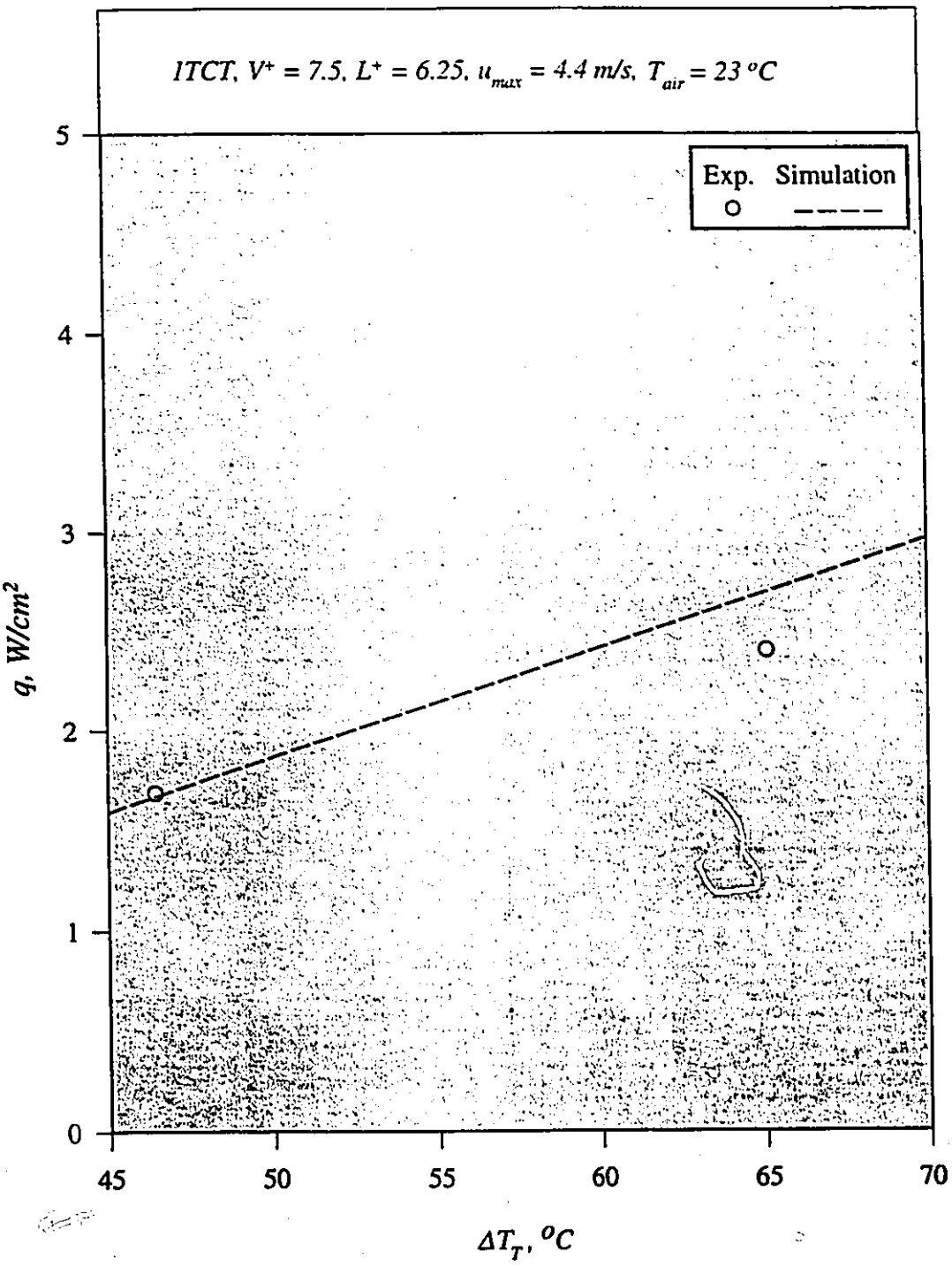

Figure 5.6(b) Effect of ΔT_T on q; WF = R-113

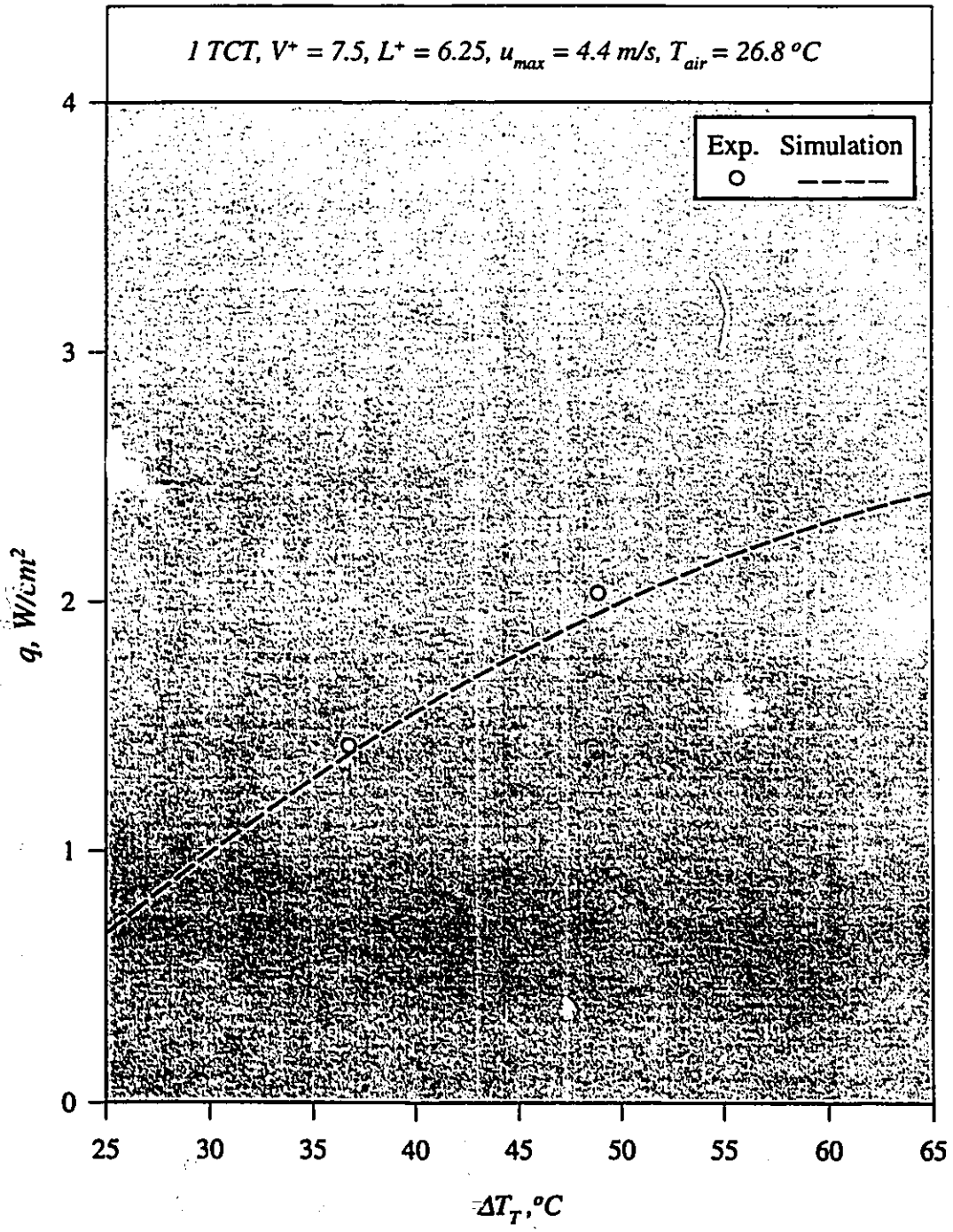

Figure 5.6(c) Effect of ΔT_T on q; WF = R-11

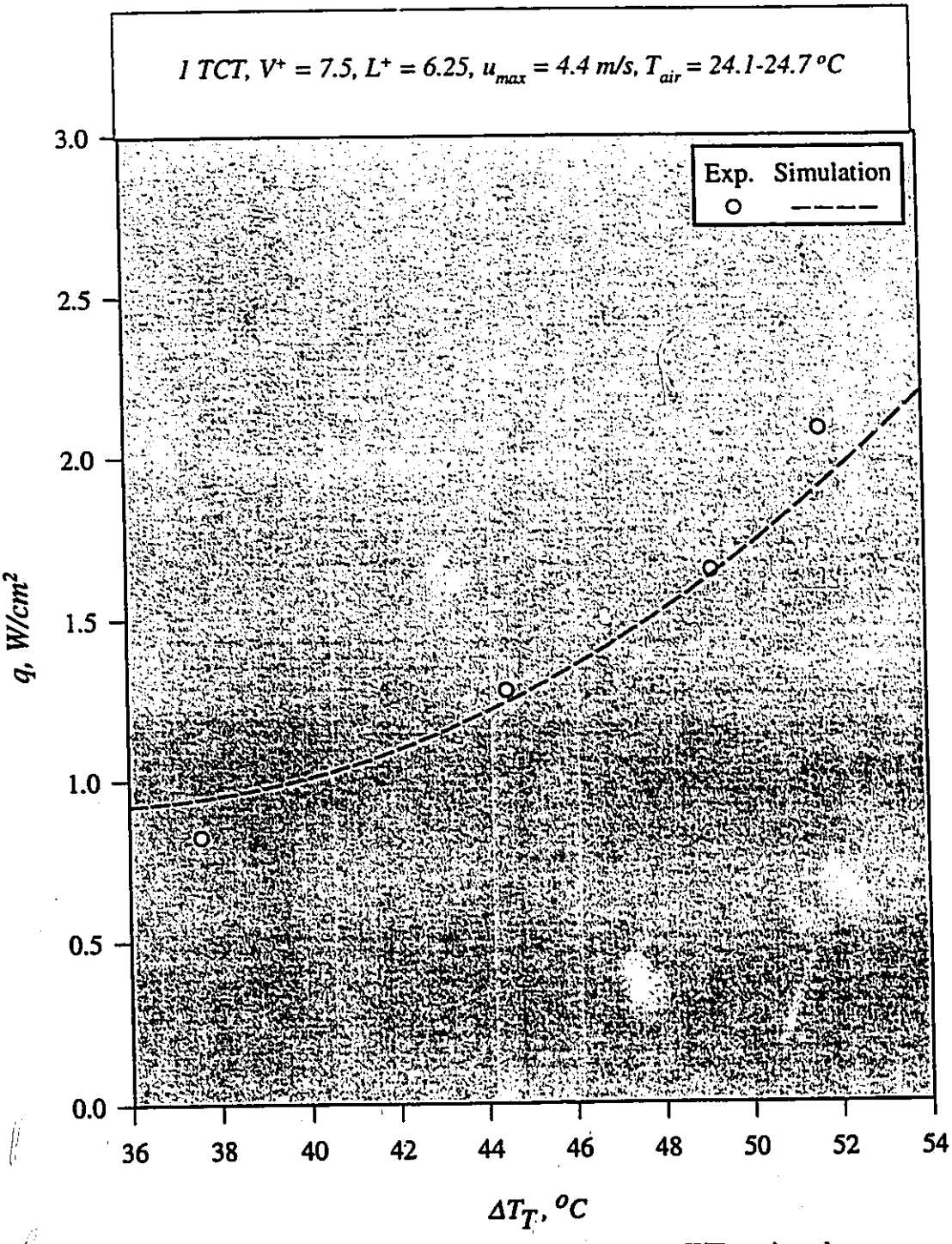

Figure 5.6(d) Effect of ΔT_T on q; WF = ethanol

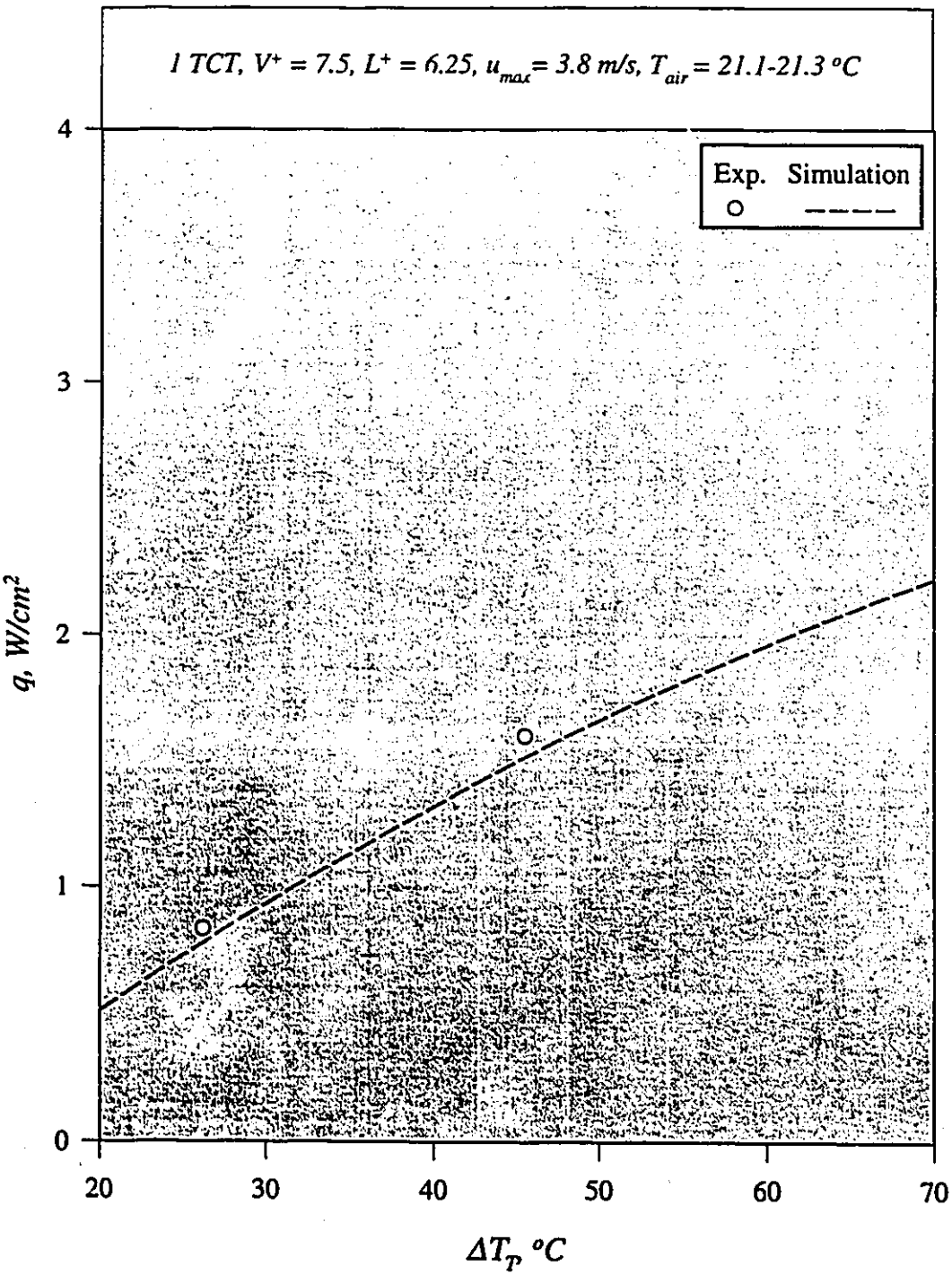

Figure 5.6(e) Effect of ΔT_T on q; WF = FC-87

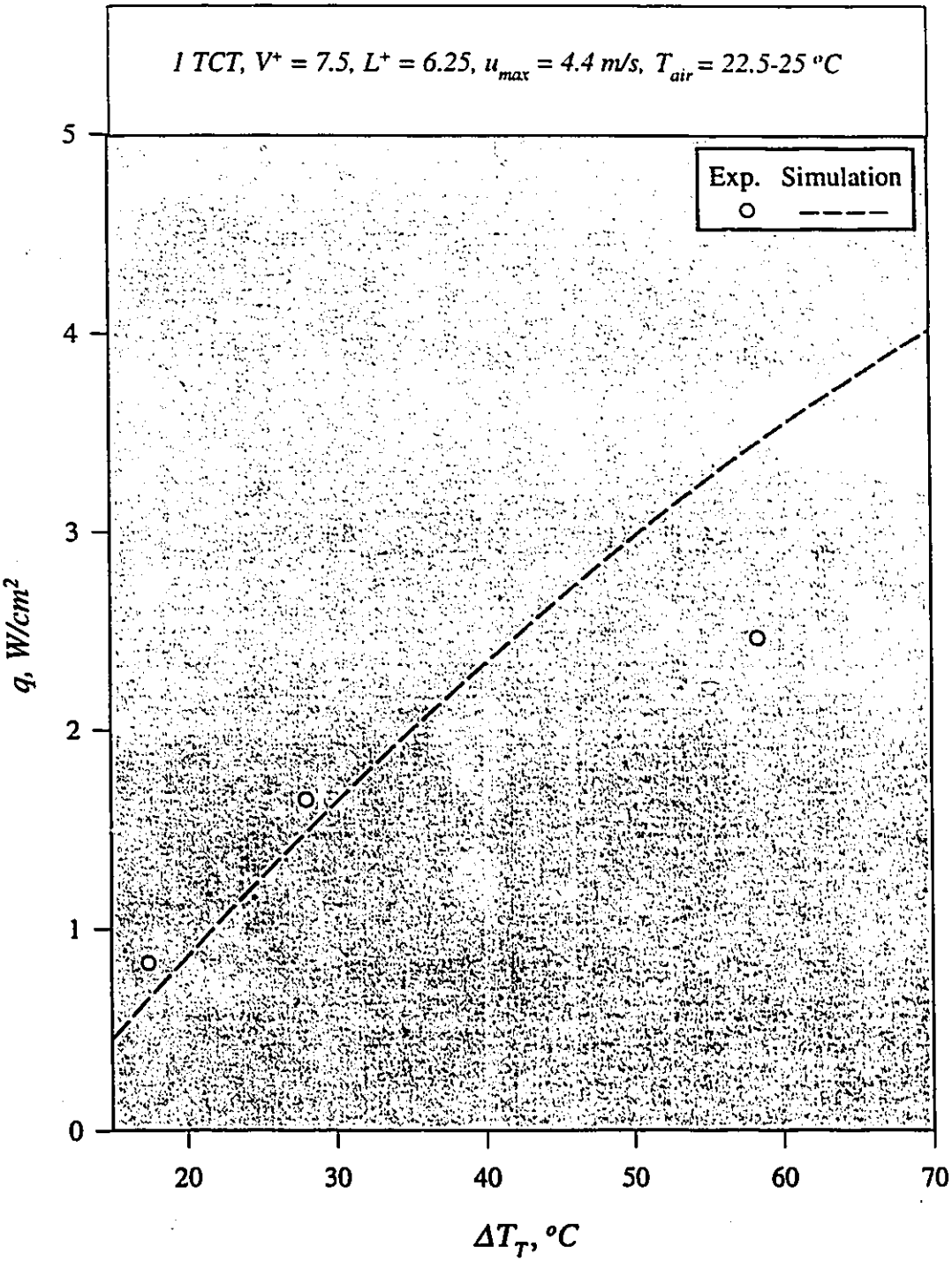

Figure 5.6(f) Effect of ΔT_T on q; WF = acetone

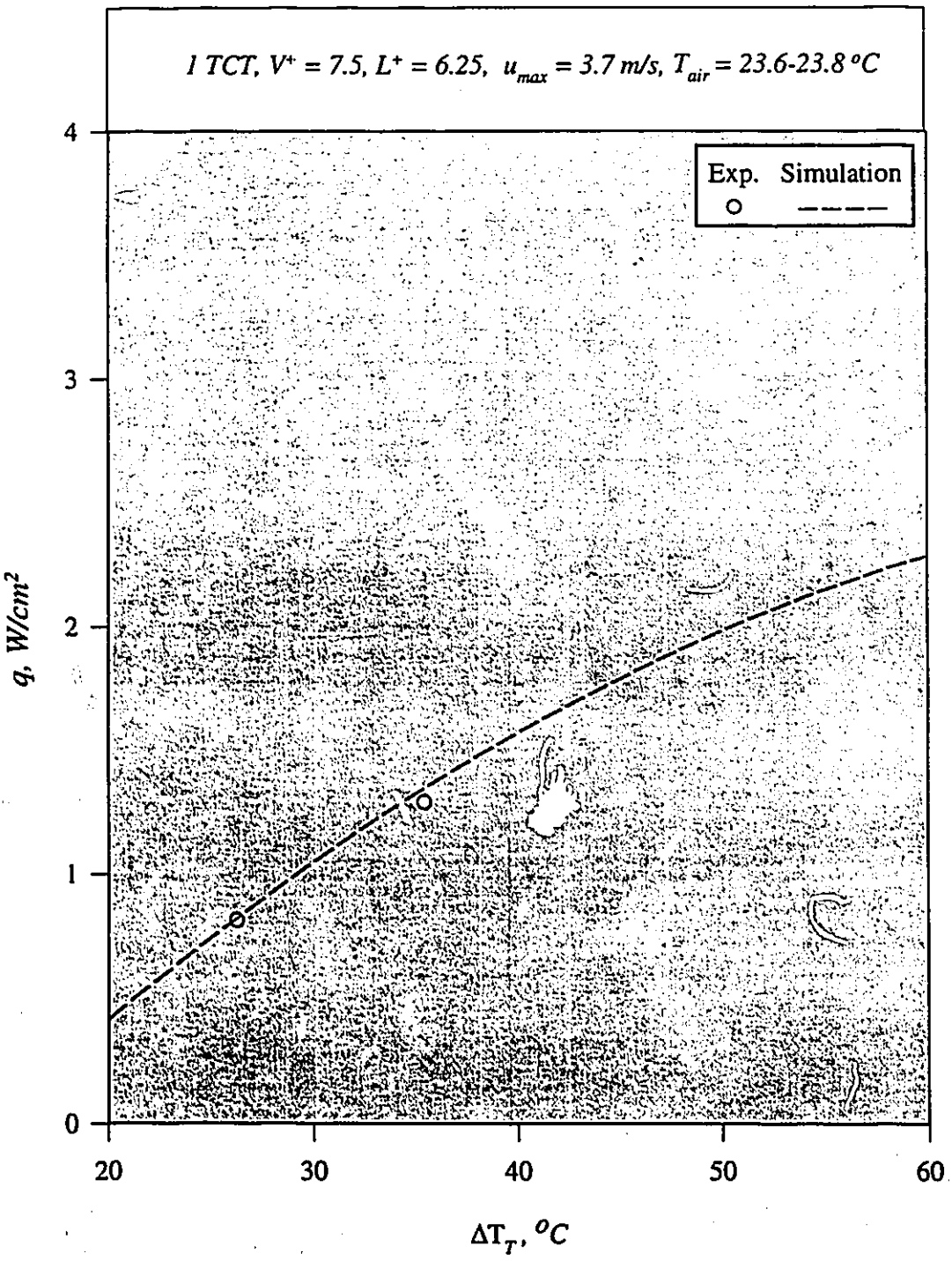

Figure 5.6(g) Effect of ΔT_T on q; WF = water

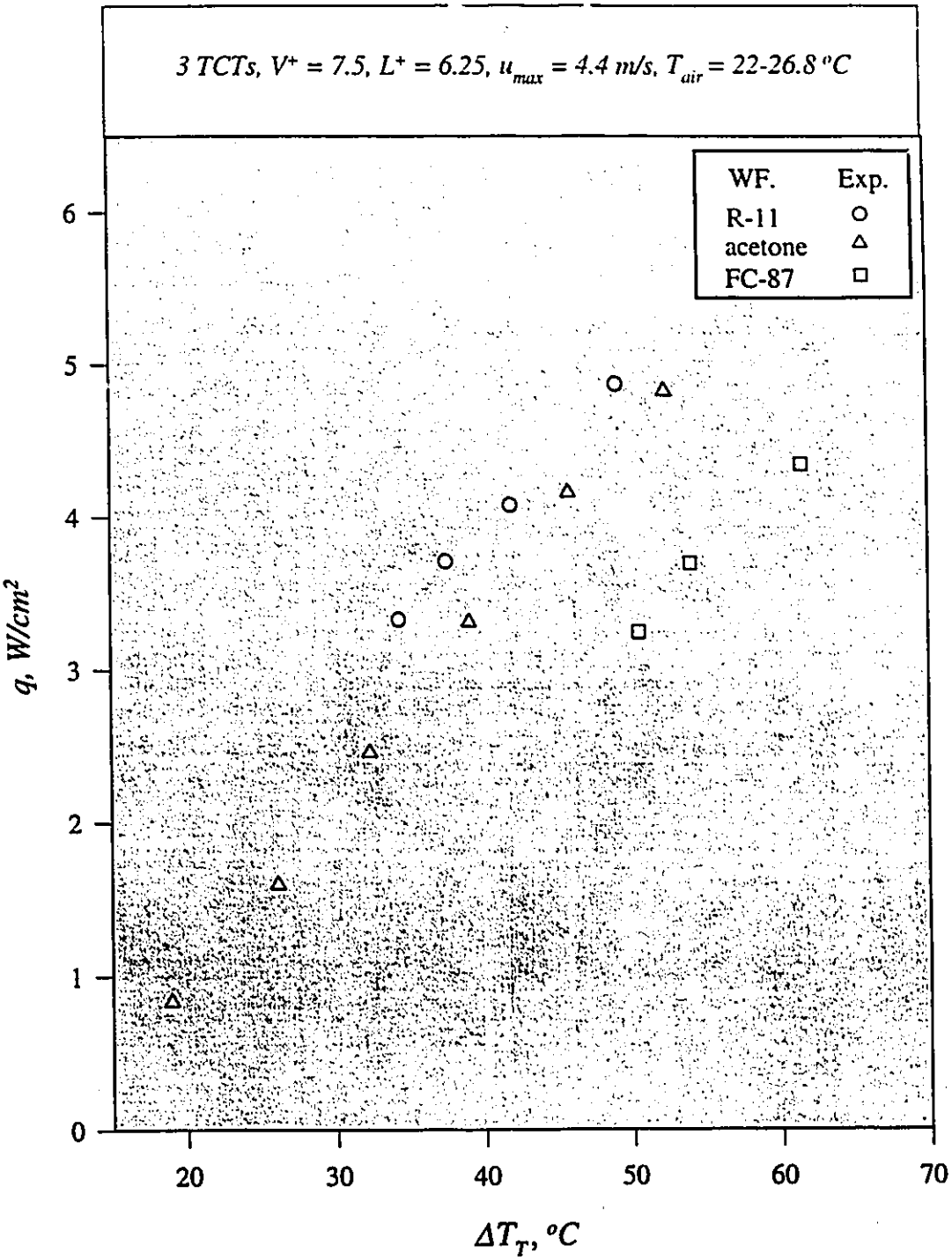

Figure 5.6(h) Effect of ΔT_T on q; Wf = R-11, FC-87, and acetone

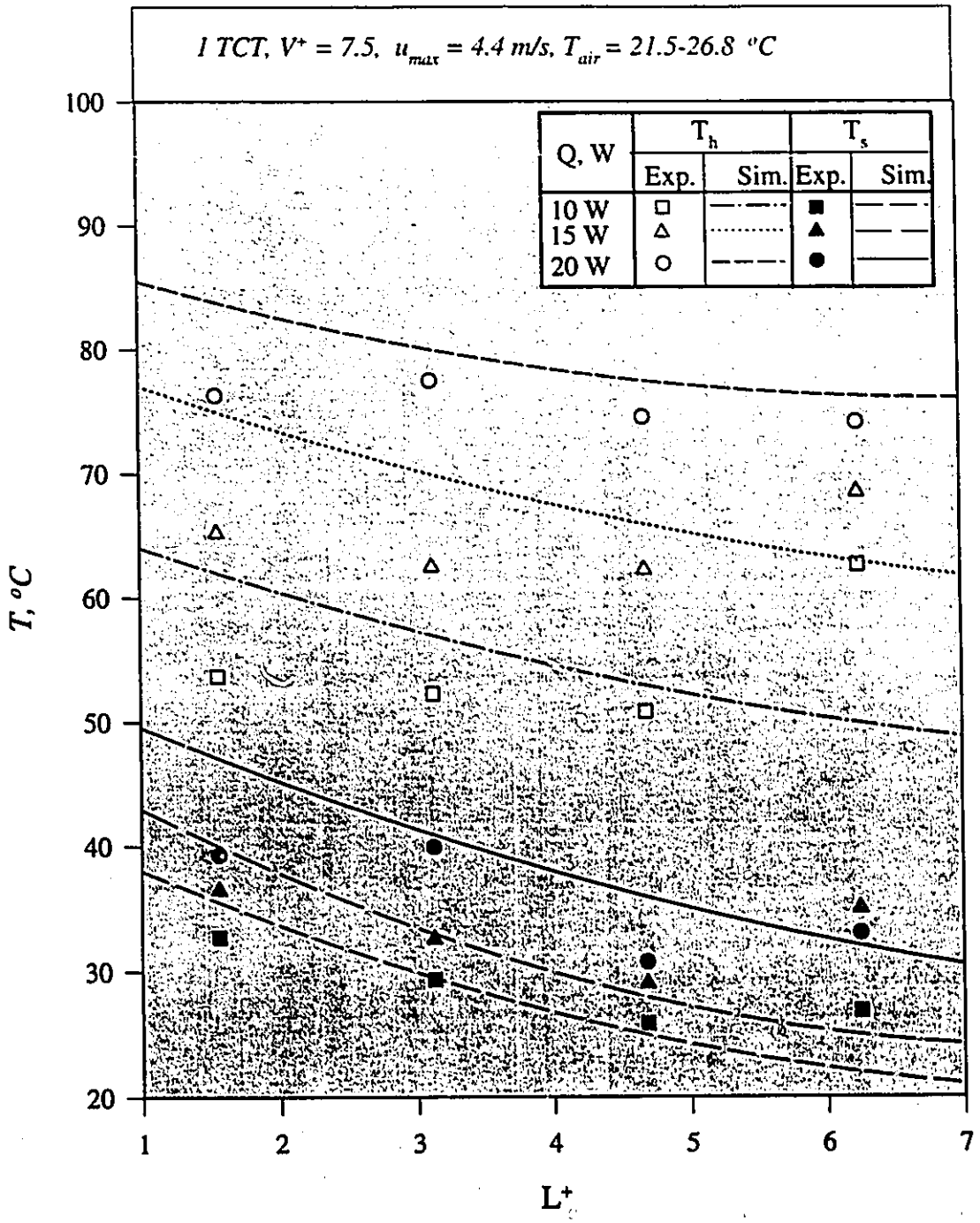

Figure 5.7(a) Effect of L^+ on T_h and T_s; WF = FC-72

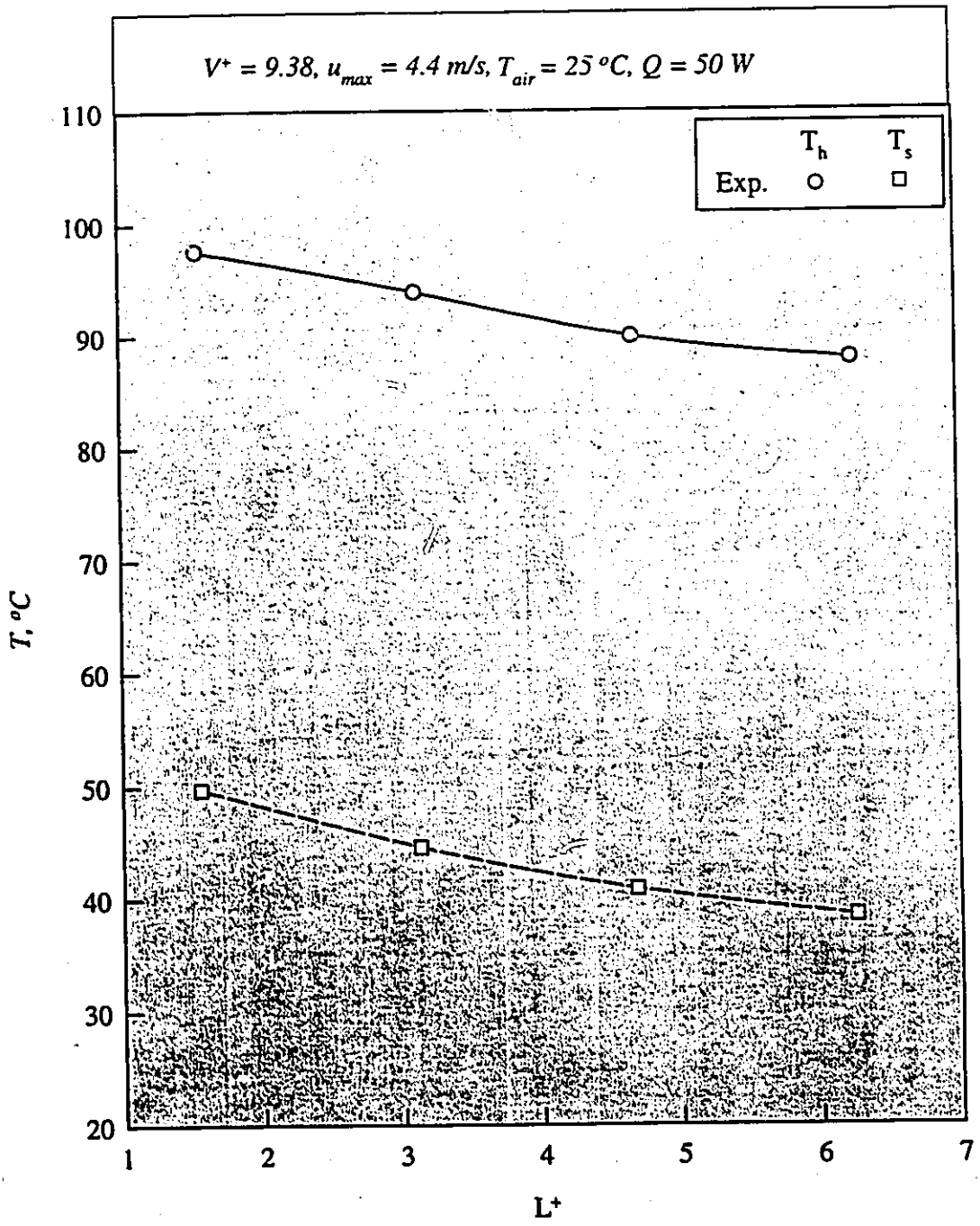

Figure 5.7(b) Effect of L^+ on T_h and T_s with 3 TCTs; WF = FC-87

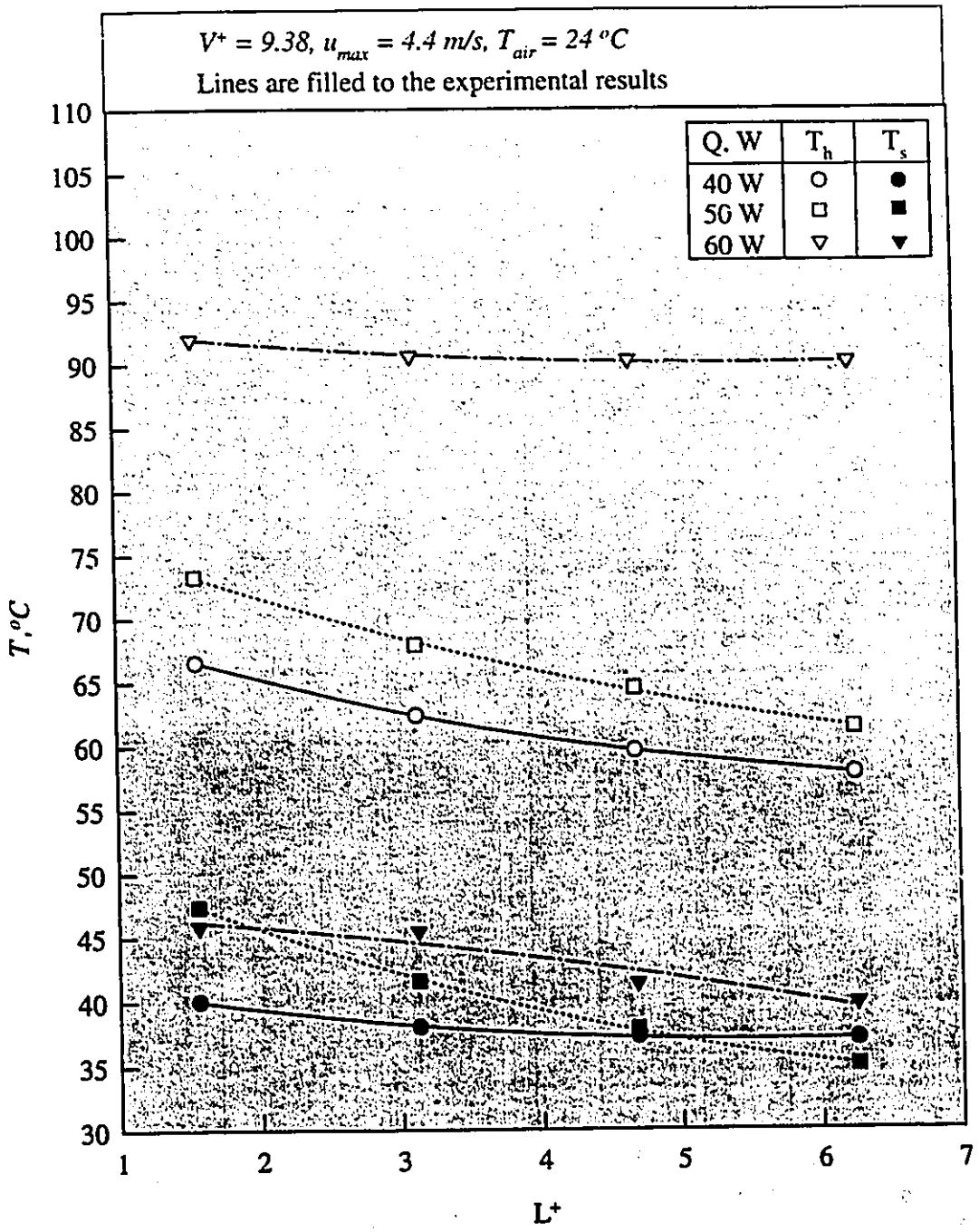

Figure 5.7(c) Effect of L^+ on T_h and T_s with 3 TCTs; WF = acetone

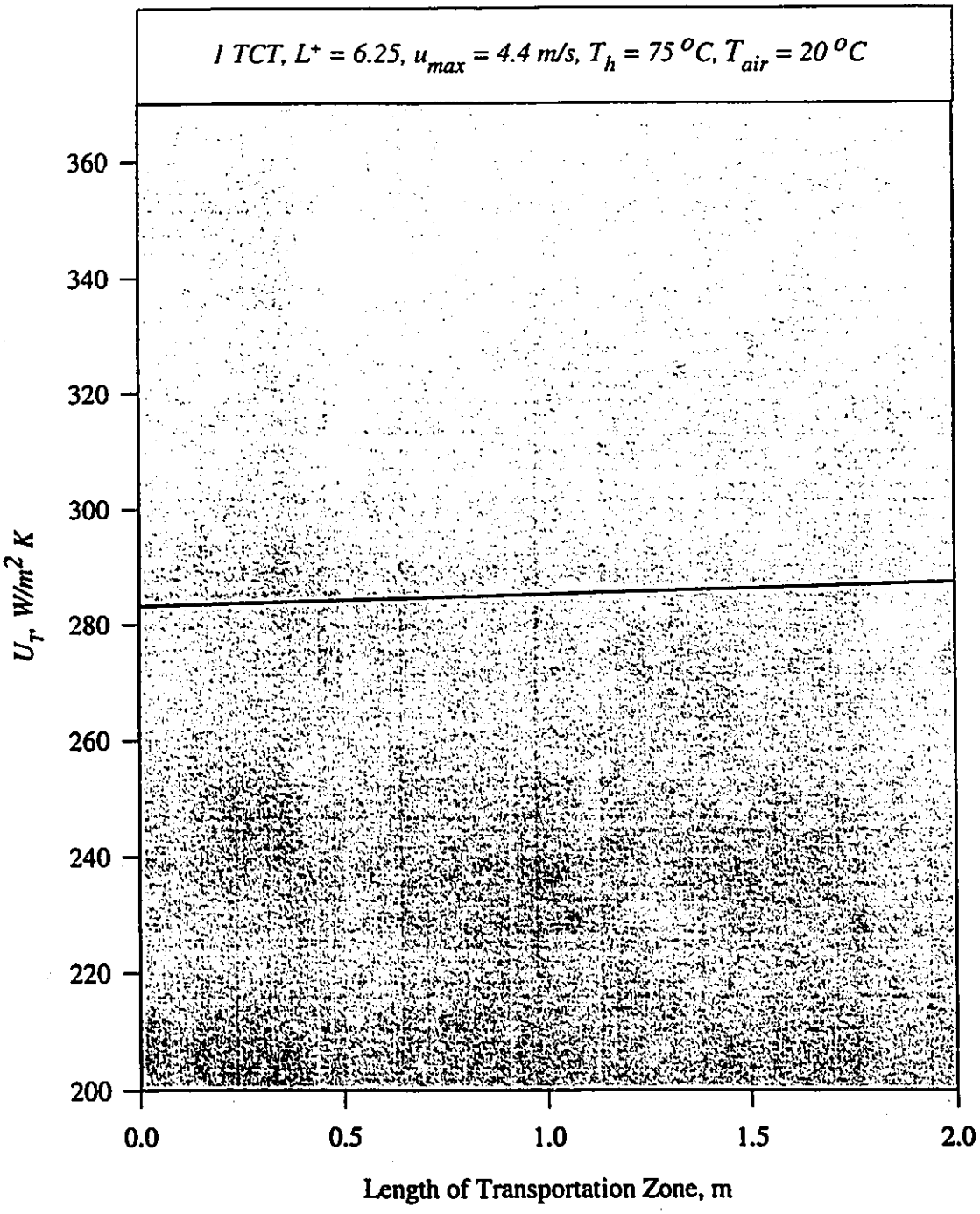

Figure 5.8 Effect of the length of transportation zone on U_T; WF = FC-72

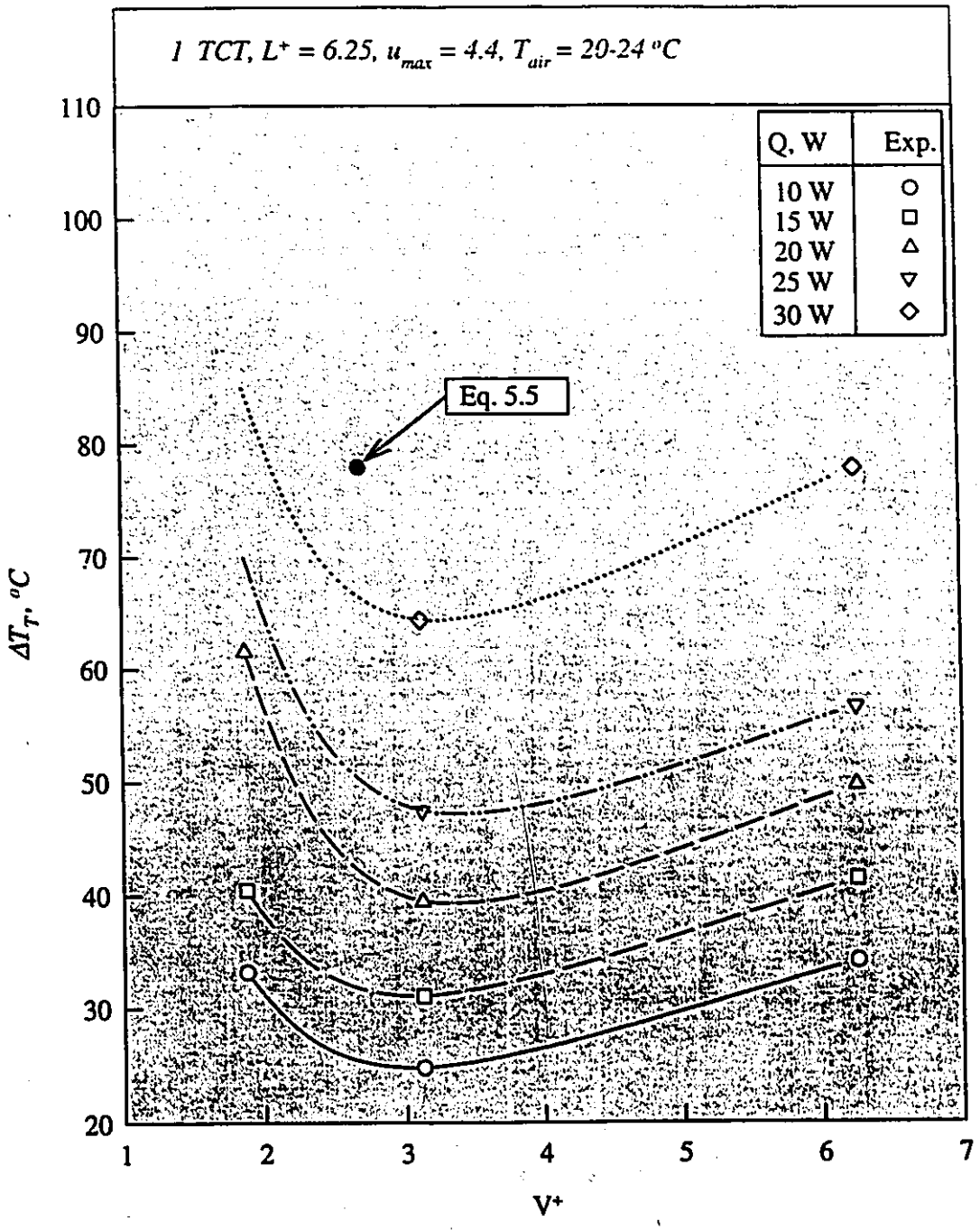

Figure 5.9(a) Effect of V^+ on ΔT_T; WF = FC-87

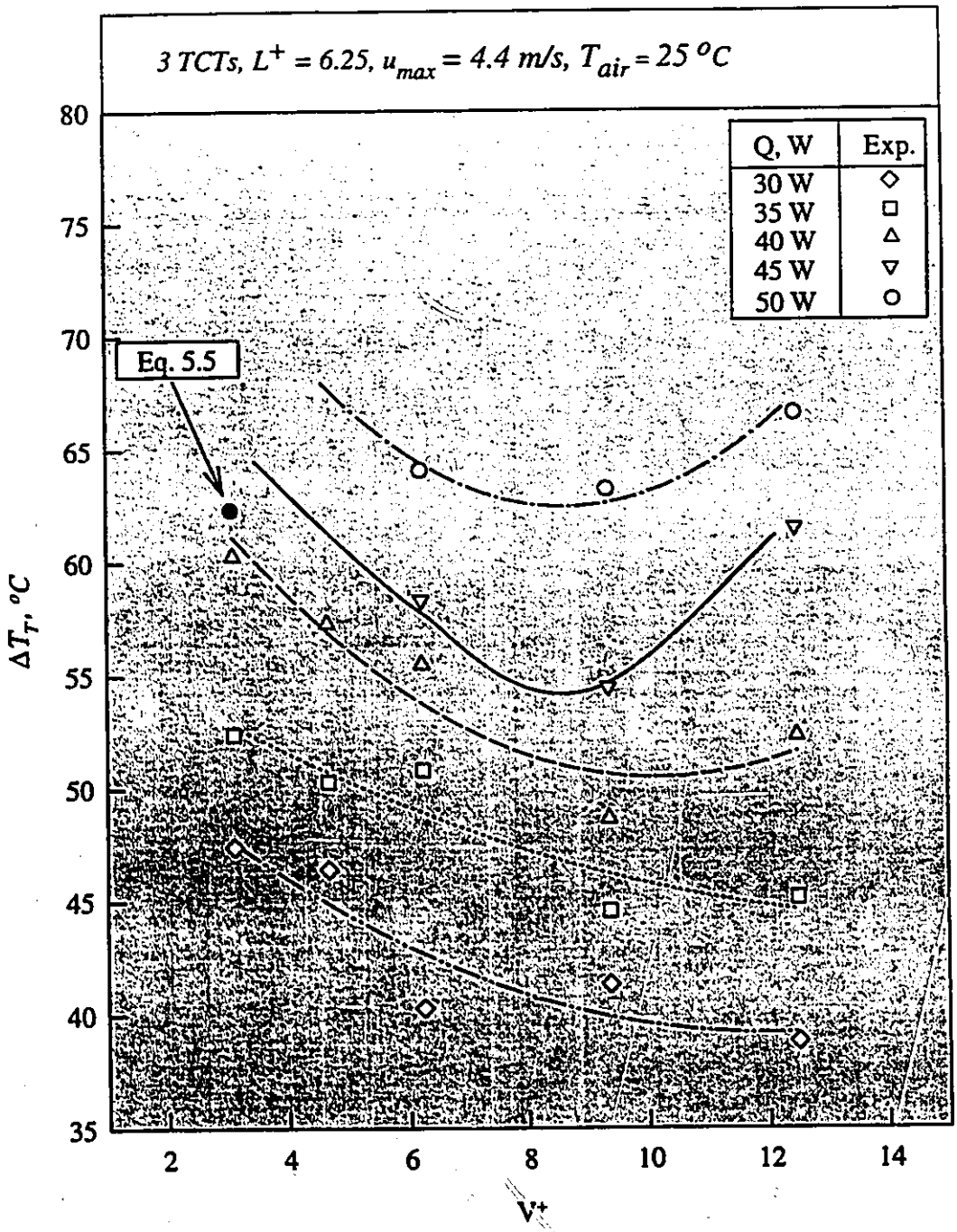

Figure 5.9(b) Effect of V^+ on ΔT_T; WF = FC-87

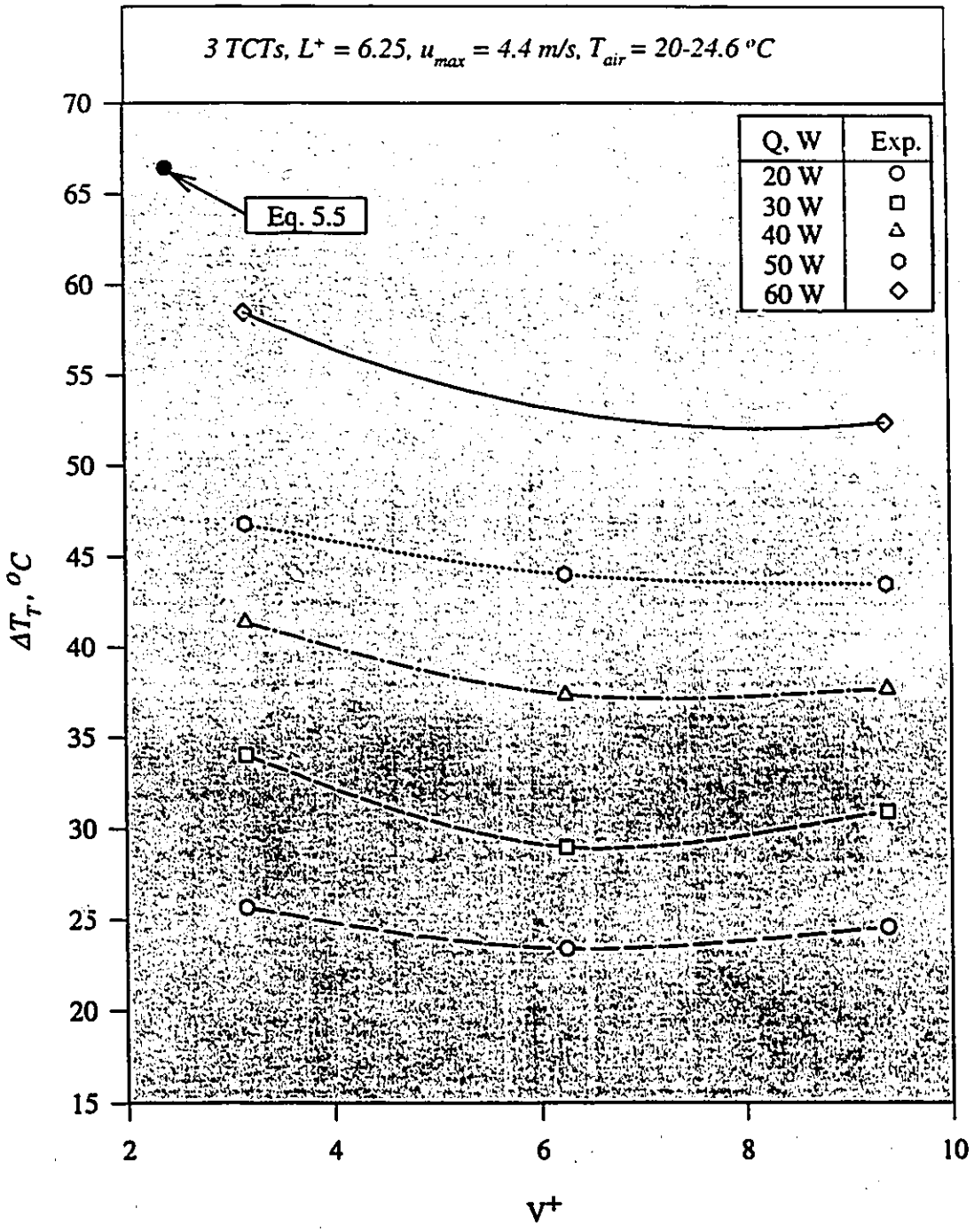

Figure 5.9(c) Effect of V^+ on ΔT_T; WF = acetone

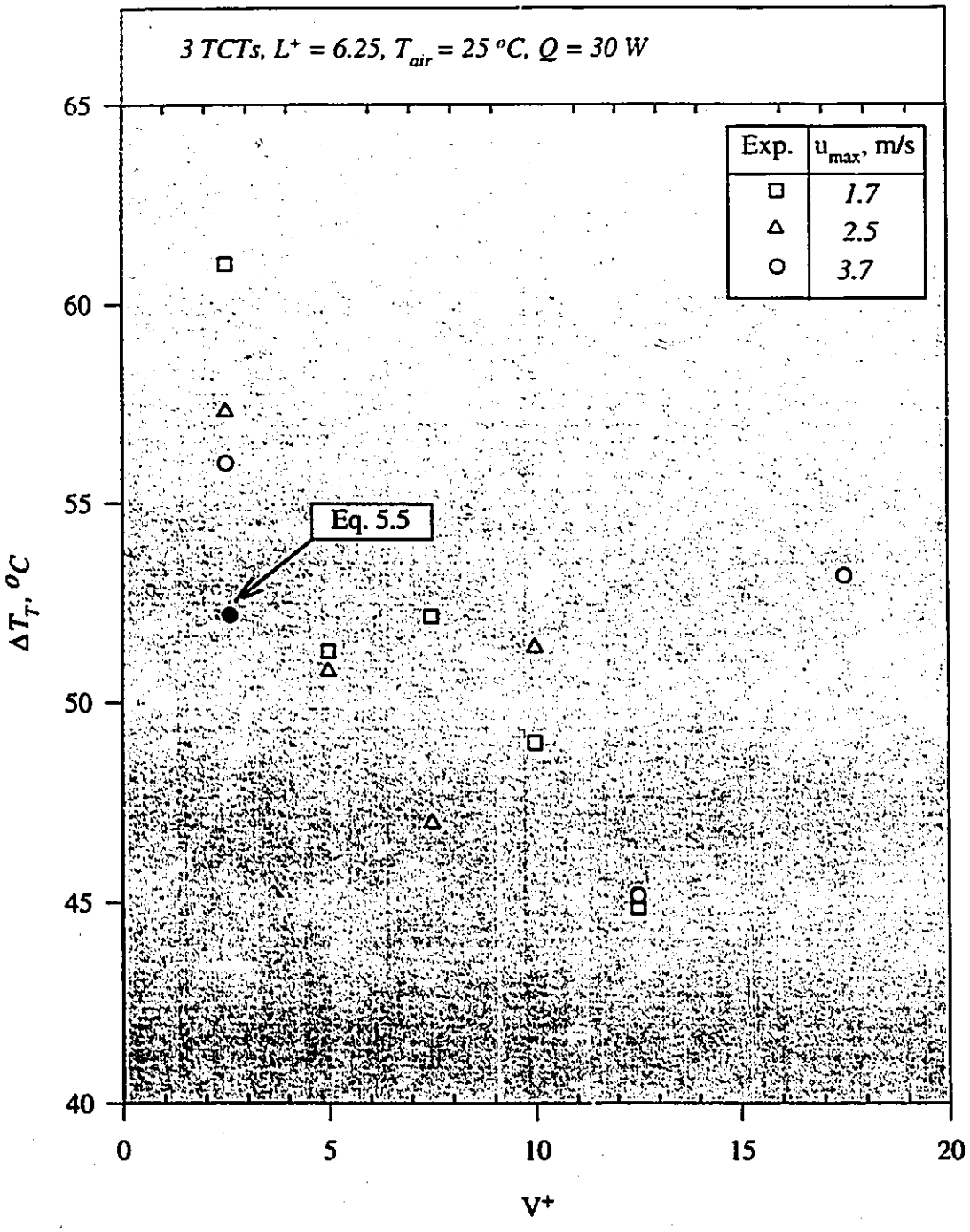

Figure 5.9(d) Effect of V^+ on ΔT_T ; WF = R-113

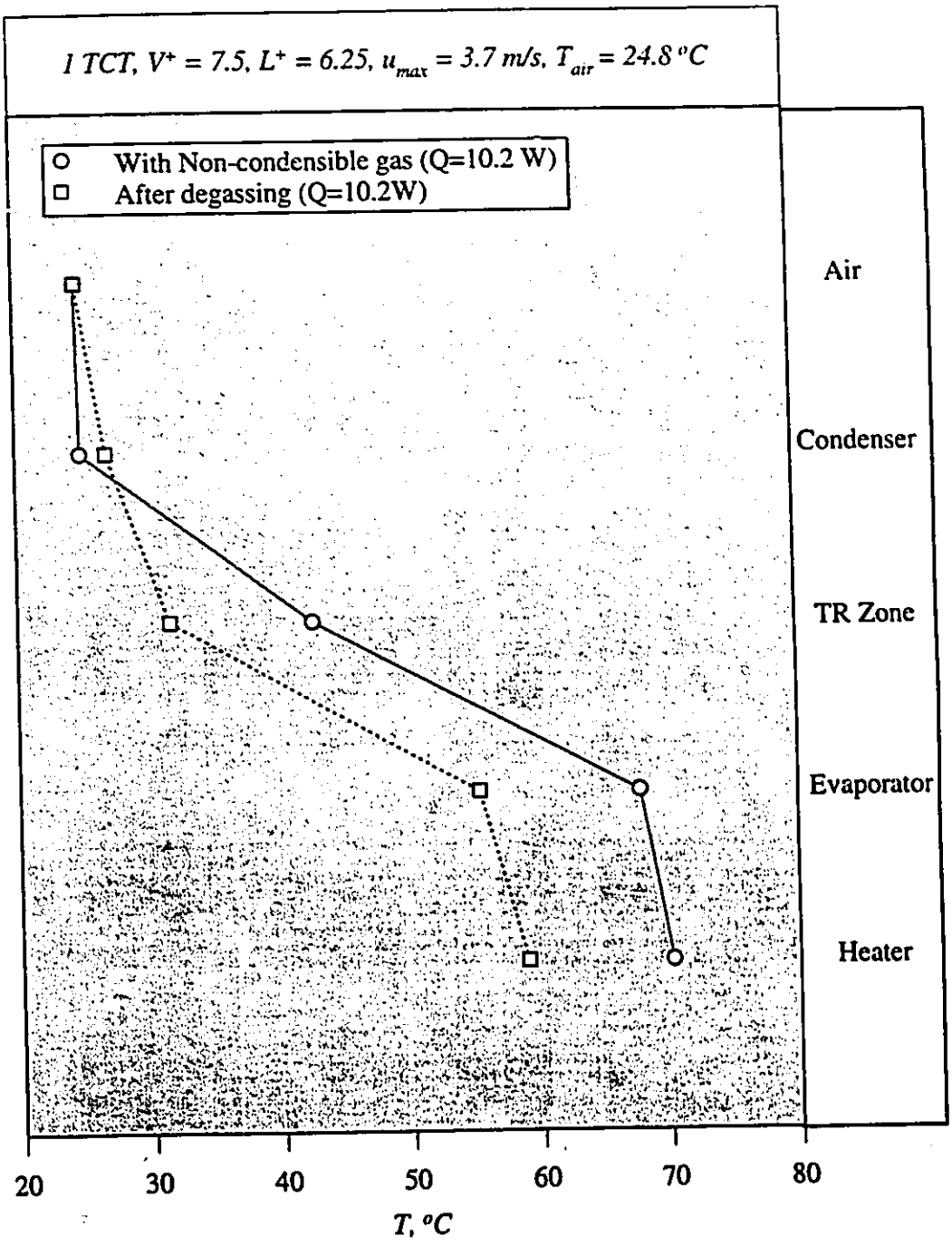

Figure 5.10 Effect of Non-condensible gas; WF = FC-72

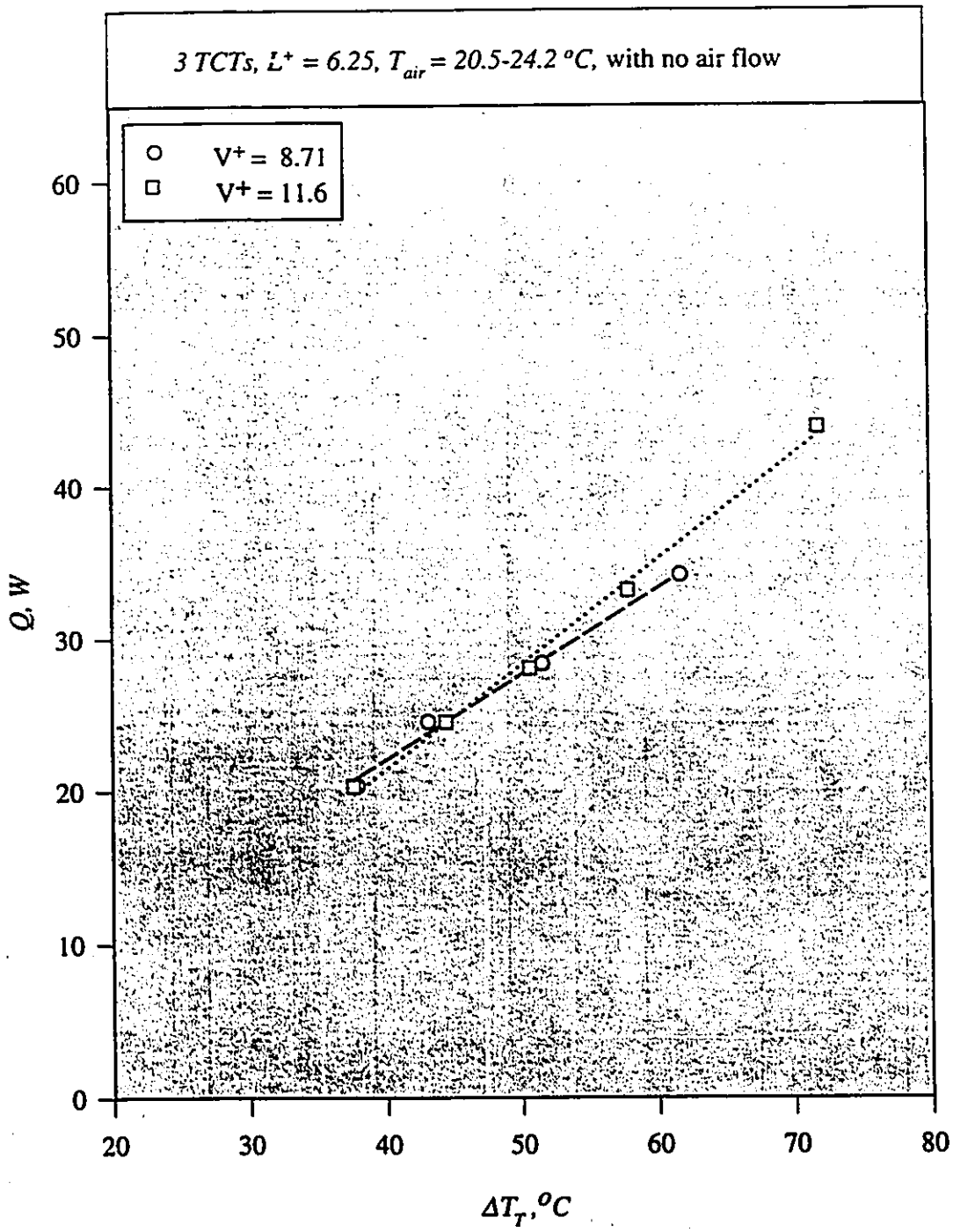

Figure 5.11(a) Effect of Absence of the Cooling Fan; WF = FC-87

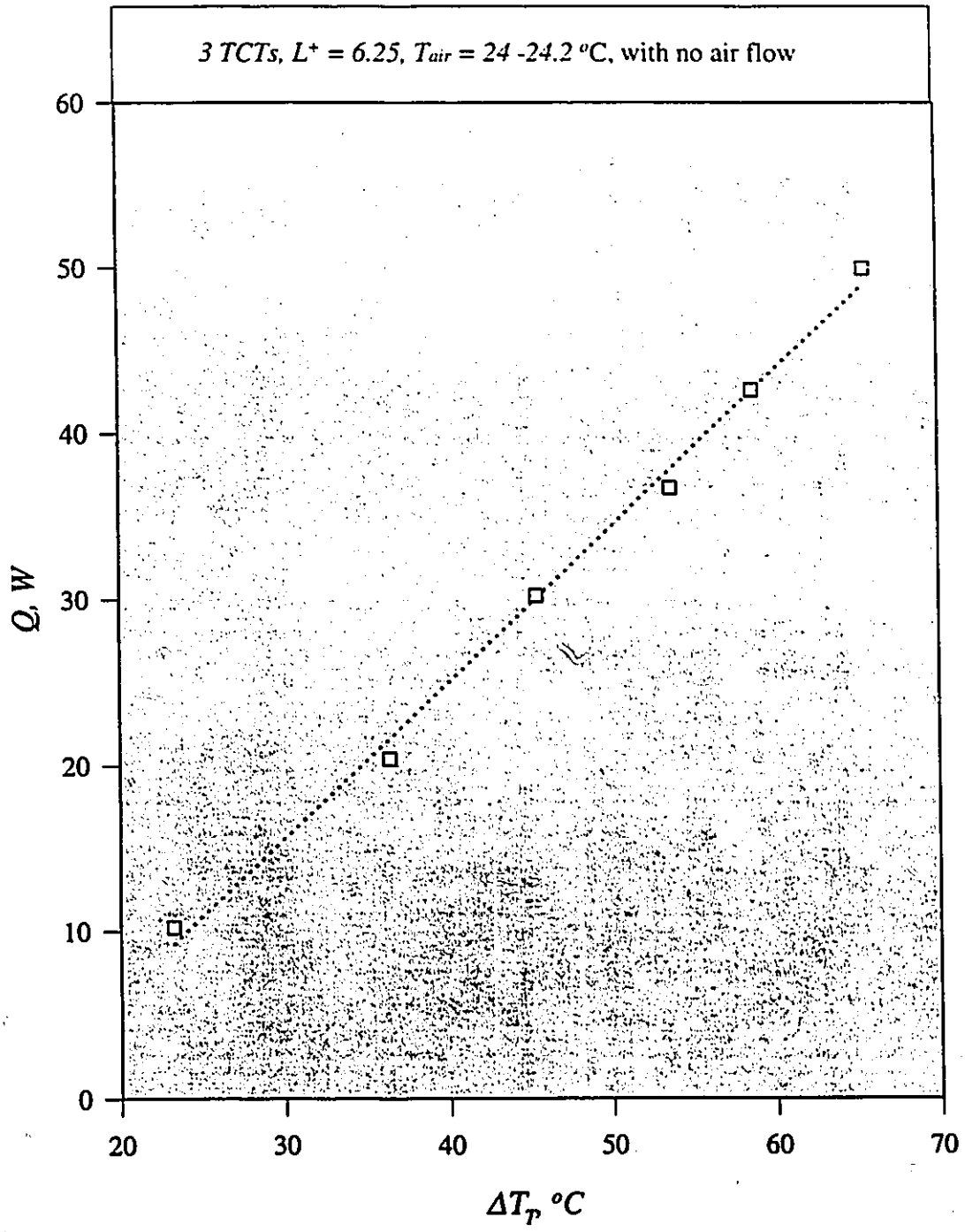

Figure 5.11(b) Effect of Absence of the Cooling Fan; WF = acetone

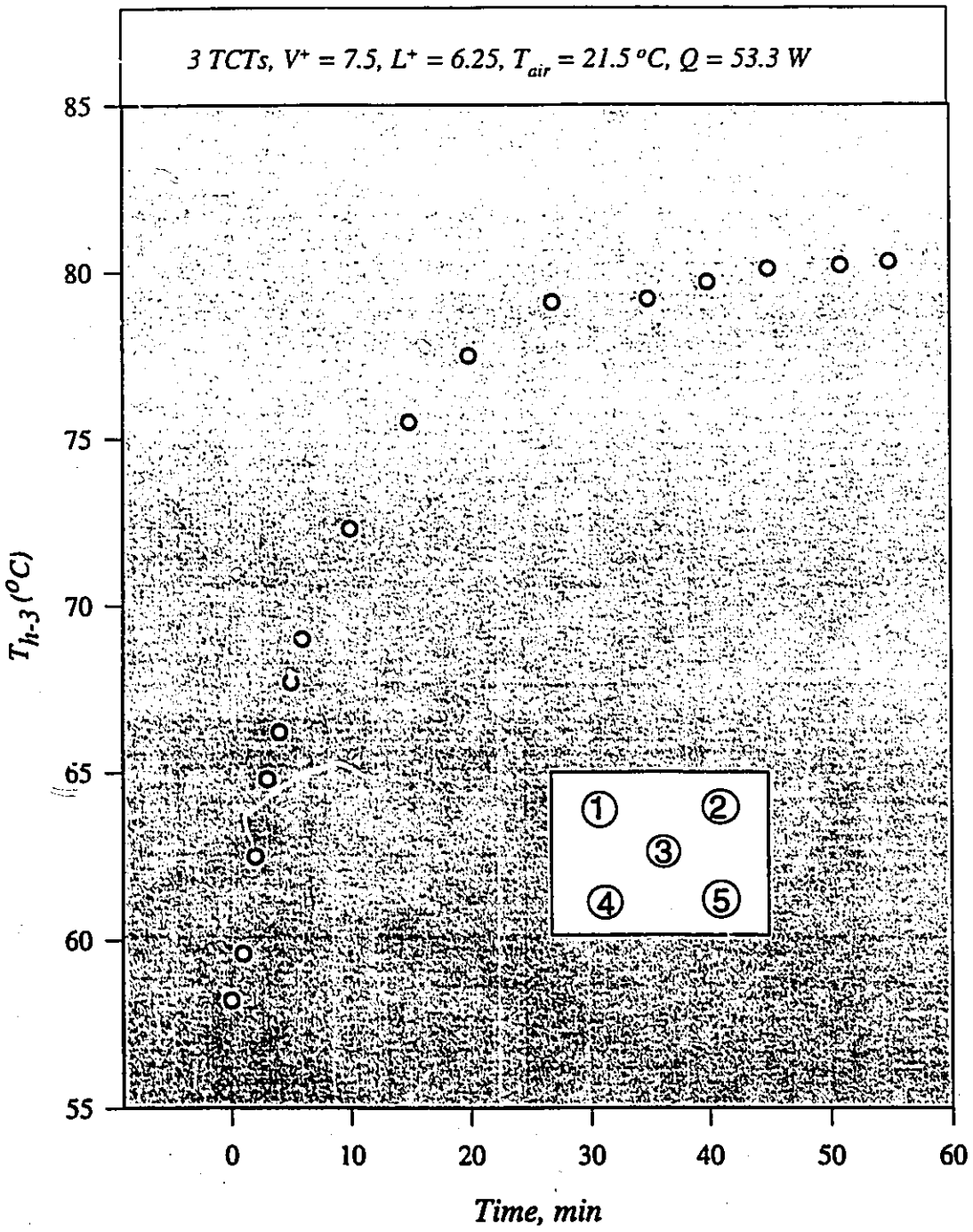

Figure 5.11(c) Temperature from Fan off ; WF = acetone

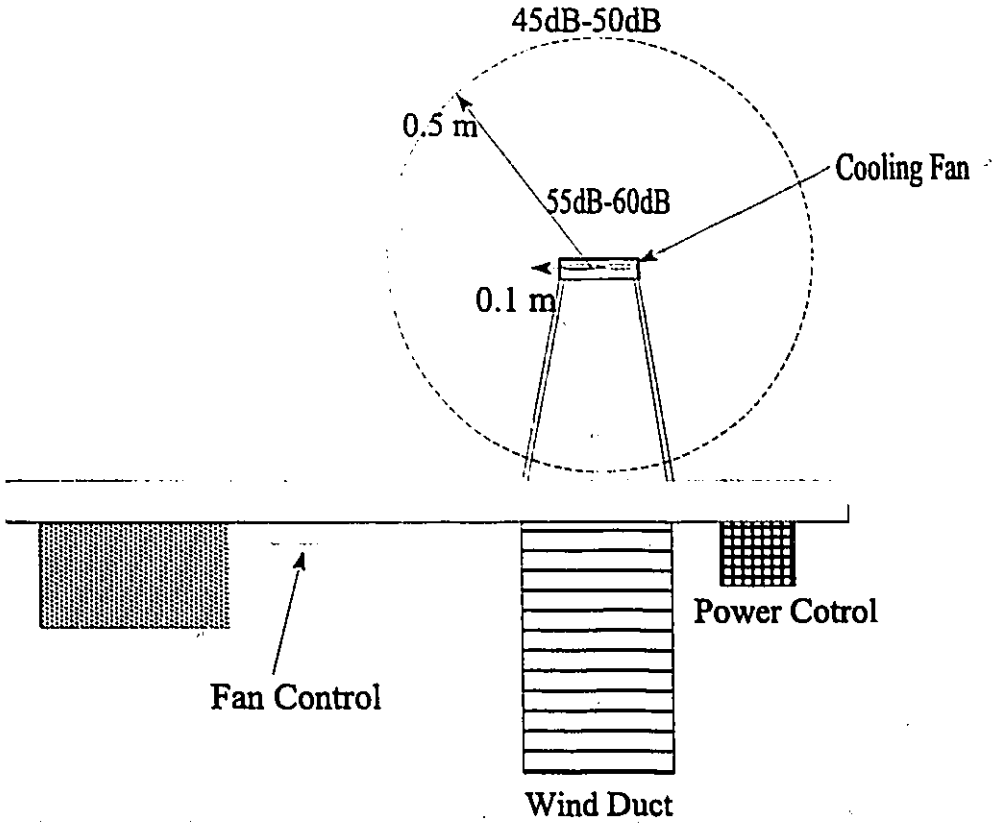

Test Conditions	
u_{max}	3.7 m/sec
T_{air}	22.4°C
Room ventilation off	

Figure 5.12 Cooling Fan Noise Test